Master of Science in Advanced Mathematics and Mathematical Engineering
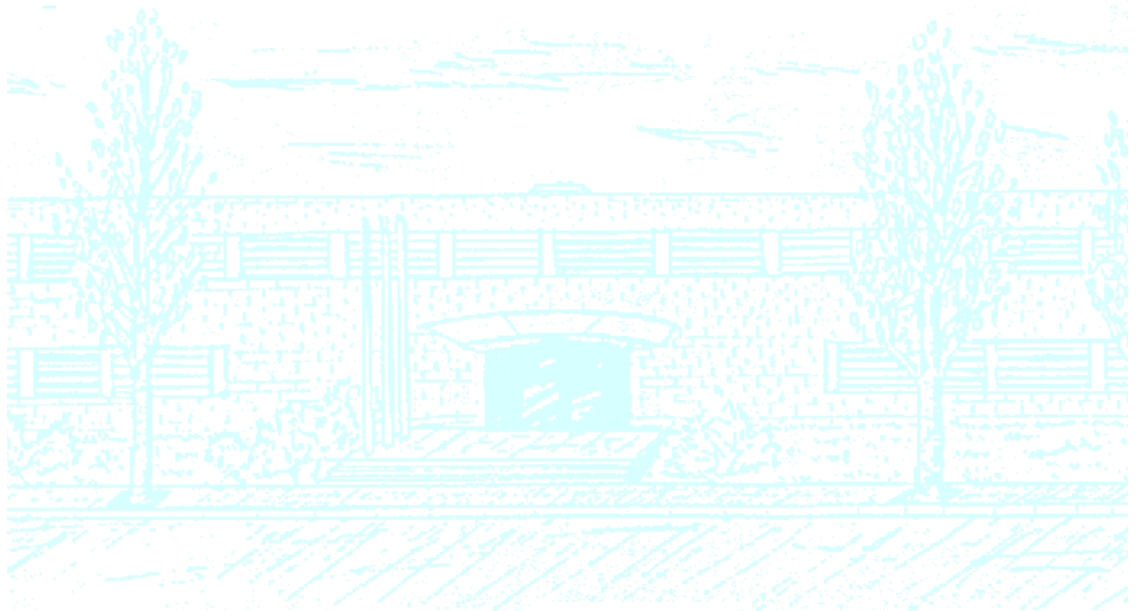
MASTER'S THESIS

Title: Assessment of air pollution health co-benefits of Net-zero climate policies

Author: Clàudia Rodés Bachs

Advisor: Lara Aleluia Reis

Department: Department of Mathematics

Academic year: 2021-2022

UNIVERSITAT POLITÈCNICA DE CATALUNYA
BARCELONATECH
Facultat de Matemàtiques i Estadística

Universitat Politècnica de Catalunya

Facultat de Matemàtiques i Estadística

Master in Advanced Mathematics and Mathematical Engineering
Master's thesis

Assessment of air pollution health co-benefits of Net-zero climate policies

Clàudia Rodés Bachs

Supervised by Lara Aleluia Reis

June, 2022

Abstract

Outdoor air pollution is responsible for a substantial amount of premature deaths and severe illnesses. Just in 2019, according to the GBD, it caused 124.21 million (95% CI 98.89-147.63) DALYs and 4.505 million (95% CI 3.625-5.364) deaths. Several air pollution co-benefits derive directly from the climate change mitigation policies, that have recently included a new carbon budget design: the *net-zero* pathway. However, a lot of factors add uncertainty to the estimation of health impacts.

We aim to study the main drivers of uncertainty in mortality, as well as their interaction, with a special focus on the relative risk impact functions in the role of the decarbonization path. To do so, the climate mitigation scenarios from the ENGAGE database are considered, as well as a source-receptor model to estimate concentrations and several relative risk impact functions to compute premature deaths. The study further identifies that *net-zero* climate policies rise the health co-benefits and reduce the risk of extreme mortality outcomes. Moreover, this is of especial importance for stringent climate targets aiming to limit the temperature increase well below 2°C, with particular relevance in Asia and Africa.

Keywords

Contents

1. Introduction

Outdoor air pollution is known to be a major contributor to mortality, morbidity, and productivity loss [45]. In 2019, according to the HIME database [33], 4.5 million deaths worldwide were caused by fine particulate matter ($PM_{2.5}$) and ozone (O_3) air pollution. Of those deaths, 5.7% were due to O_3, and the rest to $PM_{2.5}$ [33]. Moreover, more than 80% of the world's population is exposed to pollutant concentrations exceeding the World Health Organization (WHO) recommended levels [6, 68]. Besides, air pollution does not only impact on human health, it also constitutes an economical problem, endangers the planetary health, destroys ecosystems, and is linked to global climate change [23, 38, 72].

Precisely, O_3 and $PM_{2.5}$ are the two main health-harmful air pollutants [7], originated mainly from fossil fuel combustion and greenhouse gas (GHG) emissions [12, 34, 44, 69]. This means that air pollution and climate change are closely linked since GHG emissions are responsible for the Earth's temperature increase, which in turn leads to the widely known climate change problem [62]. In this context, several climate policies have been designed aiming to meet a global average temperature increase by the end of the century (i.e. 2100), as assessed in the last IPCC AR6 [70]. These long-term global scenarios are generally produced by integrated assessment models (IAMs), which project economic growth, population, energy consumption, land use and agriculture along with associated GHG and pollutant emissions [42]. To that extent, it is important to consider the air pollution health dimension in the design of policies [56].

Generally, the climate policies aim to cut down the use of highly pollutant fuels and to switch away from inefficient technologies to mitigate the GHG damages [53]. Indubitably, the effects on the mitigation depend directly on the policy stringency and strategy [54, 57]. Historically, global climate mitigation policies allow overshooting of emissions and temperature, that is, a period of time in which warming is increasing past some "dangerous" threshold and then cooling back down. In this traditional climate policy design, the majority of climate models predict a period of climate overshoot, with years if not decades of higher global temperatures before stabilizing at the temperature increase target, for instance, 1.5°C or 2°C as set by the Paris Agreement [70]. Then, to meet the emissions goal, the models predict a period of net-negative emissions, that is, removing directly the pollutant from the atmosphere.

Recently, the use of *net-zero* carbon budget policies has been analysed through a multi-model studio [23, 70]. This kind of policy constrains the world to never have net-negative emissions. Consequently, they impose earlier climate mitigation strategies to reduce the overshoot. Our goal is to analyse the air pollution mortality impact of non-overshooting climate policies.

1.1 State of the art and contributions

A substantial amount of work has been done to estimate the numbers of current and future premature deaths due to $PM_{2.5}$ and O_3 concentration levels [2, 11, 34, 68]. Typically, the air pollution co-benefits literature often considers only the uncertainty associated with the model input, that is the uncertainty associated with emissions, commonly derived by a range of IAMs [67]. However, there are other sources of uncertainty such as method uncertainty. The calculation of concentration from emissions also entails large uncertainties, as even complex chemical transport models often provide different values for concentration depending on their assumptions and parameterizations [4, 63]. Finally, the extent to which a change in concentration entails a change in mortality is also subject of uncertainty [35]. As a result, our aim is to study these sources of uncertainty as well as their interactions.

This study contributes to the air pollution co-benefits literature by providing the first assessment of

air pollution outcomes from non-overshooting climate policies. To the best of my knowledge, a sensitivity analysis on *net-zero* carbon budget policies has never been undertaken. Previous studies have looked at the IAMs uncertainty of *net-zero* carbon scenarios [23, 59] with the focus on climate mitigation. Other studies have performed uncertainty analysis along some impact functions, the methods used to estimate mortality, although without considering different scenarios [10, 11] and especially not considering the most recent IPCC AR6 climate scenario design. This study combines the novelty of the newly designed *net-zero* carbon budget policies and the sensitivity and uncertainty analyses, providing robust findings of the impacts of the climate policy design on air pollution mortality.

The goal of this thesis is: to provide robust insight on the co-benefits of *net-zero* carbon budget policies for air pollution mortality; and to identify and quantify the sources of uncertainty related to air pollution mortality estimates. Furthermore, we aim to answer the following questions: do *net-zero* scenarios have significantly more co-benefits for air pollution? What contributes more to the uncertainty in air pollution mortality: emissions uncertainty or impact function uncertainty? And does *net-zero* climate policy lower the probability of nasty mortality outcomes?

1.2 Organization of the thesis

This Master's Degree Thesis is structured into the following chapters:

- Preliminaries: where an overview of the considered pollutants and their health impacts is given, as well as an explanation of the scenarios and policies, and a detailed mathematical description of the impact functions.

- Methodology: where the data sources are detailed, as well as the pre-processing data methodology. Moreover, an overview of TM5-FASST(R) is provided, along with a description of the implemented impact functions.

- Uncertainty and sensitivity analyses: where the mathematical background of the uncertainty and sensitivity analyses is given.

- Results: where all methods and procedures are applied and the results detailed.

- Conclusion: where we summarize the achievements of this thesis and lay out future work that may stem from here.

2. Preliminaries

2.1 Chemical overview

Outdoor air pollution is a major contributor to the burden of disease worldwide [61]. Most of the global population currently resides in places where air pollution levels, because of emissions from major sources such as industry, power generation, transportation, and domestic burning, considerably exceed the World Health Organization (WHO) health-based air-quality guidelines [6, 68].

It has been widely proved that some ambient pollutants have a direct impact on our health, depending on their concentration level. Some of the most relevant ones are particulate matter $PM_{2.5}$ and PM_{10}, ozone (O_3), nitrogen dioxide (NO_2), sulfur dioxide (SO_2), and carbon monoxide (CO) [49].

In this study, we will focus on $PM_{2.5}$ and O_3. $PM_{2.5}$ refers to fine particulate matter, which are particles with an aerodynamic diameter equal to or less than 2.5 µm [49]. The chemical composition of $PM_{2.5}$ differs spatially and temporally. Its most commonly found chemical compounds are ammonium (NH_4^+), sulfate (SO_4^{-2}), nitrate (NO_3^-), black carbon (BC), organic carbon (OC), sodium (Na), silicon (Si) and other metals [22]. Particularly, the main $PM_{2.5}$ precursor pollutants are SO_2, NO_x, BC, OC, and NH_3 [21].

Particulate matter pollution is often divided into two types: ambient (outdoor) particulate matter pollution and household (indoor) air pollution from the use of solid fuels for cooking, including coal, charcoal, wood, agricultural residue, and animal dung [33], as well as tobacco smoke, biomass, and fossil fuel combustion [68]. Here we tackle the health impacts of ambient air pollution.

Furthermore, $PM_{2.5}$ is composed both of primary and secondary $PM_{2.5}$. The former refers to the pollution that is directly emitted and remains in the atmosphere, without reacting, in the form of fine particulate matter (e.g. BC and OC). Secondary pollution, on the other hand, refers to particulate matter that is not directly emitted but is formed in the atmosphere through chemical reactions (e.g. ammonium sulphates and nitrates). As a remark, primary $PM_{2.5}$ may include *natural* $PM_{2.5}$, like sea salt and desert dust; in fact, it is in the deserts where $PM_{2.5}$ concentrations may be the highest [49].

Long-term exposure to $PM_{2.5}$ increases morbidity and mortality [9]. More precisely, total exposure to $PM_{2.5}$ caused 6.45 million (5.72–7.24) deaths and 210 million (95% CI 186–235) disability-adjusted life years (DALYs) in 2019 according to the Global Burden of Disease (GBD) database [33]. Elevated risks in several countries for $PM_{2.5}$-adult-related deaths from ischemic heart disease (IHD), chronic obstructive pulmonary disease (COPD), lung cancer (LC), and stroke, called also cerebrovascular disease, that comprehends ischaemic stroke and haemorrhagic stroke, were illustrated in a large amount of studies [3, 9, 39]. As well as elevated risks for $PM_{2.5}$-children-related deaths from acute lower respiratory illness (ALRI) [3, 39]. $PM_{2.5}$ is a set of particles of particular health concern because it contains numerous toxic compounds (e.g., acids and heavy metals), and can penetrate deeper into the lung than the larger PM generated by natural processes, such as most windblown soil particle mass [68].

The GBD defined the level of risk exposure that minimises risk in the population, usually referred to as counterfactual or theoretical minimum risk exposure level (TMREL). Since 2015, the counterfactual exposure for $PM_{2.5}$ is established as a uniform distribution between 2.4 and 5.9 $\mu g\,m^{-3}$ [55]. This means that below the lower bound no increased risk of mortality is assumed to exist, and above the upper bound there is expected no additional risk of mortality either.

On the other hand, O_3 is a pollutant that is not directly emitted by primary sources. Rather, it is formed through a series of complex reactions driven mainly by volatile organic compounds (VOCs), nitrogen oxides (NOx), and methane (CH_4) [49, 68]. Precisely, the GBD defines the ambient ozone pollution as the

highest seasonal (six-month) average of eight-hour daily maximum ozone concentrations and in 2019 set the counterfactual exposure to a uniform distribution between 29.1 and 35.7 parts per billion (ppb) [33].

In 2019, O_3 pollution accounted for 11.1% (95% CI 5.3–17.0) of COPD deaths globally, for a total of 365.000 deaths (175.000–564.000), and 6.21 million (2.99 to 9.63) disability-adjusted life years (DALYs) [33]. Moreover, field experiments have demonstrated that atmospheric O_3 can damage crops, leading to yield reduction and deteriorating crop quality, resulting in economic losses and threat to food security [72].

To sum up, in 2019, $PM_{2.5}$ was considered the 4th-leading deaths risk factor of Level 3 and the 2nd one regarding DALYs, while O_3 was placed in the 31th position concerning deaths and in the 43rd one with respect to DALYs [33].

Both constitute an important environmental health risk that contributes to human premature mortality and crop loss that calls for better mitigation policies.

2.2 Scenarios overview

One of the main objectives of the Paris Agreement is to limit warming well below 2°C and pursue limiting it to 1.5°C. The pathways through which such global temperature outcomes can be achieved have been explored widely by the Intergovernmental Panel on Climate Change (IPCC), for example, in its Sixth Assessment Report (AR6; [70]).

To meet different temperature targets, various carbon budgets have been considered. These values indicate the cumulative CO_2 emissions over the period 2018-2100 and they directly imply different temperature outcomes by the the end of the century [59]:

Table 1: Temperature increase and carbon budget relation.

Temperature increase	Carbon budgets (GtCO$_2$)
Range around 1.5°C	200, 300, 400, 500, 600, 700, 800, 900
Range around 1.5-2°C	1000, 1200, 1400, 1600, 1800, 2000
Higher budgets	2500, 3000

This long-term temperature target is consistent with two different carbon budget scenario designs, that from now on we will refer to as climate policy designs. The *end-of-century* (EoC) climate policy design implements the remaining carbon budget without restriction, while the *net-zero* (NZ) climate policy design implements the remaining carbon budget until CO_2 emissions reach net-zero emissions. After that point, net CO_2 emissions are kept at zero. In this way, the temperature peaks and stabilizes.

Traditionally, the models used the EoC climate policy design, which mainly employs overshooting, i.e., there exists a time period in which warming is increasing past the 1.5°C mark and then cooling back down. This suggests that net-negative emissions techniques will be used later in the century to ensure that the carbon budget targets are met. They have been widely criticised and new pioneer studies have analysed the so-called NZ scenarios, where overshooting is limited through global *net-zero* emission goals, as just introduced [59, 66].

As a recap, while both EoC and NZ climate policies achieve the same carbon budget, their paths to the target imply different GHG emissions over time, and therefore, different technology pathways. This will also have implications for air pollution emissions. Bear in mind that to compute the future emissions

according to each policy and scenario assumption, the IAMs are essential. They are a very useful tool to provide guidance in policy design and estimate climate and economic impacts.
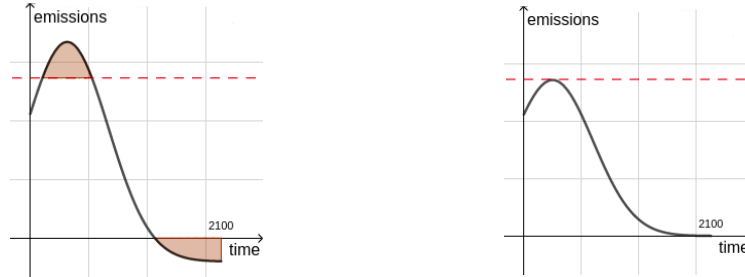

Figure 1: Sketch of overshooting (left) vs non-overshooting emissions (right). Notice that the area above the threshold and below the X-axis is the same, as well as the two areas comprehend between the X-axis and the threshold of the two figures.

Besides the long-term assumption (climate policy and carbon budget), short-term policies play also an important role. Following the ENGAGE project database [60], we can distinguish between [73]:

- National Policy (NPi): scenario that includes the currently implemented reference policy. Thus, models should follow the current national policy implementation to 2020.

- Nationally Determined Contribution (NDC): scenario that assumes the implementation of the Nationally Determined Contributions (NDCs) by 2030, but no further intensification of emission reduction commitments beyond the NDCs after 2030.

- No Policy: scenario that does not include any policy.

All in all, each scenario deals with the following information:

- The long-term assumption (climate policy): *net-zero* or *end-of-century*.

- The short-term assumption (policy): NPi, NDC, or *no-policy*.

- The long-term assumption (carbon budget): ranging form 200 $GtCO_2$ to 3000 $GtCO_2$.

For further details on the scenario design and description, please see [59].

2.3 Impact functions overview

Taking as input the concentration of each pollutant per region and year, it is possible to estimate several health metrics. For instance, the premature deaths or the avoided deaths, the years of life lived with disability, the years of life lost, or the disability-adjusted life years, among others [33]. All of them need the Population Attributable Fraction (PAF) value, that links the concentrations with the health risks. Subsequently, the impact made by it is the same on each health metric, and hence, it is only necessary to study one of them. In this project, the focus is on premature deaths.

To compute the premature deaths due to air pollution we consider the following formula:

$$\Delta Mort = y_0 \cdot PAF \cdot pop \tag{1}$$

provided by several references such as [2] and widely used in worldwide studies. The variable y_0 refers to the baseline mortality, whereas *pop* accounts for the exposed population. *PAF* is the acronym for Population Attributable Fraction. Consequently, $\Delta Mort$ is the proportional reduction in population disease or mortality that would occur if exposure to a risk factor were reduced to an alternative ideal exposure scenario [48].

As previously explained, PM$_{2.5}$ is responsible for IHD, STROKE, LC, COPD, and ALRI. On the other hand, O$_3$ has a direct impact on COPD. Except for ALRI, which affects children (< 5 years old), the other causes of death are studied among the adult population (≥ 25 or ≥ 30 years old depending on the study). Therefore, the exposed population value will be different for ALRI than for the rest of the illnesses.

The PAF can be obtained as

$$PAF = \left(\frac{RR - 1}{RR} \right) \tag{2}$$

as described in [53], where *RR* refers to Relative Risk, which is the ratio of the probability of an outcome in an exposed group to the probability of an outcome in an unexposed group. This value is different for each disease and concentration's exposure and can be computed in multiple ways. The selected parameters to compute them and the methods chosen for the analysis are gathered in Table 3 and along the Methodology section 3.3 respectively.

Since the first impact function to compute the relative risk appeared, new impact functions aiming to improve the existing ones have been developed through the years.

Figure 2: PM$_{2.5}$ impact functions timeline.

One of the simplest and ancient methods to compute the relative risk is the Log-Linear (LL) model, developed approximately one decade ago [40]:

$$LL(X) = \exp\{\beta(X - X_0)\}, \tag{3}$$

where β is the parameter that characterises its shape, X is the concentrations exposure, and X_0 is the counterfactual value. This formulation has some difficulties when dealing with high levels of outdoor PM$_{2.5}$ since it is usually assumed no additional risk beyond $30\,\mu g\,m^{-3}$ [11].

As it can be appreciated, this function only depends on the difference in concentrations, $X - X_0$, not on their individual magnitudes. This fact is also present in other relative risk functions.

The Integrated Exposure-Response (IER) model, developed by the GBD, has become the state-of-the-art exposure-response model for estimating the PM$_{2.5}$ mortality relative risk since its introduction in 2013 [11, 12, 26]. It has the following formulation,

$$IER(X) = 1 - \nu(1 - \exp\{-\omega z^\delta\}), \quad z = \max(0, X - X_0), \tag{4}$$

where the parameters (ν, ω, δ) are estimated using non-linear regression methods. This formulation allows to deal with arbitrary high PM$_{2.5}$ expositions, while considering other sources of PM$_{2.5}$, particularly, secondhand and active smoking [11]. However, it assumes equal toxicity per unit dose across these nonoutdoor sources, as well as presumes a counterfactual value, which adds uncertainty to the model [10].

To relax these assumptions, the Shape Constrained Health Impact Function (SCHIF) was developed, aiming to model the mortality due to $PM_{2.5}$ using data within any specific cohort [46].

$$logSCHIF(z) = \theta f(z)l(z), \quad z = X - \min(X), \tag{5}$$

where $l(z) = (1 + \exp\{-(z - \mu)/\tau r\})^{-1}$ is a logistic function in concentration, and $f(z)$ can take two forms. Either linear, $f(z) = z$, or logarithmic, $f(z) = log(z + 1)$. Note, $logSCHIF(0) = 0$. The parameters (θ, μ, τ) are estimated from data [11] and notice that this formulation endogenizes the counterfactual value, considering it simply as the minimum concentration of $PM_{2.5}$ in the study set.

An improvement of this impact function arrived with a well-known relative risk model: the Global Exposure Mortality Model (GEMM) [11].

$$logGEMM(z) = \theta \frac{log(\frac{z}{\alpha+1})}{1 + \exp\{-\frac{z-\mu}{\tau r}\}}, \quad z = X - \min(X).$$

The parameter α was added to make the SCHIF more flexible. In particular, α controls the amount of curvature, with less curvature for larger values of α. In this way, the formulation of the previous SCHIF equation 5 can be simplified transforming the two forms of $f(z)$ by $log\left(\frac{1+z}{\alpha}\right)$. Consequently, the predictions of relative risk beyond the observed exposure range have a logarithmic form with diminishing changes in relative risk as exposure increases [11].

In this function, the parameters are constrained such that the change in relative risk for higher concentrations declined as concentrations increased. Moreover, as in the SCHIF equation 5, it has the counterfactual value endogenized. Remark that this model is usually used without the logarithmic form:

$$GEMM(z) = \exp\left\{\frac{\theta \log\left(\frac{z}{\alpha+1}\right)}{1 + \exp\{-\frac{z-\mu}{\nu}\}}\right\}, \quad z = X - \min(X). \tag{6}$$

Besides, there are other functions to compute the relative risk due to some specific diseases, such as the one suggested by *Ostro et al.* [14]. It is a rational function used for lung cancer as well as cardiopulmonary diseases (CP), which are the sum of chronic obstructive pulmonary disease, acute respiratory illness, ischemic heart disease, and stroke. It has the following formulation,

$$RR(X) = \left(\frac{X+1}{X_0+1}\right)^{\beta}, \tag{7}$$

where the coefficient β is chosen according to the disease, the region, the educational level, and the economic status among others [14].

To compute the relative risk for O_3 there is a large consensus to use the Long-Linear function [15]. Since the GBD used it in 2010, it was reported by many authors [34, 40].

$$LL(X) = \exp\{\beta(X - X_0)\}, \tag{8}$$

3. Methodology

Uncertainty analysis requires large amounts of data. Therefore, data should be gathered and handled before proceeding with the final goal. This procedure is composed of three main steps: first, the pre-processing of the emissions' data given by the ENGAGE project database 3.1.1. Secondly, the computation of $PM_{2.5}$ and O_3 concentrations through TM5-FASST(R) 3.2. Finally, the computation of premature deaths using different impact functions 3.3. Recall that only the first and the third step might produce uncertainty since different ways of computing the emissions and the mortality are respectively considered; however, after computing the concentrations, a detail analysis will be performed to see the relation between all the components.
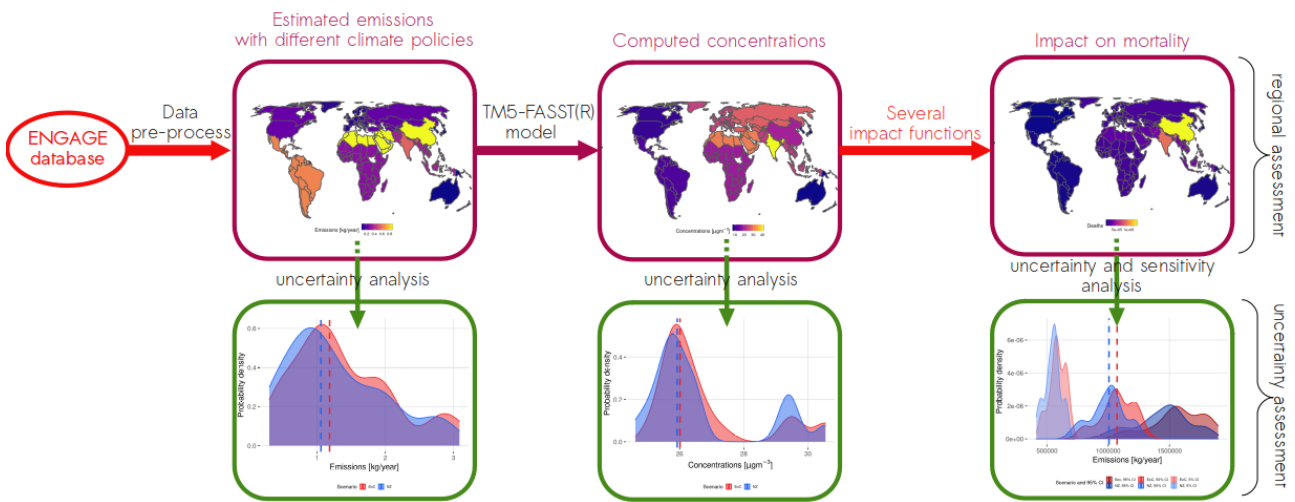
Figure 3: Schematic representation of the methodology framework. In red the uncertainty sources, in purple the regional assessment, and in green the uncertainty and sensitivity analyses.

3.1 Data

Different data is required in different parts of the workflow. For instance, data regarding the emissions, data on the baseline mortalities, or data about the population exposure. Each one is obtained through different sources that are detailed below.

3.1.1 Emissions data

The emissions data, as already mentioned above, is obtained through the ENGAGE project database [60], which includes 36 scenarios and 9 global integrated assessment models (IAMs). However, we only consider 6 of the models (AIM/CGE [28, 29], IMAGE [65], MESSAGEix-GLOBIOM [32], POLES-JRC ENGAGE [20], REMIND-MAgPIE [37, 43], and WITCH [5, 25]) since the other three (COFFEE [50], GEM-E3 [13, 24], and TIAM-ECN [71]) only report SO_2 and CH_4, which are not enough to estimate O_3 and $PM_{2.5}$. We use the harmonized regional air pollution emissions ($R10$) and include world emissions such as aircraft and shipping. This means, that we divide the overall countries into 10 regions (R10AFRICA, R10CHINA+, R10EUROPE, R10INDIA+, R10LATIN-AM, R10MIDDLE-EAST, R10NORTH-AM, R10PAC-OCED, R10REF-ECON, and R10REST-ASIA, see figure 4) and also consider an extra one devoted to aircraft and shipping.

On the other hand, emissions from eight pollutants that contribute to the formation of O_3 and $PM_{2.5}$ are taken into account: BC, OC, NOx, SO_2, CO, CH_4, NH_3 and VOC.
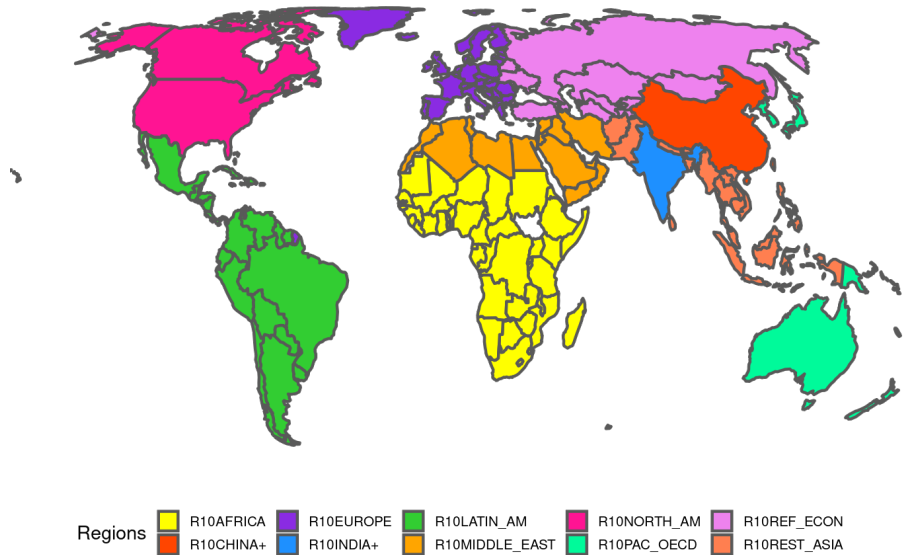

Figure 4: R10 World division.

The ENGAGE scenarios are the results of a multi-model exercise that includes several levels of climate stringency, through different carbon budgets allowed. As detailed in 2.2, it includes different levels of short-term policies, such as NPi, NDC, and *no-policy*. Remark that this last one will be considered as a reference (REF) scenario in this project, as well as the already considered reference scenarios in the ENGAGE project database. Importantly the ENGAGE project database distinguishes from the more conventionally used EoC climate policy and the NZ one [59]. While the former relies solely on the resulting budget in 2100, the latter constrains world emissions to stay at net-zero not allowing the world to go net negative at any moment, as described in 2.2.

The ENGAGE database is regionalized, that is, the emissions are given by region and not by country. Since TM5-FASST(R) requires the annual pollutant emission data aggregated at the regional level, we could directly run it with the original data, without down-scaling it.

3.1.2 Impact functions data

As mentioned above, the formula to compute premature deaths is 1:

$$\Delta Mort = y_0 \cdot PAF \cdot pop,$$

where y_0 and *pop* are data. Both values are taken directly from *VanDingenen et al* [21]. Remark that the baseline mortality is different for each disease, as well as the exposure population value, which changes for age group and pollutant. In particular, for $PM_{2.5}$ it is the annual average daily exposure, while for

O_3 it is the seasonal hourly maximum concentration. According to the literature, some authors used the sixth-month hourly maximum concentration, whereas some others used the three-months one.

3.2 TM5-FASST(R)

To estimate the concentrations of $PM_{2.5}$ and O_3 from emissions provided by the ENGAGE scenario database we used an R version of the TM5-FASST Scenario Screening Tool (TM5-FASST(R)), from now on simply denoted by FASST [21]. It is a global reduced-form air quality source–receptor model from the TM5 chemical transport model. As an idea, it is constructed from pre-computed emission-concentration transfer matrices between pollutant source regions and receptor regions. These matrices emulate underlying meteorological and chemical atmospheric processes for a predefined set of meteorological and emission data and have the advantage that concentration responses to emission changes are obtained by a simple matrix multiplication, avoiding expensive numerical computations. The method has been widely used [57].

Since FASST was needed to be run for each model-scenario pair, that is, 278 times, and each run required approximately 20 minutes, Zeus [64], the supercomputer of the Euro-Mediterranean Center on Climate Change (CMCC) was used to run all the model-scenario combinations in parallel.

3.3 Impact functions

As already mentioned, to estimate the premature deaths we use equation 1. On the one hand, the *PAF* value is computed through different impact functions. This study considers impact functions starting from 2000. On the other hand, the baseline mortality value y_0 and the population exposure value *pop* are obtained from literature, as detailed in 3.1.2.

As it can be seen in Table 3, five different sources for $PM_{2.5}$'s parameter values and two for O_3 are considered. Nevertheless, some papers provided more than one set of parameters, which enabled us to finally collect eight relative risk parameter sets for $PM_{2.5}$ and two ones for O_3. Regarding the variety of methods, four different ones are used for $PM_{2.5}$ and only one is used for O_3.

To really comprehend each set of parameters, let us look carefully one by one to see how the values were obtained and, in the case of considering different parameter sets from the same paper, under which rules have been derived.

A recent study of *Burnett et al.* [10] followed the GEMM model 6 to compute the relative risk value of $PM_{2.5}$. Among the causes of death that they considered, four match with our aim of study: LC, IHD, STROKE, and COPD. The counterfactual value was set to the lowest one of the GBD $PM_{2.5}$-TMREL distribution, $2.4\,\mu g\,m^{-3}$. To perform the study, they considered 15 research groups globally that, independently, conducted analyses to characterize the shapes of $PM_{2.5}$–mortality associations in their respective cohorts. Among these 15 cohorts was a study of Chinese men with long-term outdoor $PM_{2.5}$ exposures up to $84\,\mu g\,m^{-3}$, thus greatly extending the range of exposures observed in cohort studies conducted in high-income countries in Europe and North America. Therefore, they did the study both including and not including them, and consequently, in this project, two separate sets are considered. The adult population considered in the study was people older than 25 years old.

It is worth mentioning that these same parameter values were used in subsequent studies, for instance, in [11].

In 2016, the GBD together with the WHO [52] re-calibrated the IER model's parameters 4 from the 2013 ones. They focused on five illnesses, but only four coincided with the diseases tackled in this study:

LC, IHD, STROKE, and COPD. Once again, the study was done for $PM_{2.5}$ and considered the adult population as people older than 25 years old. The provided data was especially extensive since they used a spatial resolution ($1° \times 1°$) globally to estimate the exposures of $PM_{2.5}$. Therefore, 1000 values were present for each cause of death and age group.

To deal with them, we determine to split the data using the counterfactual exposure. In particular, three groups are created according to the GBD $PM_{2.5}$-TMREL distribution:

$$LOW = (2.4, 3.56), \qquad MEDIUM = (3.57, 4.73), \qquad HIGH = (4.74, 5.9).$$

Then, by illness, the median of each parameter was considered, as well as the counterfactual value.

Based on previous studies of *Pope et al.* [51], *Ostro et al.* [14] did a study for $PM_{2.5}$ and PM_{10} to assess their environmental burden of disease at national and local levels. The function used was the rational one 7 for two illnesses: LC and CP. The suggested values for β were taken directly from [51] and for the counterfactual values, they suggested two different ways of choosing them: either using the background concentration of $PM_{2.5}$ in the region or the lowest observed concentration in the original study. Therefore, a sensitivity analysis among the uniform distribution suggested by the GBD will be performed.

Two impact functions were already implemented in FASST [21]. For $PM_{2.5}$, they follow the IER model 4 with the parameter values from *Burnett et al. 2014* [12], while for O_3 they used the ones described in *Jerret et al. 2009* [34] following the LL method 8. Other studies used also these values, such as [2].

The IER parameters are computed for COPD, LC, ALRI, STROKE, and IHD. They were driven from [15], which used a Bayesian framework through the STAN fitting algorithm. Importantly, the counterfactual value was set different for each disease.

Besides, for O_3 the study was done for COPD, with a flexible counterfactual value. Hence, we will do sensitivity analysis on it through the uniform distribution of O_3 that was set by the GBD in that year: U(33.3–41.9) ppb. In the published paper [34], only the PAF value was available. Thus, since we need the value of the parameter β for our study, we use the following approach to compute the relative risk value:

$$RR = \frac{1}{1 - PAF}, \tag{9}$$

$$\beta = \frac{\log(RR)}{10}. \tag{10}$$

As mentioned before and detailed in the reference paper [21], the exposure of O_3 used was the six-monthly hourly maximum concentration.

Ananberg et al. [2] and *Jerret et al.* [34] also used the LL method 3 to compute the relative risk of $PM_{2.5}$ for LC, IHD, and CP. Precisely, they used the relative risk values of *Krewski et al.* [36]. However, to do our analysis we require from the value of the parameter β, thus we obtain it using equation 10. Once again, the counterfactual value was not clearly fixed, hence, we will do sensitivity analysis considering values of the uniform distribution for $PM_{2.5}$ set by the GBD, that is U(2.4–5.9) $\mu g\,m^{-3}$.

Finally, in 2015 the GBD used the LL model 8 for O_3. The study was done for COPD, with a flexible counterfactual value. In the published paper, only the PAF was available. Thus, since we need the value of the parameter β for our study, we use the equations 9 and 10 to obtain it. As mentioned before and detailed in the reference paper [55], the exposure of O_3 used was the three-monthly hourly maximum concentration. In this case, the counterfactual value was again not distinctly fixed; thus, a sensitivity analysis will be performed with the GBD distribution values of that year, which are once again U(33.3–41.9) ppb.

Remark that some studies consider adult population people older than 25 years old, while some others people older than 30 years old. In this assessment, the exposure value of the adult population is homogenized for the sake of simplicity and to avoid another source of variation, accounting for people older than 30 years old.

Regarding the counterfactual concentration value, we use the ones specified in each paper where the parameters' values were taken or, in the case of no explicit value, the GBD counterfactual value of that year, when possible. For $PM_{2.5}$, they use to match with the ones posted in the GBD 2019 report (U(2.4–5.9) $\mu g\,m^{-3}$; [17]); thus, this uniform distribution was taken for all functions; whereas for O_3, all both coincide with the previous counterfactual values defined by the GBD in 2017 (U(33.3–41.9) ppb; [61]); and consequently, these are the values considered.

4. Uncertainty and sensitivity analysis

When dealing with the future, it is often impossible to predict with certainty outcomes or events. Therefore, models are used to foresee tendencies and quantify the outcomes of policies. However, some assumptions must be made while imposing a policy or scenario, and our aim is to quantify the impact of normative choices, such as the choice of a given parameter, method or dataset. To do so, both sensitivity and uncertainty analyses are performed.

On the one hand, sensitivity analysis procedures explore and quantify the impact of each model input on the uncertainty of the predicted model output. Simple sensitivity analysis procedures can be used to illustrate either graphically or numerically the consequences of alternative assumptions about the future. On the other hand, uncertainty analysis is a mathematical approach that employs probabilistic descriptions of model inputs deriving probability distributions of model outputs [41].

Recall the two sources of uncertainty in our study: i) input uncertainty, as for the same climate policy design each IAM estimates different emission pathways; ii) impact functions uncertainty, since they are employed to compute the premature deaths. To study the uncertainty and sensitivity of all of them, as well as their interaction, some tests and graphs are considered.

Bear in mind that our final goal is to assess the difference between climate policies: NZ and EoC. However, other elements play an important role, such as the region, the carbon budget or the year, among others. Hence, the wide majority of tests and figures are done separately by different factors. Given the large number of carbon budgets present in the scenarios, three groups have been configured following the expected temperature rise in Table 1:

Table 2: Carbon budget groups.

Name	Carbon budget interval (GtCO$_2$)	Description
low carbon budgets	< 1000	accounts for temperature increase around 1.5°C
medium carbon budgets	$[1000, 2000]$	accounts for temperature increase around 1.5–2°C
high carbon budgets	> 2000	accounts for higher temperature increase

Besides, considering the different nature and values' ranges of the pollutants' emissions, they are used to be analysed separately.

Although graphical analyses give powerful information, we would like to complement it by quantifying the differences between either scenarios and climate policies or input parameters. Consequently, some statistical tests are run, such as the Kolmogorov-Smirnov test or the Binomial test. In this way, the differences between probability distributions and the probability of having longer tails are assessed, as done in previous studies such as [23]. This information will help us to quantify the impact of the NZ and EoC climate policy among pollutants and regions. Other tests could have been helpful, namely ANOVA or MANOVA, but the normality assumptions were not satisfied.

Each test considers a statistical hypothesis, i.e., a conjecture or affirmation about the distribution of one or more random variables. A hypothesis test is simply a procedure to decide if the hypothesis is accepted or rejected.

Definition 4.1. [19] Consider a statistical problem where the value of a parameter $\theta \in \Omega$ is unknown. Suppose that

$$\Omega = \Omega_0 \cup \Omega_1, \quad \text{such that } \Omega_0 \cap \Omega_1 = \emptyset.$$

Our aim is to decide whether $\theta \in \Omega_0$ or $\theta \in \Omega_1$.

Denote by

$$\begin{cases} H_0: & \theta \in \Omega_0 \\ H_1: & \theta \in \Omega_1. \end{cases}$$

Since $\theta \in \Omega$, where $\Omega = \Omega_0 \cup \Omega_1$ and $\Omega_0 \cap \Omega_1 = \emptyset$, one of the two hypotheses must be true. This kind of problem is called **hypothesis test problem**.

Recall two important definitions:

Definition 4.2. [19] On the above assumptions, H_0 is the **null hypothesis** and H_1 is the **alternative hypothesis**.

Remark 4.3. We will denote by $\Pi(\theta)$ the probability of rejecting the null hypothesis. When doing such a decision we could make a mistake (if H_0 was true), generally called *type I error*. To ensure that the test performs well, usually a level $\hat{\alpha}$ is fixed such that the probability of making a *type I error* is lower than this threshold.

Definition 4.4. [19] The **size of a test** $\hat{\alpha}$ is defined as

$$\hat{\alpha} = \sup_{\theta \in \Omega_0} \Pi(\theta),$$

which is the maximum probability, among all the values θ that satisfy H_0, of making an incorrect decision. Consequently, the **significance level of a test** α is

$$\sup_{\theta \in \Omega_0} \Pi(\theta) \leq \alpha.$$

Finally, recall the Fundamental Theorem of the Mathematical Statistics:

Theorem 4.5. [Glivenko-Cantelli] *[31] Let $\{X_n\}_{n \geq 1}$ be a succession of independent random variables identically distributed in a probabilistic space $(\Omega, \mathcal{A}, P)$, with a common distribution function F_X. Denote by S_n the empirical distribution function obtained from the n first random variables $X_1, \cdots, X_n$. Then, $S_n(x)$ converges uniformly to $F_X(x)$ with probability 1, that is,*

$$P[\lim_{n \to \infty} \sup_{-\infty < x < \infty} |S_n(x) - F_X(x)| = 0] = 1.$$

Once this short definitions reminder is done, let us describe in detail the figures and tests applied to the three data sets.

4.1 Probability distribution and cumulative frequency graphs

For emissions, concentrations, and mortality, the probability distribution and cumulative frequency graphs are considered. The first one shows the likelihood of obtaining possible values that a variable can take. In our case, the estimated emissions, the pollutants' concentrations, or the premature deaths estimation. Considering different probability distributions per climate policy, we can see which one predicts higher values of our variables. Moreover, by plotting the median we can detect if although the distributions are different, the output trends coincide.

Besides, the cumulative frequency graph represents the total number of values up to the current point. In this way, we can appreciate how the tendencies of each variable are, and more importantly, see the differences between climate policies: if both cumulative frequency lines are overlapped, no discrepancy between them is expected, whereas if the lines are somehow different, we can study if one climate policy estimates more emissions, concentrations, or premature deaths, or either if the dominant climate policy changes among factors.

Both graphs are complementary and give powerful and visual information. However, we feel the necessity of quantifying the differences between climate policies.

4.2 Kolmogorov-Smirnov two-sample test

This non-parametric test is an adaptation of the Kolmogorov-Smirnov (K-S) one-sample test. It compares the empirical distribution functions of two samples. Intuitively, the test answers the question "What is the probability that these two sets of samples were drawn from the same (but unknown) probability distribution?"

Consider two data samples of size m and n from continuous populations F_X and F_Y denoted by

$$X_1, X_2, \cdots, X_m, \quad \text{and} \quad Y_1, Y_2, \cdots, Y_n.$$

Their respective empirical continuous distribution functions, denoted by $S_m(x)$ and $S_n(x)$, are defined as

$$S_i(x) = \begin{cases} 0 & \text{if } x < X_1 \\ \frac{k}{i} & \text{if } X_k \leq x < X_{k+1}, \ k = 1, 2, \cdots, i-1, \quad \text{where } i = m, n. \\ 1 & \text{if } x \geq X_i, \end{cases}$$

The hypothesis of the test is the following:

$$\begin{cases} H_0: & F_X(x) = F_Y(x) \ \ \forall x, \\ H_1: & F_X(x) \neq F_Y(x) \ \ \text{for some } x, \end{cases}$$

which means that if the null hypothesis is true, both population distributions are identical and the samples are from the same population. Thanks to Glivenko-Cantelli theorem 4.5, we know that as m (analogously n) increases, the step function $S_m(x)$, approaches the true distribution function $F_X(x)$. Therefore, for large samples' size, the deviations between the true function and its statistical image, $|S_m(x) - F_X(x)|$, should be small for all values of x. This result suggests that the statistic

$$D_{m,n} = \max_x |S_m(x) - S_n(x)|$$

is, for any m and n, a reasonable measure of the accuracy of our estimate, and the rejection region is in the upper tail, defined by

$$D_{m,n} \geq c_\alpha, \text{ where } P(D_{m,n} \geq c_\alpha | H_0) \leq \alpha.$$

Once again, as a consequence of Glivenko-Cantelli theorem 4.5, the test is consistent and the p-value is

$$p = P(D_{m,n} \geq D_0 | H_0),$$

where D_0 is the observed value of the two-sample K-S statistic [31].

For our purpose, the significance level is set to 0.05, and the two data samples considered are the values of emissions, concentrations, and premature deaths estimated by the NZ and EoC climate policies. Remark each test is run by groups of region, pollutant, carbon budget interval, and year. In the case of premature deaths, also by impact function as well as by counterfactual and parameters percentile level.

Precisely, our hypothesis is:

$$\begin{cases} H_0: & \text{NZ and EoC climate policies have the same distribution function,} \\ H_1: & \text{NZ and EoC climate policies have different distribution functions,} \end{cases}$$

and we look for statistical evidence to reject the H_0.

Thus, for high p-values no difference due to the climate policy is expected, while for low p-values we can state that the climate policy plays some role. Remark that if a p-value is lower than the significance level we can state, with a 95% of assurance, that the climate policy is decisive, whereas if it's higher than 0.95, we can say that it has no influence on the data.

Linking the results of this test with the previous graphs in Section 4.1, observe that for low p-values we will observe a difference between the climate policies in the probability distribution plots, as well as among the cumulative plots. In particular, as higher the differences between both graphs, the lower the p-value will be.

4.3 Tail heaviness analysis

In the case of premature mortalities computation, we are also interested in studying the tail heaviness of the NZ and EoC distributions and whether there is a significant difference between them.

There is no unique definition of a heavy-tailed distribution. Indeed, this notion only makes sense in the context of each considered model. What we usually expect when we talk about heavy-tailed phenomena is some kind of different qualitative behaviour of the underlying model, i.e., some deviation from the "normal behaviour" which is caused by the extremes of the sample [8]. Precisely because of that, heavy-tailed distributions tend to have many outliers with very high values. The heavier the tail, the larger the probability to have one or more disproportionate values in a sample; and in our case, larger probability of nasty mortality outcomes.

Although it does not exist a universal definition, there is a general consensus and acceptance of the following one:

Definition 4.6. [27] A probability distribution $F(x)$ is **heavy-tailed** if and only if

$$\int_{\mathbb{R}} e^{\lambda x} F(x) dx = \infty, \ \forall \lambda > 0.$$

Analogously, a probability distribution $F(x)$ is **light-tailed** if and only if

$$\int_{\mathbb{R}} e^{\lambda x} F(x) dx < \infty, \ \text{for some } \lambda > 0.$$

Intuitively, a probability distribution is called *heavy-tailed* if it has a tail that's heavier than an exponential distribution [8]. In other words, a distribution that is heavy-tailed goes to zero slower than one with exponential tails. On the contrary, if a function is *light-tailed*, it goes to zero quicker than one with exponential tails.
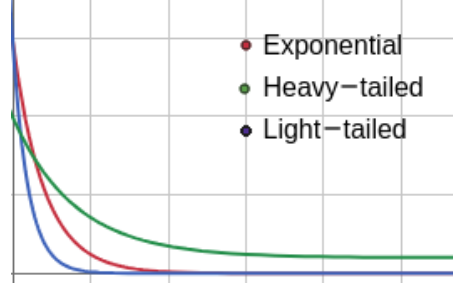
Figure 5: Sketch of a *heavy-tailed* (green) and a *light-tailed* (blue) function with respect to the exponential function (red).

One way of measuring the tail heaviness is computing the tail index [18]. However, for a given impact function, year, region, and pollutant we do not have enough data to obtain reliable estimates. Thus, we proceed as in [23] exploiting a finite sample argument relative to the binomial random behaviour of threshold exceedances.

Specifically, for a given region and pollutant we focus on the sequence of premature deaths, represented by the random variable X_t, where $t = 2020, \dots, 2050$ is the time index. Then, we consider a "high" threshold h given by the 90th percentile obtained from all premature deaths values by region and pollutant available with the NZ data. This threshold value has been chosen since it represents the mortality extremeness. Now, we consider the exceeding probability

$$p = P(X_r > h), \ t = 2020, \dots, 2050.$$

In this way, for each year we have n premature death values, obtained through different carbon budgets and impact functions. For simplicity, it can be assumed that these values are observations generated from the independent random variables $X_t^{(i)}$, $i = 1, 2, \cdots, n$. Since $\mathbb{1}(X_t > h)$ is a Bernoulli random variable, then

$$\sum_{i=1}^{n} \mathbb{1}\left(X_t^{(i)} > h\right) \sim \text{Bin}(n, p),$$

i.e., the number of exceedances on n trials follows a binomial distribution with success probability p. This probability provides an indication of the heaviness of the tail distribution. In particular, as p increases, fatter is the distribution's tail. Although with this procedure we can not obtain a precise indication of the tail heaviness, we do identify the distribution with the heavier tail, which fits exactly our analysis aim.

All in all, we estimate the exceeding probability p by each sample group. Furthermore, applying the exact Pearson-Klopper method we can also estimate the 95% confidence interval for p. This method allows to obtain the binomial confidence interval as follows:

$$p \in (p_L, p_U), \ \text{where}$$

$$p_L = \left\{ p \mid P[\text{Bin}(n; p) \leq x] > \frac{\alpha}{2} \right\} \quad \text{and} \quad p_U = \left\{ p \mid P[\text{Bin}(n; p) \geq x] > \frac{\alpha}{2} \right\},$$

where α is the significance level and $0 \leq x \leq n$ is the number of successes observed in the sample [1].

As will be commented soon, the estimated exceeding probability p is often higher with the EoC data than with the NZ one. Therefore, we consider the binomial test with the following hypothesis:

$$\begin{cases} H_0: & p^{(EoC)} \leq p^{(NZ)}, \\ H_1: & p^{(EoC)} > p^{(NZ)}, \end{cases}$$

where $p^{(EoC)}$ is the exceeding probability of the EoC distribution and $p^{(NZ)}$ is the exceeding probability of the NZ distribution. Once again, we look for empirical evidence to reject the null hypothesis H_0.

The binomial test follows the same idea than the K-S test. However, now the p-value is simply computed with the binomial probability function:

$$p = \sum_{i=0}^{k} P(X \leq i) = \sum_{i=0}^{k} \binom{n}{i} \pi_0^i (1 - \pi_0)^{n-i},$$

where k is the number of successes in the sample of size n, corresponding to $p^{(EoC)}$ in our specific case, and π_0 is the threshold value of the hypothesis, $p^{(NZ)}$ in our procedure [47].

Finally, for the test to be coherent, we need the same amount of NZ and EoC data samples. However, not all models from the ENGAGE database are run with both climate policies for each carbon budget. Therefore, it is necessary to select only the ones that run both climate policies types before computing the test.

4.4 Sensitivity analysis of the impact functions

For the premature death data, we also study the sensitivity of the impact functions parameters and the counterfactual value percentile level, both independently and related.

For this purpose, we consider a graphical visualization of the medians and the confidence interval of each parameter by impact function, carbon budget interval, year, and region. In this way, we can see the uncertainty produced by each factor, as well as their interaction.

4.5 IAMs and impact functions uncertainty

Finally, to assess if either the IAMs or the impact functions produce more uncertainty to the final mortality outcome, probability distributions of the estimated deaths with all impact functions for each IAM and probability distributions of the estimated deaths with all IAMs for each impact functions will be compared.

4.6 Code availability

The reproducible source code used for the data analysis and the figures can be found at `https://github.com/klau506/SensitivityAirPollution.git`.

5. Results

First of all, we will analyse the overall estimated premature deaths. Due to the different sources of uncertainty, we do not expect to have a unique mortality value for each region and scenario. Therefore, after analysing the global mortality results, we will focus on the sources of uncertainty assessing which one contributes the most to the final output.

Since the vast majority of graphs and test visualizations are done by region, among other factors, we generally obtain ten figures per plot (one for region). They can be all found in appendices C, D, E, and F, but in this section, to facilitate a dynamic discourse, only the whole globe graphs and comparison figures are displayed. Nevertheless, the results are discussed considering them all.

Recall that *climate policy* refers to the choice of NZ or EoC long-term policy scenario.

All in all, to commence the analysis of the results, consider figure 6 (and appendix E.3), where the medians of the avoided deaths among all impact functions are displayed by year, carbon budget and climate policy, as well as the 95% CI. To compute them, the premature deaths estimated by the each climate policy are subtracted to the ones estimated by the REF.
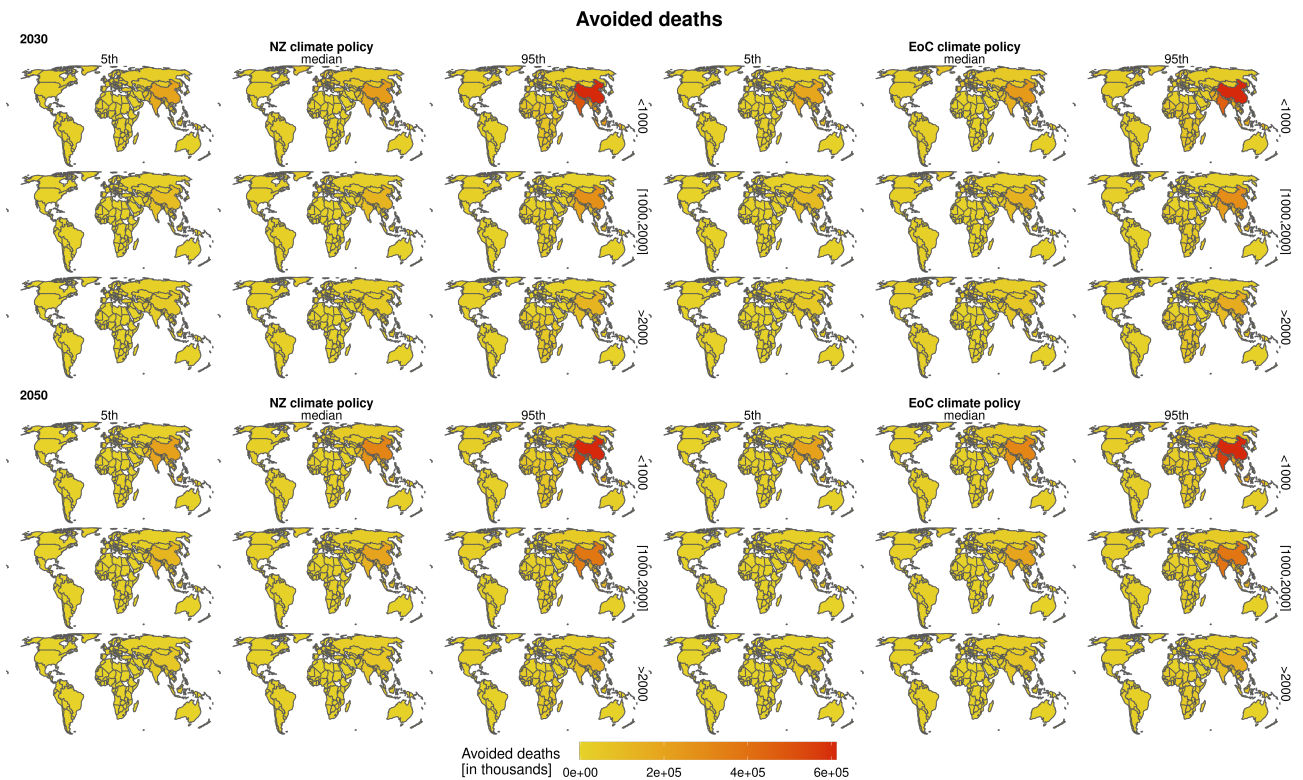
Figure 6: Overall ($PM_{2.5} + O_3$) avoided deaths by region, carbon budget, and climate policy in 2030 and 2050 using the premature deaths median among the projections done by all impact functions. The colors correspond to the median value, and there is also displayed the 95% CI. To compute the avoided deaths, the premature deaths estimated by the each climate policy are subtracted to the ones estimated by the REF.

In general terms, the NZ data determines fewer premature deaths than the EoC data, which in turn estimates fewer fatalities than the REF one. Furthermore, the number of estimated deaths increases directly

with the carbon budget, while the number of avoided deaths has the inverse behavior: is higher for low carbon budgets and lower for high carbon budgets. If the reader wants to directly compare the mortality values, please look at E.3.

At the same time, it can be detected that R10CHINA+ is the region where more premature deaths can be avoided, followed closely by R10INDIA+ and, with a whole order of magnitude behind, by R10REST-ASIA. Recall that these three regions involve some of the most populated countries where millions of people are exposed to very high pollution levels. These regions are also the home to many mid to low-income countries.

These trends continue through time, even though slightly fewer avoided deaths are estimated in mid-century, when in fact fewer premature deaths are forested since the policies should have had more effect and the emissions should have been reduced in both climate policies due to the deployment of air pollution controls.

Regarding the CI, there is a pretty huge range of values. In particular, in some cases, the 95th percentile can even double the median deaths, such as in R10NORTH-AM in 2050 for low carbon budgets. In fact, R10NORTH-AM, R10LATIN-AM, and R10EUROPE are the regions where the upper percentile presents more variability. On the other hand, the 5th percentile is more stable and, at most, decreases a 66% of the median mortality values, such as in R10LATIN-AM in 2050 for low and medium carbon budgets. The regions more affected by the 5th percentile variability are R10LATIN-AM and R10REF-ECON.

With these results in mind, we can start the uncertainty analysis to find out the most important variability sources. It will begin with the emissions' uncertainty assessment. Then, the uncertainty on concentrations will be discussed; and the study will finish with the mortality sensitivity and uncertainty analyses.

5.1 Uncertainty and sensitivity of emissions

In order to study the contribution of the climate policy on the emissions' uncertainty, we start by considering the probability distribution and cumulative frequency graphs. They are done for five pollutants, although for BC and OC the emissions are summed, aiming to understand the general behaviour of carbon emissions since they are both precursors of primary $PM_{2.5}$. In the same line, NO_x and SO_2 are chosen, because they account for secondary $PM_{2.5}$. Finally, also VOC emissions are shown, given that together with NO_x are two of the most important originators of O_3.

The impact of the NZ relative to EoC climate policy is more explicit for low carbon budgets (< 1000), i.e. more stringent climate policies (see figure 7 and appendix C.1). It can be seen that, in this case, the distribution functions have some differences when considering each climate policy. In general, there are lower emissions values in the NZ data than in the EoC data. This behaviour is supported by the cumulative graphs, where the NZ line is almost always the dominant, i.e., it is above or overlapped with the EoC cumulative function, indicating that less the NZ climate policy, lower the emissions of the main air pollutants. This happens because in more stringent climate policies, i.e. with lower carbon budgets, there is less flexibility in the choice of the emitting technologies. In these cases, the IAMs are constrained to make faster technology shifts towards less carbon-intensive technologies, which in turn are also less polluting. With the carbon budget increment, both climate policies become similar and the differences become less visually perceived. Particularly, for medium carbon budgets ($[1000, 2000]$) we can still distinguish some contrast in NO_x and to some extent in SO_2, whereas for very high carbon budgets (> 2000) the probability distributions and the cumulative frequencies between both climate policies are indistinguishable. This suggests that for high carbon budgets the climate policy has no importance.

Emissions probability distribution and cumulative frequency of WORLD
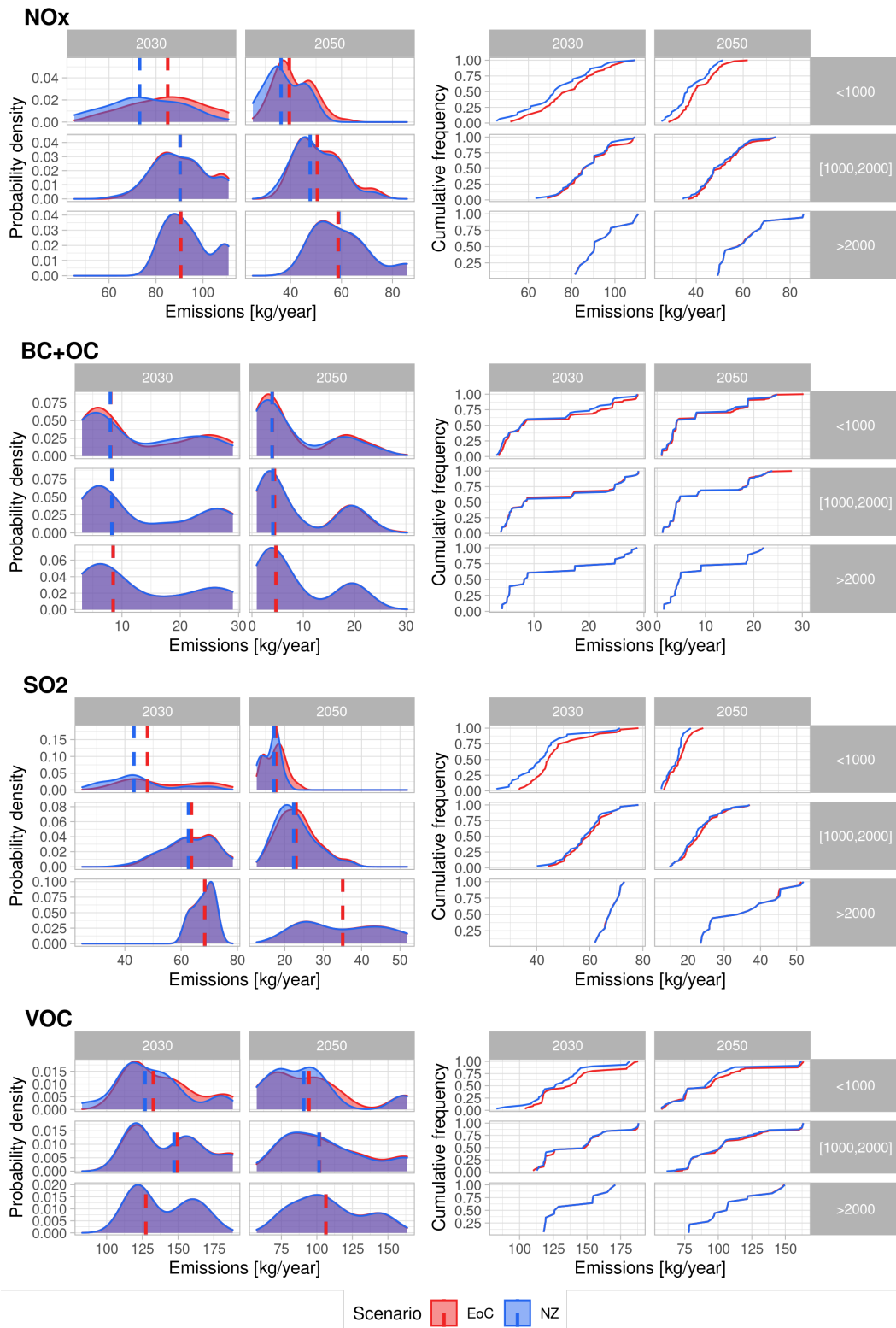
Figure 7: Probability density distribution (left) and cumulative frequency (right) of World's emissions of BC and OC, SO$_2$, NO$_x$, and VOC. Includes median line by climate policy.

Analysing through time, all pollutants perform equally: the differences between climate policies tend to reduce in 2050 for low carbon budgets and to increase for medium carbon budgets. This could be explained by the fact that in low carbon budgets, the strategies of the NZ policies tend to anticipate action towards less polluting fuels and technologies. Therefore, their differences are more appreciable in the early years. On the other hand, for medium carbon budgets, since the climate policies are milder, the mitigation strategies could be taken some years later. As a result, the strategies between the NZ and EoC climate policies start to differ some years later, and so, the difference between them is more appreciable in the middle of the century.

In addition, NO_x and SO_2 show in general more contrast between NZ and EoC than the other pollutants. Recall that they are both precursors of the secondary $PM_{2.5}$ and NO_x is one of the main precursors of secondary O_3. Since O_3 is only formed by secondary pollution, this last pollutant is expected to be more responsive to the climate policy.

Looking close at the shapes of the probability distribution functions, we can detect some similarities between regions. For instance, R10EUROPE 21 and R10NORTH-AM 25 present similar distributions, that are also close to the ones of R10PAC-OECD 26 and R10LATIN-AM 23. We can distinguish as well, another regions-group, established by R10INDIA+ 22, R10REST-ASIA 28, and R10REF-ECON 27.

Finally, observe that for Shipping and aviation 29 the cumulative frequency shows a pronounced step at the 75% of the accumulated frequency. Along the regions, we can find also this cumulative frequency behaviour only for BC and OC, but in a softer way and at higher levels. The other cumulative frequency shapes are more or less linear.

To quantify the differences between NZ and EoC climate policy, the K-S two-samples test is applied (see figure 8). Corroborating the analysis of the probability distribution and cumulative graphs, we see the importance of the climate policy for low carbon budgets in both years and for all regions, while for high carbon budgets all p-values are exactly 1, meaning that with 95% of assurance, the climate policy design does not play any role. This statement is logical, since for low carbon budgets the final amount of CO_2 is highly restricted, which means that global CO_2 emissions must decrease sharply, leading to higher and faster deployment of cleaner technology. However, for high carbon budgets, the restrictions are mild and both climate policies can perform similarly, reducing slowly the amount of CO_2 through the years.

Notice also the differences between pollutants. As expected by the cumulative and distribution graphs, BC and OC together with VOC have higher p-values than NO_x and SO_2. Particularly, only for this last pollutant, the null hypothesis can be rejected in some cases with a 95% of certainty. Specifically, for low carbon budgets in 2030 in R10INDIA+, R10CHINA+, and R10PAC-OECD. This could be explained by the fact that SO_2 emissions are often related to coal use in mid to low-income countries; and when a climate policy is applied, the first fuel that is often phased out, with a high agreement between models, is coal. Moreover, the emissions of BC and OC seem to be much lower in the R10INDIA+ and R10CHINA+, the most reducing regions, than everywhere else.

Furthermore, a tendency between regions throughout the years and the carbon budgets can be seen. For instance, R10INDIA+ and R10CHINA+ have usually the lowest p-value, suggesting that they are the most sensitive regions to the climate policy choice. This may be justified by the fact that air pollution emissions in these regions are very high due to generally poor end-of-pipe (also called control measures) technology deployment. Since the cost of IAMs expects reduction to occur where the marginal abatement cost is lower, these regions often see high emissions reduction in optimal cost-effective models, leading to lower emissions also in air pollution.

Finally, as mentioned before, for medium carbon budgets the climate policy has a higher effect in

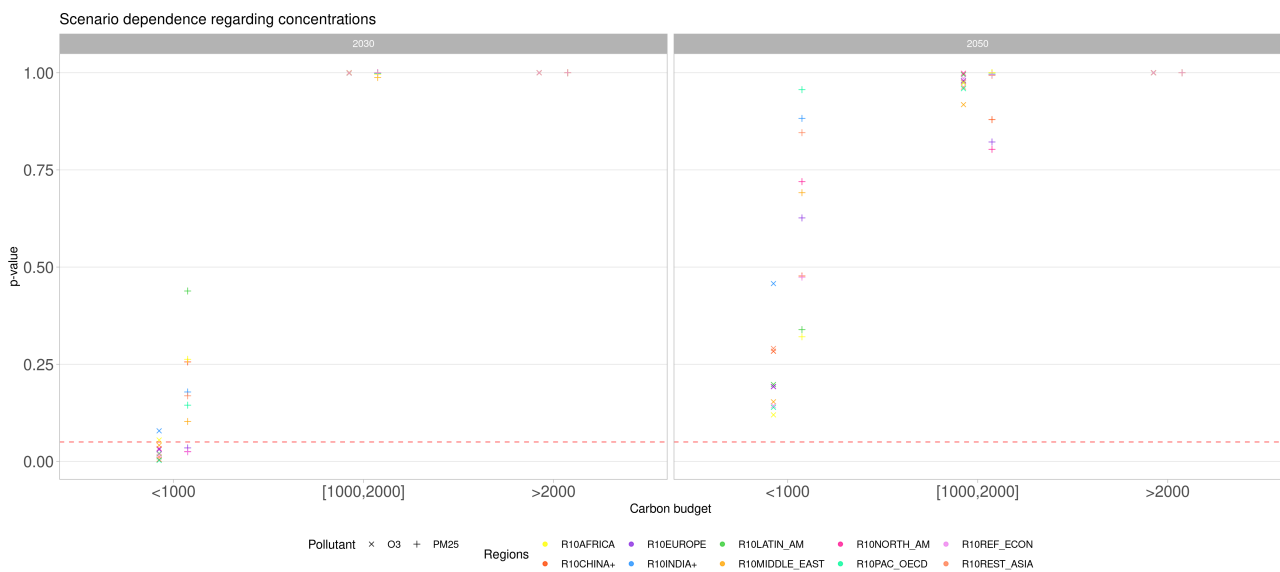mid-century than in 2030, but only in NO_x and SO_2 emissions.
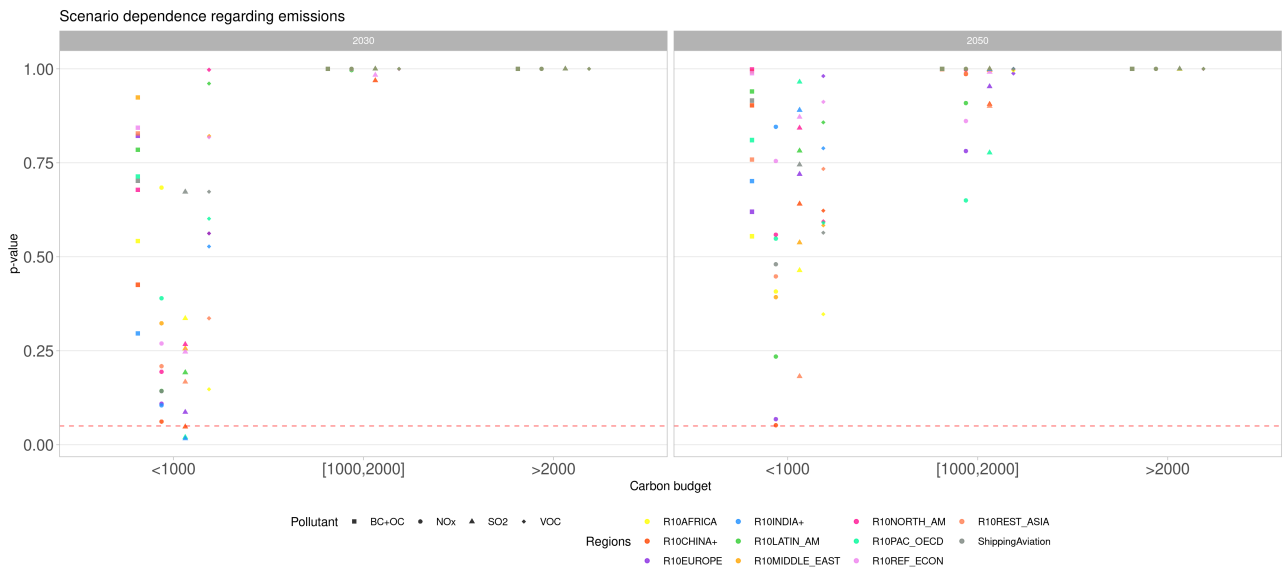
Figure 8: Climate policy dependence by region, year, and carbon budget. On the Y-axis there is the p-value of the K-S two-samples test done separately by pollutant, region, year, and carbon budget. The dashed red line indicates the significance level threshold.

5.2 Uncertainty and sensitivity of concentrations

After running FASST we obtain the $PM_{2.5}$ and O_3 concentrations. As done in the previous section, we start by looking at the probability distribution and cumulative frequency graphs (see figure 9 and appendix D.1).

Once again, as seen in the previous section and found in previous studies [23, 59], more differences can be seen for low carbon budgets, while for high carbon budgets the climate policies are indistinguishable. For both pollutants and low carbon budgets, the NZ climate policy estimates always fewer concentrations, since the distribution plots are more to the left than the EoC ones. It can be also seen through the cumulative frequency graph, where the NZ climate policy line ends sooner.

It seems that for low carbon budgets the climate policies are more distinguishable in 2030, while for medium carbon budgets it happens in 2050, in line with what has been found for emissions. Importantly, the climate policy choice affects differently to both pollutants: although they perform equally along all carbon budgets, the median of the distribution by climate policy is significantly more different regarding O_3; especially for low carbon budgets. As an example, see R10LATIN-AM 34 and R10INDIA+ 33 figures.

Finally, notice the range in the concentrations' values. There are some regions, such as R10PAC-OECD 37 or R10EUROPE 32, where the concentrations' amount is almost constant; especially concerning $PM_{2.5}$. This is due to the fact that these plots account for the regional concentrations' average for each model, scenario, and climate policy. Therefore, the whole data is shrunk and, due to the presence of outliers in some regions, the average is driven by producing similar concentration's values for any given model and scenario. Howbeit, more differences are expected to be seen in the mortality plots, since the premature deaths are computed using the entire concentrations data and account for the population's factor. In this way, if a lot of people live in a certain place on the Earth, the concentration in that point will be considered, whereas if no one lives in a singular place on the planet, the concentration there will not be used to estimate
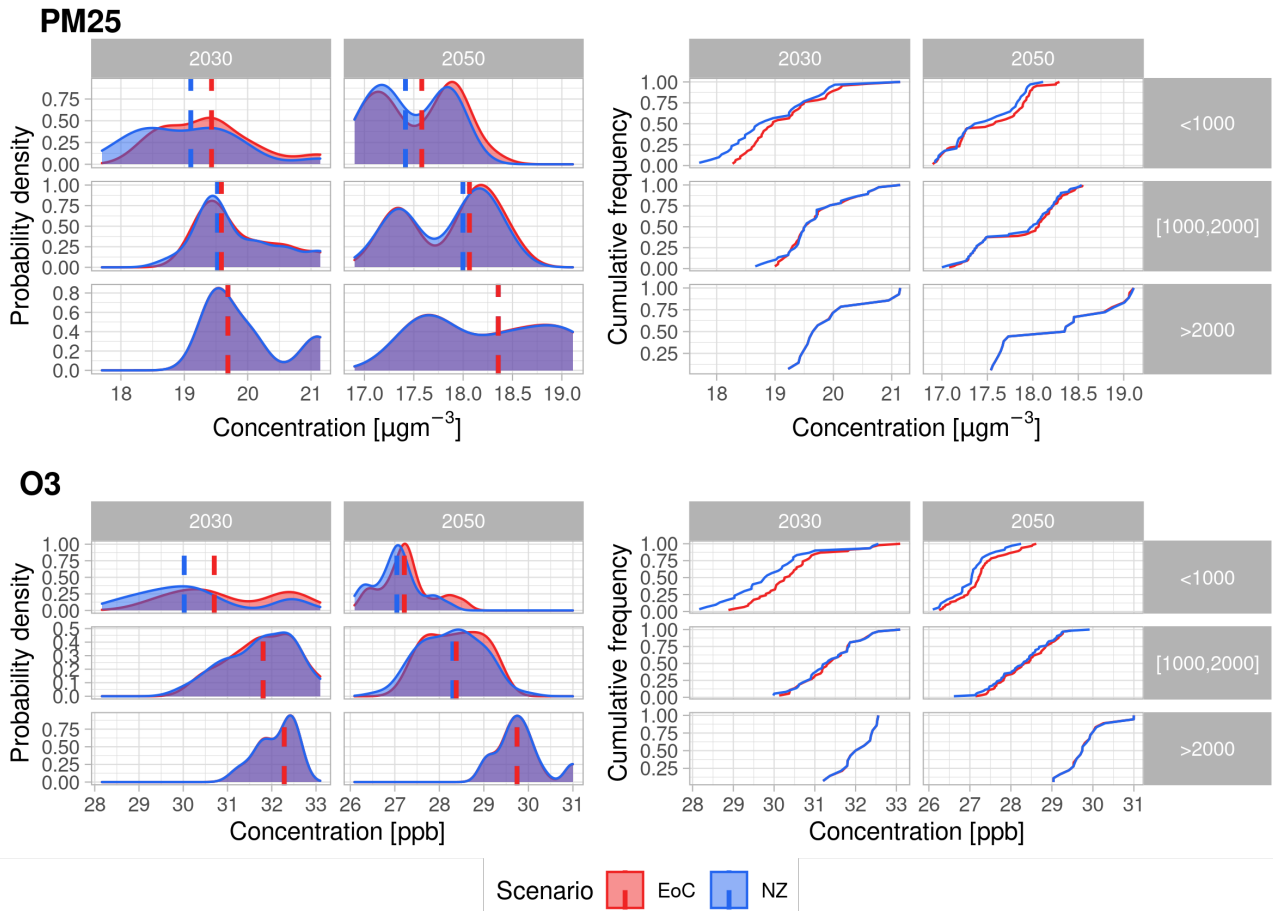
Figure 9: Probability density distribution (left) and cumulative frequency (right) of World's concentrations of $PM_{2.5}$ and O_3. Includes median line by climate policy. Data has been averaged by model and scenario.

premature deaths since no one is exposed to that pollution level.

Nevertheless, to really see the uncertainty produced by the models on the concentrations, the probability distribution and the cumulative frequency graphs have been done, as well, using the complete concentration's data, that is, using each point of the whole globe grid, without computing the average. As appreciated in the figures, (see appendix D.2) the concentration's values use to vary between 0–50 $\mu g \, m^{-3}$ in the case of $PM_{2.5}$, and between 20–60 $\mu g \, m^{-3}$ in the case of O_3. Notice that some regions such as R10EUROPE 42, R10PAC-OECD 47, and R10LATIN-AM 44 present out-of-range values, coinciding with the regions in which its $PM_{2.5}$ concentration's values were almost constant in the previous plots. Moreover, the World figure 50 does not almost change, since in both methods, to depict the whole globe plots, the average values among all the regions are accounted.

As before, we use the K-S two-samples test to quantify the differences between NZ and EoC climate policy on concentrations of both pollutants (see figure 10). Without surprise, we detect that the climate policy choice is far more decisive for low carbon budgets than for high carbon budgets. That is, for stringent carbon policies, a NZ emission pathway will generate more air pollution co-benefits. We also appreciate

that the p-value is exactly 1 for all regions in the highest carbon budget interval. It can also be seen a difference between years: while for low carbon budgets the differences between climate policies decrease with time, for medium carbon budgets increases. However, this decrease is light compared with the increase in low carbon budgets.

On the other hand, for low carbon budgets, the p-value is quite different between pollutants: the climate policy has more impact on O_3 than on $PM_{2.5}$ concentrations. This result was expected since we have already seen that NO_x emissions are very sensitive to the climate policy factor and they are the main precursors of O_3. Hence, they drive the O_3 concentrations to have the same behavior.

Moreover, the p-value among all regions has a shorter range for O_3 than for $PM_{2.5}$. In fact, all regions except R10INDIA+ (whose value is almost at the threshold edge) are below the significance level threshold for O_3 in 2030, which means that with a 95% of confidence, we can assert that the climate policy really makes a difference for this pollutant for low carbon budgets in 2030. Besides, $PM_{2.5}$ concentrations are slightly more dispersed among regions, but it is still clear that the impact of the climate policy is higher in lower years.

As an exception, R10REF-ECON has the $PM_{2.5}$ p-value lower than 0.05 in 2030 for low carbon budgets. Since this region has also the O_3 p-value below the significance level for the same carbon budget interval and year, we can conclude that it is the most sensitive region to the climate policy choice in these circumstances regarding the pollutant concentration.

Figure 10: Climate policy dependence by region, year, and carbon budget. On the Y-axis there is the p-value of the K-S two-samples test done separately by pollutant, region, year, and carbon budget. The dashed red line indicates the significance level threshold.

The uncertainty produced by the climate policy is the same one for emissions than for concentrations (see figure 119 in appendix F): for low carbon budgets the NZ and EoC data are always more different. However, for high carbon budgets both climate policies are equivalent. For medium carbon budgets the differences between climate policies increase with the time, while for low carbon budgets they behave inversely. Importantly, the p-value of $PM_{2.5}$ and O_3 precursors behaves similarly.

5.3 Uncertainty and sensitivity of impact functions

Following the same structure as the previous sections and to see precisely the impact of the climate policy per impact function, the probability distribution and cumulative frequency graphs are considered. Now, however, we display also the 95% confidence interval of the impact functions' parameters (see figures 11, 12 and appendix E.1). Remark that these figures are done considering the median of the counterfactual exposure when there could be uncertainty on it. Once again, we can appreciate more the climate policy impact on low carbon budgets for both pollutants. As already occurred in the emissions and concentrations case, for these carbon budgets the influence of the climate policy diminishes with the years, while for medium carbon budgets increases. For high carbon budgets, both climate policies are indistinguishable. In general, both pollutants show the same premature mortality tendencies per climate policy. However, notice that the number of fatalities due to O_3 is approximately three times the one owing to $PM_{2.5}$.

First of all, notice BURNETT2018 exhibits the same probability distribution and cumulative frequency functions' shape for both groups, and as expected, the group with the Chinese men cohort estimates more mortalities than the group without them. This is due to the fact that this cohort accounts with extreme $PM_{2.5}$ exposure values, and consequently, more deaths are estimated. In the same line, GBD2016 has the same behaviour among its three groups, whose premature death estimated values have the inverse order of their names: LOW, MEDIUM, and HIGH. This is because GBD2016-LOW has the *lowest* counterfactual value, meaning that health impacts start to be felt by humans at lower concentrations; therefore, more people will suffer from exposure to $PM_{2.5}$ than in GBD2016-HIGH, where the counterfactual value is higher. All values are detailed in Table 3.

Depending on the region, we can find different trends. Nevertheless, the OSTRO2004 impact function estimates always the highest or the second-highest number of premature deaths. For instance, in R10AFRICA 51 and R10EUROPE 53. In some cases, it is KREWSKI2009, such as in R10INDIA+ 54 and R10MIDDLE-EAST 56, while in R10NORTH-AM 57, R10LATIN-AM 55, and R10REF-ECON 59 is BURNETT2018-WITH that shows the largest numbers.

The probability distribution shape depends also on the region. On the one hand, some regions show the same trend throughout both years, all impact functions, and all carbon budgets; but some others present similar distributions in 2030 which then flatters in 2050, notably for medium and high carbon budgets. As an example, see the graphs of R10AFRICA 51 and R10LATIN-AM 55 for the first behaviour, and R10EUROPE 53 and R10INDIA+ 54 for the second one. However, each region has particularities.

Notice that the behavior of mortalities per region is different from the one previously observed in emissions and concentrations, suggesting that the impact functions play a very important role.

In the case of O_3, all regions except for R10CHINA+ 62, R10INDIA+ 64 and R10REST-ASIA 70 present the same distribution probability trend: a pronounced peak for both impact functions for all years and carbon budgets, that is clearly flattered for low carbon budgets in 2030. Whereas in the case of the three mentioned regions, the distribution is slightly more homogeneous along with the estimated premature deaths. This could be due to the very non-linear behaviour of O_3 which is a secondary photochemical pollutant.

It might seem that the differences between impact functions are larger in O_3 than in $PM_{2.5}$. However, the scales of both graphs are different, and in fact, among all the $PM_{2.5}$ impact functions, the maximum difference between the medians of premature deaths per climate policy is approximately 1×10^6.

Regarding the cumulative plot of $PM_{2.5}$, we can appreciate that in some regions such as R10CHINA+ 52 and R10REST-ASIA 60, the cumulative frequency function increases linearly with the accumulated premature deaths. On the other hand, regions such as R10NORTH-AM 57 and R10EUROPE 53 present a
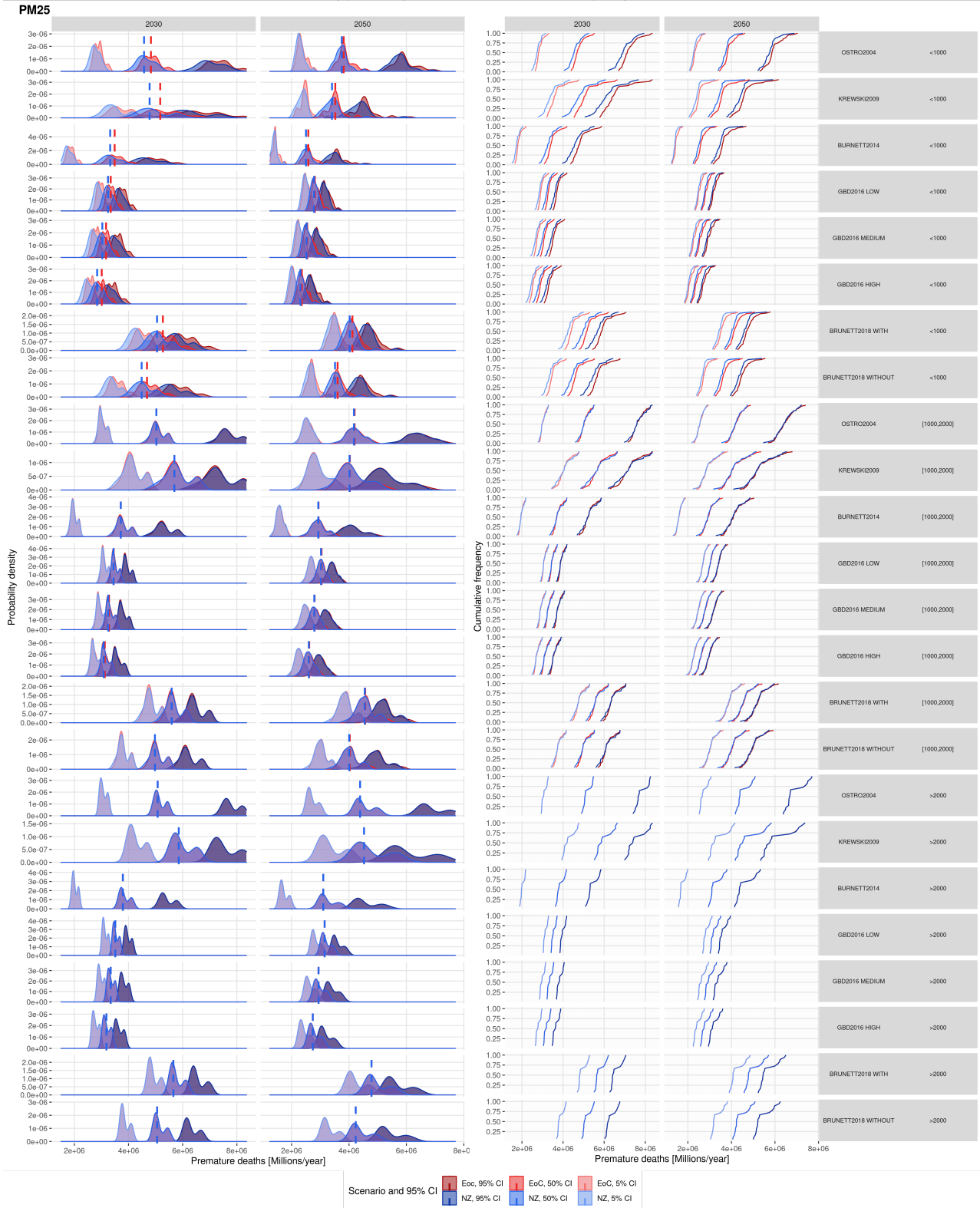
Figure 11: Probability density distribution (left) and cumulative frequency (right) of the whole globe for premature deaths due to PM$_{2.5}$. Includes line of the median by climate policy as well as 95% confidence interval of the impact function's parameter percentile. Impact functions ordered by publication's year.

noticeable step on the 50-60% of the accumulated frequencies, while R10LATIN-AM 55 and R10MIDDLE-EAST 56 do it on the 75%.
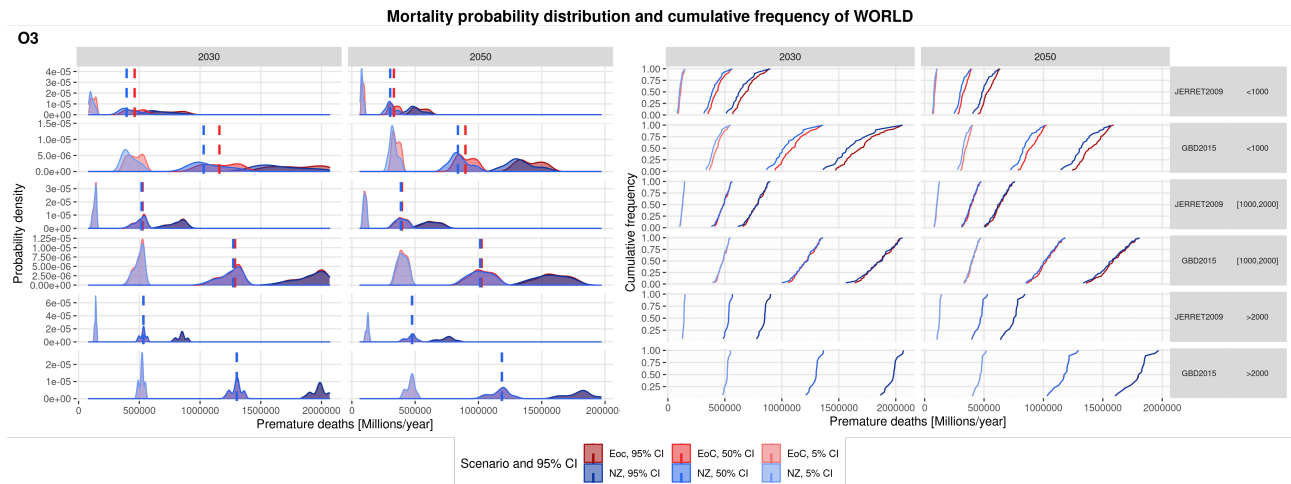
Figure 12: Probability density distribution (left) and cumulative frequency (right) of the whole globe for premature deaths due to O_3. Includes line of the median by climate policy as well as 95% confidence interval. Impact functions ordered by publication's year.

On the other hand, the cumulative frequency plots concerning O_3 are always linear. Notice that the 5th percentile line is almost straight in all regions, while the 95th percentile cumulative frequency function has a softer slope, indicating that for the former percentile less mortality uncertainty is expected than for the last one.

Studying the uncertainty given by the parameters of the impact functions, we can observe that, in the case of $PM_{2.5}$, OSTRO2004 has a wider range in all regions. However, in some of them, such as R10INDIA+ 54, R10LATIN-AM 55, and R10REST-ASIA 60, is homogeneous and in some others, for instance in R10EUROPE 53 and R10PAC-OECD 58, is especially pronounced for the 95th percentile, which can even increase 45% the value of the premature death. On the other hand, GBD2016 has the lowest uncertainty, with usually a difference of 10% on the expected mortality. Notice, that BURNETT2018-WITHOUT has a larger uncertainty than BURNETT2018-WITH. In fact, either BURNETT2018-WITHOUT or KREWSKI2009 present the second larger uncertainty for $PM_{2.5}$ impact functions.

In the case of O_3, GBD2015 has clearly the highest uncertainty, with approximately a difference of 60% with respect to the median. Besides, notice that for both pollutants, we can detect fewer differences among the climate policy in the cumulative frequency graphs when using the 5th percentile of the impact functions parameters' values.

Now is the moment to quantify the climate policy differences through the K-S two-samples test (see figure 13). The first point that should be seen is the similarities of p-values for each impact function among all regions. This fact indicates that, although the number of estimated premature deaths differs from one impact function to another one, the impact of the climate policy remains. Particularly, it is more significant for low carbon budgets and it has no effect for high carbon budgets, with a 95% of assurance. As already seen in figures 8 and 10, the climate policy role diminishes with time for low carbon budgets and increases for medium carbon budgets.

Notice the difference between both pollutants. On the one hand, O_3 is far more sensitive to the climate

policy choice since its p-values are lower than the PM$_{2.5}$ ones. Especially, in 2030 we can assert that the climate policy choice is crucial on the mortalities due to O$_3$. Also in this case, observe that all regions behave equally. On the other hand, in 2050 the impact of the climate policy on O$_3$ premature deaths presents more differences between the regions, although R10MIDDLE-EAST is still the region where it does affect less.

In the case of PM$_{2.5}$, we can appreciate that the p-values range is larger, and so, each region will be affected differently by the climate policy design. For instance, R10INDIA+ is the most responsive in 2030, while in 2050 is R10AFRICA.

It is worth mentioning that all these trends have already been seen in the concentrations figure 10, where O$_3$ had lower p-values. However, now we can precise that R10CHINA+, R10INDIA+, R10MIDDLE-EAST, R10AFRICA, and R10EUROPE are the regions more sensitive to the climate policy choice; meaning that, in these regions, more deaths can be avoided using the NZ climate policy design instead of the EoC one.
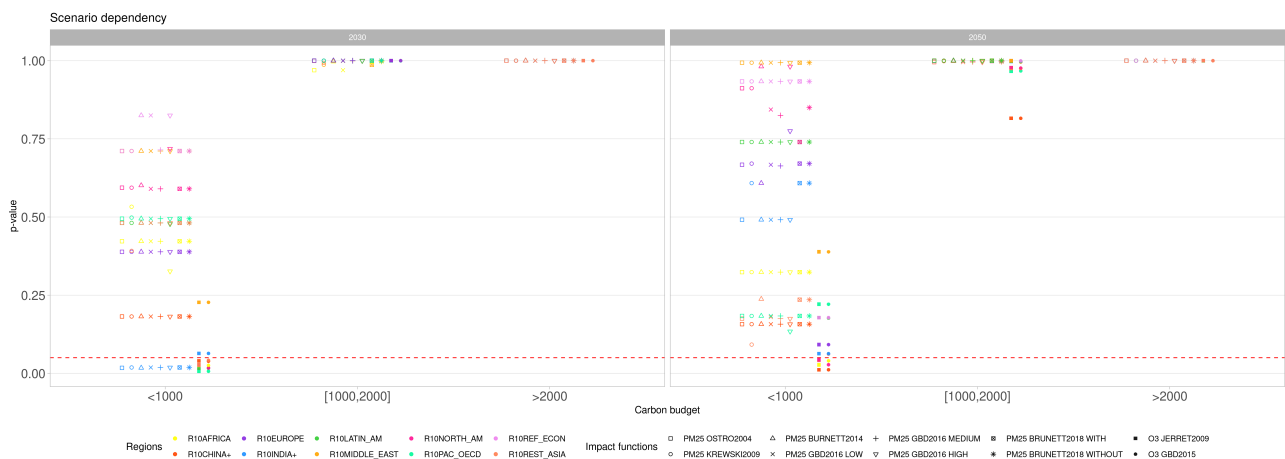
Figure 13: Climate policy dependence by region, year, and carbon budget. On the Y-axis there is the p-value of the K-S two-samples test done separately by pollutant, region, year, and carbon budget. The dashed red line indicates the significance level threshold.

To comprehend better the sensitivity of each impact function and the differences along with their confidence intervals, we consider another figure, where the counterfactual level is still fixed to its median value when uncertainty on it exists (see fig. 14 and appendix E.4). Undeniably, the climate policy is far more distinguishable for low carbon budgets, especially in 2030. Notice, as well, that for medium carbon budgets the median per climate policy is slightly more different in 2050 than in the previous years.

Regarding the differences between pollutants, notice that O$_3$ has almost no uncertainty range related to the parameter percentile, while for PM$_{2.5}$ there is. Remark that there is more uncertainty between the percentile for high carbon budgets and less uncertainty for low carbon budgets. This means that as higher the stringency of the carbon policy is, lower the risk of outliers in terms of air pollution mortality will be.

We can also distinguish that OSTRO2004 presents the higher uncertainty in all regions, but in R10CHINA+ 84, R10INDIA+ 86, R10MIDDLE-EAST 88, and R10REST-ASIA 92 the impact function KREWSKI2009 presents a higher uncertainty range within each percentile, that is, once the percentile is fixed, the error bar is the largest. Moreover, for these four regions, the uncertainty range within each percentile in PM$_{2.5}$ is much lower than in the other regions. On the contrary, they present a larger uncertainty range per percentile regarding O$_3$.

Exactly these four regions behave equally with respect to GBD2016, presenting a slightly more uncertainty range for each percentile than the other regions. Furthermore, this impact function shows the smallest uncertainty to the parameter percentile, which was expected owing to the steady behavior already seen in the cumulative frequency and probability distribution graphs.

Studying more in deep the role of the climate policy linked to the parameter percentile effect, we can detect that the general trend of the climate policy influence remains equal through years and carbon budget intervals, estimating less mortality in the NZ case. However, the climate policy's importance increases when dealing with the 95th parameter percentile, and on the contrary, its effect decreases when considering the 5th parameter percentile. Moreover, the uncertainty once the percentile is fixed, is clearly lower when dealing with the 5th percentile. Therefore, the combination of NZ climate policy together with the 5th impact function's parameter percentile reduce extreme mortality outcomes and this is robust across most impact functions.

Finally, we can distinguish two different ways of uncertainty with respect to each impact function's parameter percentile. On the one hand, there are some regions where the effect is almost homogeneous, meaning that for each percentile the median drifts the same amount and the uncertainty range within each percentile remains almost equal. On the other hand, in some other regions, the variations in the mortality outcomes are unequal and depend on the impact function's parameters percentile. In particular, they present larger drifts for the median in the 95th percentile, as well as more uncertainty range within the percentile in this case. Precisely, this happens in R10EUROPE 85, R10NORTH-AM 89, and R10PAC-OECD 90. Notice that these are the regions accounting with more high-income countries and lower pollutants concentrations. All in all, it should be mentioned that the uncertainty range for percentile increases somehow with the percentile itself.

Recall that two impact functions have as counterfactual value the minimum plausible exposure. However, for the other impact functions, the counterfactual is an exogenous parameter. Consequently, a sensitivity analysis has been performed to detect the influence of this choice and to analyse if there is any change in the climate policy influence on it. To do so, the confidence interval of the parameters of the impact functions is set to the median.

In both O_3 impact functions it has been considered 33.3 ppb as the 5th counterfactual percentile, 37.6 ppb as the median, that since we are accounting with a uniform distribution it coincides with the mean, and 41.9 ppb for the 95th percentile. In the case of $PM_{2.5}$ impact functions, except for GBD2016, the considered values are $2.4\,\mu g\,m^{-3}$ for the 5th percentile, $4.15\,\mu g\,m^{-3}$ for the median (that again coincides with the mean), and $5.9\,\mu g\,m^{-3}$ for the 95th percentile. In the particular case of GBD2016, which accounts for three groups divided precisely by counterfactual value, we took directly the values of each group: $3.00\,\mu g\,m^{-3}$ CI 95%(2.92,3.05) for the LOW, $4.18\,\mu g\,m^{-3}$ CI 95% (4.17,4.21) for the MEDIUM, and $5.29\,\mu g\,m^{-3}$ CI 95%(5.27,5.31) for the HIGH group.

Analysing the graph (see figure 15 and appendix E.5), it is very clear that for GBD2016 the counterfactual percentile has no effect. This was an expected result since each counterfactual interval is so tiny that can not divert the results. Once again, OSTRO2004 is the most responsive impact function to the parameters' choice, followed by KREWSKI2009 which has sometimes the largest uncertainty range within each percentile. Precisely, this occurs in the same regions that already happened for the impact functions' parameter percentile uncertainty. In the case of $PM_{2.5}$ (excluding GBD2016 impact function), for the high-income regions mentioned before, notice the difference in the uncertainty range: for the 5th percentile, we have more premature deaths uncertainty than for the 95th percentile. Moreover, for these regions the climate policy has more impact when considering the 5th percentile, that is, the effects of the climate
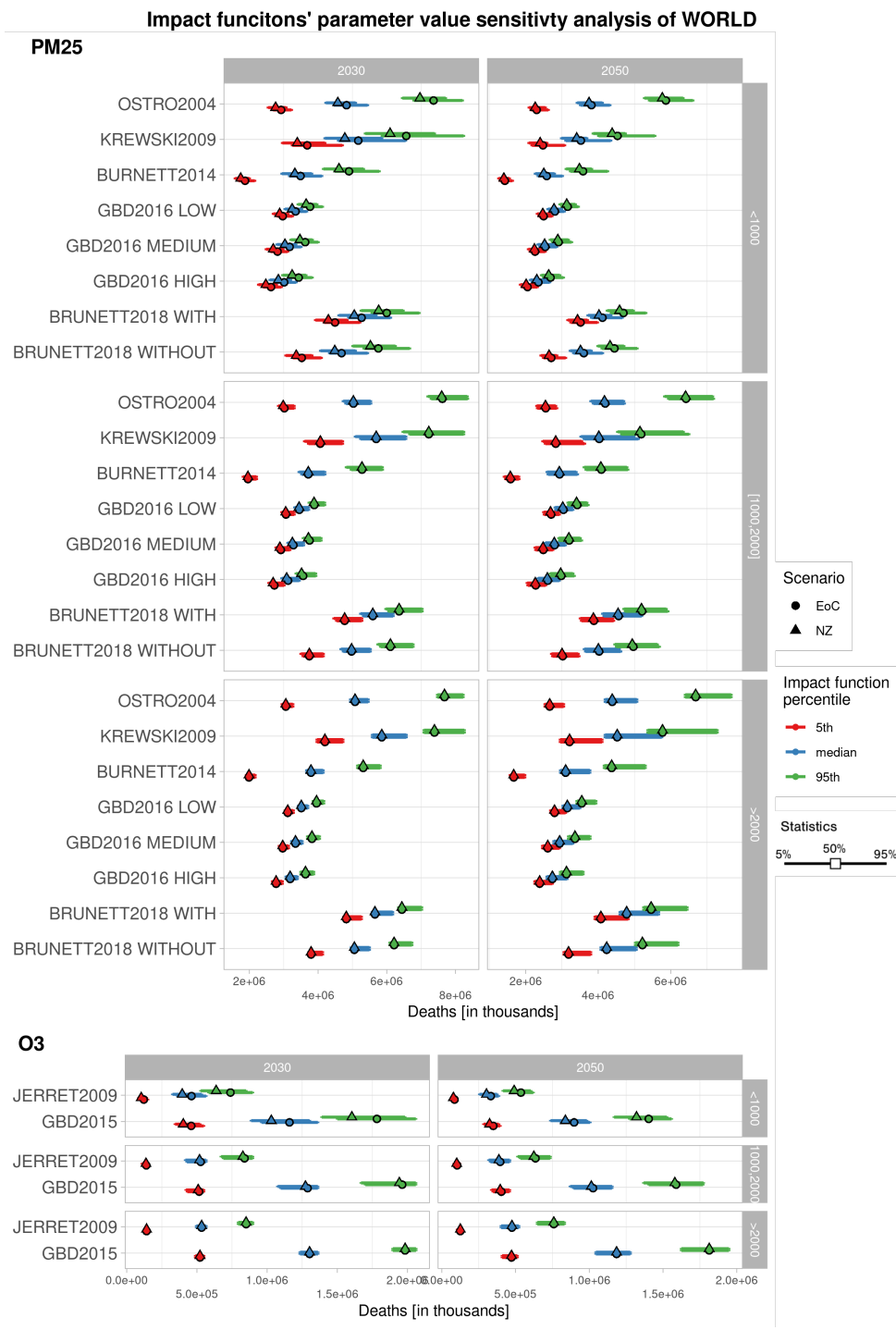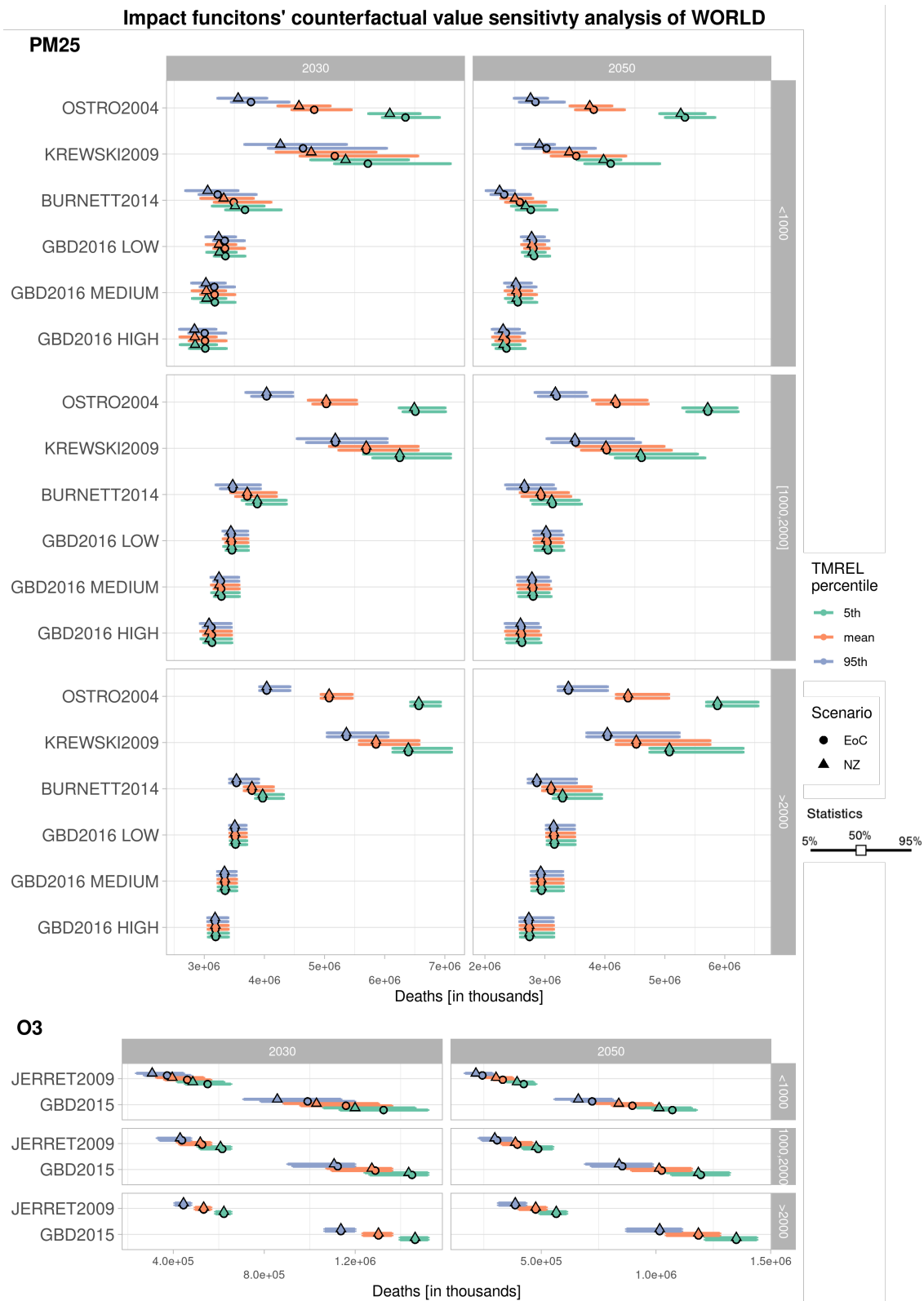
Figure 14: Influence of the impact function percentile on the estimation of premature deaths, regarding impact function, carbon budget, year, and climate policy in the whole globe. Each error bars report the uncertainty range (5-95%) across parameters' sets. The middle points represent the median of the impact function RR median. Colours represent the impact functions' parameter percentile. Impact functions are ranked according to their publication date. Parameters of the impact functions are reported in Table 3.

policy are more significant when the health impacts start to be felt by humans at lower concentrations, therefore more people are suffering from exposure. In the other regions, the climate policy is not affected by the uncertainty on the counterfactual level.

Besides, in the O_3 case, there are no differences in the climate policy on the counterfactual levels' percentile; but, it can be seen the reduction of the uncertainty range per percentile while increasing the carbon budget interval.

For the rest of the regions, we can see that the medians shift the same amount for both counterfactual percentiles, in conjunction with the maintenance of the uncertainty range within percentiles. In fact, the overall changes produced by the counterfactual uncertainty are far more uniform across both percentiles in all regions than the differences owing to the impact function's parameter percentiles. R10NORTH-AM 99 is the region which still presents more differences.

In this case, any impact function has a null uncertainty range for any percentile, i.e., once the counterfactual percentile is fixed, the 95% CI of mortalities is never negligible. However, R10CHINA+ 94, R10INDIA+ 96, R10MIDDLE-EAST 98, and R10REST-ASIA 102 show smaller uncertainty range per percentile in GBD2016 and higher uncertainty range for both O_3 impact functions than the other regions. Notice that they coincide with the four regions that presented no uncertainty range within percentiles in GBD2016 on the impact function's parameter percentile analysis.

As already observed, for high carbon budgets the climate policy does not play any role. In 2030, the climate policy is still more significant for low carbon budgets, and for middle carbon budgets, it is more important in 2050. Notice also that in the 5th percentile, the climate policy impact is slightly higher than in the 95th percentile.

To conclude the sensitivity analysis, we analyse the effect of both the impact function's parameter percentile and the counterfactual percentile altogether (see 16 and appendix E.6). It is worth mentioning the inverse behaviour of both uncertainties. On the one hand, when the counterfactual percentile increases, fewer premature deaths are estimated. On the other hand, when the parameter percentile increases, more fatalities are foreseen.

As an example, consider the GBD2016 impact function. We have already seen the uncertainty produced by the counterfactual value, which is almost null, and the uncertainty produced by the impact function's parameters, which is low but distinguishable. In this new summarizing figure 16 we can appreciate exactly this performance: there exists no difference in the mortality values if the impact function's parameter percentile is fixed, but it does exist when the counterfactual percentile is fixed.

In general, the counterfactual percentile has less effect on the 5th parameter percentile than on the 95th parameter percentile. For all regions is OSTRO2004 the impact function that commonly has a larger uncertainty among both percentiles, followed closely by KREWSKI2009, which can even have more uncertainty range within percentiles.

Analysing the relation between both uncertainties, we can determine that there are two different trends throughout the regions. On the one hand, in R10EUROPE, R10NORTH-AM, and R10PAC-OECD (the already identified as regions with the vast majority of high-income countries) together with R10LATIN-AM and R10REF-ECON, the parameter percentile produces a larger uncertainty than the counterfactual value percentile. In the other regions, the behaviour is the inverse.

At this point, it is the moment to study the tail heaviness between both NZ and EoC climate policy. To do so, we fix the impact function's parameters and counterfactual percentile to the median. Importantly

Figure 15: Influence of the counterfactual percentile on the estimation of premature deaths, regarding impact function, carbon budget, year, and climate policy in the whole globe. Each error bars report the uncertainty range (5-95%) across parameters' sets. The middle points represent the median of the impact function RR median. Colours represent the impact functions' parameter percentile. Impact functions are ranked according to their publication date. Parameters of the impact functions are reported in Table 3.
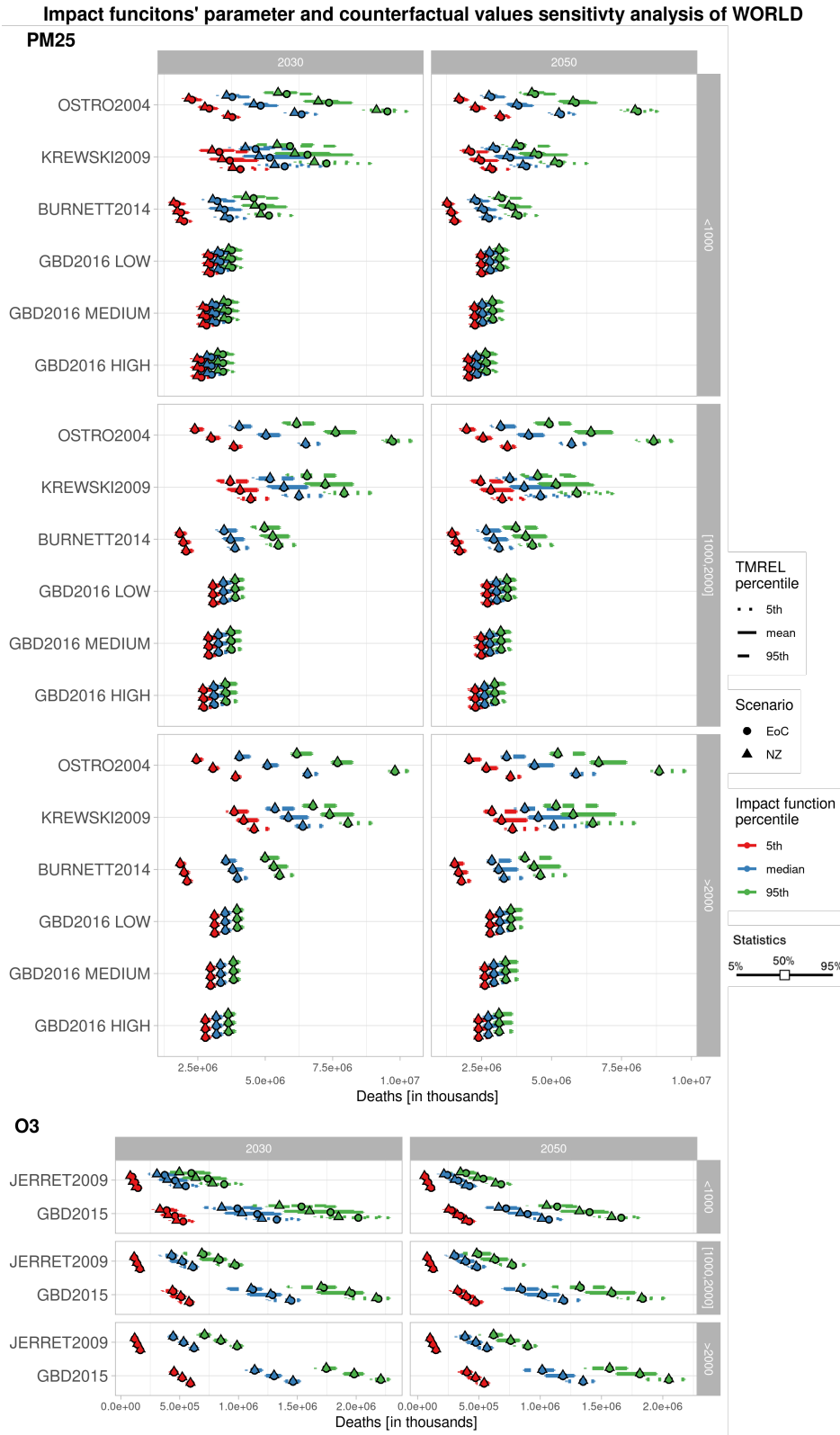
Figure 16: Influence of the relation between the impact function percentile and the counterfactual percentile on the estimation of premature deaths, regarding impact function, carbon budget, year, and climate policy in the whole globe. Each error bars report the uncertainty range (5-95%) across parameters' sets. The middle points represent the median of the impact function RR median. Colours represent the impact functions' parameter percentile. Impact functions are ranked according to their publication date. Parameters of the impact functions are reported in Table 3.

(see figure 17 and appendix E.2), in 2050 the heavy tail probability along all regions and impact functions is lower than in the previous years. Notice also the increasing tendency of the exceeding probability along with the carbon budgets.

Regarding the difference between NZ and EoC climate policy, it can be seen that it is small. Both exceeding probabilities are almost equal in all cases, and when not, the EoC climate policy is slightly higher nearly everywhere. This suggests that the impact of the tail is higher in the EoC climate policy; which is in accordance with the recently commented effect of the NZ climate policy behavior, which reduces the probability of long tails.

Analysing in-depth the differences between impact functions, notice that some of them do not present heavy tails probability in any region or carbon budget. These are GBD2016-HIGH, GBD2016-MEDIUM, and BURNETT2014 for $PM_{2.5}$, and JERRET2009 for O_3. In all these cases, the confidence interval is below the 25%, but it coincides between climate policies. Therefore, it can be stated that these impact functions are robust for both NZ and EoC climate policies.

Besides, BURNETT2018-WITH tends to have a longer tail than BURNETT2018-WITHOUT, which is in accordance with their used data. Recall that BURNETT2018-WITH accounts with an extreme Chinese men cohort; thus, the quantity of outliers is expected to be higher. It is interesting to see that along all regions, BURNETT2018-WITH exhibits the longer tail, sometimes tied with other impact functions, but in R10AFRICA 71 it has no heavy tail at all.

On the other hand, R10EUROPE 73, R10NORTH-AM 77, and R10PAC-OCED 78, again the three regions home to the major part of high-income regions, have shorter tails. Especially low are the probabilities of exceedance in OSTRO2004, KREWSKI2009, and GBD2016-LOW. For the other regions, OSTRO2004 and KREWSKI2009 tend to perform equally, sometimes having one longer tail than the other, but no pattern can be distinguished.

Finally, the long tail in GBD2015 clearly increases with the carbon budget group and is almost identical throughout all regions.

Last but not least, we are ready to assert if either the impact functions or the IAMs produce more uncertainty. With this goal in mind, the distribution probabilities accounting for all impact functions for each IAM are compared with the distribution probabilities of all IAMs for each impact function (see figure 18, and appendix E.7). Since we already know that almost no difference is expected for medium and high carbon budgets, only the low carbon budgets are displayed in the figure.

It can be seen that the probability distributions for each IAM have a prominent peak, meaning that for any impact function used, the premature deaths are highly expected in a short range of values. Notice that the peak is higher in mid-century, implying that the most probable range of mortality values shrinks for later years. However, notice that the mortality values themselves slightly decrease across years, in accordance with figure 6.

This same trend can be appreciated when considering the probability distribution among all the IAMs considering all impact functions. Therefore, the accuracy of the method to estimate the concentrations improves for further years.

Besides, the probability distribution for the different impact functions is generally more uniform and flatter than for the IAMs, resulting in more uncertainty on the mortality in the former case. Moreover, whereas the peak of the probability distribution by each IAMs lays almost on the same value for all of them, the most probable mortality values by the different impact functions change considerably between them.

All in all, the impact functions produce more mortality uncertainty than the IAMs. Moreover, this
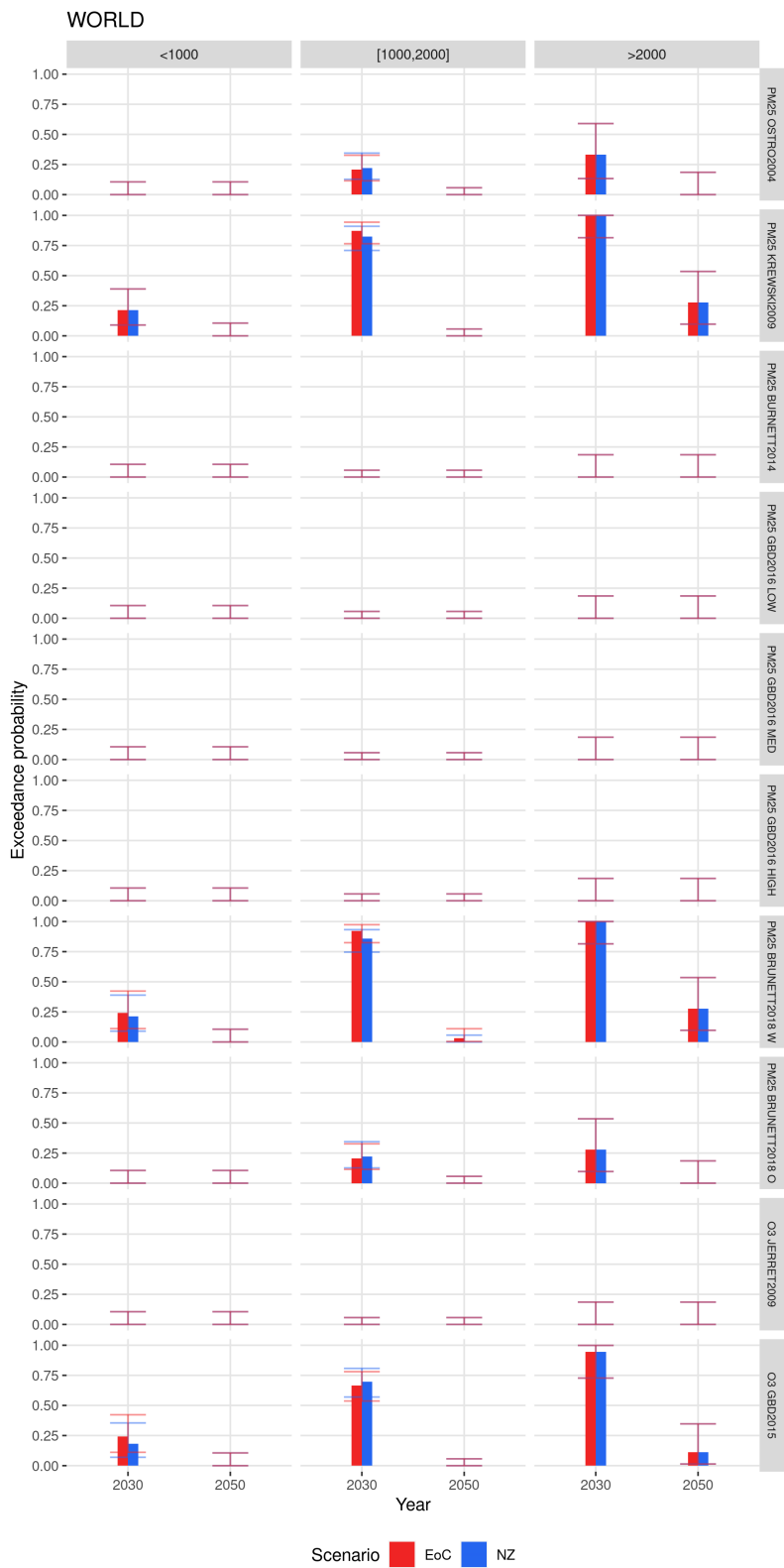
Figure 17: Exceedance probability for NZ and EoC climate policy in the whole globe with 95% CI..

is not only true for the final premature death values, but it also holds for the uncertainty linked to the climate policy, which is higher for impact functions than for IAMs. As a consequence, to have better health co-benefits estimations, regardless of the scenario and climate policy, the impact functions should be improved further.

As a note, observe that these last figures verify that OSTRO2004 is the $PM_{2.5}$ impact function with more uncertainty associated, with extreme cases such as R10AFRICA 113; whereas GBD2015 is the O_3 impact function with more uncertainty related, especially in R10LATIN-AM 115b.
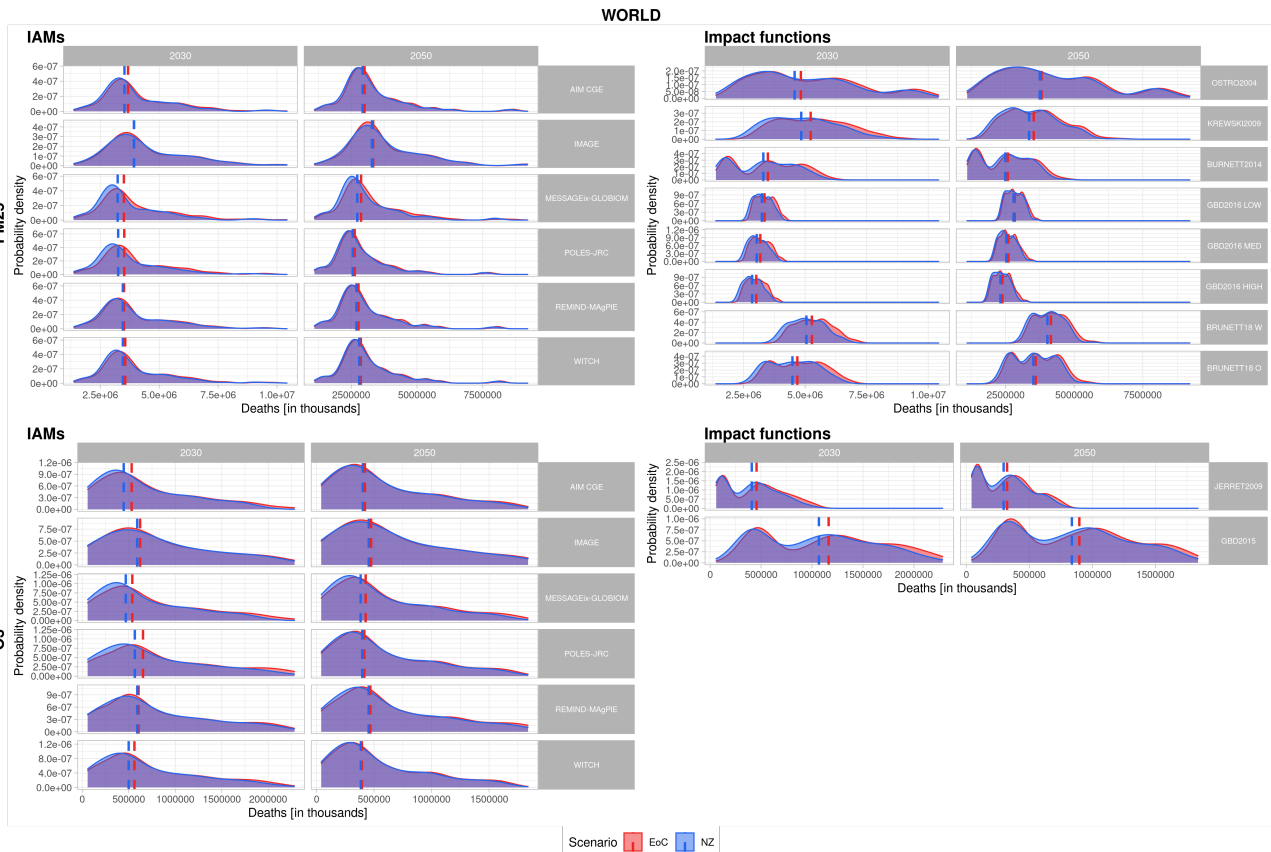
Figure 18: $PM_{2.5}$ probability distribution functions split by IAMs (left) and impact function (right), by year, carbon budget, and climate policy of the whole globe.

6. Conclusion

After this detailed analysis, it is possible to extract some general results regarding the NZ and EoC climate policy importance on different pollutants, carbon budgets, years, and regions; as well as about the uncertainty given by the impact functions parameters and counterfactual value, linked as well to the climate policy choice. Recall that while NZ solely relies on the resulting budget in 2100, the EoC climate policy constrains world emissions to stay at net-zero not allowing the world to go net negative at any moment.

On the one hand, we can conclude that the climate policy choice have more impact in low carbon budgets, than in medium carbon budgets, and almost no impact in high carbon budgets. This means that, when the aim is to limit the temperature increase to $1.5°$C, the strategies followed by both climate policies are definitely independent, while when accounting for more than $2°$C increase, both climate policies perform equally. Therefore, the more stringent the scenario is, the more sensitive the health impacts to the climate policy are. Moreover, it has been noticed that for higher carbon budgets more mortality is expected. We find that it is the combination of both NZ climate policy and stringent scenario that leads to the maximum air pollution health co-benefits.

It has been seen that the impact of the climate policy is larger for O_3. Therefore, when applying the NZ climate policy, the levels of $PM_{2.5}$ are not expected to reduce as drastically as the concentrations of O_3. This is due to the fact that the precursors of secondary pollution are the most affected by the climate policy compared with the emissions of primary pollution. Because O_3 is only constituted by secondary pollution, whereas $PM_{2.5}$ is composed both of a primary and a secondary part, the former is more affected. Besides, the climate policy choice is more important in early years for low carbon budgets, and in mid-century for medium carbon budgets. As already mentioned, this is plausible since with low carbon budgets the strategies of the NZ policies are prone to apply early measures to move towards less polluting fuels and technologies. Consequently, the differences between NZ and EoC are more appreciable in the early years. On the other hand, for medium carbon budgets, the strategies between the climate policies start to differ some years later, and so, the difference between them is more appreciable in the middle of the century.

Nevertheless, the impact of the climate policy does not only influence the emissions data and the estimated concentrations, as already mentioned, but it also affects the health of the population. But in this last point, the impact functions are required and they certainly add uncertainty to the measurements. All impact functions are based on parameters, that are estimated differently throughout the literature and the different kinds of impact functions. Moreover, some of them have also an exogenous counterfactual value. It has been detected that the climate policy has rather more impact when using the 95th percentile of the impact function's parameters. Therefore, under these circumstances, the premature deaths estimated with NZ and EoC data differ more.

Not all impact functions have the same uncertainties. In fact, the oldest impact functions for $PM_{2.5}$ have wider uncertainty ranges (OSTRO2004 and KREWSKI2009), as well as the impact functions whose parameters have been estimated using more heterogeneous cohorts (BURNETT2018-WITH). On the other hand, for O_3, JERRET2009 has less uncertainty than GBD2015.

Precisely the impact functions with more related uncertainty are the ones with larger tails; thus, with more probability of nasty mortality outcomes. The probability of having outliers is slightly higher in the EoC data, but the difference is almost negligible. However, the tails increase with the carbon budget interval, which suggests that there is more variability in high carbon budgets. This is reasonable, since when the temperature rise is less constrained, the ways of achieving the targets enhance and the efforts required diminish. Consequently, both climate policies apply mild mitigation measures in tardy years and

less premature deaths can be avoided.

Two groups can be established by analysing the uncertainty of the impact functions throughout the ten regions. For R10EUROPE, R10NORTH-AM, R10PAC-OECD, R10LATIN-AM, and R10MIDDLE-EAST the parameters of the impact functions add more uncertainty than the counterfactual value. On the other hand, for the other regions (R10CHINA+, R10INDIA+, R10AFRICA, R10REST-ASIA, and R10REF-ECON), it is the counterfactual value that introduces more uncertainty to the premature deaths. Notice the difference of income per capita on both groups: while the former is composed mainly of mid to high-income countries, the latter accounts generally for mid to low-income countries.

According to the willingness to improve the health predictions, it can be stated that more efforts should be made on the refinement of the impact functions rather than in the IAMs, given that the first ones are responsible of the largest uncertainty.

On the whole, the NZ climate policy always estimates less than or the same amount of premature deaths than the EoC climate policy, meaning that it has significantly more co-benefits for air pollution. The climate policy choice is decisive when cutting the temperature rise to $1.5°C$, while it has no effect when the temperature rise is higher than $2°C$, implying that the more stringent the policy is, more crucial is the choice between climate policies. Moreover, the NZ climate policy diminishes the probability of extreme mortality outcomes, resulting in more robust predictions. For O_3, the climate policy has more impact than for $PM_{2.5}$, and the uncertainty of the impact functions for this pollutant barely changes the climate policy significance. Besides, the counterfactual value uncertainty is higher in Asia and Africa, while the impact function's parameter uncertainty is more notorious in Europe, America and Oceania, suggesting that R10CHINA+, R10INDIA+, R10AFRICA, R10REST-ASIA, and R10REF-ECON are the regions more at risk and that would benefit the most of the NZ climate policy.

Some further work could assess also the uncertainty given by the method used to estimate concentrations. For instance, using a source-receptor model, as FASST [21], as well as an empirical based model, such as CLAQC-elastic net and the CLAQC-xgboost [58]. In this way, the overall uncertainty between the NZ and EoC climate policies could be analysed.

Furthermore, this study could be extended to welfare damages, estimating the economical implications of each climate policy and the related uncertainty.

7. Bibliography

References

1. Alan Agresti and Brent A. Coull. Approximate is better than "exact" for interval estimation of binomial proportions. *The American Statistician*, 52(2):119–126, 1998.

2. Susan Anenberg, Larry Horowitz, Daniel Tong, and Jason West. An estimate of the global burden of anthropogenic ozone and fine particulate matter on premature human mortality using atmospheric modeling. *Environmental health perspectives*, 118:1189–95, 04 2010.

3. Rob Beelen, Ole Raaschou-Nielsen, Zorana Andersen, Gudrun Weinmayr, Barbara Hoffmann, Kathrin Wolf, Evi Samoli, Paul Fischer, Mark Nieuwenhuijsen, Paolo Vineis, Wei Xun, Klea Katsouyanni, Konstantina Dimakopoulou, Anna Oudin, Bertil Forsberg, Lars Modig, Aki Havulinna, Timo Lanki, and Gerard Hoek. Effects of long-term exposure to air pollution on natural-cause mortality: An analysis of 22 european cohorts within the multicentre escape project. *Lancet*, 383, 12 2013.

4. C.A. Belis, D. Pernigotti, G. Pirovano, O. Favez, J.L. Jaffrezo, J. Kuenen, H. Denier van Der Gon, M. Reizer, V. Riffault, L.Y. Alleman, M. Almeida, F. Amato, A. Angyal, G. Argyropoulos, S. Bande, I. Beslic, J.-L. Besombes, M.C. Bove, P. Brotto, G. Calori, D. Cesari, C. Colombi, D. Contini, G. De Gennaro, A. Di Gilio, E. Diapouli, I. El Haddad, H. Elbern, K. Eleftheriadis, J. Ferreira, M. Garcia Vivanco, S. Gilardoni, B. Golly, S. Hellebust, P.K. Hopke, Y. Izadmanesh, H. Jorquera, K. Krajsek, R. Kranenburg, P. Lazzeri, F. Lenartz, F. Lucarelli, K. Maciejewska, A. Manders, M. Manousakas, M. Masiol, M. Mircea, D. Mooibroek, S. Nava, D. Oliveira, M. Paglione, M. Pandolfi, M. Perrone, E. Petralia, A. Pietrodangelo, S. Pillon, P. Pokorna, P. Prati, D. Salameh, C. Samara, L. Samek, D. Saraga, S. Sauvage, M. Schaap, F. Scotto, K. Sega, G. Siour, R. Tauler, G. Valli, R. Vecchi, E. Venturini, M. Vestenius, A. Waked, and E. Yubero. Evaluation of receptor and chemical transport models for PM10 source apportionment. *Atmospheric Environment: X*, 5:100053, jan 2020.

5. Valentina Bosetti, Marzio Galeotti, Massimo Tavoni, Carlo Carraro, and Emanuele Massetti. A world induced technical change hybrid model. *The Energy Journal*, Hybrid Modeling:13–38, 09 2006.

6. Michael Brauer, Markus Amann, Rick Burnett, Aaron Cohen, Frank Dentener, Majid Ezzati, Sarah Henderson, Michal Krzyzanowski, Randall Martin, Rita Van Dingenen, Aaron Donkelaar, and George Thurston. Exposure assessment for estimation of the global burden of disease attributable to outdoor air pollution. *Environmental science and technology*, 46:652–60, 12 2011.

7. Michael Brauer, Greg Freedman, Joseph Frostad, Aaron van Donkelaar, Randall V Martin, Frank Dentener, Rita van Dingenen, Kara Estep, Heresh Amini, Joshua S Apte, Kalpana Balakrishnan, Lars Barregard, David Broday, Valery Feigin, Santu Ghosh, Philip K Hopke, Luke D Knibbs, Yoshihiro Kokubo, Yang Liu, Stefan Ma, Lidia Morawska, José Luis Sangrador, Gavin Shaddick, H Ross Anderson, Theo Vos, Mohammad H Forouzanfar, Richard T Burnett, and Aaron Cohen. Ambient air pollution exposure estimation for the global burden of disease 2013. *Environmental science and technology*, 50:79–88, 01 2016.

8. M. Bryson. *Heavy Tailed Distributions: Properties and Tests*, volume 16(1). 02 1974.

9. Xiang Bu, Zhonglei Xie, Jing Liu, Linyan Wei, Xiqiang Wang, Mingwei Chen, and Hui Ren. Global pm2.5-attributable health burden from 1990 to 2017: Estimates from the global burden of disease study 2017. *Environmental Research*, 197:111123, 2021.

10. Richard Burnett, Hong Chen, Mieczysław Szyszkowicz, Neal Fann, Bryan Hubbell, C. Pope, Joshua Apte, Michael Brauer, Aaron Cohen, Scott Weichenthal, Jay Coggins, Qian Di, Bert Brunekreef, Joseph Frostad, Stephen Lim, Haidong Kan, Katherine Walker, George Thurston, Richard Hayes, and Joseph Spadaro. Global estimates of mortality associated with long-term exposure to outdoor fine particulate matter. *Proceedings of the National Academy of Sciences*, 115:201803222, 09 2018.

11. Richard Burnett and Aaron Cohen. Relative risk functions for estimating excess mortality attributable to outdoor pm2.5 air pollution: Evolution and state-of-the-art. *Atmosphere*, 11:589, 06 2020.

12. Richard Burnett, C. Pope, Majid Ezzati, Casey Olives, Stephen Lim, Sumi Mehta, Hwashin Shin, Gitanjali Singh, Bryan Hubbell, Michael Brauer, H Anderson, Kirk Smith, John Balmes, Nigel Bruce, Haidong Kan, Francine Laden, Annette Prüss-Ustün, Michelle Turner, Susan Gapstur, and Aaron Cohen. An integrated risk function for estimating the global burden of disease attributable to ambient fine particulate matter exposure. *Environmental health perspectives*, 122, 02 2014.

13. Pantelis Capros, Leonidas Paroussos, Panagiotis Fragkos, Stella Tsani, Baptiste Boitier, Fabian Wagner, Sebastian Busch, Gustav Resch, Markus Blesl, and Johannes Bollen. Description of models and scenarios used to assess european decarbonisation pathways. *Energy Strategy Reviews*, 2, 02 2014.

14. Aaron Cohen, H Anderson, Bart Ostro, Kiran Pandey, Michal Krzyzanowski, Nino Künzli, Kersten Gutschmidt, C. Pope, Isabelle Romieu, Jonathan Samet, and Kirk Smith. The global burden of disease due to outdoor air pollution. *Journal of toxicology and environmental health. Part A*, 68:1301–7, 07 2005.

15. Aaron Cohen, Michael Brauer, Richard Burnett, H Anderson, Joseph Frostad, Kara Estep, Kalpana Balakrishnan, Bert Brunekreef, Lalit Dandona, Rakhi Dandona, Valery Feigin, Greg Freedman, Bryan Hubbell, Amelia Jobling, Haidong Kan, Luke Knibbs, Yang Liu, Randall Martin, Lidia Morawska, and Mohammad Forouzanfar. Estimates and 25-year trends of the global burden of disease attributable to ambient air pollution: An analysis of data from the global burden of diseases study 2015. *The Lancet*, 389, 04 2017.

16. Aaron J Cohen, H Ross Anderson, Bart Ostro, K Dev Pandey, Michal Krzyzanowski, Nino Künzli, Kersten Gutschmidt, C Arden Pope III, Isabelle Romieu, Jonathan M Samet, et al. Urban air pollution. *Comparative quantification of health risks: global and regional burden of disease attributable to selected major risk factors*, 2:1353–1433, 2004.

17. GBD 2019 Risk Factors Collaborators. Global burden of 87 risk factors in 204 countries and territories, 1990-2019: a systematic analysis for the global burden of disease study 2019. *Lancet*, 396(10258)(17):1223–1249, Oct 2020.

18. Laurens de Haan and Ana Ferreira. *Extreme Value Theory: An Introduction*. Springer series in Operations reasarch and Financial Engineering. New York, EEUU, 2006.

19. Pedro Delicado, Guadalupe Gómez, and Jan Graffelman. Estadística, 2 2015.

20. Jacques Després, Kimon Keramidas, Andreas Schmitz, Alban Kitous, Burkhard Schade, Ana Raquel Diaz-Vazquez, Silvana Mima, Hans Peter Russ, , and Tobias Wiesenthal. Poles-jrc model documentation - updated for 2018. *JRC Research Reports from Joint Research Centre (Seville site)*, JRC113757, 11 2018.

21. Rita Van Dingenen, Frank Dentener, Monica Crippa, Joana Leitao, Elina Marmer, Shilpa Rao, Efisio Solazzo, and Luana Valentini. TM5-FASST: a global atmospheric source–receptor model for rapid impact analysis of emission changes on air quality and short-lived climate pollutants. *Atmospheric Chemistry and Physics*, 18(21):16173–16211, November 2018.

22. Francesca Dominici, Yun Wang, Andrew Correia, Majid Ezzati, C. Pope, and Douglas Dockery. Chemical composition of fine particulate matter and life expectancy: In 95 us counties between 2002 and 2007. *Epidemiology (Cambridge, Mass.)*, 26, 04 2015.

23. Laurent Drouet, Valentina Bosetti, Simone A. Padoan, Lara Aleluia Reis, Christoph Bertram, Francesco Dalla Longa, Jacques Després, Johannes Emmerling, Florian Fosse, Kostas Fragkiadakis, Stefan Frank, Oliver Fricko, Shinichiro Fujimori, Mathijs Harmsen, Volker Krey, Ken Oshiro, Larissa P. Nogueira, Leonidas Paroussos, Franziska Piontek, Keywan Riahi, Pedro R. R. Rochedo, Roberto Schaeffer, Jun'ya Takakura, Kaj-Ivar van der Wijst, Bob van der Zwaan, Detlef van Vuuren, Zoi Vrontisi, Matthias Weitzel, Behnam Zakeri, and Massimo Tavoni. Net zero-emission pathways reduce the physical and economic risks of climate change. *Nature Climate Change*, 11(12):1070–1076, nov 2021.

24. E2Mlab. Model manual. 2, 2017.

25. Johannes Emmerling, Laurent Drouet, Lara A. Reis, Michela Bevione, Loïc Berger, Valentina Bosetti, Samuel Carrara, Enrica De Cian, Gauthier de Maere d'Aertrycke, Thomas Longden, Michele Malpede, Giacomo Marangoni, Fabio Sferra, Massimo Tavoni, Jan Witajewski-Baltvilks, and Petr Havlik. The witch 2016 model - documentation and implementation of the shared socioeconomic pathways. 06 2016.

26. Peter Fantke, Thomas E. McKone, Marko Tainio, Olivier Jolliet, Joshua S. Apte, Katerina S. Stylianou, Nicole Illner, Julian D. Marshall, Ernani F. Choma, , and John S. Evans. Global effect factors for exposure to fine particulate matter. *Environ Sci Technol*, 53(12):6855–6868, 06 2019.

27. Sergey Foss, S.G. Serguei, Dmitry Korshunov, and Stan Zachary. *Heavy-Tailed and Long-Tailed Distributions*. 01 1970.

28. S. Fujimori, T. Hasegawa, T. Masui, and K. Takahashi. Land use representation in a global cge model for long-term simulation: Cet vs. logit functions. *Food Secur.*, 6:685–699, 2014.

29. S. Fujimori, T. Masui, and Matsuoka. Aim/cge [basic] manual discussion. *Paper Series.*, 2012.

30. GBD. Gbd 2016 ier estimates. 2016.

31. Jean Dickinson Gibbons and Subhabrata Chakraborti. *Nonparametric Statistical Inference*. Springer Berlin Heidelberg, Berlin, Heidelberg, 2011.

32. Daniel Huppmann, Matthew Gidden, Oliver Fricko, Peter Kolp, Clara Orthofer, Michael Pimmer, Nikolay Kushin, Adriano Vinca, Alessio Mastrucci, Keywan Riahi, and Volker Krey. The messageix integrated assessment model and the ix modeling platform (ixmp): An open framework for integrated and cross-cutting analysis of energy, climate, the environment, and sustainable development. *Environmental Modelling and Software*, 112:143–156, 2019.

33. IHME. Gbd 2019 cause and risk summaries, 2019.

34. Michael Jerrett, Richard Burnett, C. Pope, Kazuhiko Ito, George Thurston, Daniel Krewski, Yuanli Shi, Eugenia Calle, and Michael Thun. Long-term ozone exposure and mortality. *The New England journal of medicine*, 360:1085–95, 03 2009.

35. Sasha Khomenko, Marta Cirach, Evelise Pereira-Barboza, Natalie Mueller, Jose Barrera-Gómez, David Rojas-Rueda, Kees de Hoogh, Gerard Hoek, and Mark Nieuwenhuijsen. Premature

mortality due to air pollution in european cities: a health impact assessment. *The Lancet Planetary Health*, 5(3):e121–e134, mar 2021.

36. Daniel Krewski, Michael Jerrett, Richard T Burnett, Renjun Ma, Edward Hughes, Yuanli Shi, Michelle C Turner, C Arden Pope III, George Thurston, Eugenia E Calle, et al. *Extended follow-up and spatial analysis of the American Cancer Society study linking particulate air pollution and mortality*, volume 140. Health Effects Institute Boston, MA, 2009.

37. Elmar Kriegler, Nico Bauer, Alexander Popp, Florian Humpenöder, Marian Leimbach, Jessica Strefler, Lavinia Baumstark, Benjamin Leon Bodirsky, Jérôme Hilaire, David Klein, Ioanna Mouratiadou, Isabelle Weindl, Christoph Bertram, Jan-Philipp Dietrich, Gunnar Luderer, Michaja Pehl, Robert Pietzcker, Franziska Piontek, Hermann Lotze-Campen, Anne Biewald, Markus Bonsch, Anastasis Giannousakis, Ulrich Kreidenweis, Christoph Müller, Susanne Rolinski, Anselm Schultes, Jana Schwanitz, Miodrag Stevanovic, Katherine Calvin, Johannes Emmerling, Shinichiro Fujimori, and Ottmar Edenhofer. Fossil-fueled development (ssp5): An energy and resource intensive scenario for the 21st century. *Global Environmental Change*, 42:297–315, 2017.

38. Philip J Landrigan, Richard Fuller, Nereus J R Acosta, Olusoji Adeyi, Robert Arnold, Niladri (Nil) Basu, Abdoulaye Bibi Baldé, Roberto Bertollini, Stephan Bose-O'Reilly, Jo Ivey Boufford, Patrick N Breysse, Thomas Chiles, Chulabhorn Mahidol, Awa M Coll-Seck, Maureen L Cropper, Julius Fobil, Valentin Fuster, Michael Greenstone, Andy Haines, David Hanrahan, David Hunter, Mukesh Khare, Alan Krupnick, Bruce Lanphear, Bindu Lohani, Keith Martin, Karen V Mathiasen, Maureen A McTeer, Christopher J L Murray, Johanita D Ndahimananjara, Frederica Perera, Janez Potočnik, Alexander S Preker, Jairam Ramesh, Johan Rockström, Carlos Salinas, Leona D Samson, Karti Sandilya, Peter D Sly, Kirk R Smith, Achim Steiner, Richard B Stewart, William A Suk, Onno C P van Schayck, Gautam N Yadama, Kandeh Yumkella, and Ma Zhong. The lancet commission on pollution and health. *The Lancet*, 391(10119):462–512, 2018.

39. J Lelieveld, John Evans, M Fnais, Despina Giannadaki, and A Pozzer. The contribution of outdoor air pollution sources to premature mortality on a global scale. *Nature*, 525:367–71, 09 2015.

40. Stephen S Lim, Theo Vos, Abraham D Flaxman, Goodarz Danaei, Kenji Shibuya, Heather Adair-Rohani, Markus Amann, H Ross Anderson, Kathryn G Andrews, Martin Aryee, Charles Atkinson, Loraine J Bacchus, Adil N Bahalim, Kalpana Balakrishnan, John Balmes, Suzanne Barker-Collo, Amanda Baxter, Michelle L Bell, Jed D Blore, Fiona Blyth, Carissa Bonner, Guilherme Borges, Rupert Bourne, Michel Boussinesq, Michael Brauer, Peter Brooks, Nigel G Bruce, Bert Brunekreef, Claire Bryan-Hancock, Chiara Bucello, Rachelle Buchbinder, Fiona Bull, Richard T Burnett, Tim E Byers, Bianca Calabria, Jonathan Carapetis, Emily Carnahan, Zoe Chafe, Fiona Charlson, Honglei Chen, Jian Shen Chen, Andrew Tai-Ann Cheng, Jennifer Christine Child, Aaron Cohen, K Ellicott Colson, Benjamin C Cowie, Sarah Darby, Susan Darling, Adrian Davis, Louisa Degenhardt, Frank Dentener, Don C Des Jarlais, Karen Devries, Mukesh Dherani, Eric L Ding, E Ray Dorsey, Tim Driscoll, Karen Edmond, Suad Eltahir Ali, Rebecca E Engell, Patricia J Erwin, Saman Fahimi, Gail Falder, Farshad Farzadfar, Alize Ferrari, Mariel M Finucane, Seth Flaxman, Francis Gerry R Fowkes, Greg Freedman, Michael K Freeman, Emmanuela Gakidou, Santu Ghosh, Edward Giovannucci, Gerhard Gmel, Kathryn Graham, Rebecca Grainger, Bridget Grant, David Gunnell, Hialy R Gutierrez, Wayne Hall, Hans W Hoek, Anthony Hogan, H Dean Hosgood, Damian Hoy, Howard Hu, Bryan J Hubbell, Sally J Hutchings, Sydney E Ibeanusi, Gemma L Jacklyn, Rashmi Jasrasaria, Jost B Jonas, Haidong Kan, John A Kanis, Nicholas Kasse-

baum, Norito Kawakami, Young-Ho Khang, Shahab Khatibzadeh, Jon-Paul Khoo, Cindy Kok, Francine Laden, Ratilal Lalloo, Qing Lan, Tim Lathlean, Janet L Leasher, James Leigh, Yang Li, John Kent Lin, Steven E Lipshultz, Stephanie London, Rafael Lozano, Yuan Lu, Joelle Mak, Reza Malekzadeh, Leslie Mallinger, Wagner Marcenes, Lyn March, Robin Marks, Randall Martin, Paul McGale, John McGrath, Sumi Mehta, George A Mensah, Tony R Merriman, Renata Micha, Catherine Michaud, Vinod Mishra, Khayriyyah Mohd Hanafiah, Ali A Mokdad, Lidia Morawska, Dariush Mozaffarian, Tasha Murphy, Mohsen Naghavi, Bruce Neal, Paul K Nelson, Joan Miquel Nolla, Rosana Norman, Casey Olives, Saad B Omer, Jessica Orchard, Richard Osborne, Bart Ostro, Andrew Page, Kiran D Pandey, Charles D H Parry, Erin Passmore, Jayadeep Patra, Neil Pearce, Pamela M Pelizzari, Max Petzold, Michael R Phillips, Dan Pope, C Arden Pope, John Powles, Mayuree Rao, Homie Razavi, Eva A Rehfuess, Jürgen T Rehm, Beate Ritz, Frederick P Rivara, Thomas Roberts, Carolyn Robinson, Jose A Rodriguez-Portales, Isabelle Romieu, Robin Room, Lisa C Rosenfeld, Ananya Roy, Lesley Rushton, Joshua A Salomon, Uchechukwu Sampson, Lidia Sanchez-Riera, Ella Sanman, Amir Sapkota, Soraya Seedat, Peilin Shi, Kevin Shield, Rupak Shivakoti, Gitanjali M Singh, David A Sleet, Emma Smith, Kirk R Smith, Nicolas J C Stapelberg, Kyle Steenland, Heidi Stöckl, Lars Jacob Stovner, Kurt Straif, Lahn Straney, George D Thurston, Jimmy H Tran, Rita Van Dingenen, Aaron van Donkelaar, J Lennert Veerman, Lakshmi Vijayakumar, Robert Weintraub, Myrna M Weissman, Richard A White, Harvey Whiteford, Steven T Wiersma, James D Wilkinson, Hywel C Williams, Warwick Williams, Nicholas Wilson, Anthony D Woolf, Paul Yip, Jan M Zielinski, Alan D Lopez, Christopher J L Murray, Majid Ezzati, Mohammad A AlMazroa, and Ziad A Memish. A comparative risk assessment of burden of disease and injury attributable to 67 risk factors and risk factor clusters in 21 regions, 1990-2010: a sys-

tematic analysis for the global burden of disease study 2010. *Lancet*, 380(9859):2224–60, December 2012. Copyright © 2012 Elsevier Ltd. All rights reserved.

41. Daniel P. Loucks, Eelco van Beek, Jery R. Stedinger, Jozef P.M. Dijkman, and Monique T Villars. *Water resources systems planning and management: an introduction to methods, models and applications*. UNESCO digital library, 2005.

42. Shilpa IRao, Zbigniew Klimont, Steven Smith, Rita Van Dingenen, Frank Dentener, Alexander Bouwman, Keywan Riahi, Markus Amann, Benjamin Bodirsky, Detlef Vuuren, Lara A. Reis, Katherine Calvin, Laurent Drouet, Oliver Fricko, Shinichiro Fujimori, David Gernaat, Petr Havlík, J.H.M. Harmsen, Tomoko Hasegawa, and Massimo Tavoni. Future air pollution in the shared socio-economic pathways. *Global Environmental Change*, 42, 07 2016.

43. Gunnar Luderer, Robert Pietzcker, Christoph Bertram, Elmar Kriegler, Malte Meinshausen, and Ottmar Edenhofer. Economic mitigation challenges: How further delay closes the door for achieving climate targets. *Environmental Research Letters*, 8:034033, 09 2013.

44. Anil Markandya, Jon Sampedro, Steven Smith, Rita Van Dingenen, Cristina Pizarro-Irizar, Iñaki Arto, and Mikel González-Eguino. Health co-benefits from air pollution and mitigation costs of the paris agreement: a modelling study. *The Lancet Planetary Health*, 2:e126–e133, 03 2018.

45. Christopher J L Murray, Aleksandr Y Aravkin, Peng Zheng, Cristiana Abbafati, Kaja M Abbas, Mohsen Abbasi-Kangevari, Foad Abd-Allah, Ahmed Abdelalim, Mohammad Abdollahi, Ibrahim Abdollahpour, et al. Global burden of 87 risk factors in 204 countries and territories, 1990–2019: a systematic analysis for the global burden of disease study 2019. *The Lancet*, 396(10258):1223–1249, oct 2020.

46. Masoud Nasari, Mieczysław Szyszkowicz, Hong Chen, Dan Crouse, Michelle Turner, Michael Jerrett, C. Pope, Bryan Hubbell, Neal Fann,

Aaron Cohen, Susan Gapstur, W. Diver, David Stieb, Mohammad Forouzanfar, Sun-Young Kim, Casey Olives, Daniel Krewski, and Richard Burnett. A class of non-linear exposure-response models suitable for health impact assessment applicable to large cohort studies of ambient air pollution. *Air Quality, Atmosphere and Health*, 9, 12 2016.

47. The Concise Encyclopedia of Statistics. *Binomial Test*. Springer New York, New York, NY, 2008.

48. World Healt Organization. Global health observatory resources.

49. World Health Organization. Who global air quality guidelines. particulate matter (pm2.5 and pm10), ozone, nitrogen dioxide, sulfur dioxide and carbon monoxide. *Geneva*, page 250, 2021.

50. R Pedro. Development of a global integrated energy model to evaluate the brazilian role in climate change mitigation scenarios. *DSc thesis, Programa de Planejamento Energético, COPPE/UFRJ.*, 2016.

51. C. A. Pope, R. T. Burnett, M. J. Thun, E. E. Calle, D. Krewski, K. Ito, and G. D. Thurston. Lung cancer, cardiopulmonary mortality, and long-term exposure to fine particulate air pollution. *JAMA*, 287(9):1132–1141, 2002.

52. Social Public Health and World Health Organization Environmental Determinants of Health Department. Burden of disease from the joint effects of household and ambient air pollution for 2016. *Global Health Estimates Technical Paper*, 2018.

53. Air quality co-benefits for human health and agriculture counterbalance costs to meet Paris Agreement pledges. Toon vandyck and kimon keramidas and alban kitous and joseph v. spadaro and rita van dingenen and mike holland and bert saveyn. *Nature Communications*, 9(4939), 2018.

54. Shilpa Rao, Zbigniew Klimont, Steven J. Smith, Rita Van Dingenen, Frank Dentener, Lex Bouwman, Keywan Riahi, Markus Amann, Benjamin Leon Bodirsky, Detlef P. van Vuuren, Lara Aleluia Reis, Katherine Calvin, Laurent Drouet, Oliver Fricko, Shinichiro Fujimori, David Gernaat, Petr Havlik, Mathijs Harmsen, Tomoko Hasegawa, Chris Heyes, Jérôme Hilaire, Gunnar Luderer, Toshihiko Masui, Elke Stehfest, Jessica Strefler, Sietske van der Sluis, and Massimo Tavoni. Future air pollution in the shared socio-economic pathways. *Global Environmental Change*, 42:346–358, jan 2017.

55. K Reddy. Global burden of disease study 2015 provides gps for global health 2030. *The Lancet*, 388, 10 2016.

56. Lara Aleluia Reis, Laurent Drouet, and Massimo Tavoni. Internalising health-economic impacts of air pollution into climate policy: a global modelling study. *The Lancet Planetary Health*, 6(1):e40–e48, jan 2022.

57. Lara Aleuia Reis, Laurent Drouet, Rita Dingenen, and Johannes Emmerling. Future global air quality indices under different socioeconomic and climate assumptions. *Sustainability*, 10(10):3645, oct 2018.

58. Stefania Renna, Francesco Granella, Lara Aleluia Reis, and Paulina Antipa. Claqc - country level air quality calculator. https://datashowb.shinyapps.io/CLAQC/.

59. Keywan Riahi, Christoph Bertram, Daniel Huppmann, Joeri Rogelj, Valentina Bosetti, Anique-Marie Cabardos, Andre Deppermann, Laurent Drouet, Stefan Frank, Oliver Fricko, Shinichiro Fujimori, Mathijs Harmsen, Tomoko Hasegawa, Volker Krey, Gunnar Luderer, Leonidas Paroussos, Roberto Schaeffer, Matthias Weitzel, Bob van der Zwaan, Zoi Vrontisi, Francesco Dalla Longa, Jacques Després, Florian Fosse, Kostas Fragkiadakis, Mykola Gusti, Florian Humpenöder, Kimon Keramidas, Paul Kishimoto, Elmar Kriegler, Malte Meinshausen, Larissa P. Nogueira, Ken

Oshiro, Alexander Popp, Pedro R. R. Rochedo, Gamze Ünlü, Bas van Ruijven, Junya Takakura, Massimo Tavoni, Detlef van Vuuren, and Behnam Zakeri. Cost and attainability of meeting stringent climate targets without overshoot. *Nature Climate Change*, 11(12):1063–1069, November 2021.

60. Keywan Riahi, Christoph Betram, Laurent Drouet, Tomoko Hasegawa, Francesco Dalla Longa, Jacques Desprès, Florian Fosse, Kostas Fragkiadakis, Oliver Fricko, Mykola Gusti, Florian Humpenöder, Kimon Keramidas, Paul Kishimoto, Elmar Kriegler, Larissa P. Nogueira, Ken Oshiro, Alexander Popp, Pedro R.R. Rochedo, Junya Takakura, Gamze Ünlü, Bas van Ruijven, Detlef van Vuuren, Behnam Zakeri, Valentina Bosetti, Anique-Marie Cabardos, Andre Deppermann, Harmen-Sytze de Boer, Johannes Emmerling, Stefan Frank, Shinichiro Fujimori, Mathijs Harmsen, Petr Havlik, Jérôme Hilaire, Daniel Huppmann, Kimon Keramidas, Volker Krey, Gunnar Luderer, Aman Malik, Malte Meinshausen, Yuki Ochi, Leonidas Paroussos, Joeri Rogelj, Deger Saygin, Roberto Schaeffer, Massimo Tavoni, Bob van der Zwaan, Zoi Vrontisi, and Matthias Weitzel. Engage global scenarios, 2021.

61. GBD 2017 risk factor collaborators. Gbd 2017 risk factor collaborators. global, regional, and national comparative risk assessment of 84 behavioural, environmental and occupational, and metabolic risks or clusters of risks for 195 countries and territories, 1990-2017: a systematic analysis for the global burden of disease study 2017. *Lancet*, 392(20159):1923–1994, Nov 2017.

62. Jon Sampedro, Steven J. Smith, Iñaki Arto, Mikel González-Eguino, Anil Markandya, Kathleen M. Mulvaney, Cristina Pizarro-Irizar, and Rita Van Dingenen. Health co-benefits and mitigation costs as per the paris agreement under different technological pathways for energy supply. *Environment International*, 136:105513, 2020.

63. Alqamah Sayeed, Ebrahim Eslami, Yannic Lops, and Yunsoo Choi. CMAQ-CNN: A new-generation of post-processing techniques for chemical transport models using deep neural networks. *Atmospheric Environment*, 273:118961, mar 2022.

64. Super Computing Center (SCC). Zeus supercomputer.

65. E. Stehfest, Detlef Vuuren, Tom Kram, Alexander Bouwman, Rob Alkemade, Michel Bakkenes, H. Biemans, A. Bouwman, Michel Elzen, Jan Janse, Paul Lucas, Jelle van Minnen, M. Müller, and Anne Prins. Integrated assessment of global environmental change with image 3.0. model description and policy applications. 01 2014.

66. Katsumasa Tanaka and Brian O'Neill. The paris agreement zero-emissions goal is not always consistent with the 1.5 ˚c and 2 ˚c temperature targets. *Nature Climate Change*, 8:1–6, 04 2018.

67. Philippe Thunis, Monica Crippa, Cornelis Cuvelier, Diego Guizzardi, Alexander de Meij, Gabriel Oreggioni, and Enrico Pisoni. Sensitivity of air quality modelling to different emission inventories: A case study over europe. *Atmospheric Environment: X*, 10:100111, apr 2021.

68. Michelle Turner, Zorana Andersen, Andrea Baccarelli, W. Diver, Susan Gapstur, C. Pope, Diddier Prada, Jonathan Samet, George Thurston, and Aaron Cohen. Outdoor air pollution and cancer: An overview of the current evidence and public health recommendations. *CA: A Cancer Journal for Clinicians*, 70, 08 2020.

69. Michelle C Turner, Michael Jerrett, C Arden 3rd Pope, Daniel Krewski, Susan M Gapstur, W Ryan Diver, Bernardo S Beckerman, Julian D Marshall, Jason Su, Daniel L Crouse, and Richard T Burnett. Long-term ozone exposure and mortality in a large prospective study. *American journal of respiratory and critical care medicine*, 193:1134–42, 05 2016.

70. Masson-Delmotte V., P. Zhai, A. Pirani, S.L. Connors, C. Péan, S. Berger, N. Caud, Y. Chen,

L. Goldfarb, M.I. Gomis, M. Huang, K. Leitzell, E. Lonnoy, J.B.R. Matthews, T.K. Maycock, T. Waterfield, O. Yelekçi, R. Yu, , and B. Zhou (eds.). Climate change 2021: The physical science basis. contribution of working group i to the sixth assessment report of the intergovernmental panel on climate change. *Cambridge University Press*, 2021.

71. B. van der Zwaan, T. Kober, F. D. Longa, A. van der Laan, and G. Jan Kramer. An integrated assessment of pathways for low-carbon development in africa. *Energy Policy*, 117:387–395, 2018.

72. R. van Dingenen, F.J. Dentener, F. Raes, M.C. Krol, L. Emberson, and J. Cofala. The global impact of ozone on agricultural crop yields under current and future air quality legislation. *Atmospheric Environment*, 43(3):604–618, 2009.

73. Heleen L. van Soest, Mathijs Harmsen, Detlef P. van Vuuren, Christoph Bertram, Michel den Elzen, Niklas Höhne, Gabriela Iacobuta, Volker Krey, Elmar Kriegler, Gunnar Luderer, Keywan Riahi, Falko Ueckerdt, Jae Edmonds, Jacques Despres, Laurent Drouet, Johannes Emmerling, Stefan Frank, Oliver Fricko, Matthew Gidden, Florian Humpenöder, Daniel Huppmann, Shinichiro Fujimori, Kostas Fragkiadakis, Keii Gi, Kimon Keramidas, Alexandre C. Köberle, Lara Aleluia Reis, Pedro Rochedo, Roberto Schaeffer, Ken Oshiro, Zoi Vrontisi, Wenying Chen, Gokul C. Iye, Maria Kannavou, Jiang Kejun, Ritu Mathur, George Safonov, and Saritha Sudharmma Vishwanathan. Cd-links wp3 global low-carbon development pathways, 06 2017.

A. Relative Risk parameters

Table 3: Relative Risk parameters with 95% CI

Ref.	Publication's year	Pollutant	Method	Levels	TMREL	Parmeter	ALRI	LC	IHD	STROKE	COPD	CP
BURNETT2018 [10]	2018	$PM_{2.5}$	GEMM 6	WITH	2.40 µg m^{-3}	θ		0.2942 (0.23273,0.35567)	0.2969 (0.27903,0.31477)	0.2720 (0.19503,0.34897)	0.2510 (0.18338,0.31862)	
						α		6.2	1.9	6.2	6.5	
						μ		9.3	12.0	16.7	2.5	
						ν		29.8	40.2	23.7	32.0	
				WITHOUT	2.40 µg m^{-3}	θ		0.2626 (0.18411,0.34109)	0.2543 (0.20841,0.30019)	0.1873 (0.10299,0.27161)	0.2095 (0.14225,0.27675)	
						α		6.7	4.9	6.2	7.2	
						μ		11.0	-21.1	14.5	2.0	
						ν		16.5	17.7	14.4	14.7	
GBD2016 [30]	2016	$PM_{2.5}$	IER 4	HIGH	5.29 µg m^{-3} (5.27,5.31)	α		73.1 (65.5,80.3)	6.40 (6.04,6.72)	2.73 (2.62,2.84)	16.3 (14.6,18.0)	
						β		0.000195 (0.000174,0.000215)	0.0123 (0.0117,0.0131)	0.0141 (0.0135,0.0147)	0.0023 (0.00204,0.00264)	
						δ		0.773 (0.766,0.779)	0.334 (0.331,0.337)	0.432 (0.427,0.437)	0.579 (0.564,0.589)	
				MEDIUM	4.18 µg m^{-3} (4.17,4.21)	α		71.5 (64.7,76.1)	6.16 (5.91,6.50)	2..72 (2.61,2.83)	15.4 (14.0,18.1)	
						β		0.000213 (0.000196 0.000239)	0.0131 (0.0124,0.0138)	0.0141 (0.0137,0.0147)	0.00228 (0.00206,0.00250)	
						δ		0.773 (0.766,0.782)	0.332 (0.329,0.335)	0.429 (0.425,0.435)	0.579 (0.568,0.589)	
				LOW	3.00 µg m^{-3} (2.92,3.05)	α		70.4 (63.4,75.6)	6.61 (6.31,6.97)	2.86 (2.75,2.99)	14.8 (13.6,16.1)	
						β		0.000205 (0.000185,0.000225)	0.0123 (0.0116,0.0129)	0.0142 (0.0136,0.0147)	0.00229 (0.00210,0.00254)	
						δ		0.777 (0.767,0.786)	0.333 (0.330,0.335)	0.425 (0.419,0.430)	0.575 (0.560 0.591)	
BURNETT2014 [12]	2014	$PM_{2.5}$	IER 4		ALRI: 5.553867502 (3.175877368,10.65856447) LC: 5.312838615 (5.263402167,5.625401066, IHD: 5.89785796 (4.9,6.917645688) STROKE: 7.261807718 (6.53033859,8.921692107) COPD: 5.787549667 (4.999997811,6.759656531)	α β δ	1.97378648 (1.436904185,2..935465288) 0.002847675 (0.001440037,1.373370217) 1.209294599 (0.879980508,1.373370217)	15.67636977 (12.30776596,47.47159043) 0.001073919 (0.000864294,0.000131904) 0.765861621 (0.659865243,1.020917868)	1.190330928 (0.947050981,1.228481327) 0.0750978 (0.025256397,0.05795739) 0.374809182 (0.4164409,0.934215573)	1.16632796 (1.410432389,1.780359822) 0.011865371 (0.016309476,0.018028539) 1.202946339 (0.477576651,1.210566232)	14.10220781 (7.440843463,14.99199458) 0.001206578 (0.002112071,0.000493862) 0.680348423 (0.648260937,0.851276683)	
KREWSKI2009 [36]	2009	$PM_{2.5}$	LL 3		U(2.4,5.9) µg m^{-3}	β		0.0104360 (0.00392207 0.0165514)	0.010436 0.0139762 (0.01043600 0.0182322)			0.0086178 (0.00582689 0.0113329)
OSTRO2004 [14]	2004	$PM_{2.5}$	Rational 7		U(2.4,5.9) µg m^{-3}	β		0.23218 (0.08563,0.37873)				0.15515 (0.0562,0.2541)
GBD2015 [55]	2015	O_3	LL 8		U(33.3,41.9) ppb	β					0.0083382 (0.0030459,0.013926)	
JERRET2009 [34]	2009	O_3	LL 8		U(33.3,41.9) ppb	β					0.0039221 (0.00099503,0.0064851)	

B. Abbreviations

List of abbreviations used in the project:

- ALRI: Acute Lower Respiratory Illness

- CEV: Cerebrovascular Disease

- CI: Confidence Interval

- COPD: Chronic Obstructive Pulmonary Disease

- CP: Cardiopulmonary Disease

- DALY: Disability-Adjusted Life Years

- EoC: End-Of-Century

- GBD: Global Burden of Disease

- GEMM: Global Exposure Mortality Model

- GHG: Greenhouse Gas

- IAM: Integrated Assessment Model

- IER: Integrated Exposure-Response Model

- IHD: Ischemic Heart Disease

- INDC: Intended Nationally Determined Contribution

- IPCC: Intergovernmental Panel on Climate Change

- LC: Lung Cancer

- LL: Log-Linear Model

- NDC: Nationally Determined Contribution

- NPi: National Policy

- NZ: Net-Zero

- PAF: Population Attributable Fraction

- PM: Particulate Matter

- ppb: parts per billion

- RESP: Respiratory Illness

- RR: Relative Risk

- TMREL: Theoretical Minimum Relative Exposure Level

- SCHIF: Shape Constrained Health Impact Function Model

- WHO: World Health Organization

C. Emissions sensitivity and uncertainty

C.1 Probability distribution and cumulative frequency emissions graphs
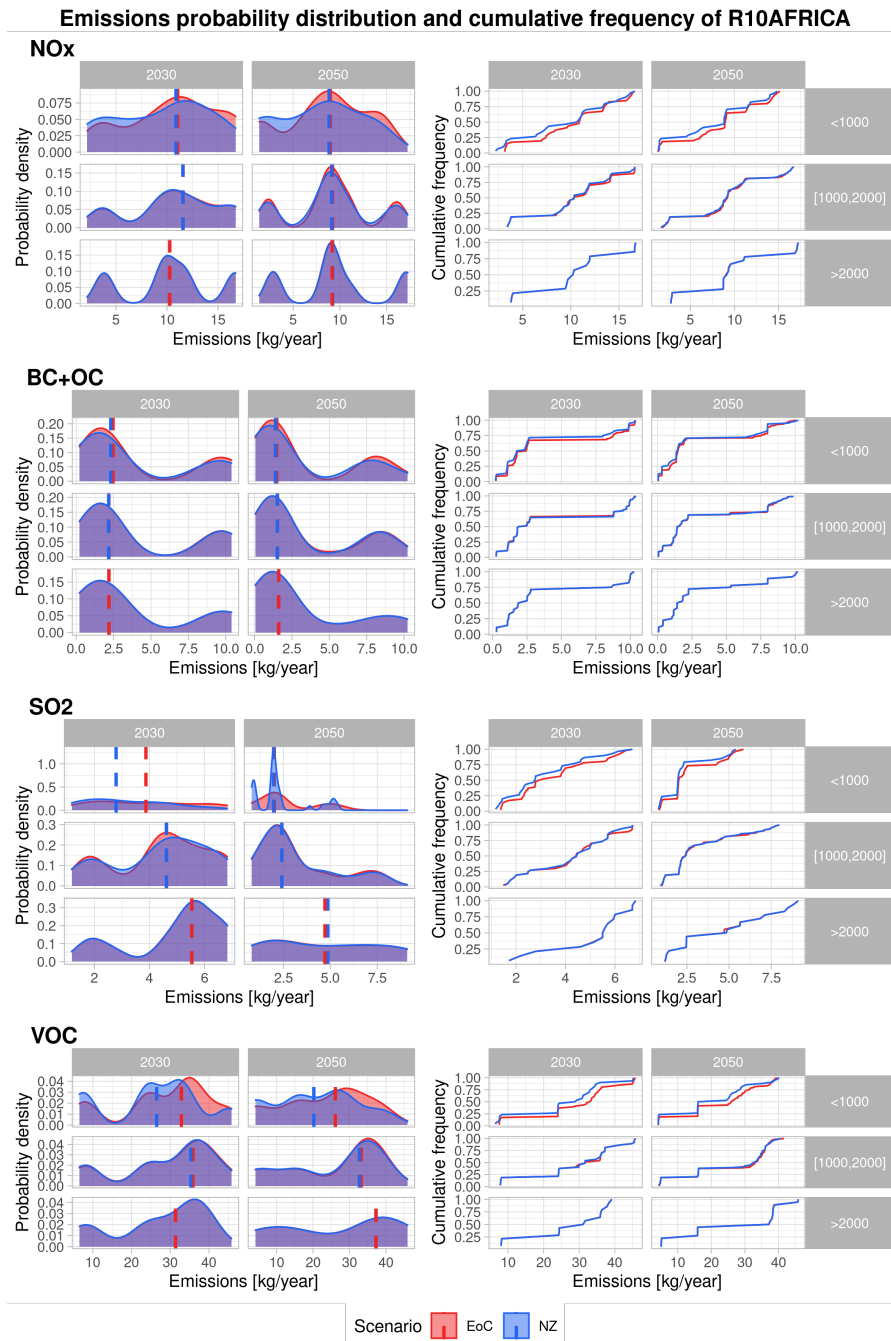
Figure 19: Probability density distribution (left) and cumulative frequency (right) for R10AFRICA for BC and OC, SO$_2$, NO$_x$, and VOC emissions. Includes median line by climate policy.
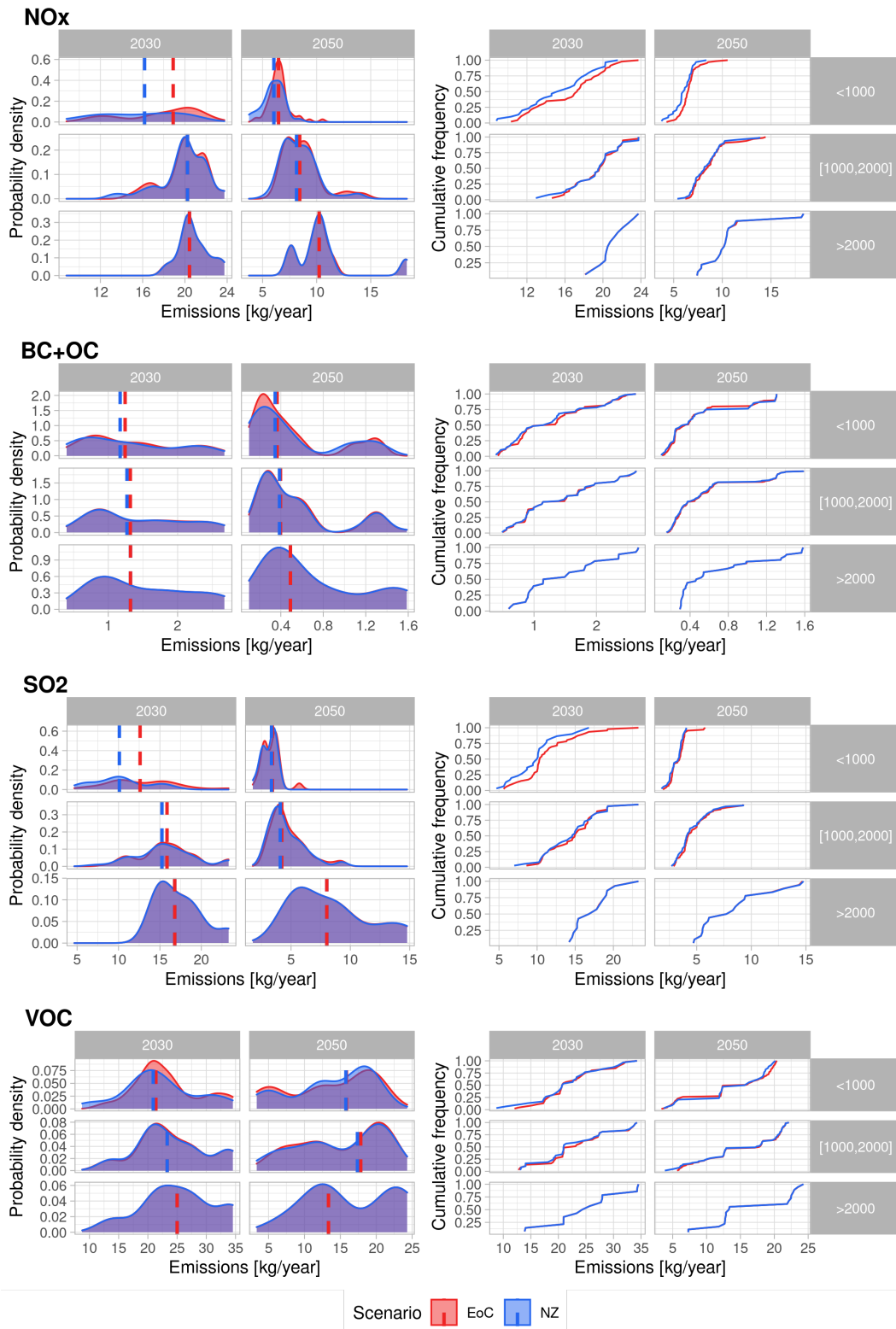
Figure 20: Probability density distribution (left) and cumulative frequency (right) for R10CHINA+ for BC and OC, SO$_2$, NO$_x$, and VOC emissions. Includes median line by climate policy.
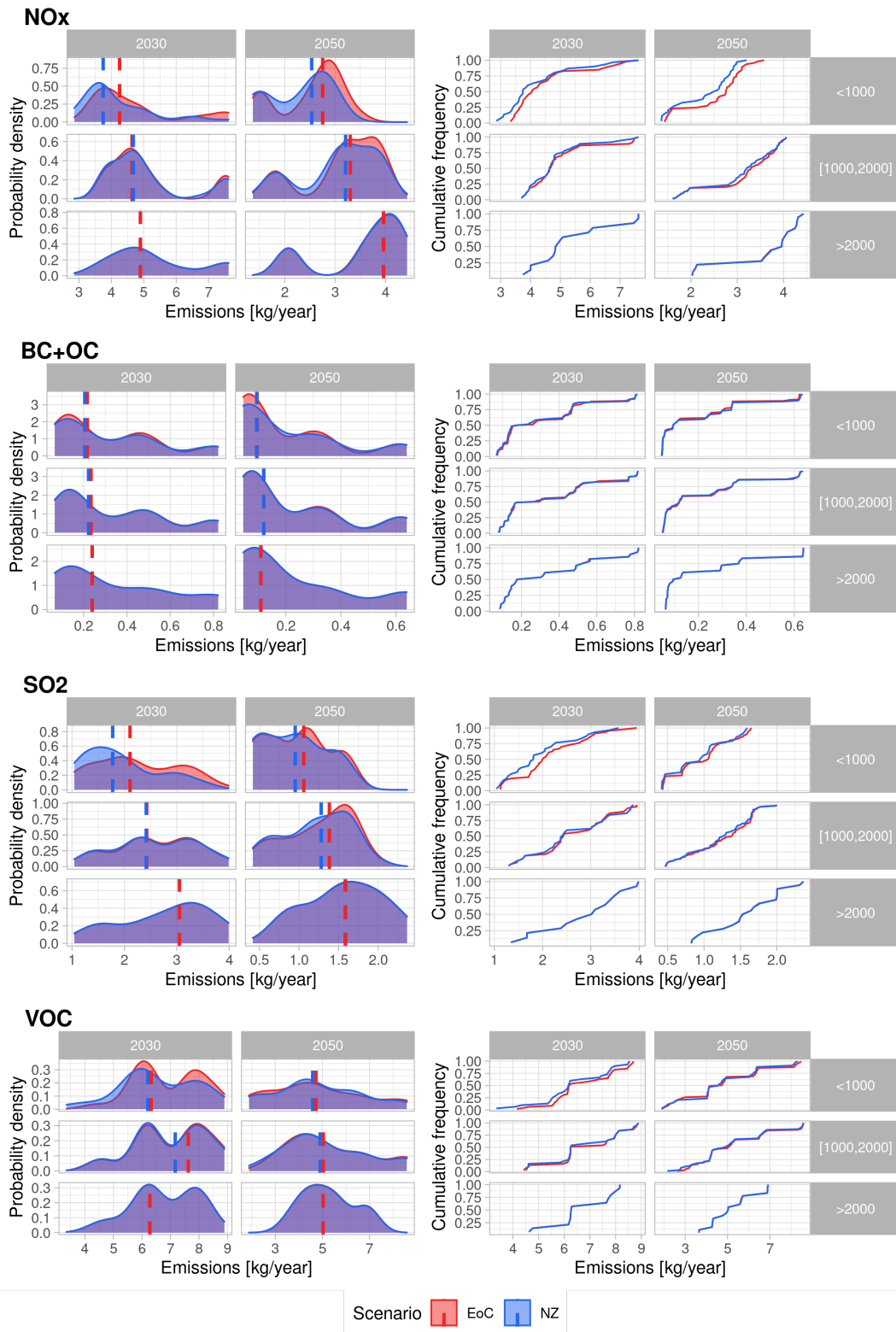
Figure 21: Probability density distribution (left) and cumulative frequency (right) for R10EUROPE for BC and OC, SO$_2$, NO$_x$, and VOC emissions. Includes median line by climate policy.
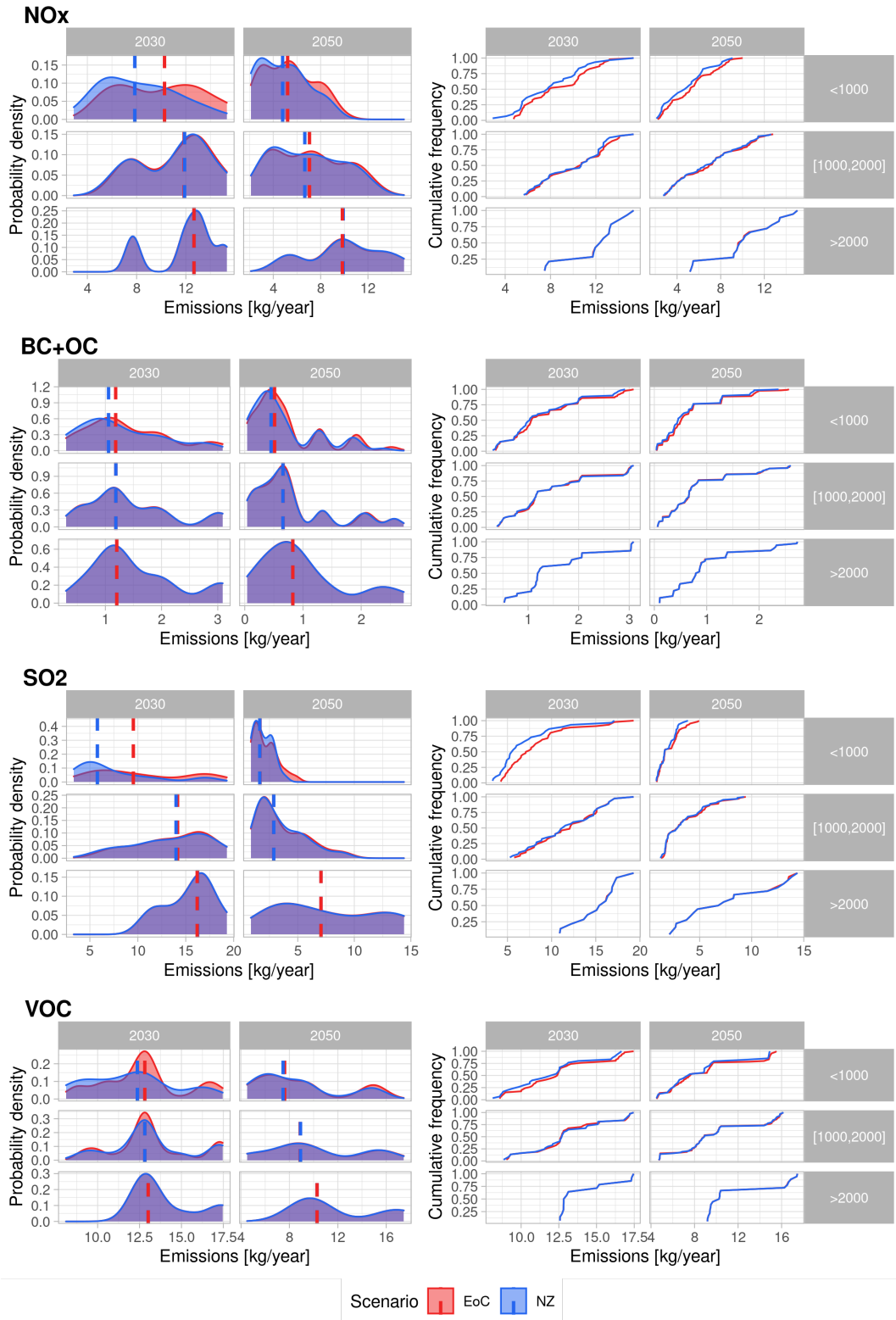
Figure 22: Probability density distribution (left) and cumulative frequency (right) for R10INDIA+ for BC and OC, SO$_2$, NO$_x$, and VOC emissions. Includes median line by climate policy.
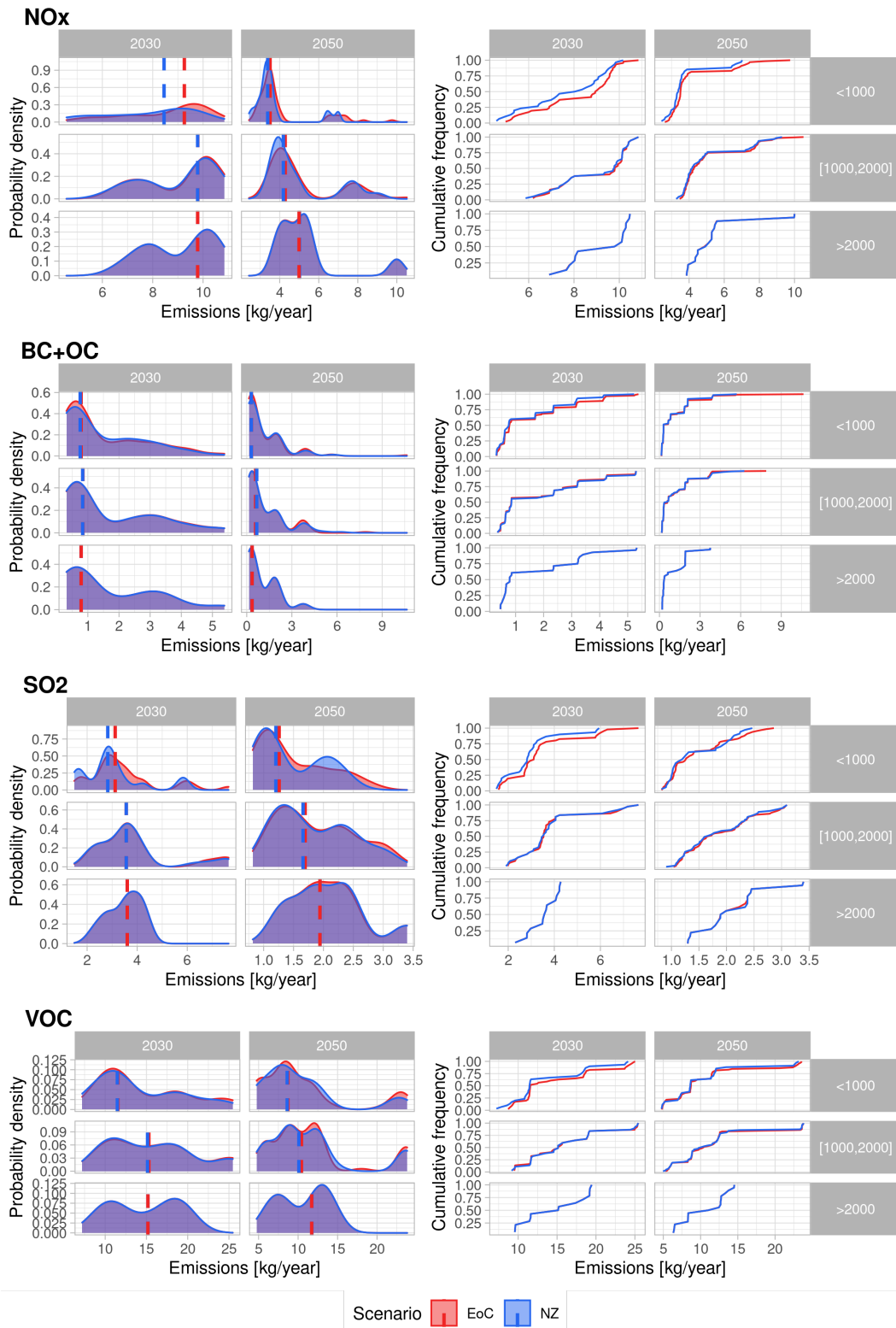
Figure 23: Probability density distribution (left) and cumulative frequency (right) for R10LATIN-AM for BC and OC, SO$_2$, NO$_x$, and VOC emissions. Includes median line by climate policy.
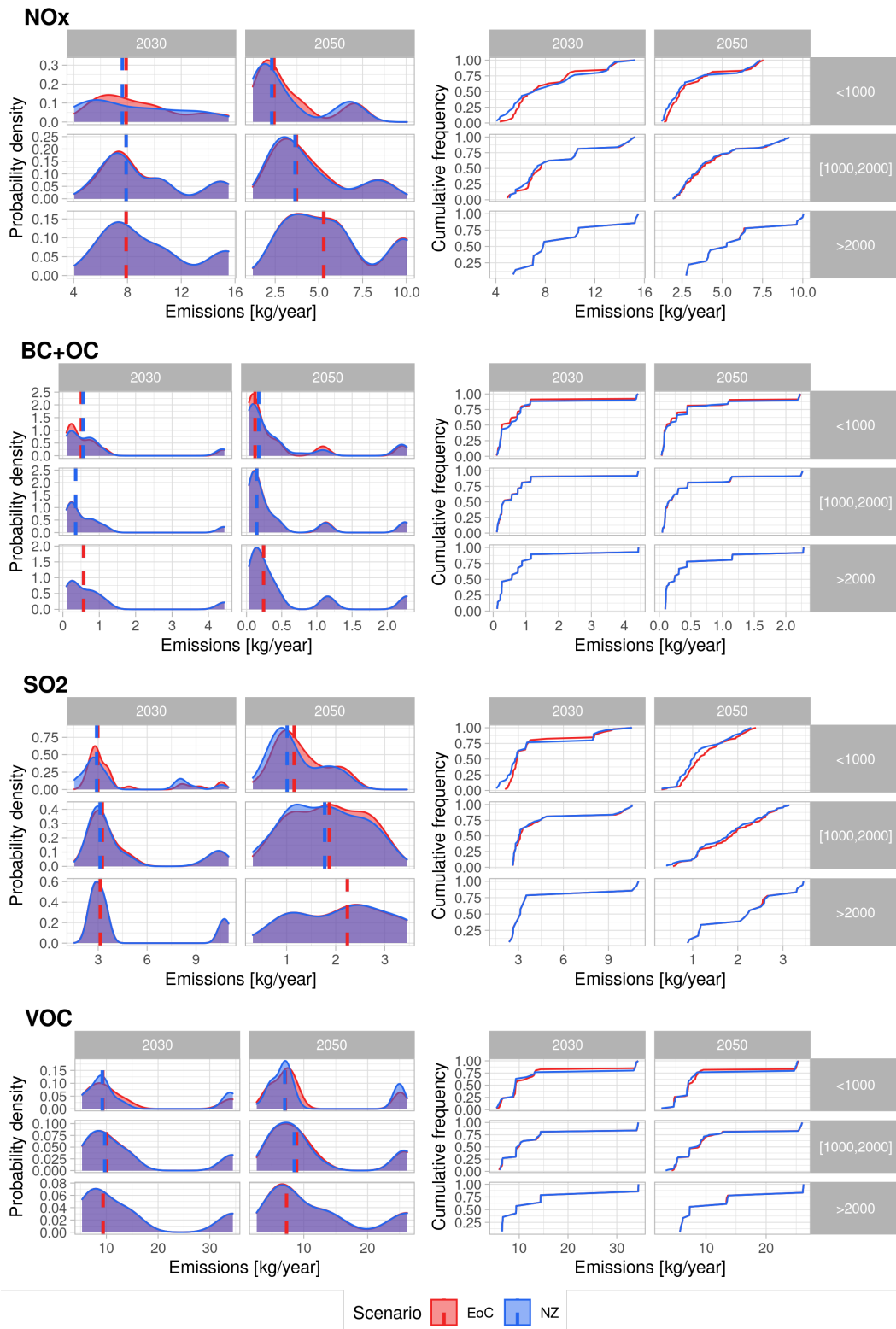
Figure 24: Probability density distribution (left) and cumulative frequency (right) for R10MIDDLE-EAST for BC and OC, SO_2, NO_x, and VOC emissions. Includes median line by climate policy.
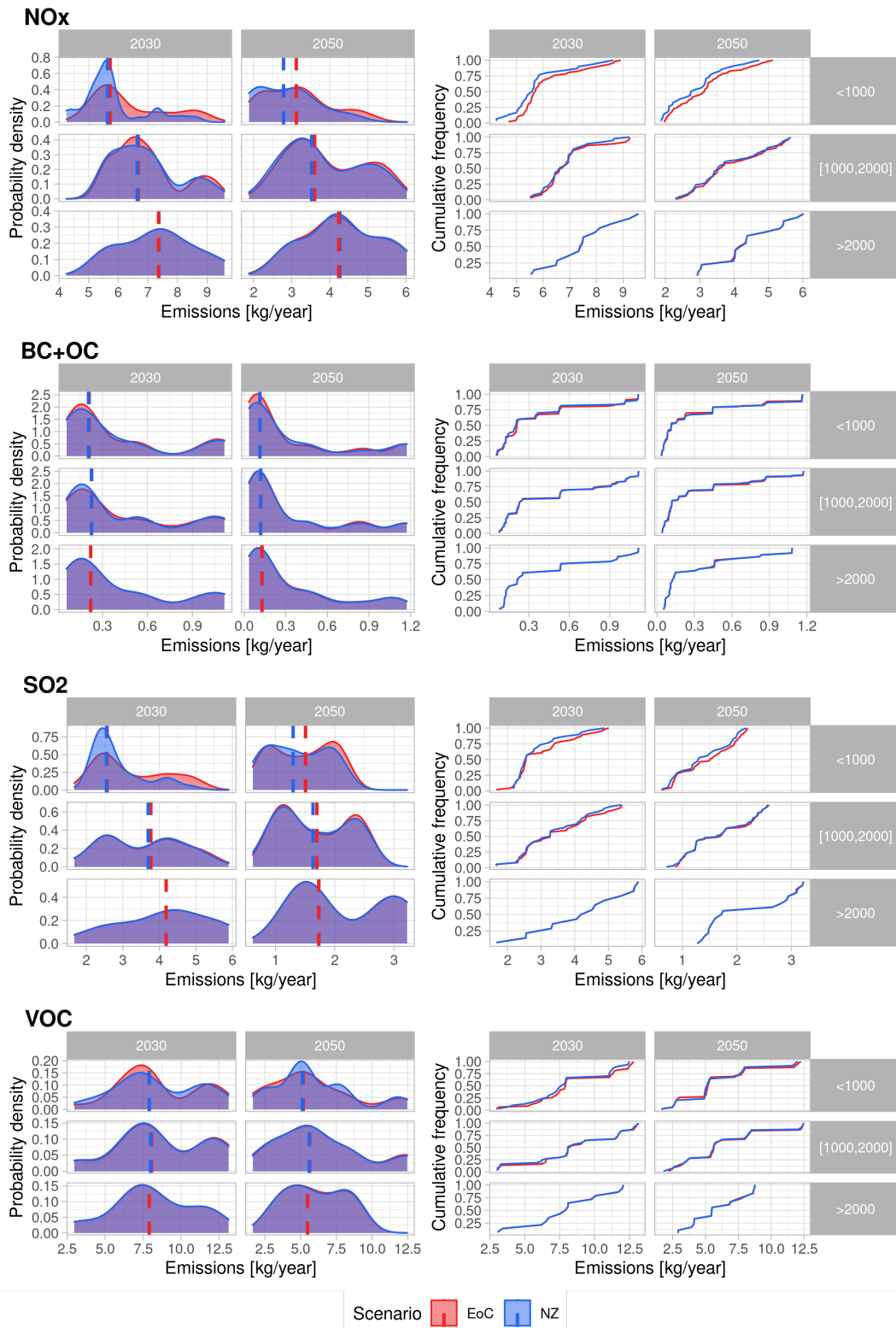
Figure 25: Probability density distribution (left) and cumulative frequency (right) for R10NORTH-AM for BC and OC, SO$_2$, NO$_x$, and VOC emissions. Includes median line by climate policy.
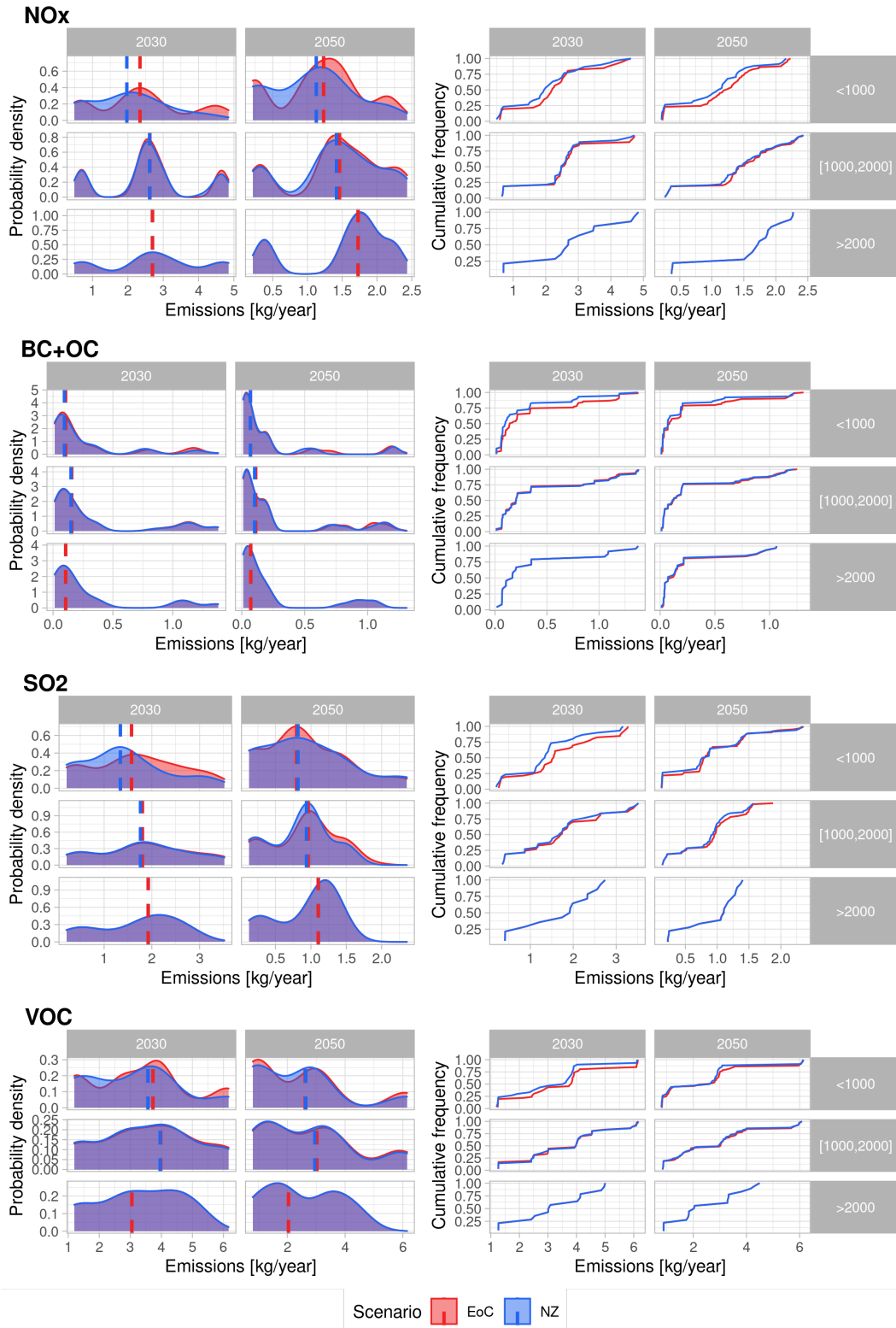
Figure 26: Probability density distribution (left) and cumulative frequency (right) for R10PAC-OECD for BC and OC, SO$_2$, NO$_x$, and VOC emissions. Includes median line by climate policy.
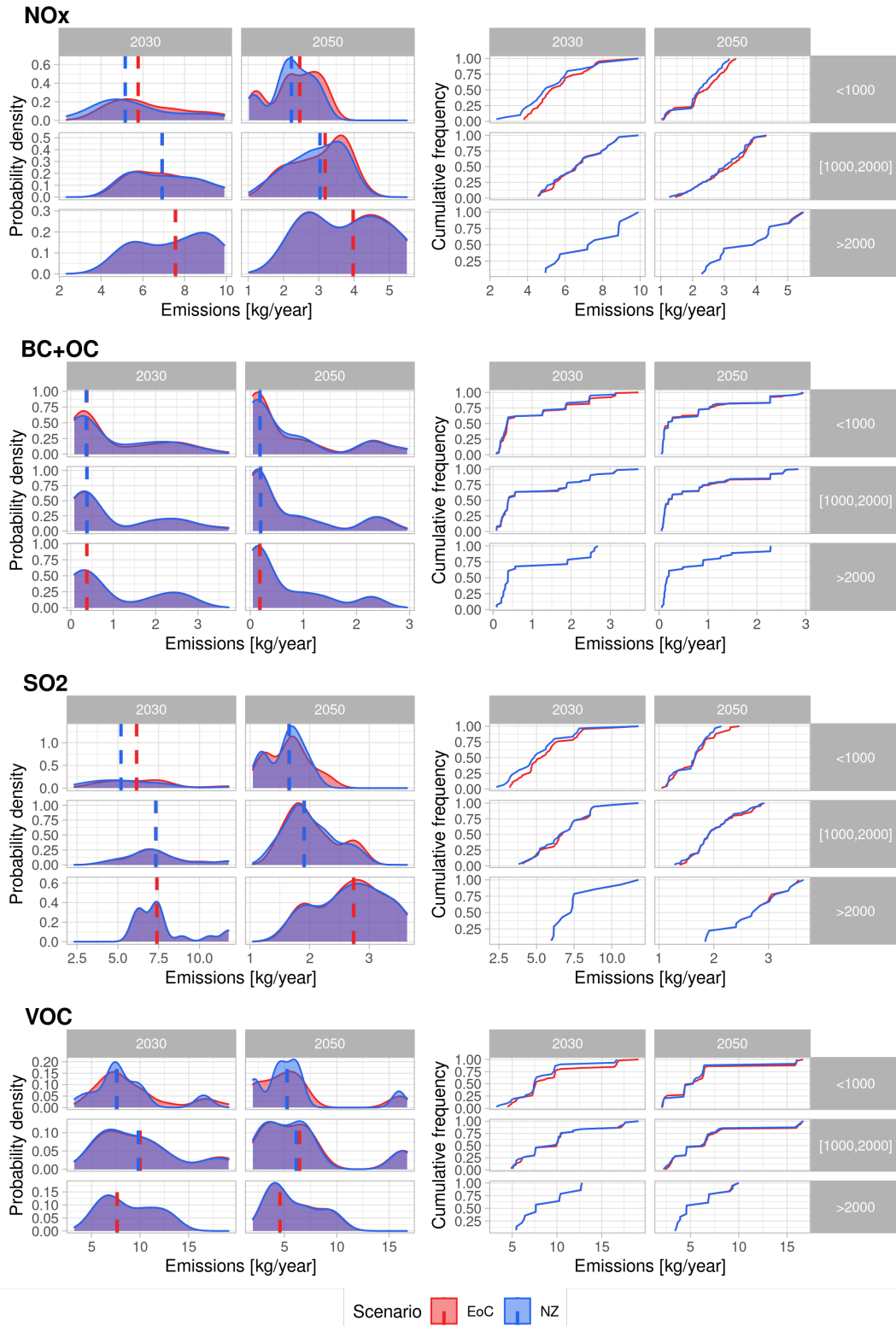
Figure 27: Probability density distribution (left) and cumulative frequency (right) for R10REF-ECON for BC and OC, SO_2, NO_x, and VOC emissions. Includes median line by climate policy.
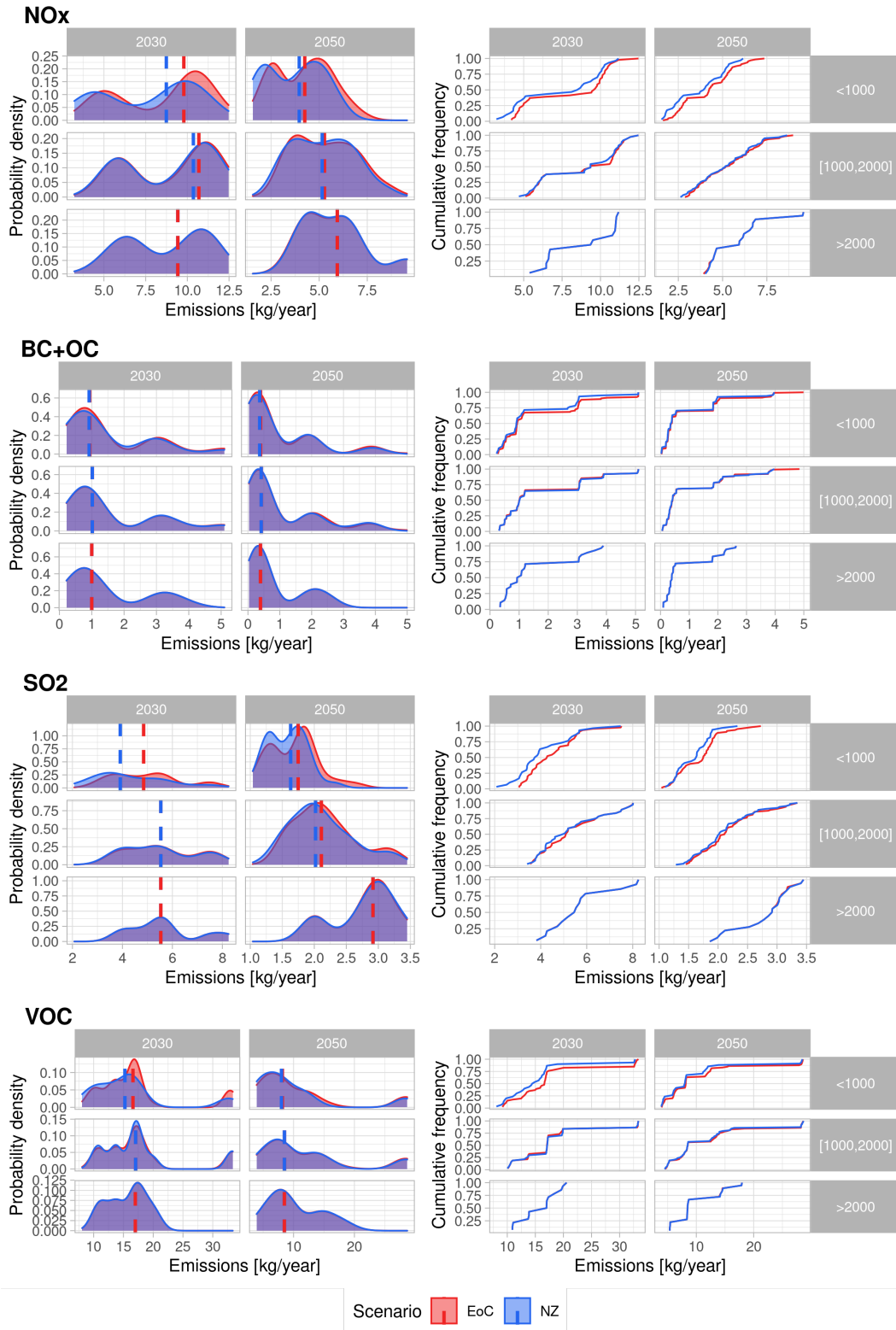
Figure 28: Probability density distribution (left) and cumulative frequency (right) for R10REST-ASIA for BC and OC, SO$_2$, NO$_x$, and VOC emissions. Includes median line by climate policy.
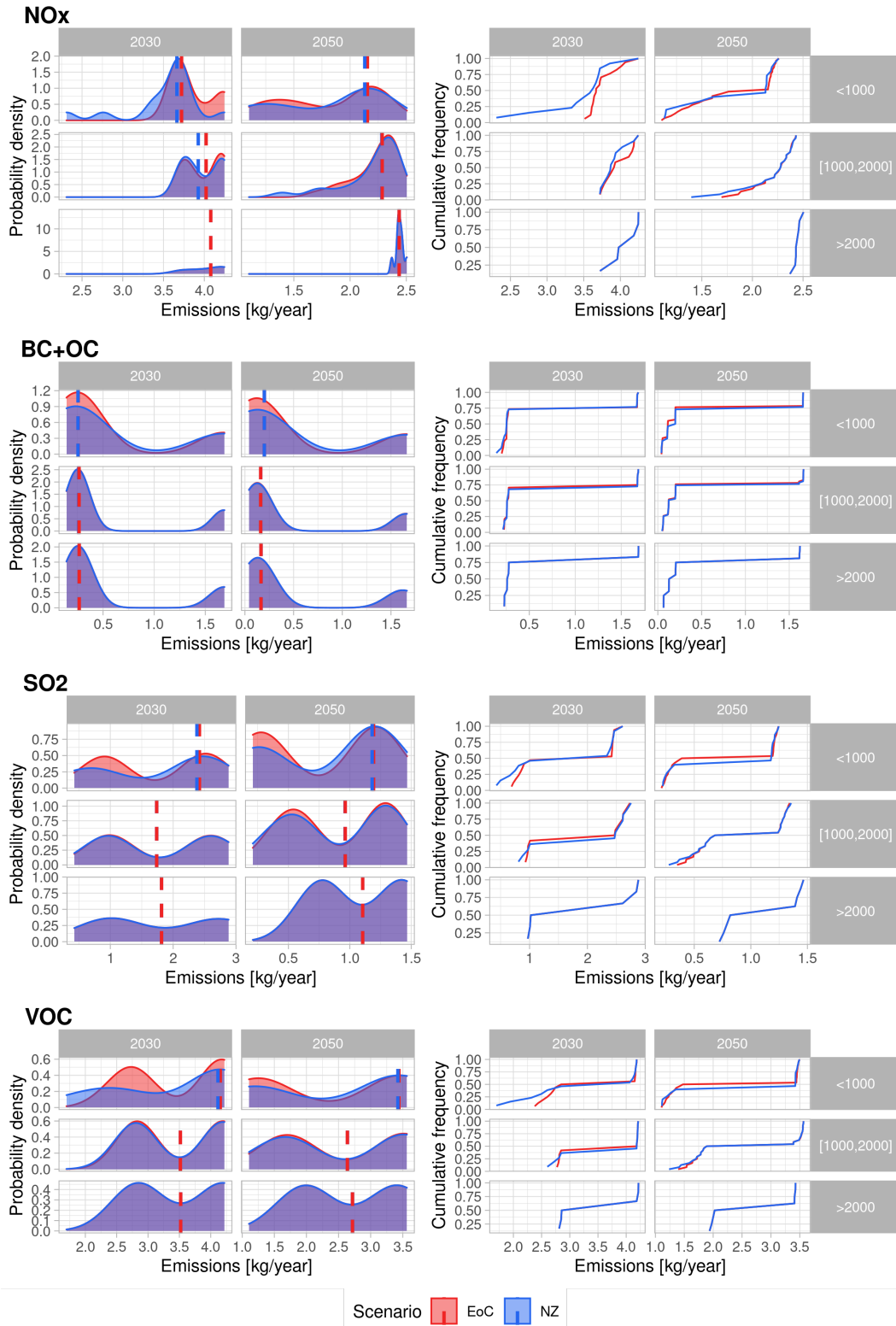
Figure 29: Probability density distribution (left) and cumulative frequency (right) for Shipping and aviation for BC and OC, SO_2, NO_x, and VOC emissions. Includes median line by climate policy.

D. Concentrations sensitivity and uncertainty

D.1 Probability distribution and cumulative frequency average concentrations graphs
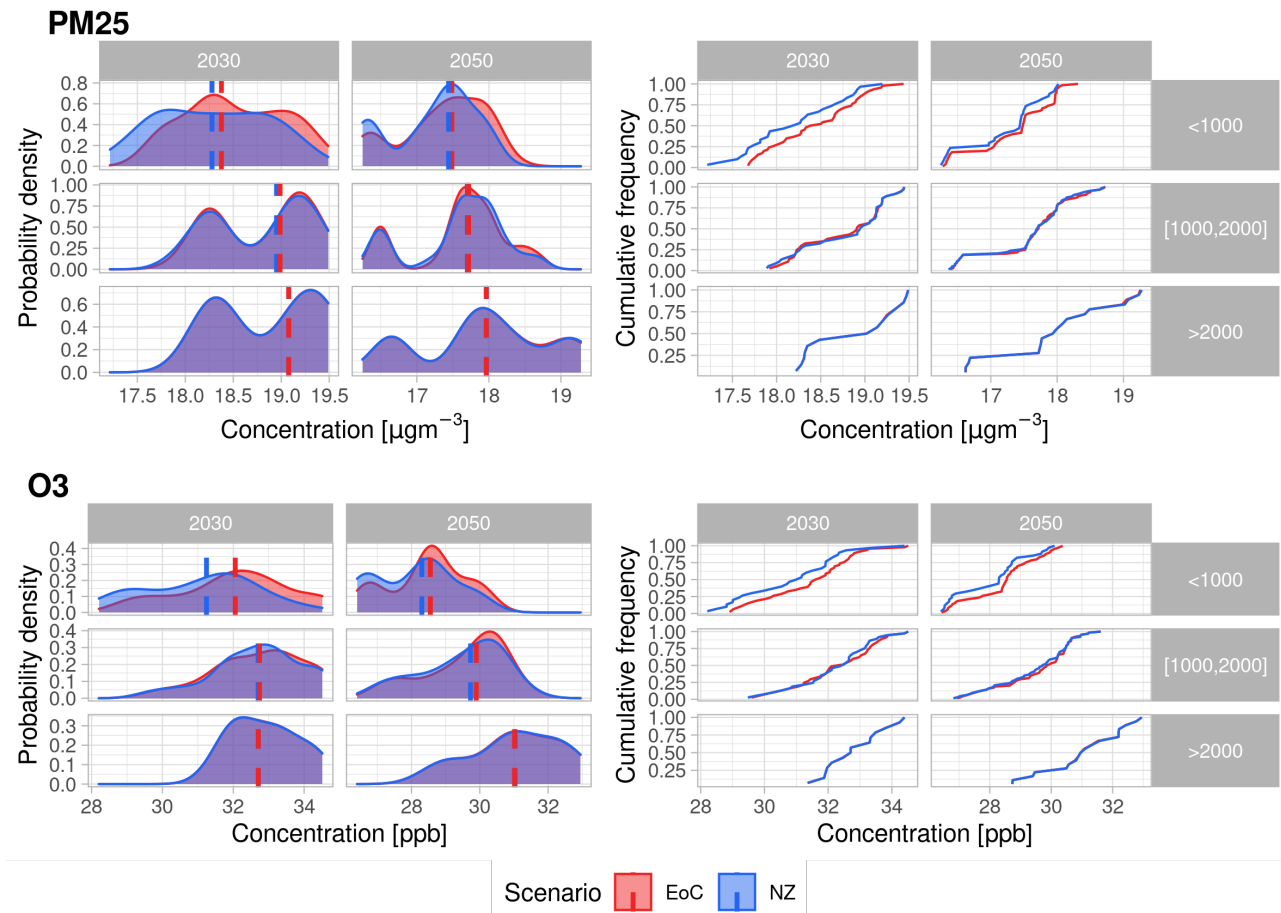
Figure 30: Probability density distribution (left) and cumulative frequency (right) for R10AFRICA for $PM_{2.5}$ and O_3 concentrations. Includes median line by climate policy. Data has been averaged by model and scenario.

Figure 31: Probability density distribution (left) and cumulative frequency (right) for R10CHINA+ for $PM_{2.5}$ and O_3 concentrations. Includes median line by climate policy. Data has been averaged by model and scenario.

Figure 32: Probability density distribution (left) and cumulative frequency (right) for R10EUROPE for $PM_{2.5}$ and O_3 concentrations. Includes median line by climate policy. Data has been averaged by model and scenario.

Figure 33: Probability density distribution (left) and cumulative frequency (right) for R10INDIA+ for $PM_{2.5}$ and O_3 concentrations. Includes median line by climate policy. Data has been averaged by model and scenario.

Figure 34: Probability density distribution (left) and cumulative frequency (right) for R10LATIN-AM for $PM_{2.5}$ and O_3 concentrations. Includes median line by climate policy. Data has been averaged by model and scenario.

Figure 35: Probability density distribution (left) and cumulative frequency (right) for R10MIDDLE-EAST for $PM_{2.5}$ and O_3 concentrations. Includes median line by climate policy. Data has been averaged by model and scenario.

Figure 36: Probability density distribution (left) and cumulative frequency (right) for R10NORTH-AM for PM$_{2.5}$ and O$_3$ concentrations. Includes median line by climate policy. Data has been averaged by model and scenario.

Concentrations probability distribution and cumulative frequency of R10PAC_OECD
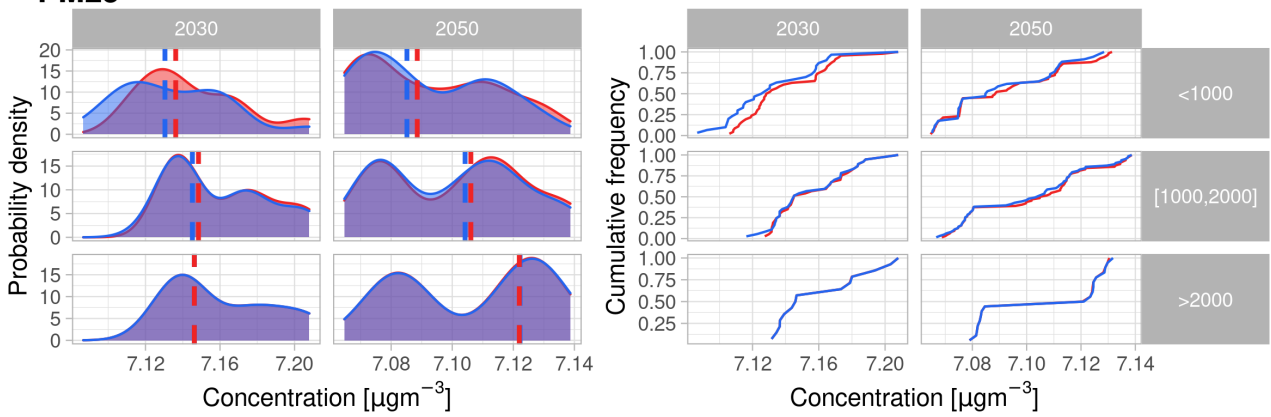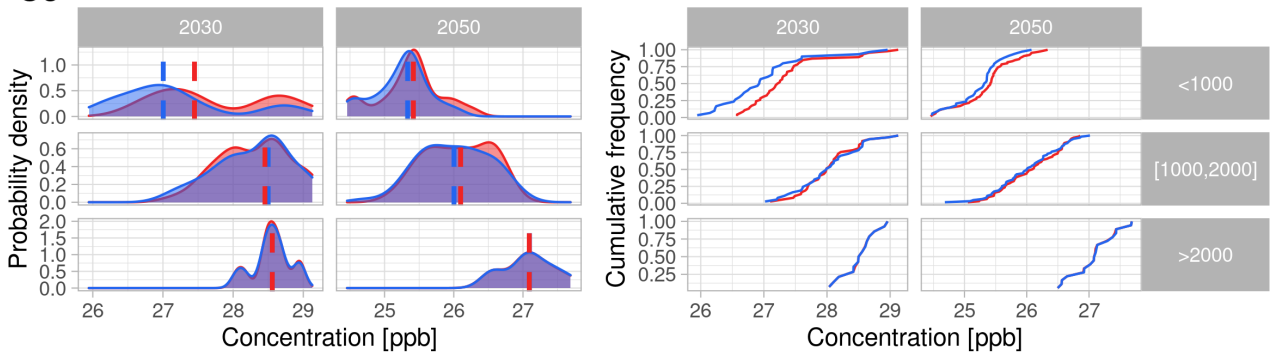
Figure 37: Probability density distribution (left) and cumulative frequency (right) for R10PAC-OECD for PM$_{2.5}$ and O$_3$ concentrations. Includes median line by climate policy. Data has been averaged by model and scenario.
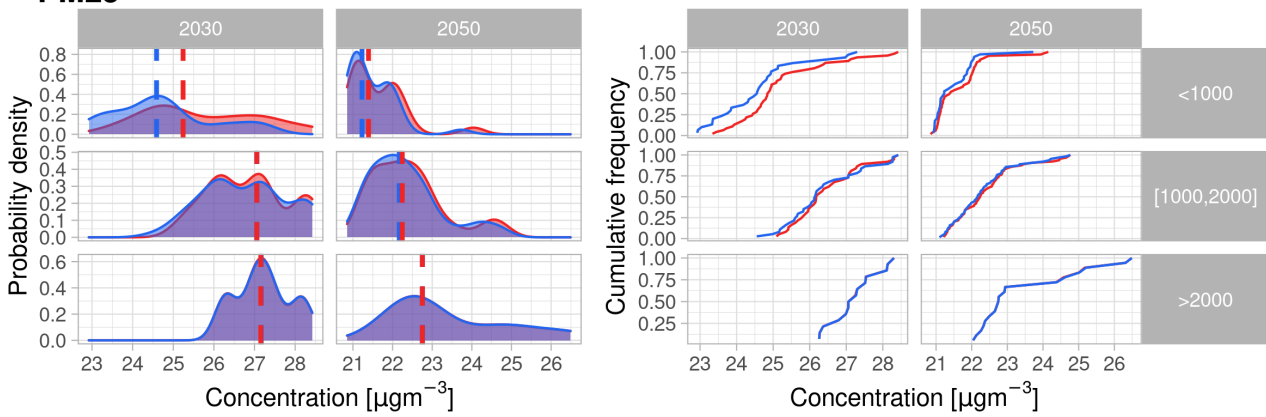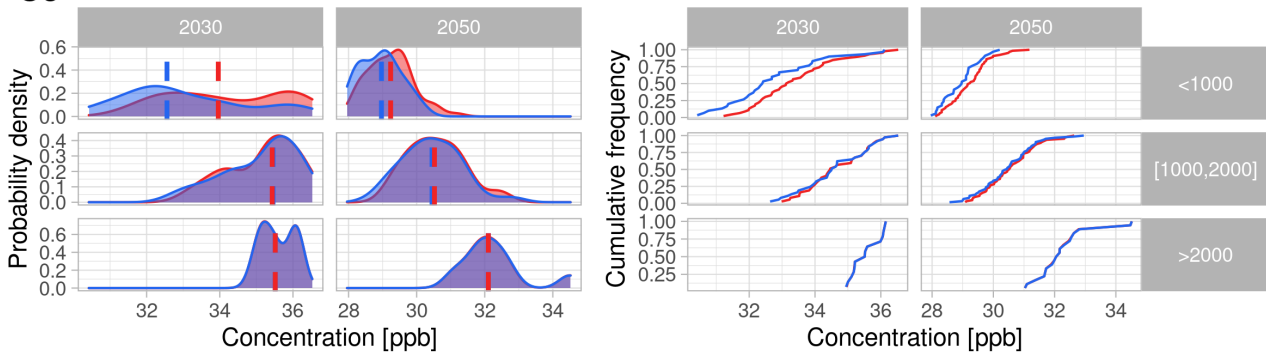
Figure 38: Probability density distribution (left) and cumulative frequency (right) for R10REF-ECON for PM$_{2.5}$ and O$_3$ concentrations. Includes median line by climate policy. Data has been averaged by model and scenario.
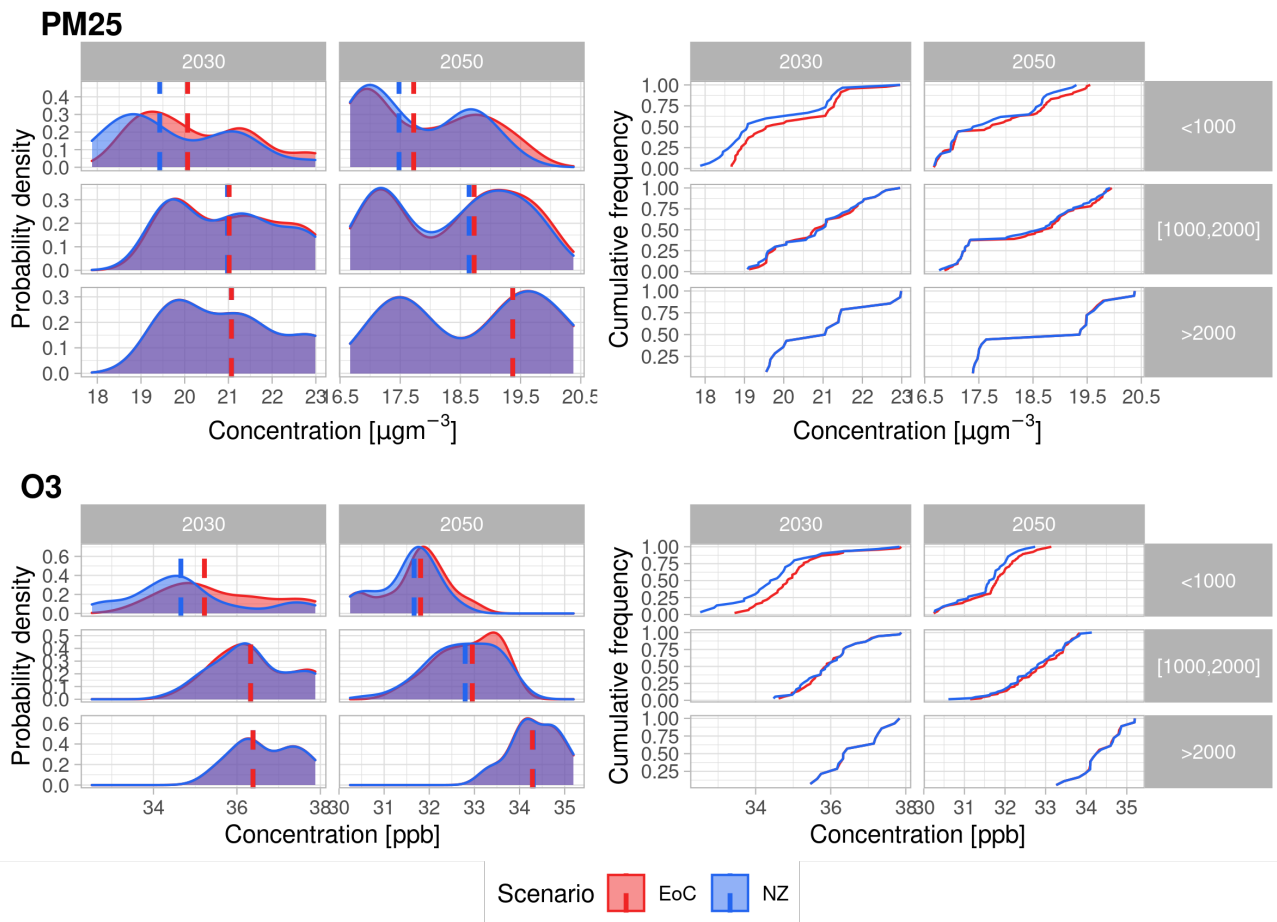
Figure 39: Probability density distribution (left) and cumulative frequency (right) for R10REST-ASIA for PM$_{2.5}$ and O$_3$ concentrations. Includes median line by climate policy. Data has been averaged by model and scenario.

D.2 Probability distribution and cumulative frequency whole grid concentrations graphs

Concentrations probability distribution and cumulative frequency of R10AFRICA
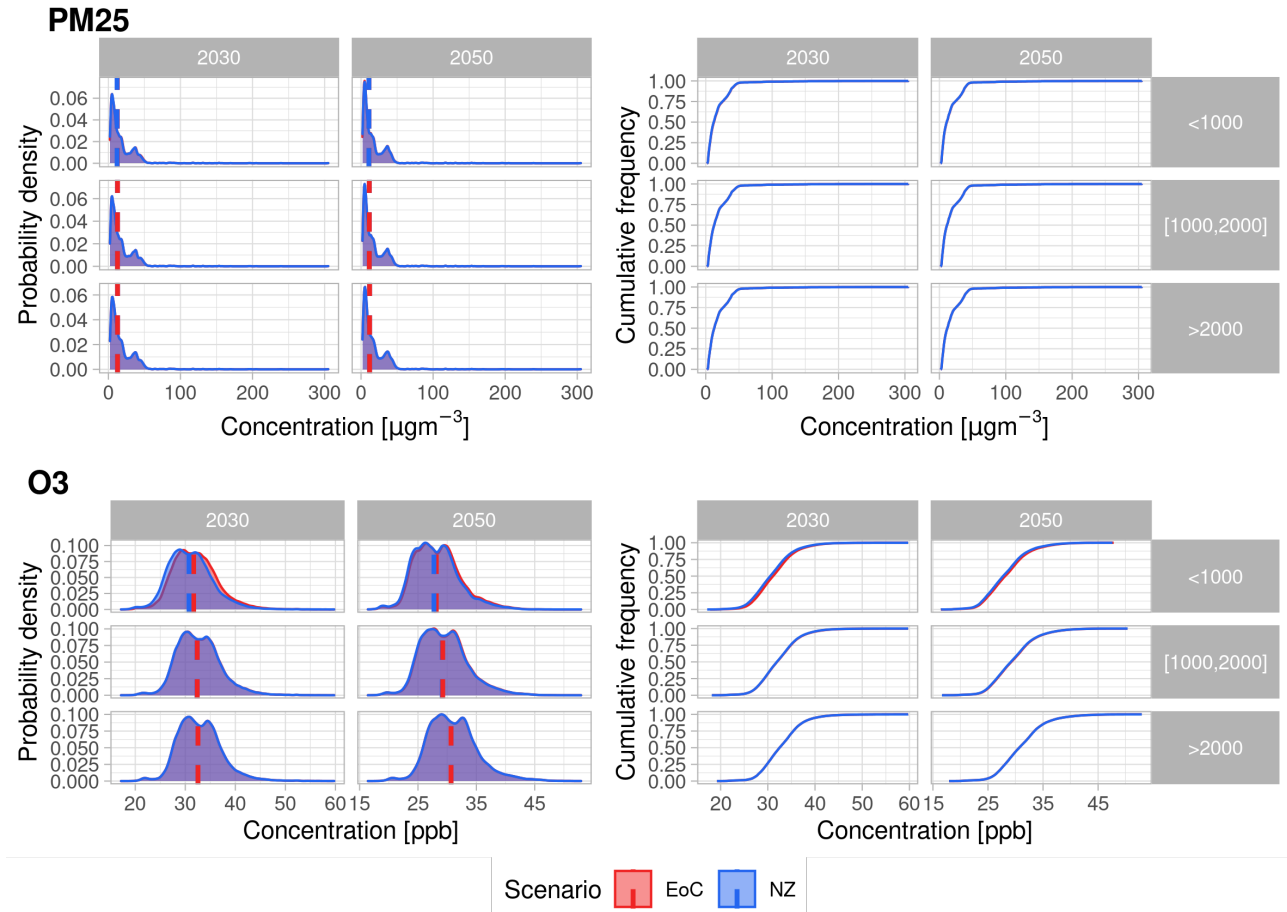
Figure 40: Probability density distribution (left) and cumulative frequency (right) for R10AFRICA for PM$_{2.5}$ and O$_3$ concentrations. Includes median line by climate policy. Data has not been averaged in any case except of World.
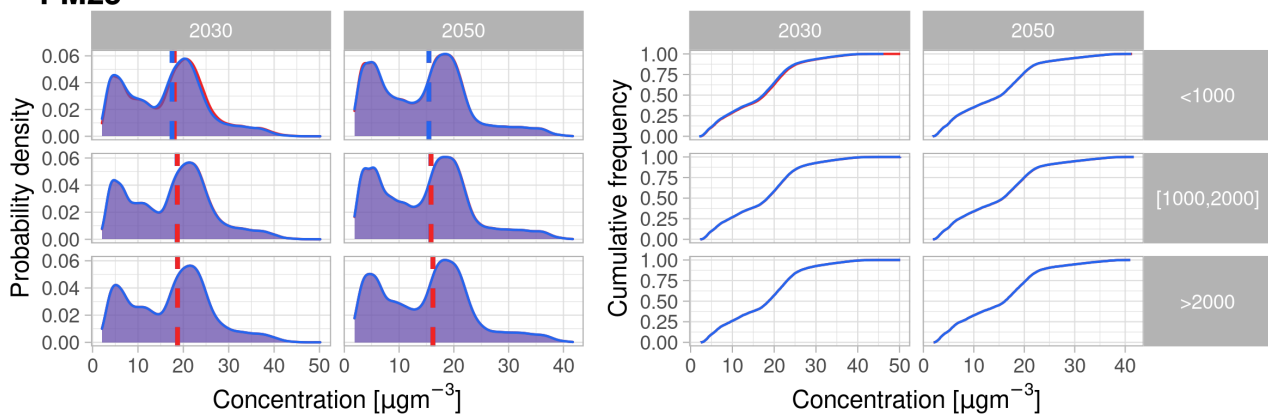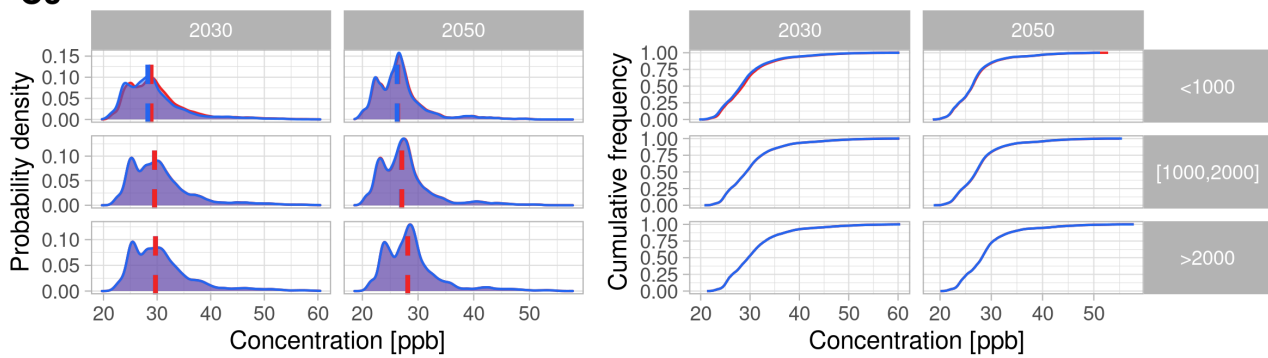
Figure 41: Probability density distribution (left) and cumulative frequency (right) for R10CHINA+ for $PM_{2.5}$ and O_3 concentrations. Includes median line by climate policy. Data has not been averaged in any case except of World.

Concentrations probability distribution and cumulative frequency of R10EUROPE

PM25

O3
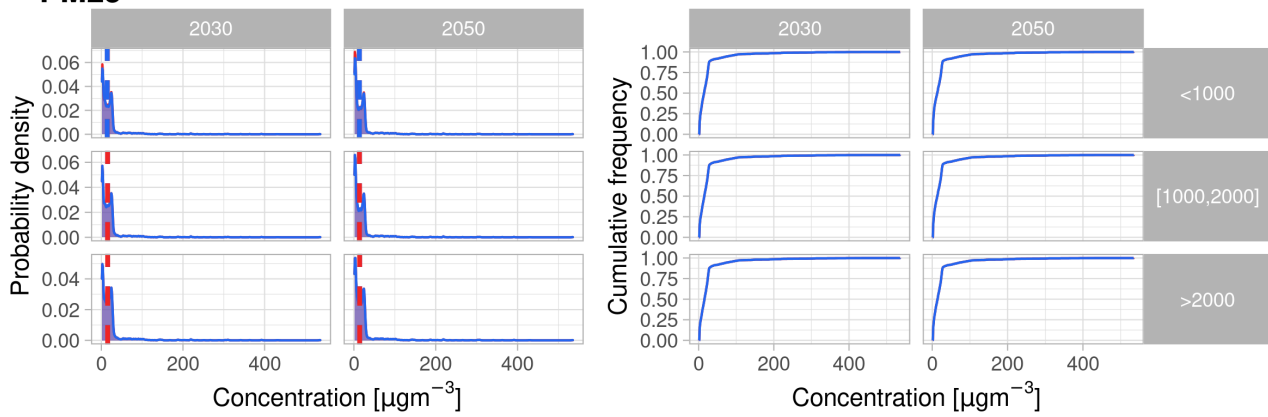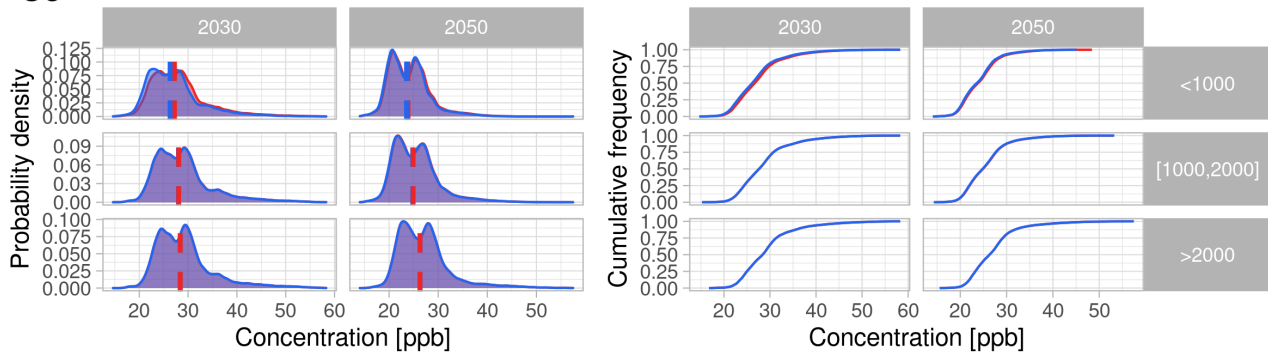
Figure 42: Probability density distribution (left) and cumulative frequency (right) for R10EUROPE for PM$_{2.5}$ and O$_3$ concentrations. Includes median line by climate policy. Data has not been averaged in any case except of World.
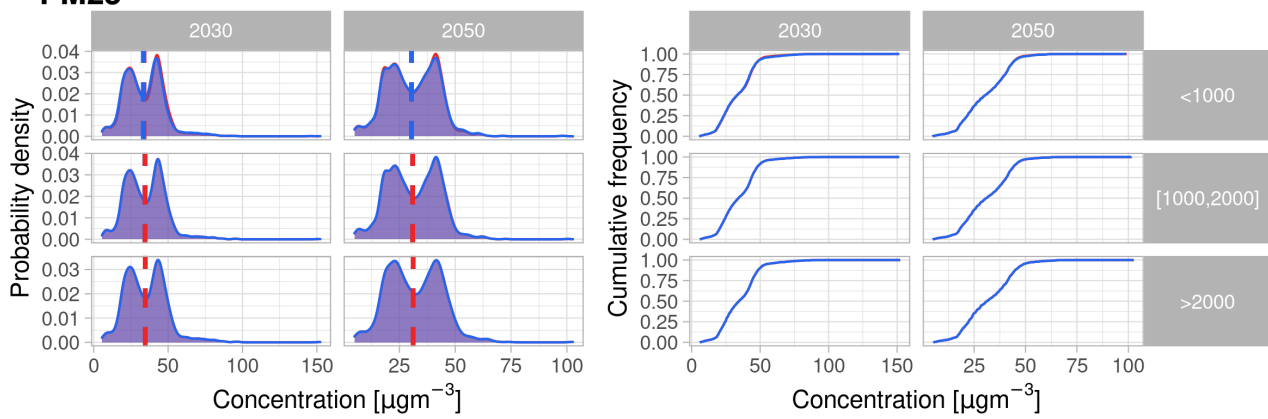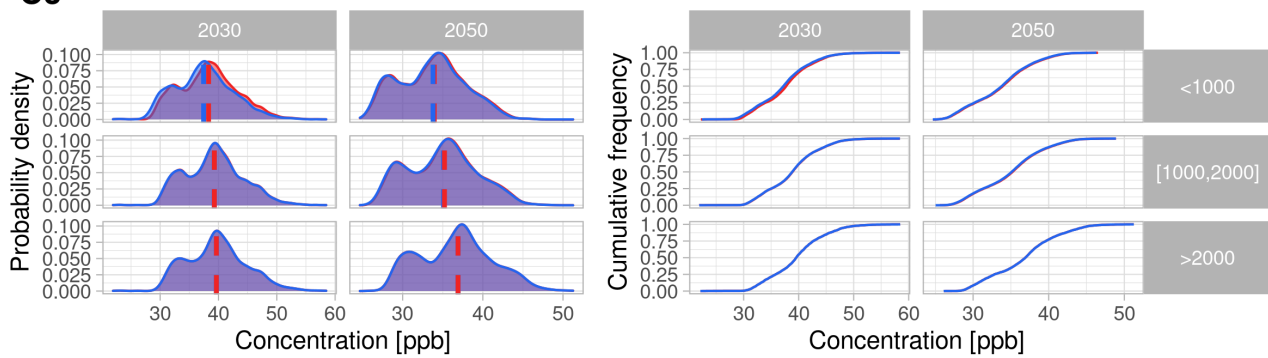
Figure 43: Probability density distribution (left) and cumulative frequency (right) for R10INDIA+ for PM$_{2.5}$ and O$_3$ concentrations. Includes median line by climate policy. Data has not been averaged in any case except of World.
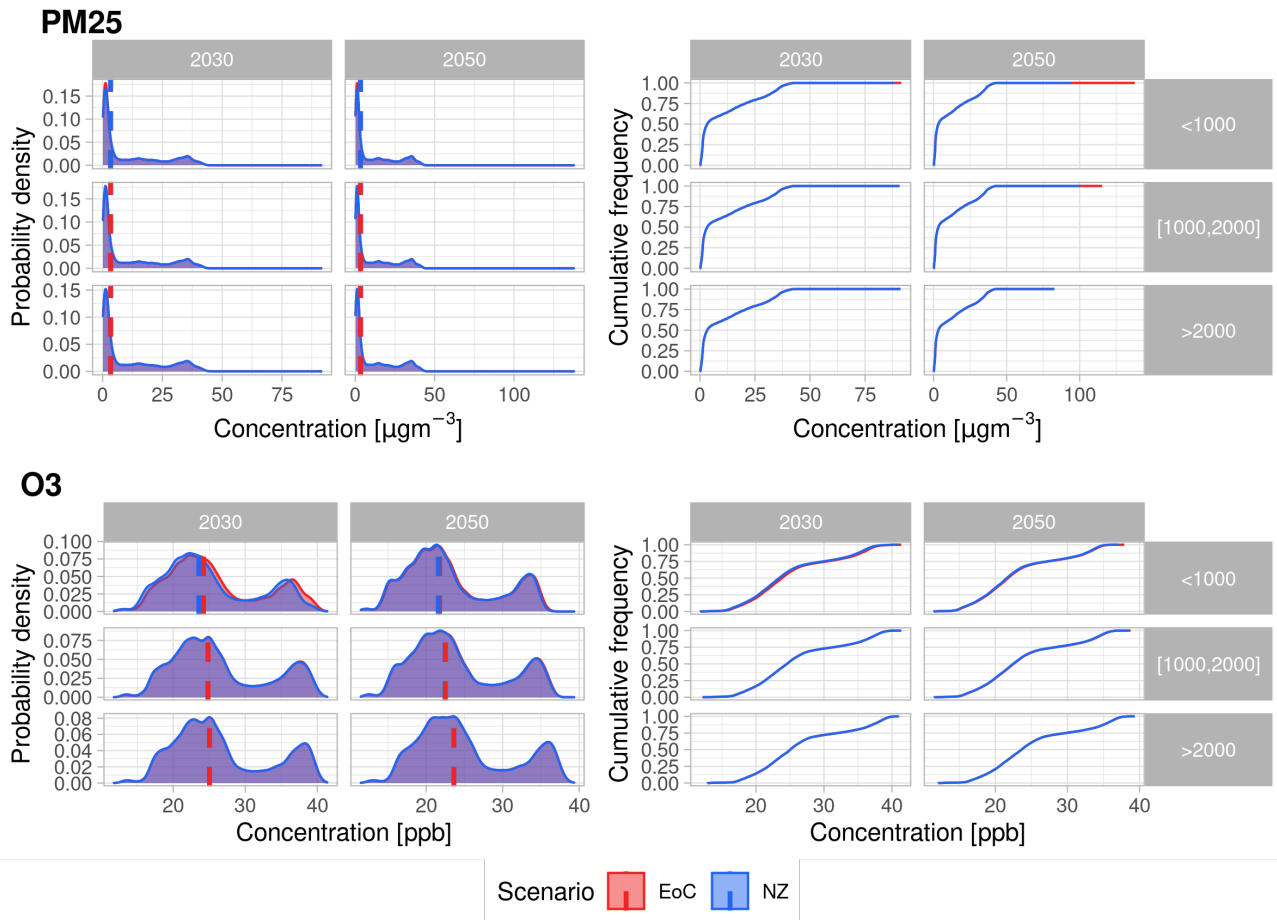
Figure 44: Probability density distribution (left) and cumulative frequency (right) for R10LATIN-AM for $PM_{2.5}$ and O_3 concentrations. Includes median line by climate policy. Data has not been averaged in any case except of World.
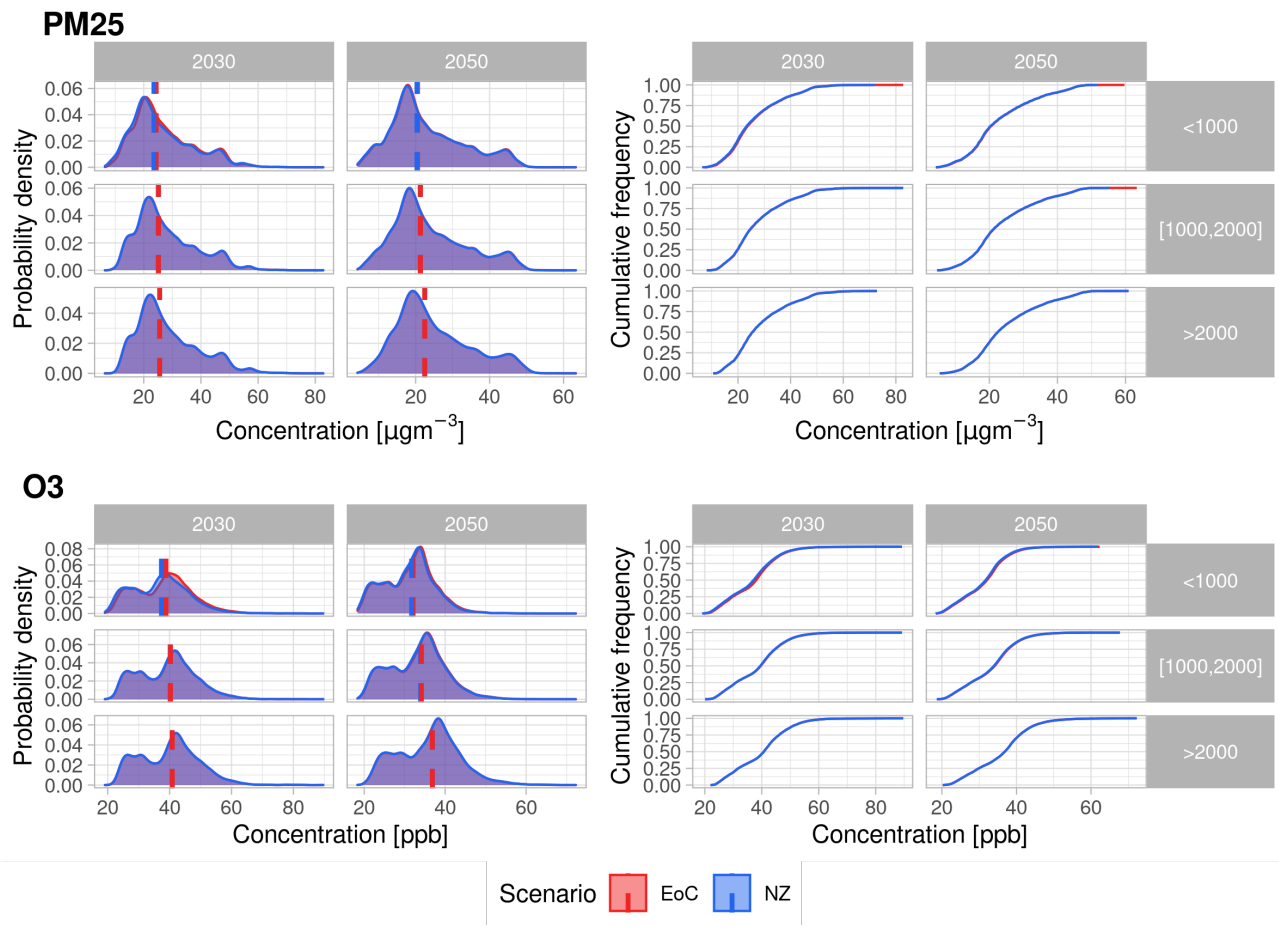
Figure 45: Probability density distribution (left) and cumulative frequency (right) for R10MIDDLE-EAST for $PM_{2.5}$ and O_3 concentrations. Includes median line by climate policy. Data has not been averaged in any case except of World.

Concentrations probability distribution and cumulative frequency of R10NORTH_AM
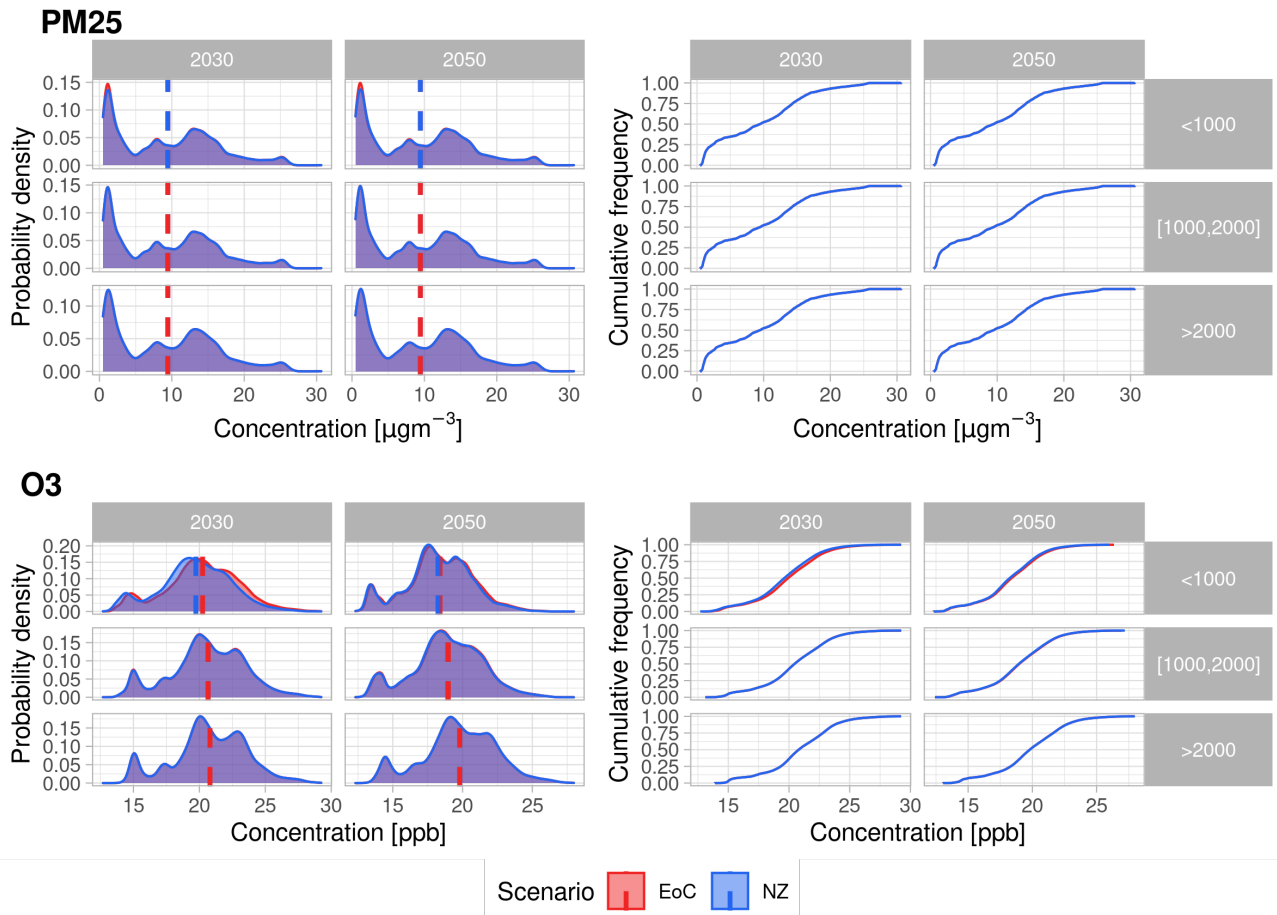
Figure 46: Probability density distribution (left) and cumulative frequency (right) for R10NORTH-AM for PM$_{2.5}$ and O$_3$ concentrations. Includes median line by climate policy. Data has not been averaged in any case except of World.

Concentrations probability distribution and cumulative frequency of R10PAC_OECD
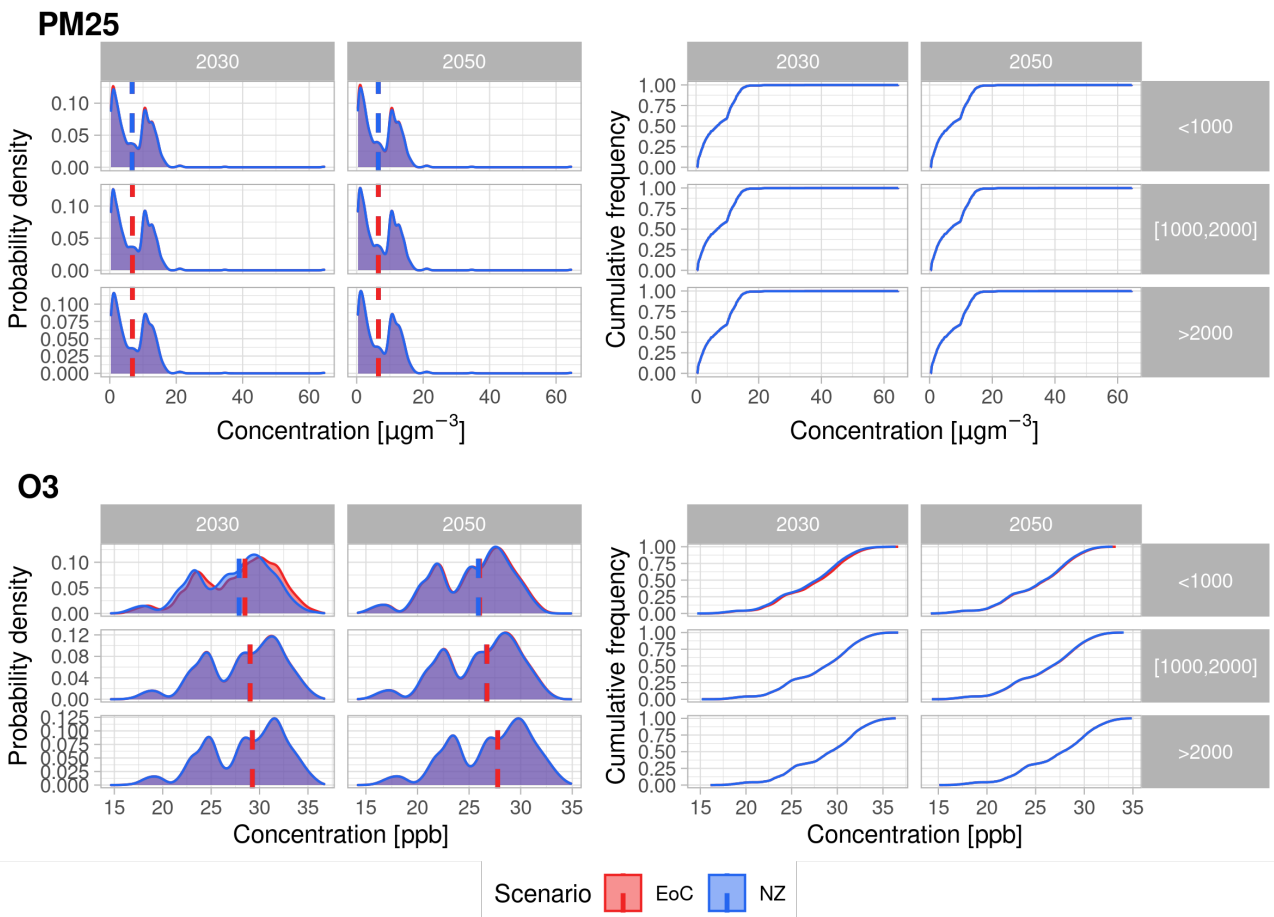
Figure 47: Probability density distribution (left) and cumulative frequency (right) for R10PAC-OECD for $PM_{2.5}$ and O_3 concentrations. Includes median line by climate policy. Data has not been averaged in any case except of World.
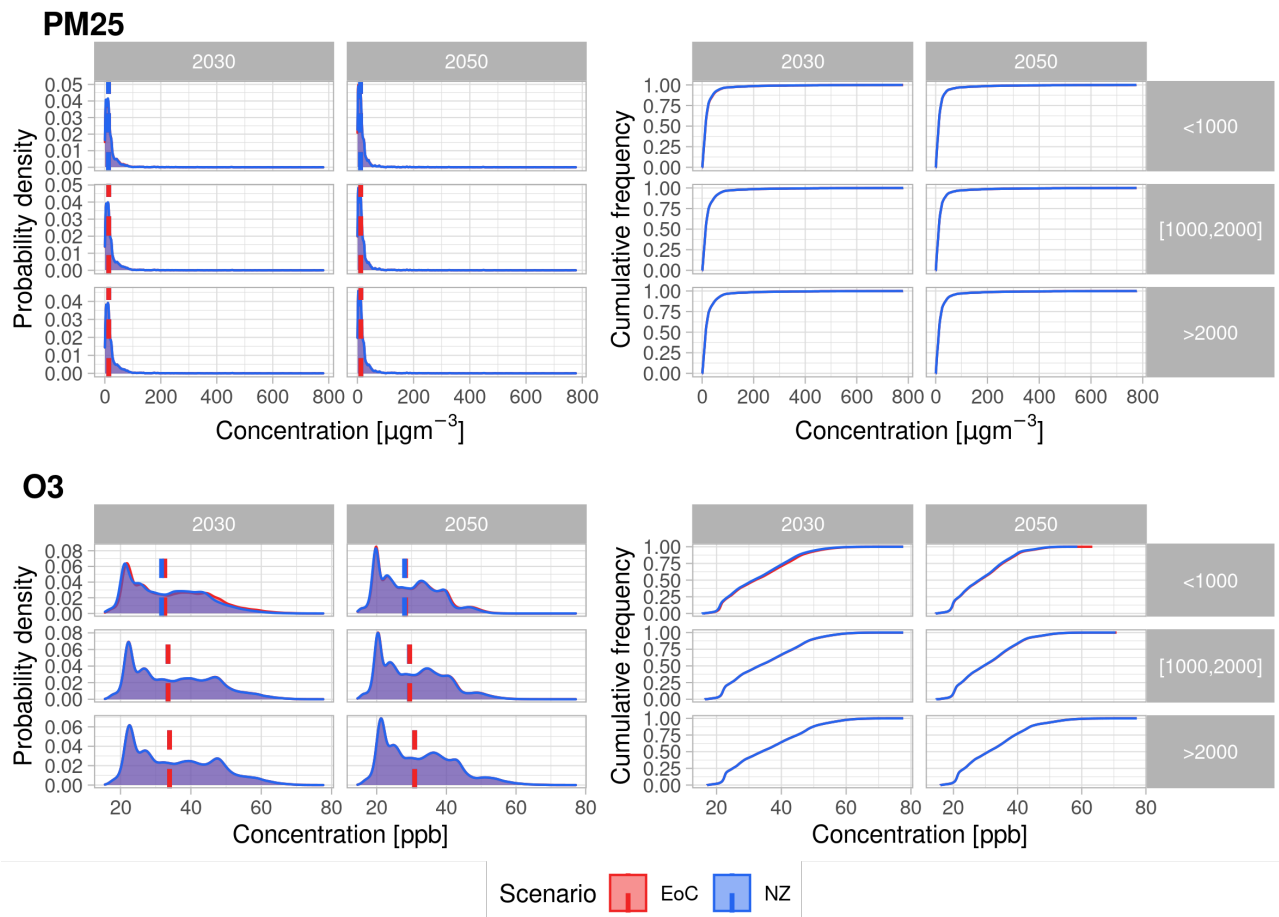
Figure 48: Probability density distribution (left) and cumulative frequency (right) for R10REF-ECON for $PM_{2.5}$ and O_3 concentrations. Includes median line by climate policy. Data has not been averaged in any case except of World.

Concentrations probability distribution and cumulative frequency of R10REST_ASIA
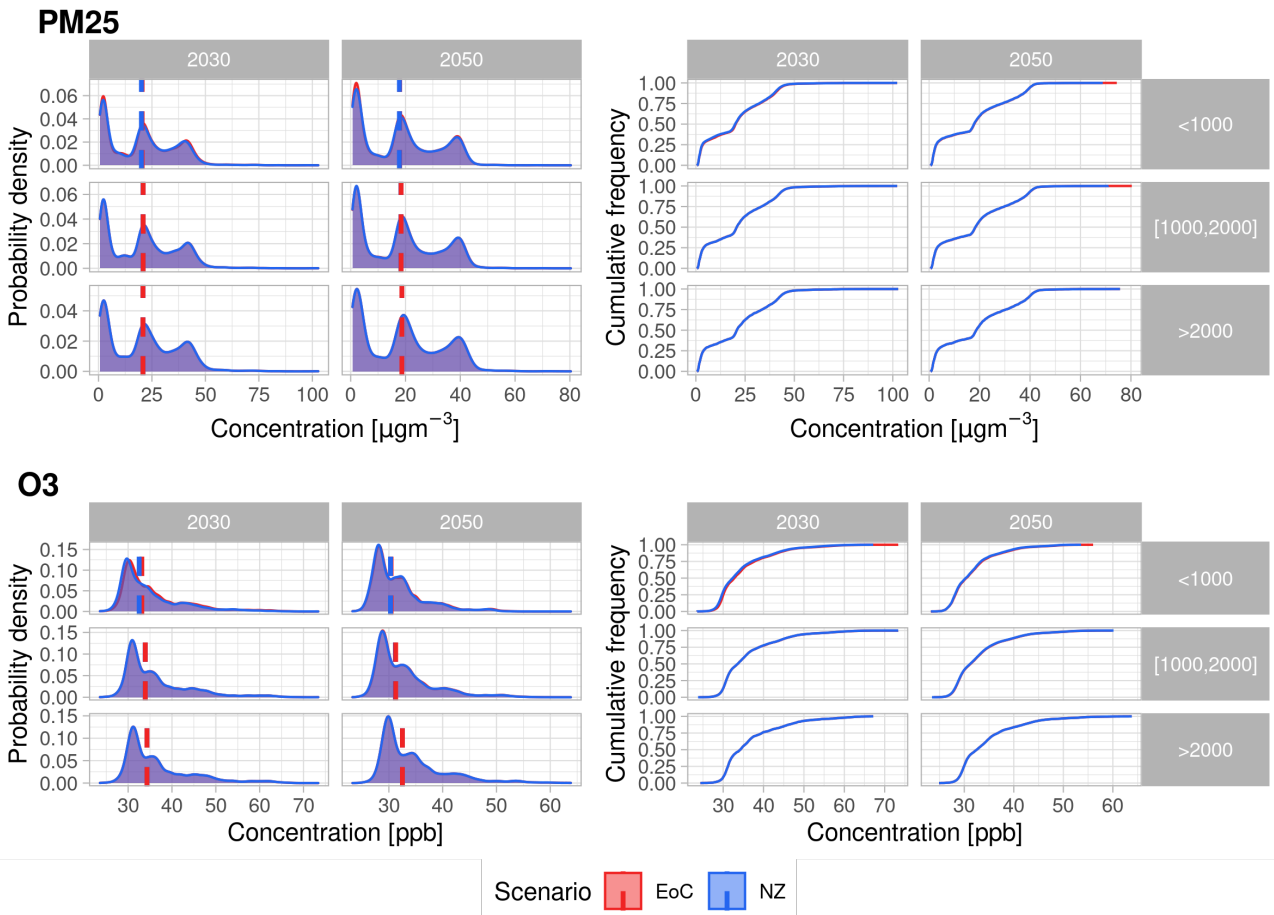
Figure 49: Probability density distribution (left) and cumulative frequency (right) for R10REST-ASIA for $PM_{2.5}$ and O_3 concentrations. Includes median line by climate policy. Data has not been averaged in any case except of World.
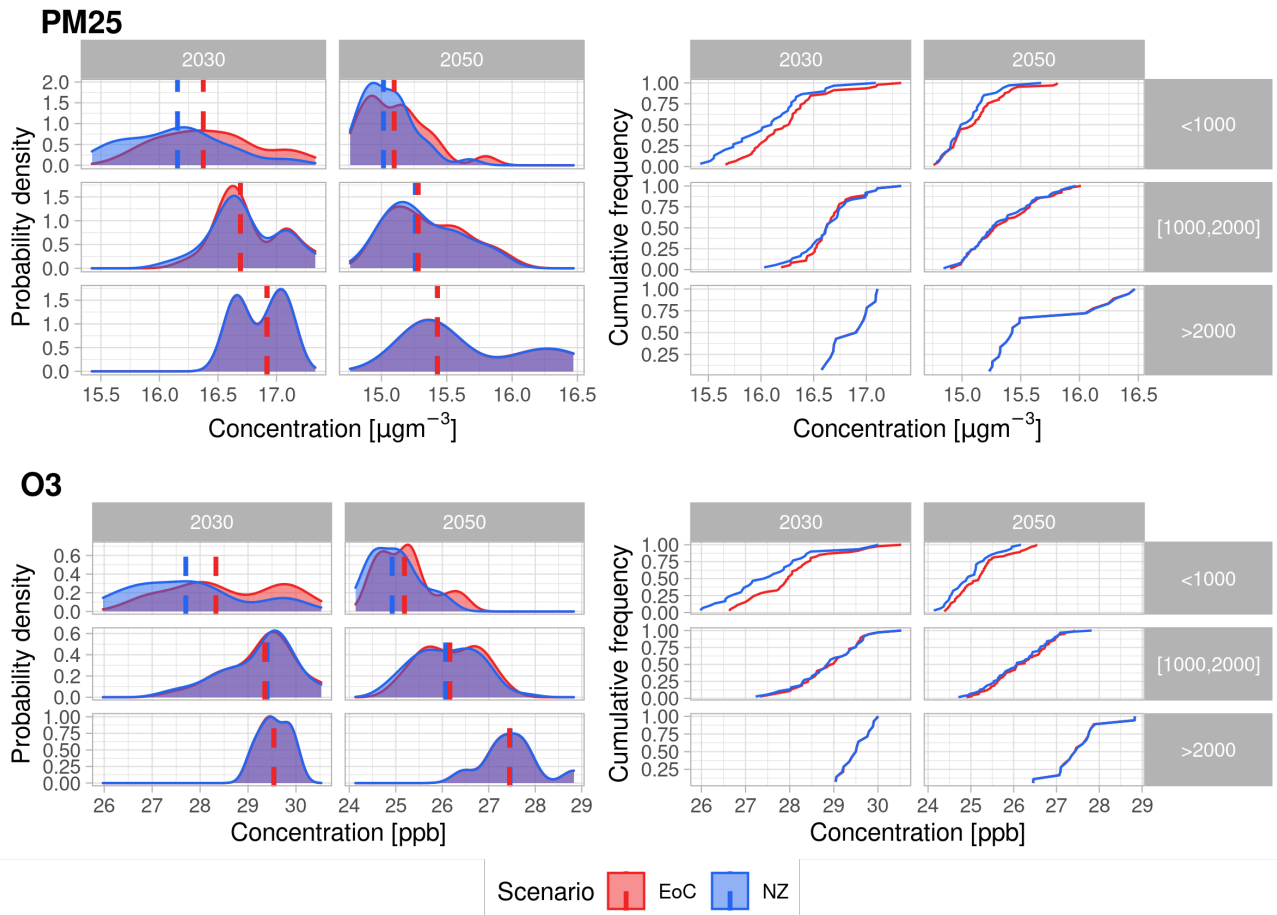
Figure 50: Probability density distribution (left) and cumulative frequency (right) for the whole globe for $PM_{2.5}$ and O_3 concentrations. Includes median line by climate policy. Data has not been averaged in any case except of World.

E. Premature deaths sensitivity and uncertainty

E.1 Probability distribution and cumulative frequency mortality graphs
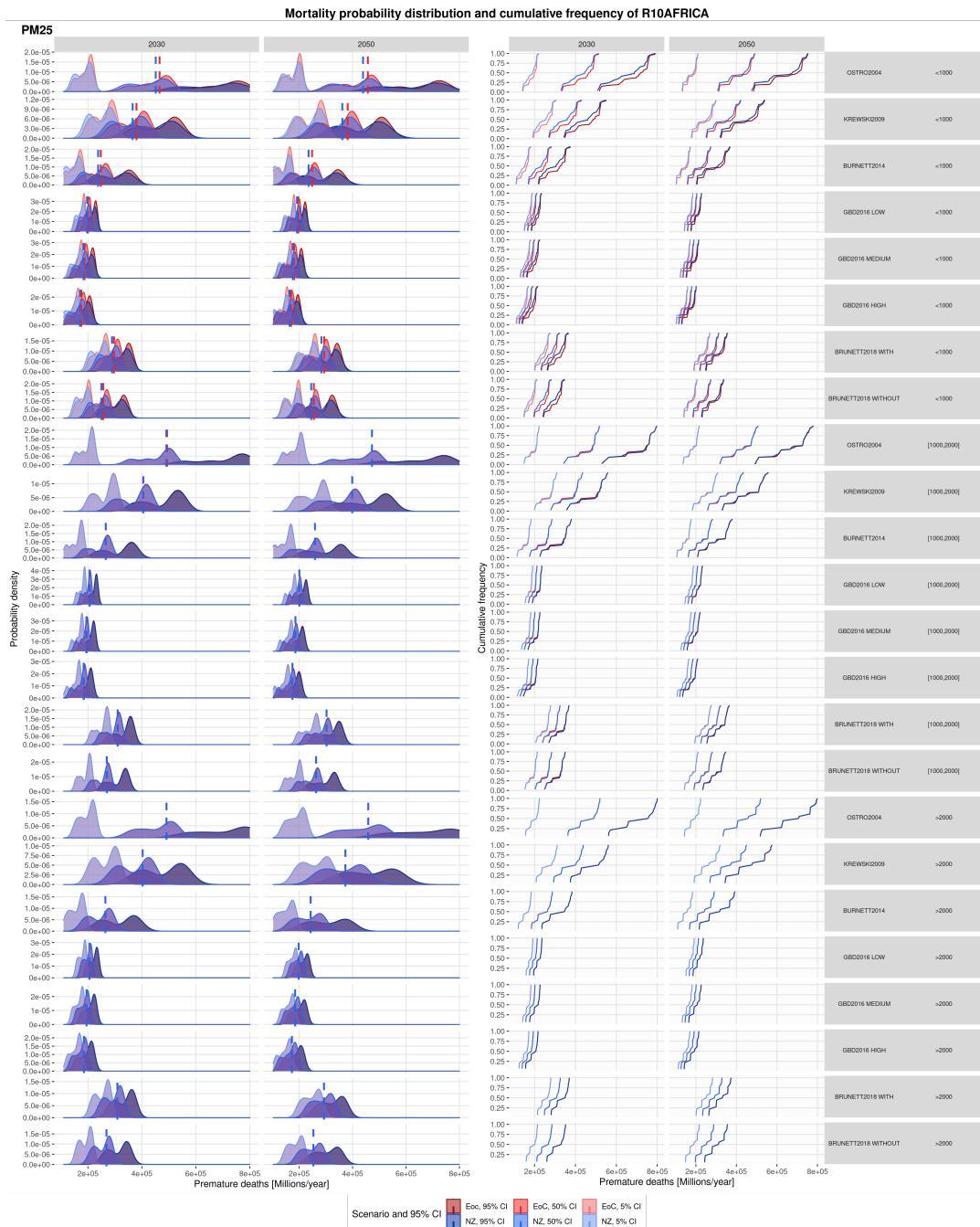
Figure 51: Probability density distribution (left) and cumulative frequency (right) for R10AFRICA for PM$_{2.5}$. Includes median line by climate policy.
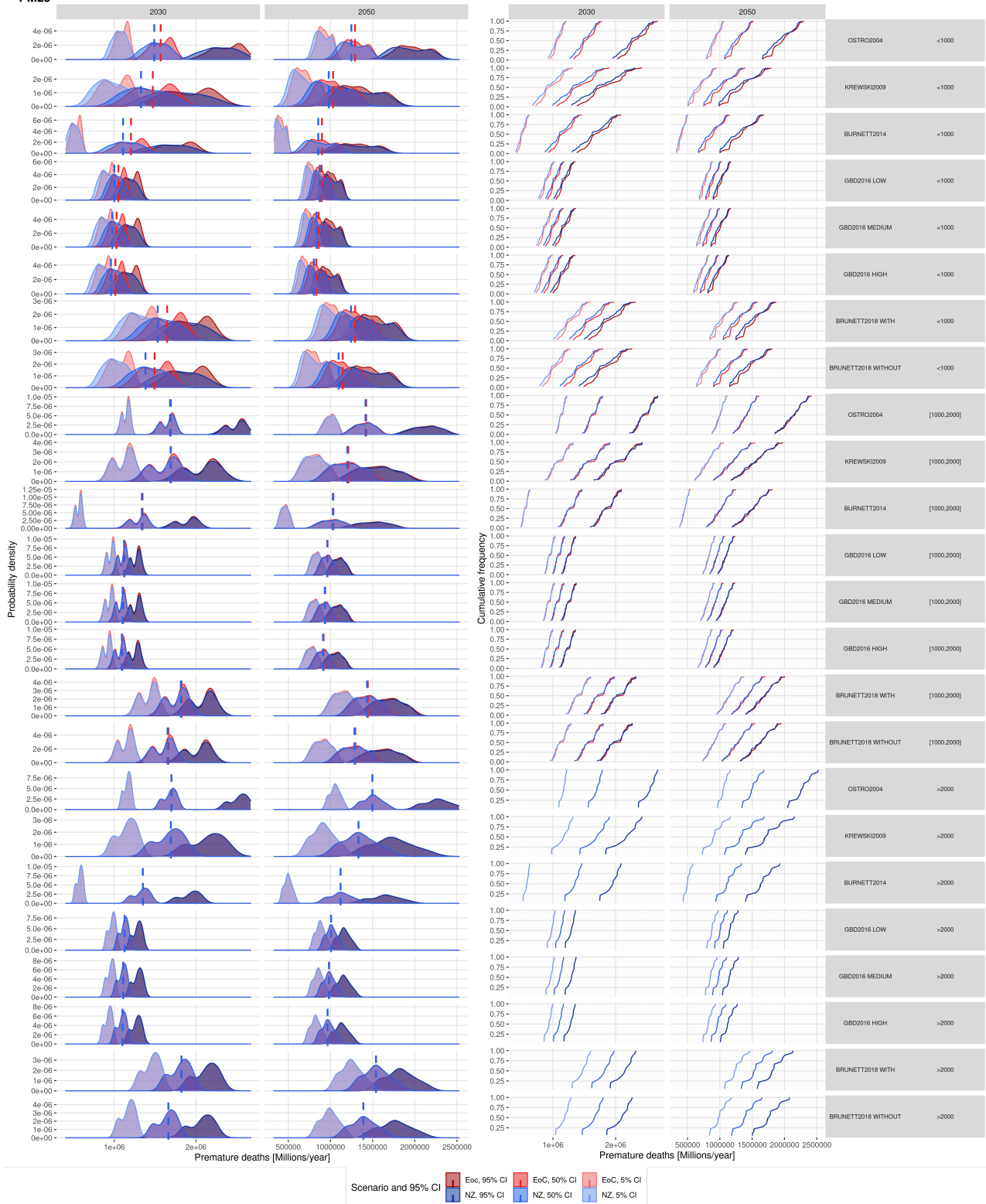
Figure 52: Probability density distribution (left) and cumulative frequency (right) for R10CHINA+ for PM$_{2.5}$. Includes median line by climate policy.
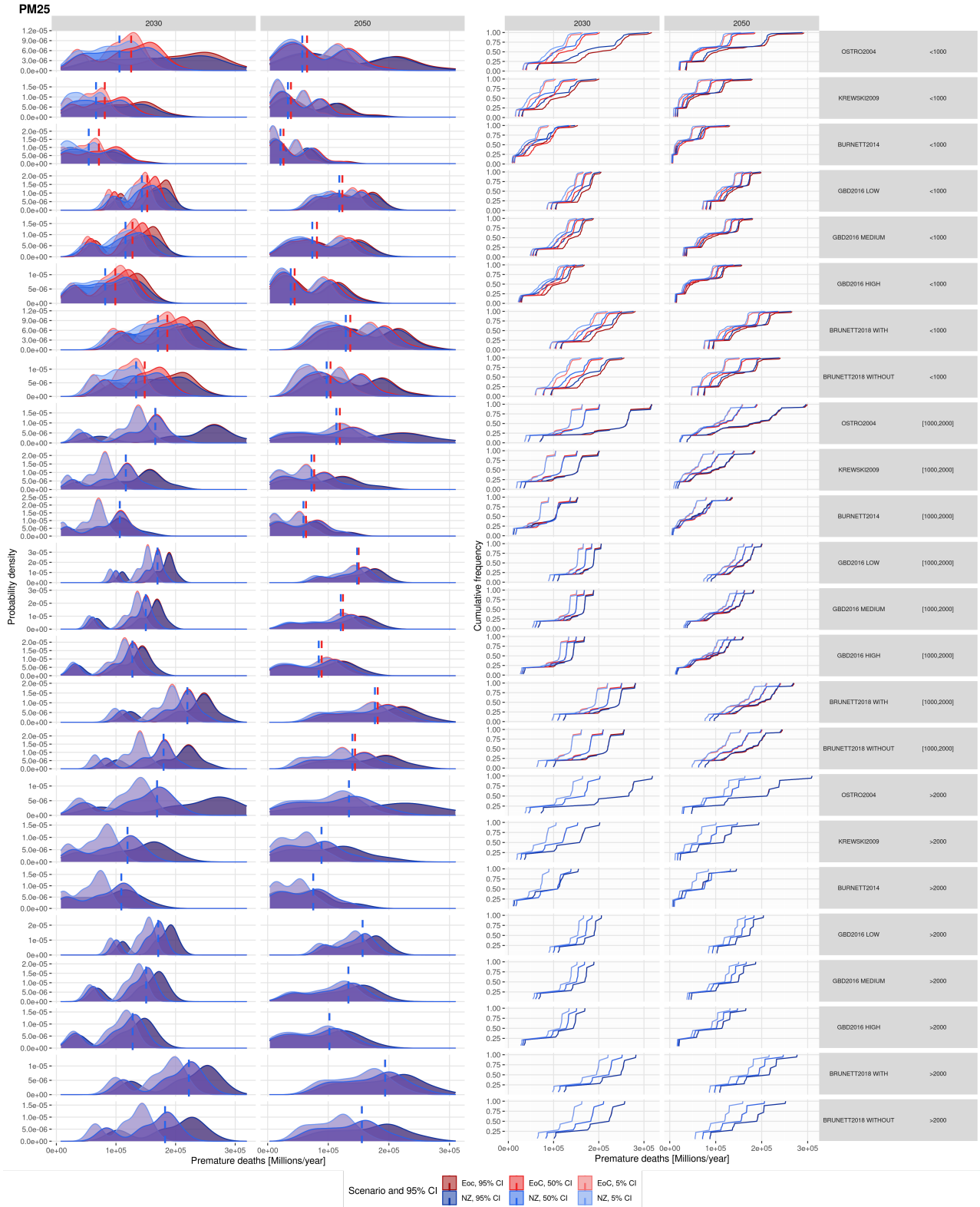
Figure 53: Probability density distribution (left) and cumulative frequency (right) for R10EUROPE for PM$_{2.5}$. Includes median line by climate policy.
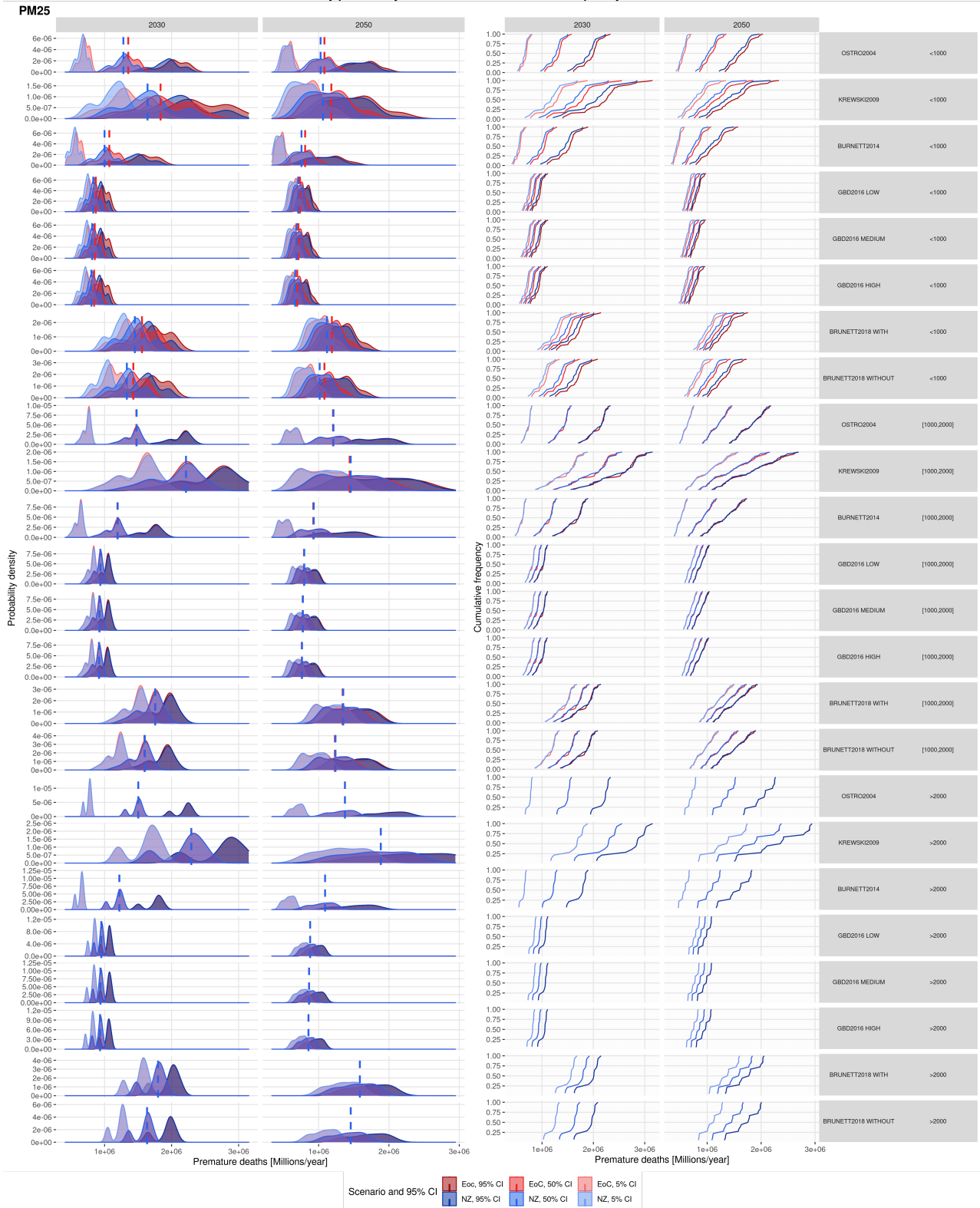
Figure 54: Probability density distribution (left) and cumulative frequency (right) for R10INDIA+ for PM$_{2.5}$. Includes median line by climate policy.
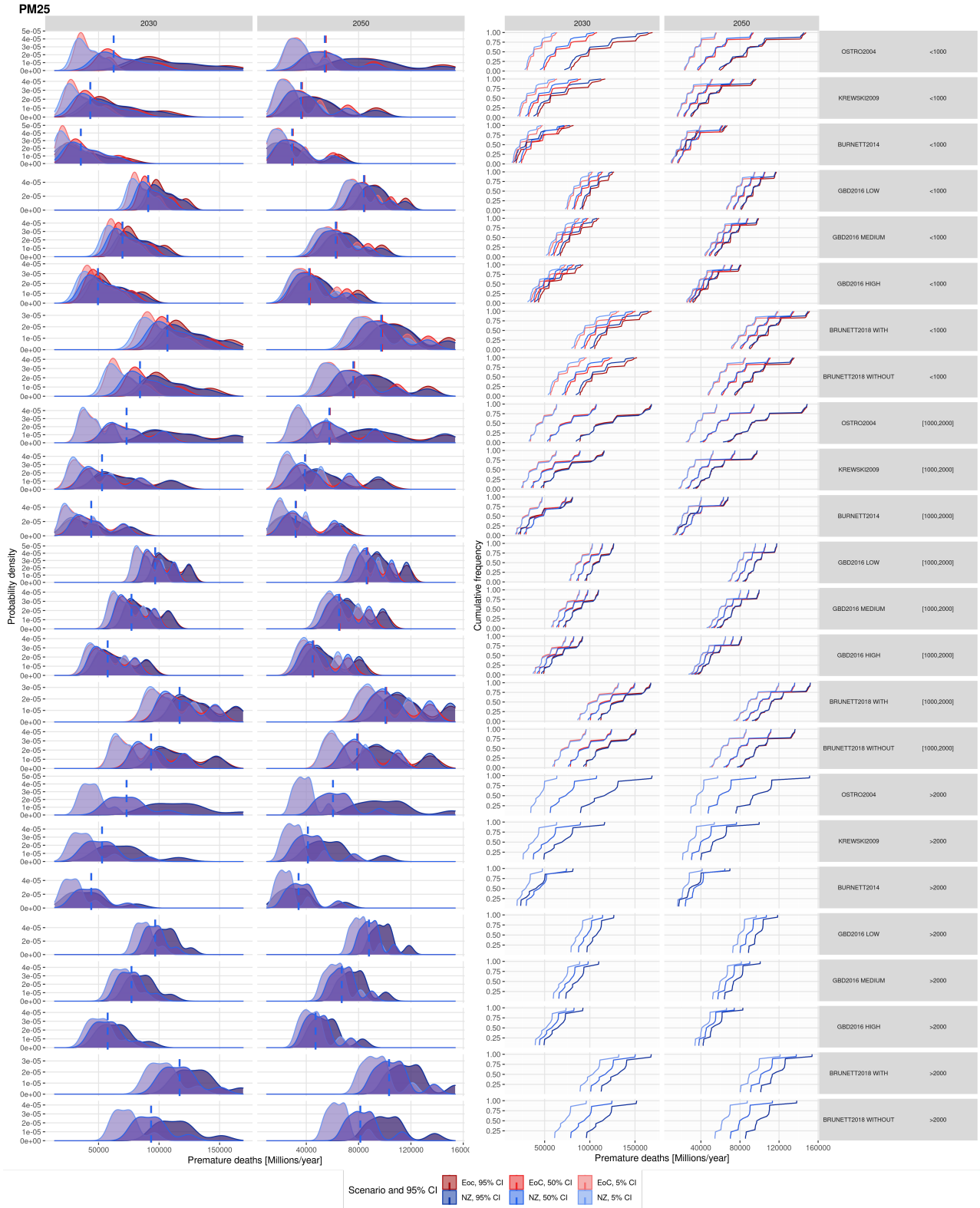
Figure 55: Probability density distribution (left) and cumulative frequency (right) for R10LATIN-AM for PM$_{2.5}$. Includes median line by climate policy.
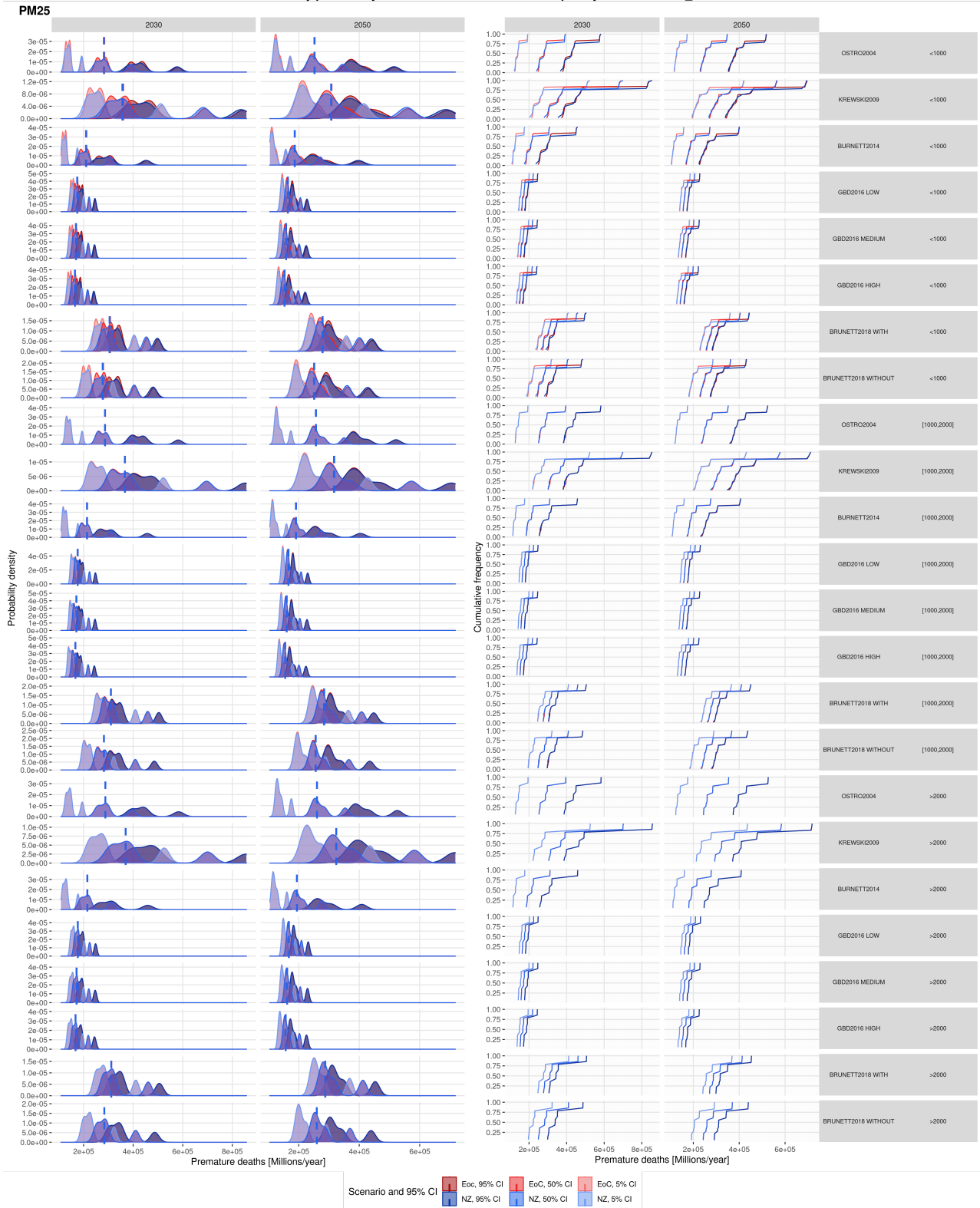
Figure 56: Probability density distribution (left) and cumulative frequency (right) for R10MIDDLE-EAST for PM$_{2.5}$. Includes median line by climate policy.
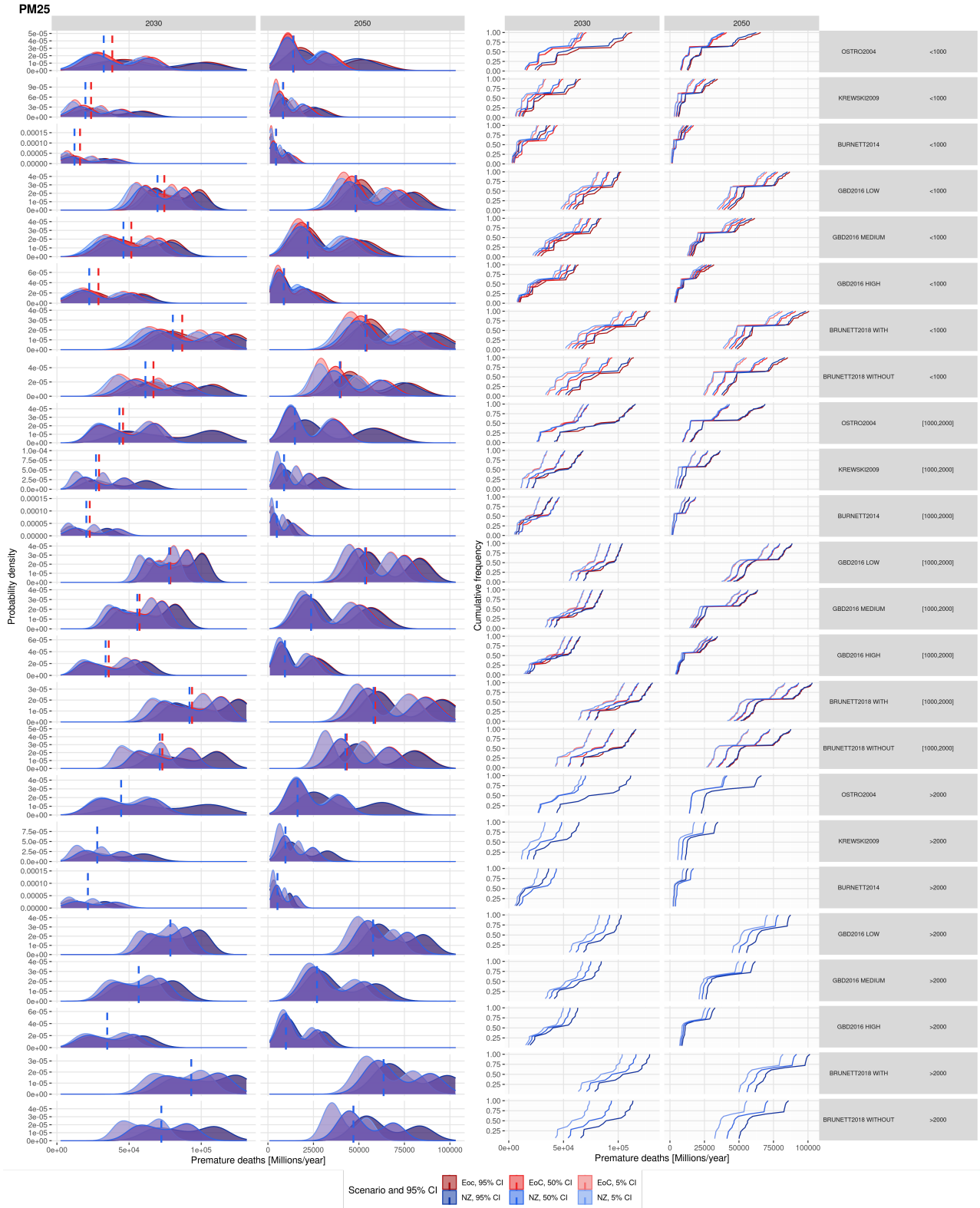
Figure 57: Probability density distribution (left) and cumulative frequency (right) for R10NORTH-AM for PM$_{2.5}$. Includes median line by climate policy.
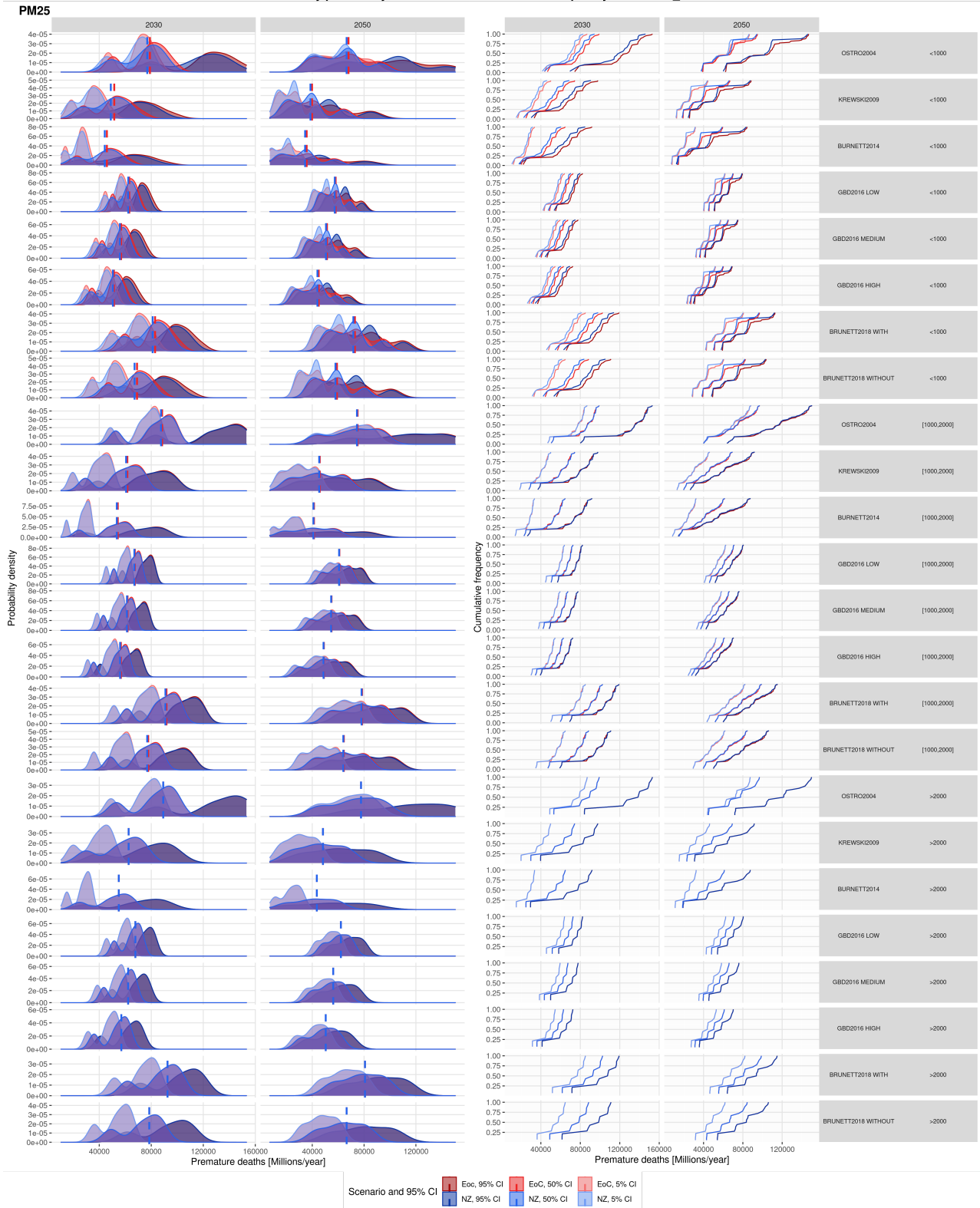
Figure 58: Probability density distribution (left) and cumulative frequency (right) for R10PAC-OECD for PM$_{2.5}$. Includes median line by climate policy.
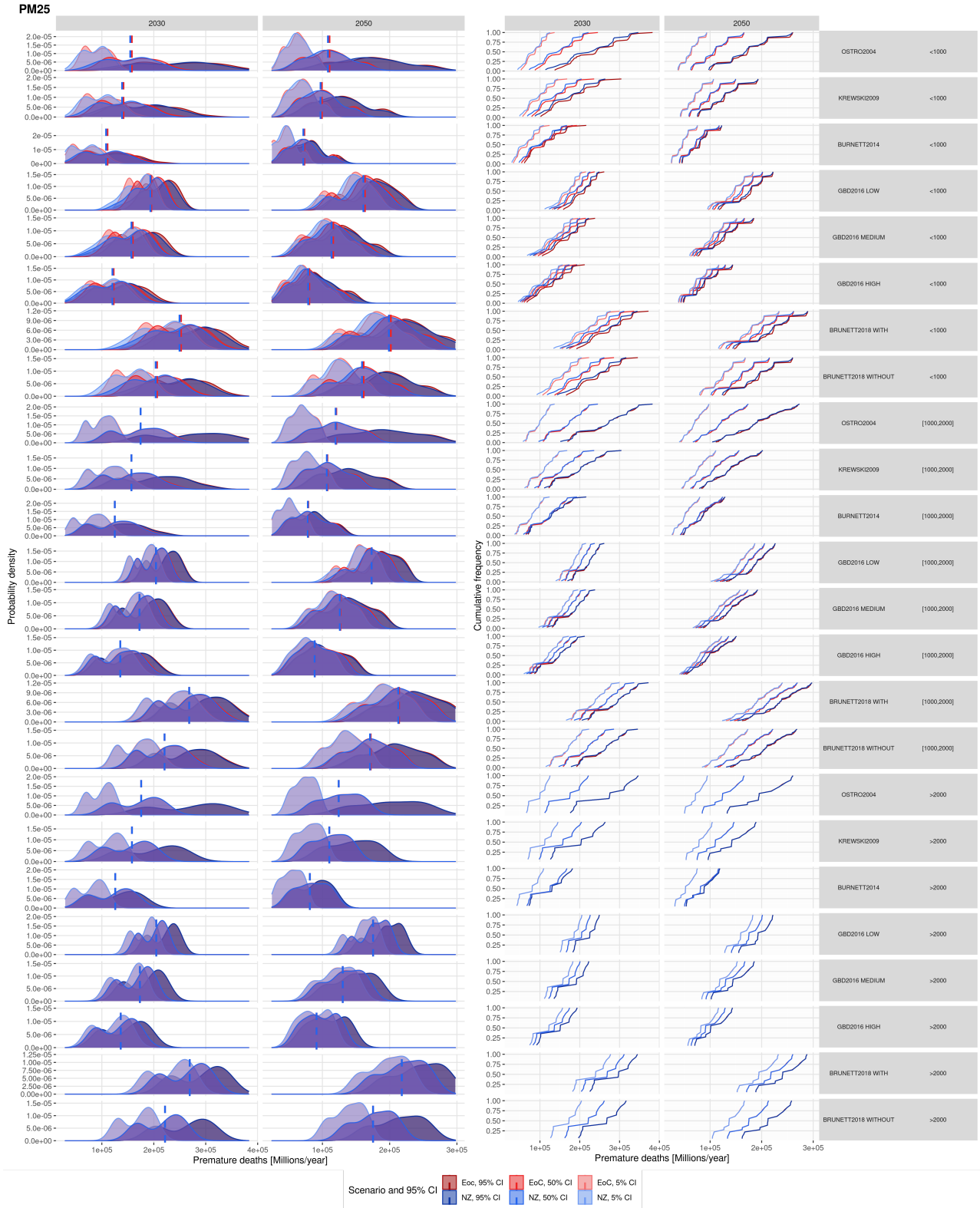
Figure 59: Probability density distribution (left) and cumulative frequency (right) for R10REF-ECON for PM$_{2.5}$. Includes median line by climate policy.
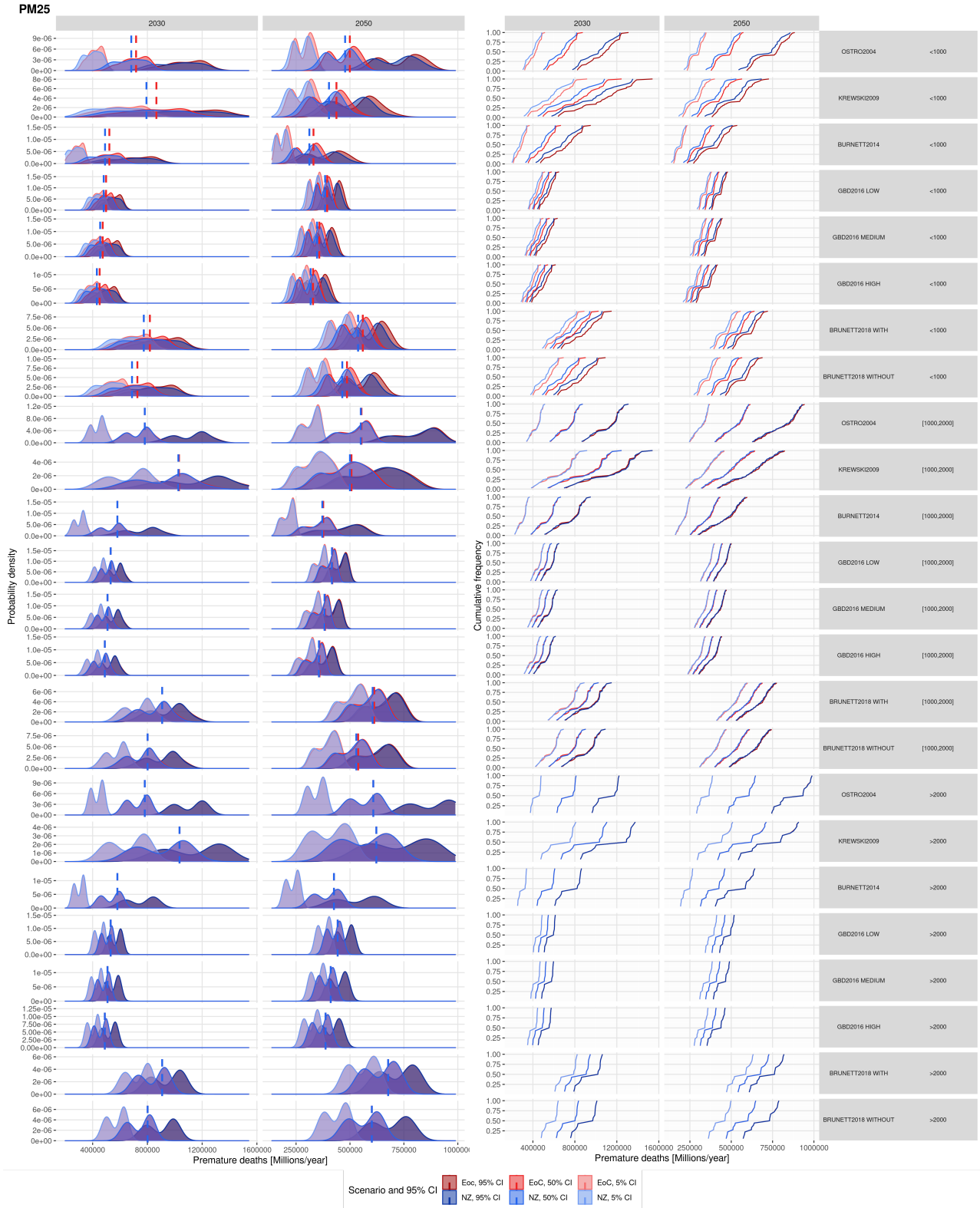
Figure 60: Probability density distribution (left) and cumulative frequency (right) for R10REST-ASIA for PM$_{2.5}$. Includes median line by climate policy.
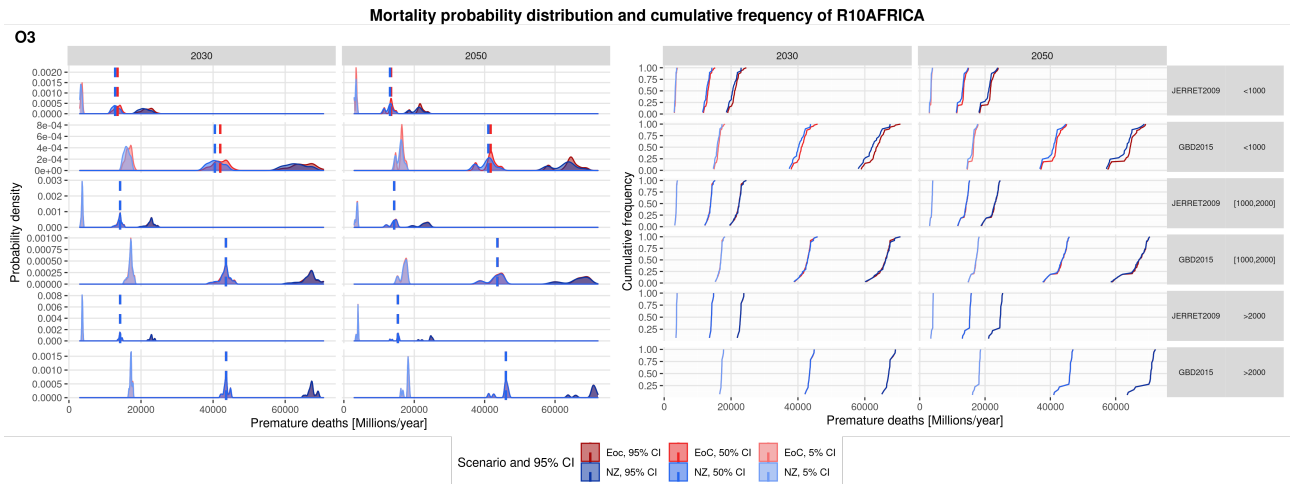
Figure 61: Probability density distribution (left) and cumulative frequency (right) for R10AFRICA for O$_3$. Includes median line by climate policy.
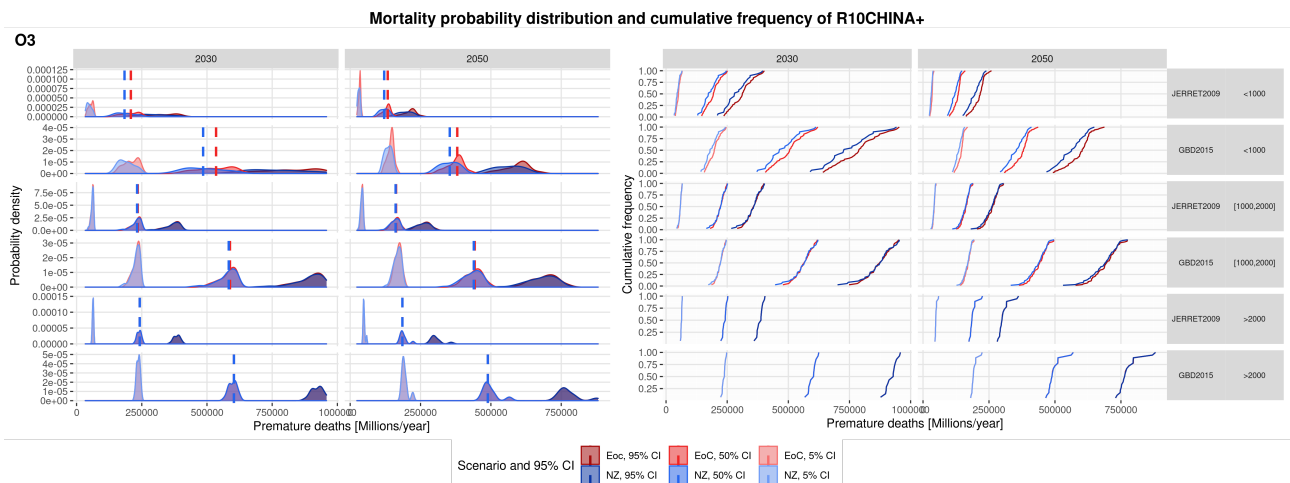
Figure 62: Probability density distribution (left) and cumulative frequency (right) for R10CHINA+ for O$_3$. Includes median line by climate policy.
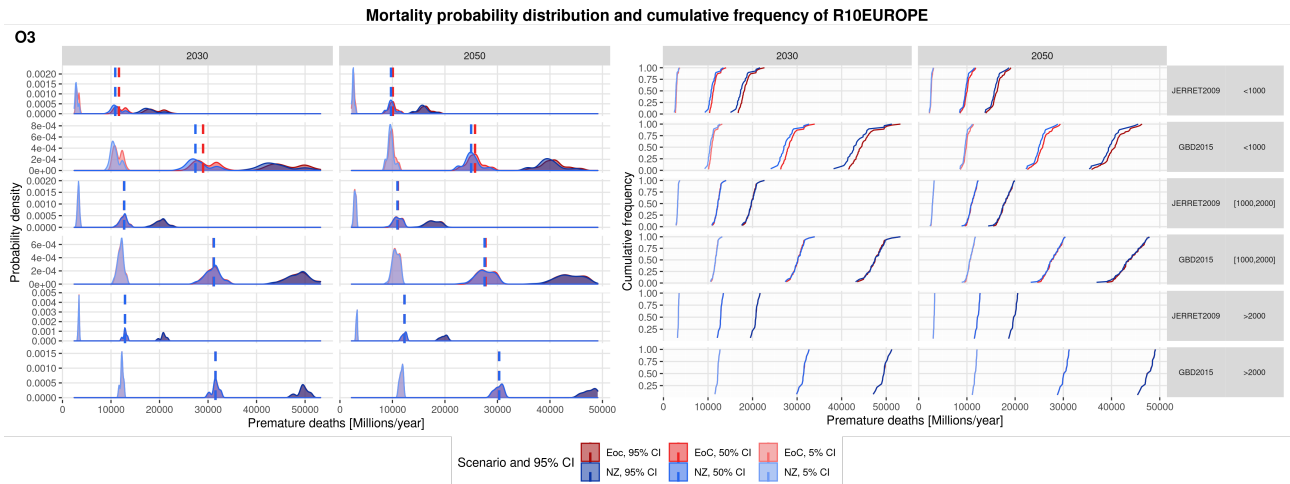
Figure 63: Probability density distribution (left) and cumulative frequency (right) for R10EUROPE for O_3. Includes median line by climate policy.
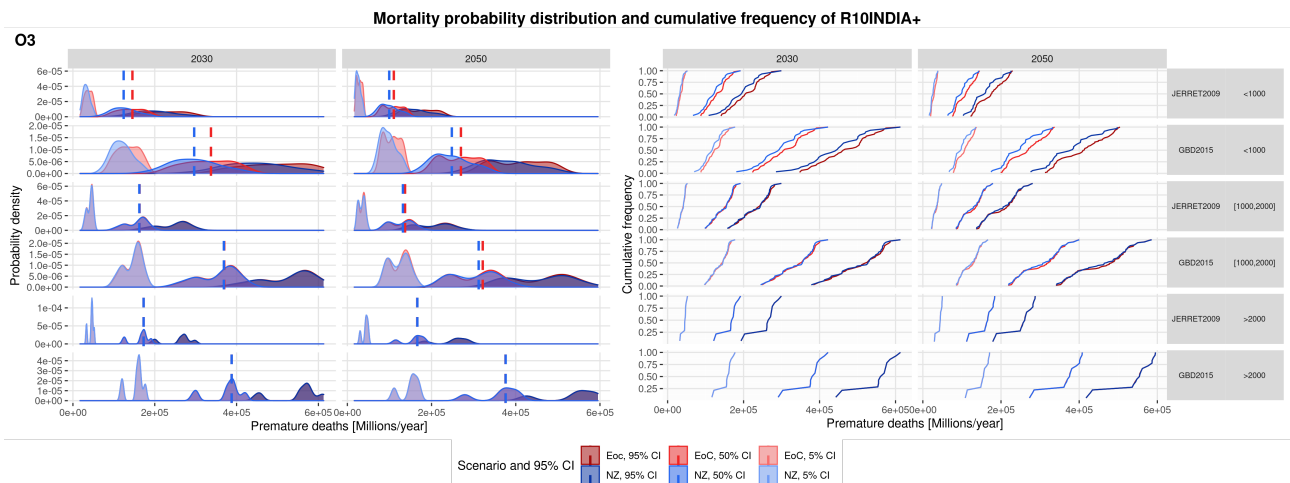
Figure 64: Probability density distribution (left) and cumulative frequency (right) for R10INDIA+ for O_3. Includes median line by climate policy.
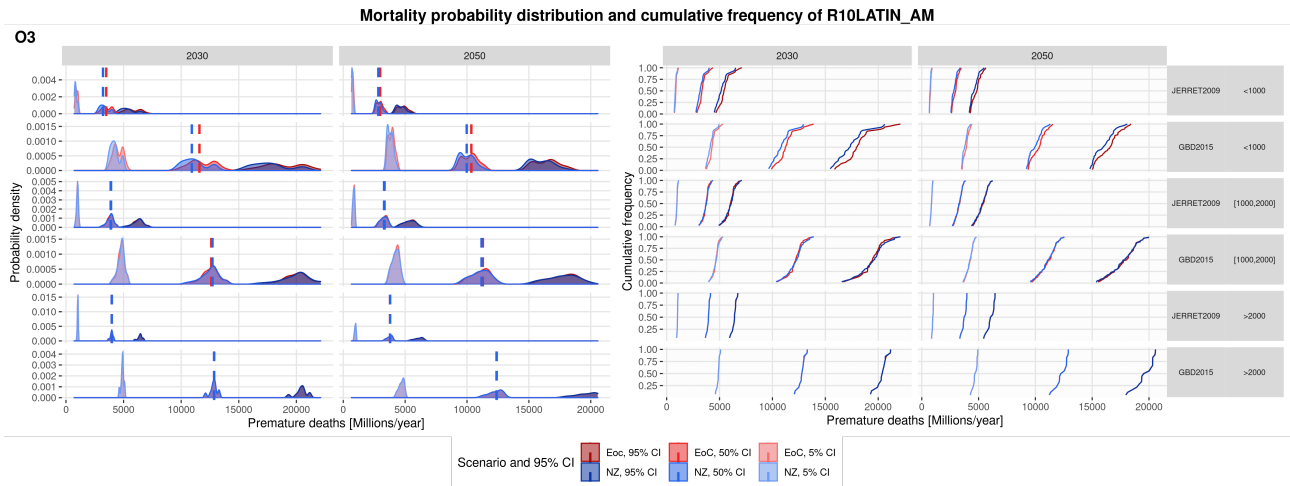
Figure 65: Probability density distribution (left) and cumulative frequency (right) for R10LATIN-AM for O_3. Includes median line by climate policy.
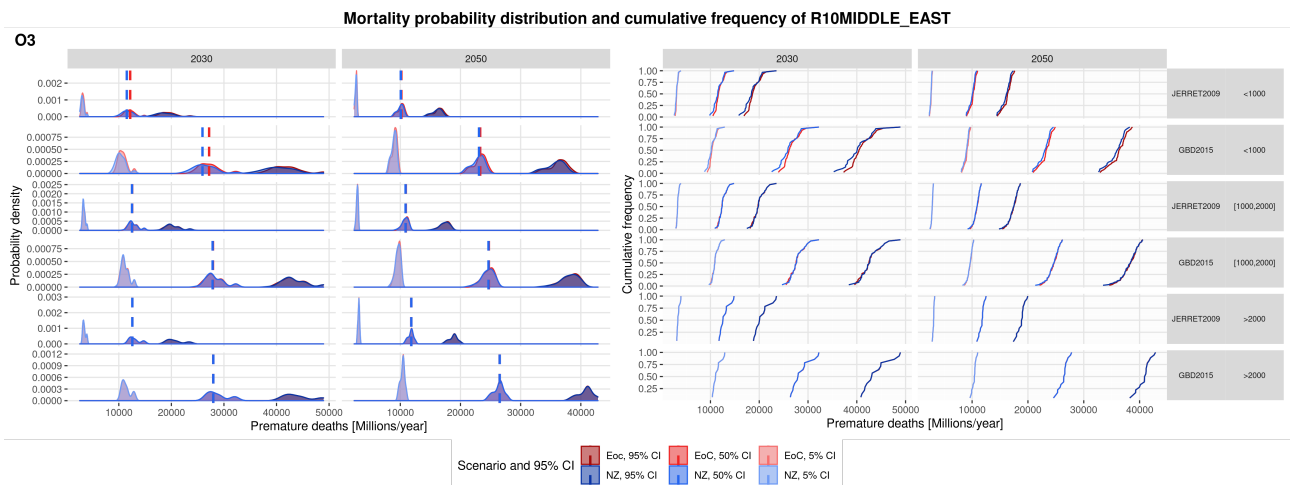
Figure 66: Probability density distribution (left) and cumulative frequency (right) for R10MIDDLE-EAST for O_3. Includes median line by climate policy.
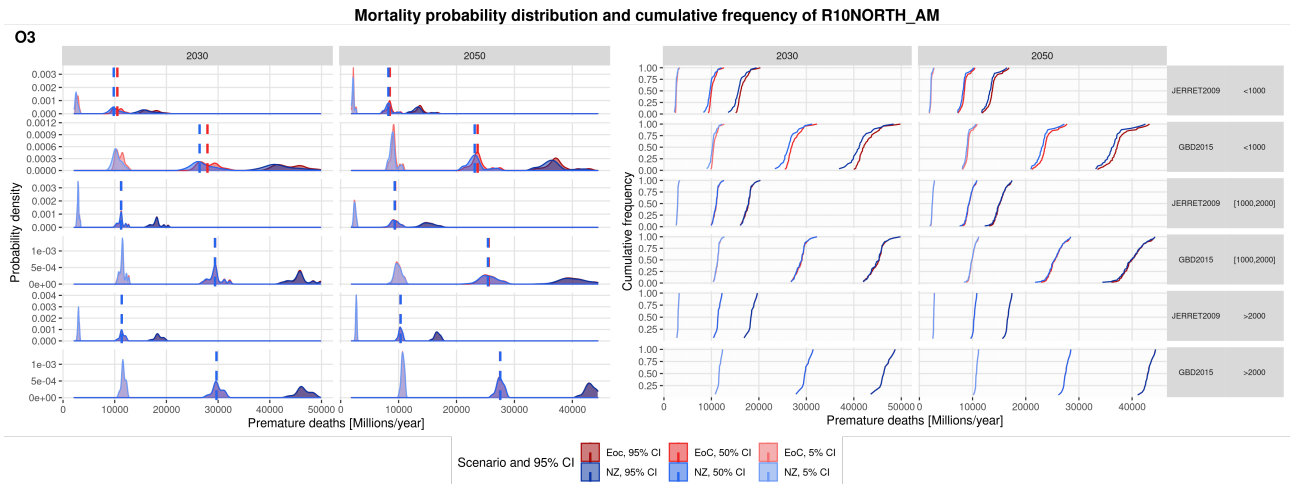
Figure 67: Probability density distribution (left) and cumulative frequency (right) for R10NORTH-AM for O_3. Includes median line by climate policy.
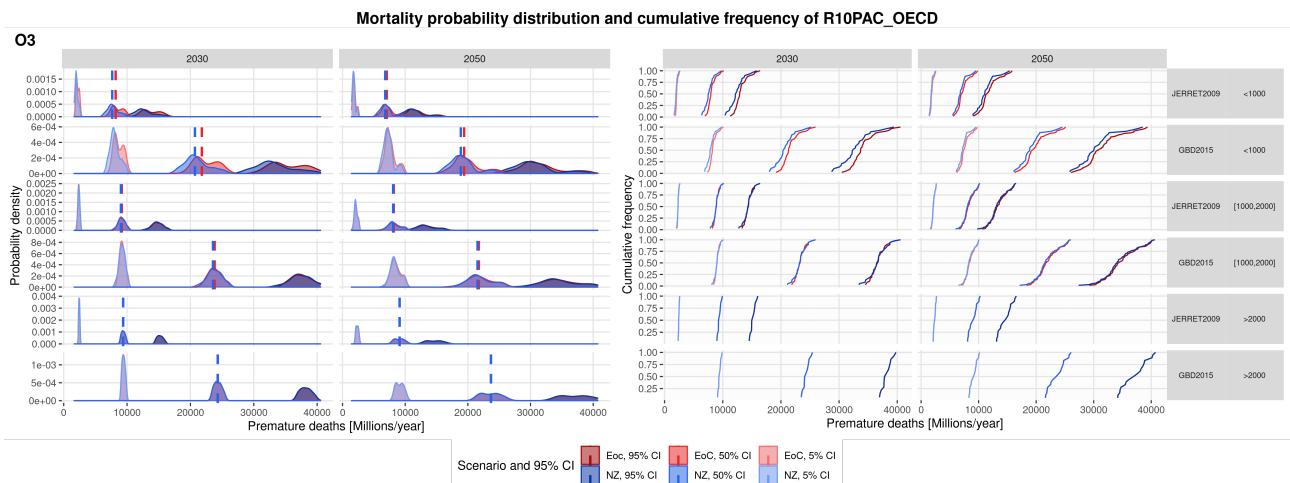
Figure 68: Probability density distribution (left) and cumulative frequency (right) for R10PAC-OECD for O_3. Includes median line by climate policy.
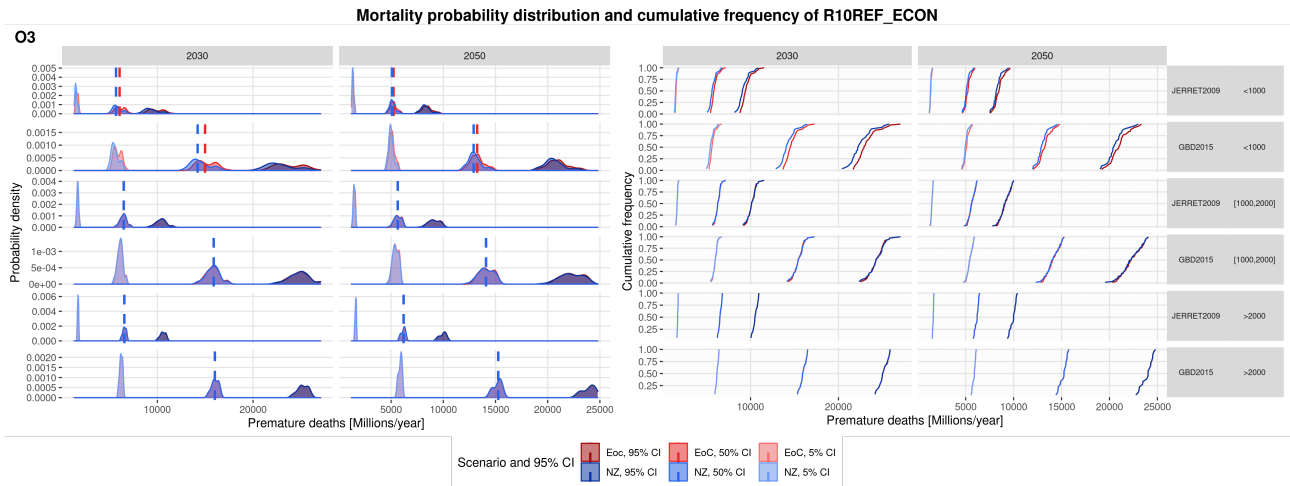
Figure 69: Probability density distribution (left) and cumulative frequency (right) for R10REF-ECON for O_3. Includes median line by climate policy.
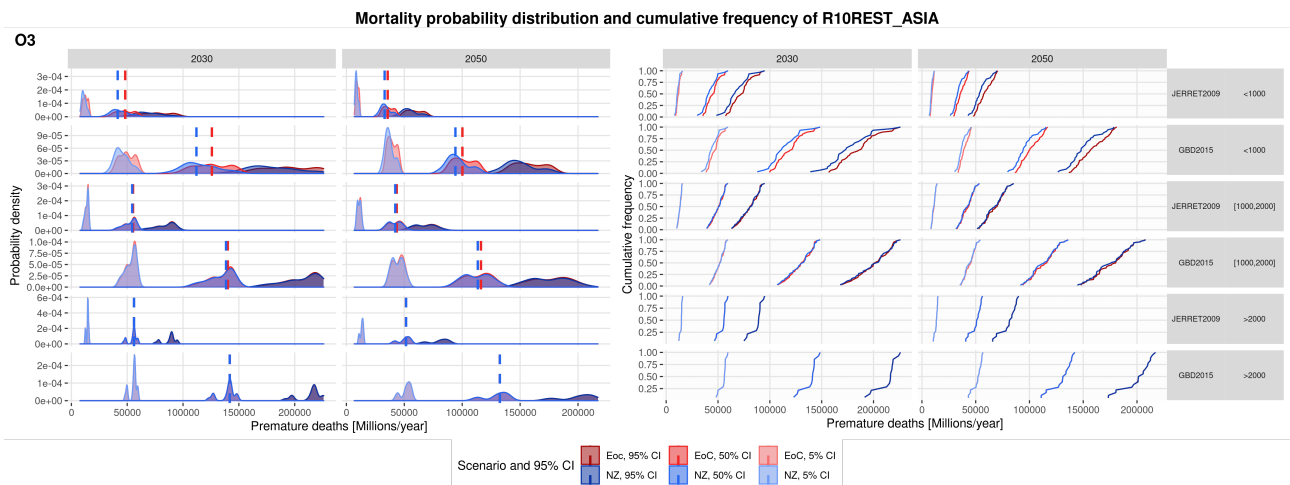
Figure 70: Probability density distribution (left) and cumulative frequency (right) for R10REST-ASIA for O_3. Includes median line by climate policy.

E.2 Exceedance probability graphs
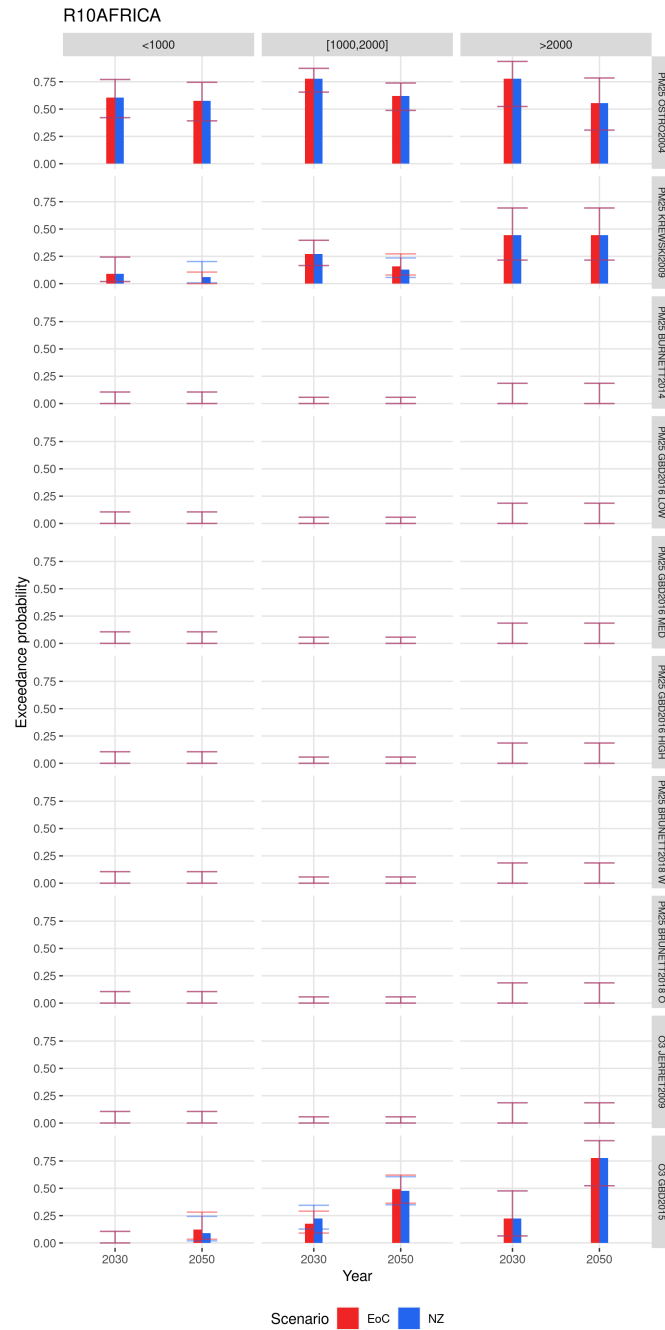
Figure 71: Exceedance probability for NZ and EoC climate policy for R10AFRICA with 95% CI. Impact functions are ranked according to their publication date.
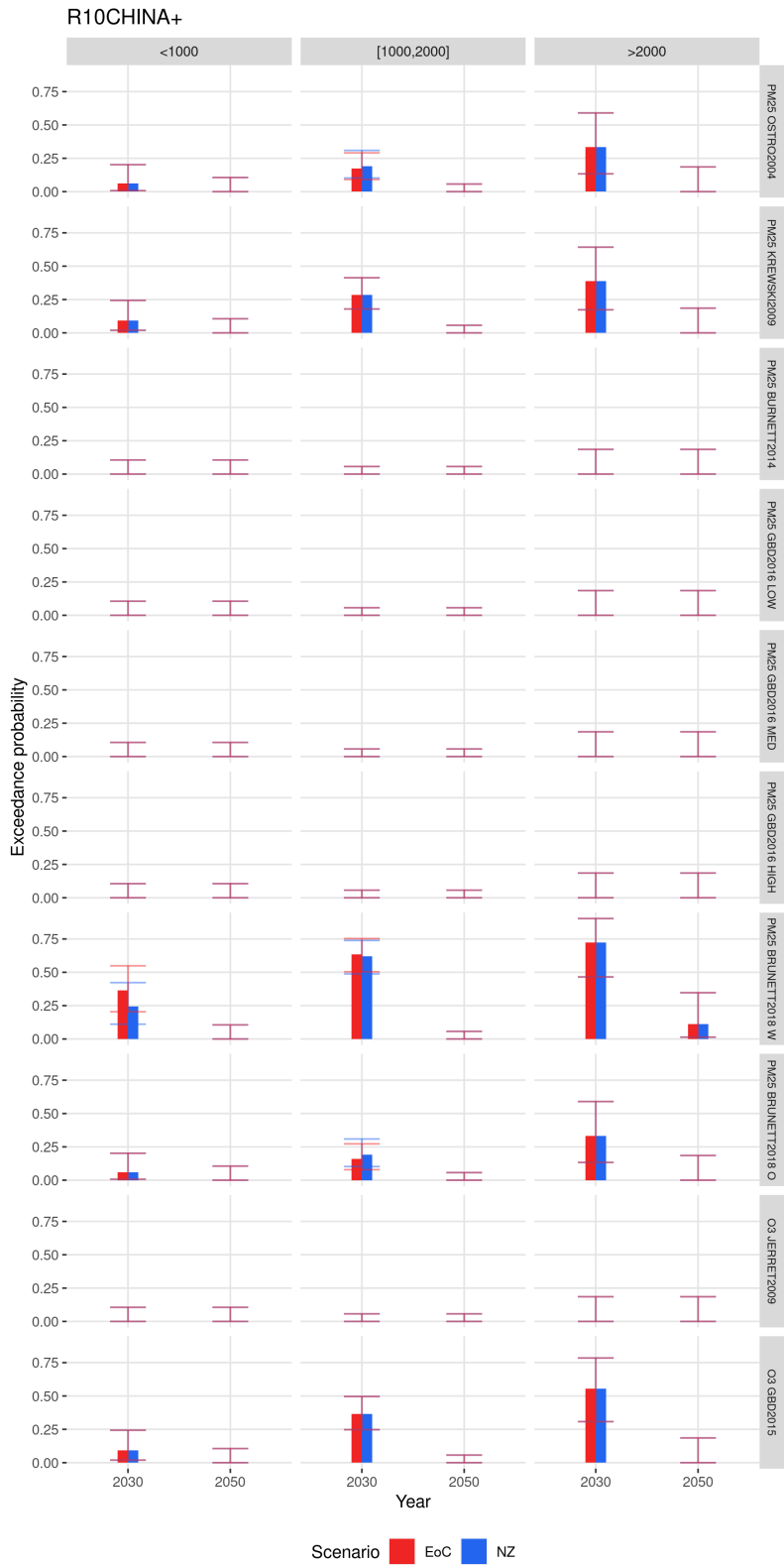
Figure 72: Exceedance probability for NZ and EoC climate policy for R10CHINA+ with 95% CI. Impact functions are ranked according to their publication date.
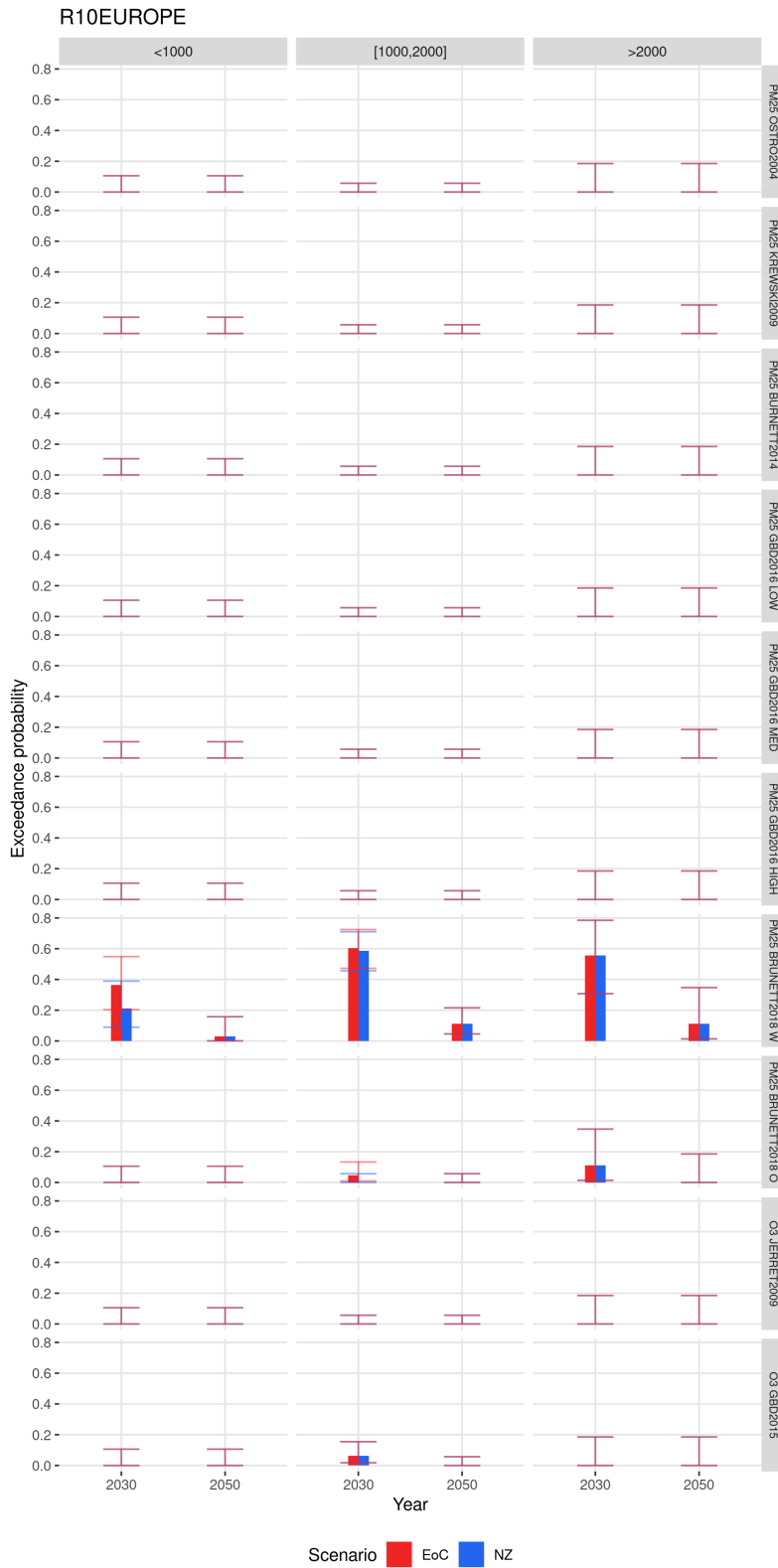
Figure 73: Exceedance probability for NZ and EoC climate policy for R10EUROPE with 95% CI. Impact functions are ranked according to their publication date.
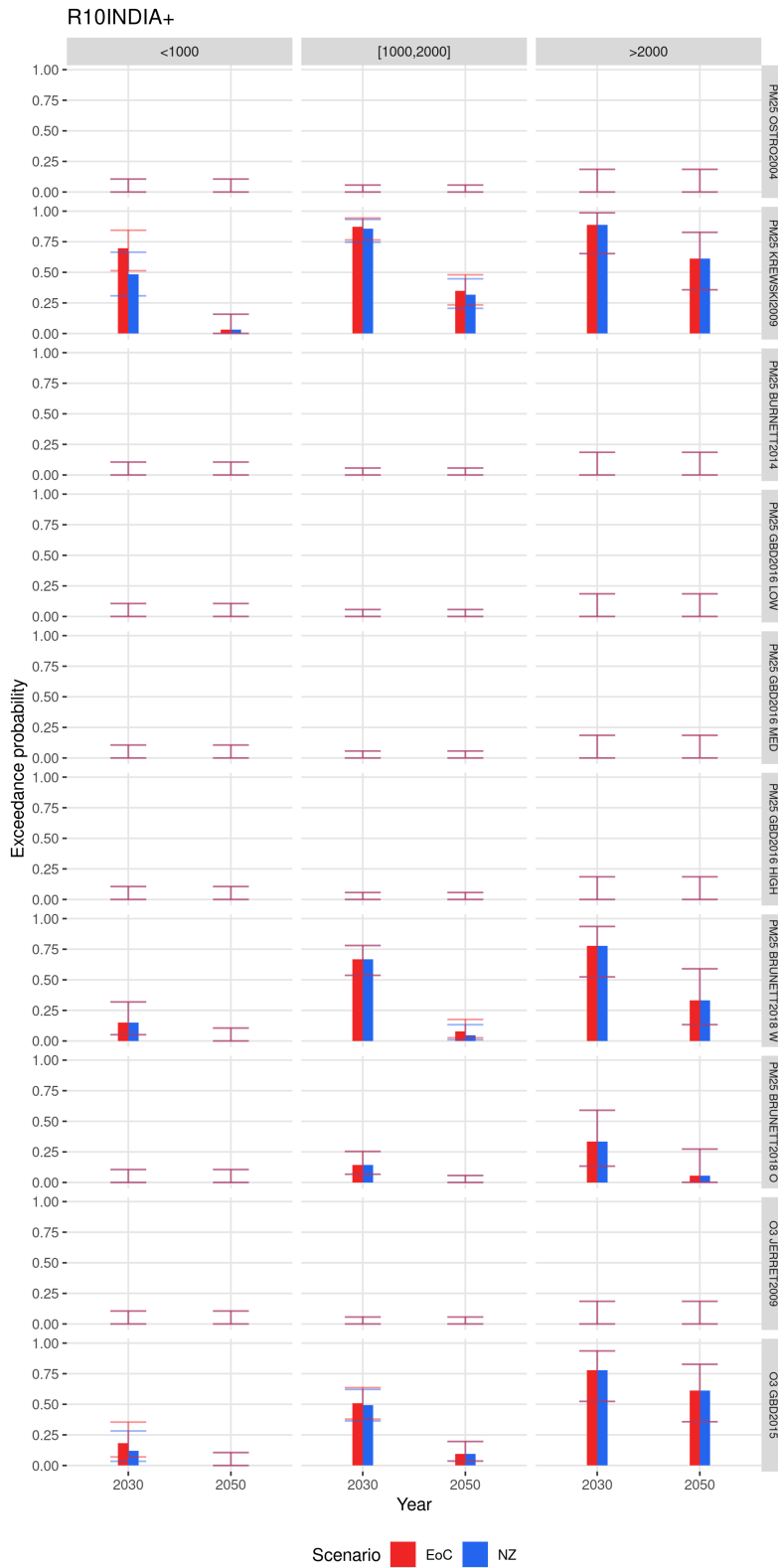
Figure 74: Exceedance probability for NZ and EoC climate policy for R10INDIA+ with 95% CI. Impact functions are ranked according to their publication date.
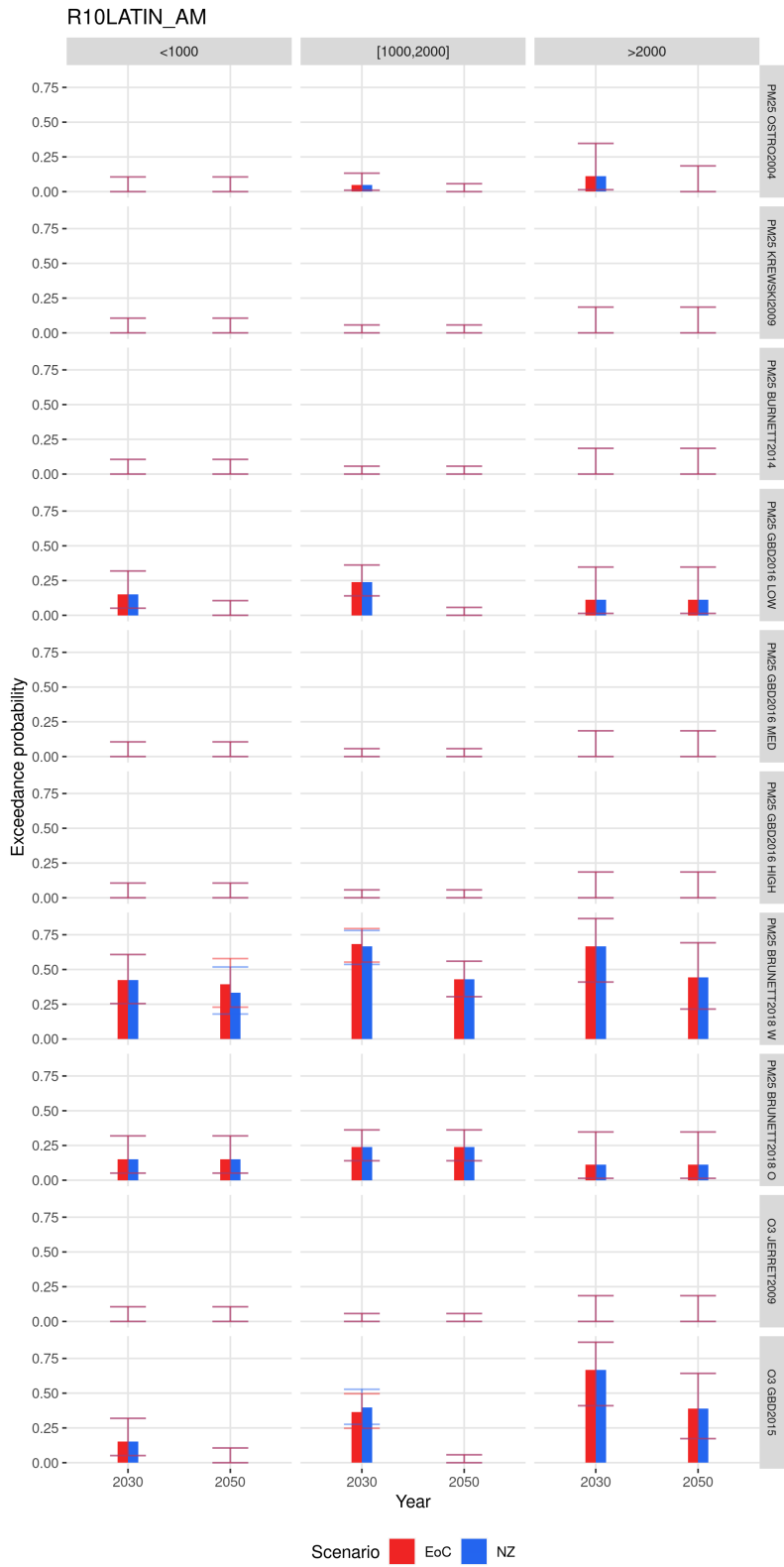
Figure 75: Exceedance probability for NZ and EoC climate policy for R10LATIN-AM with 95% CI. Impact functions are ranked according to their publication date.
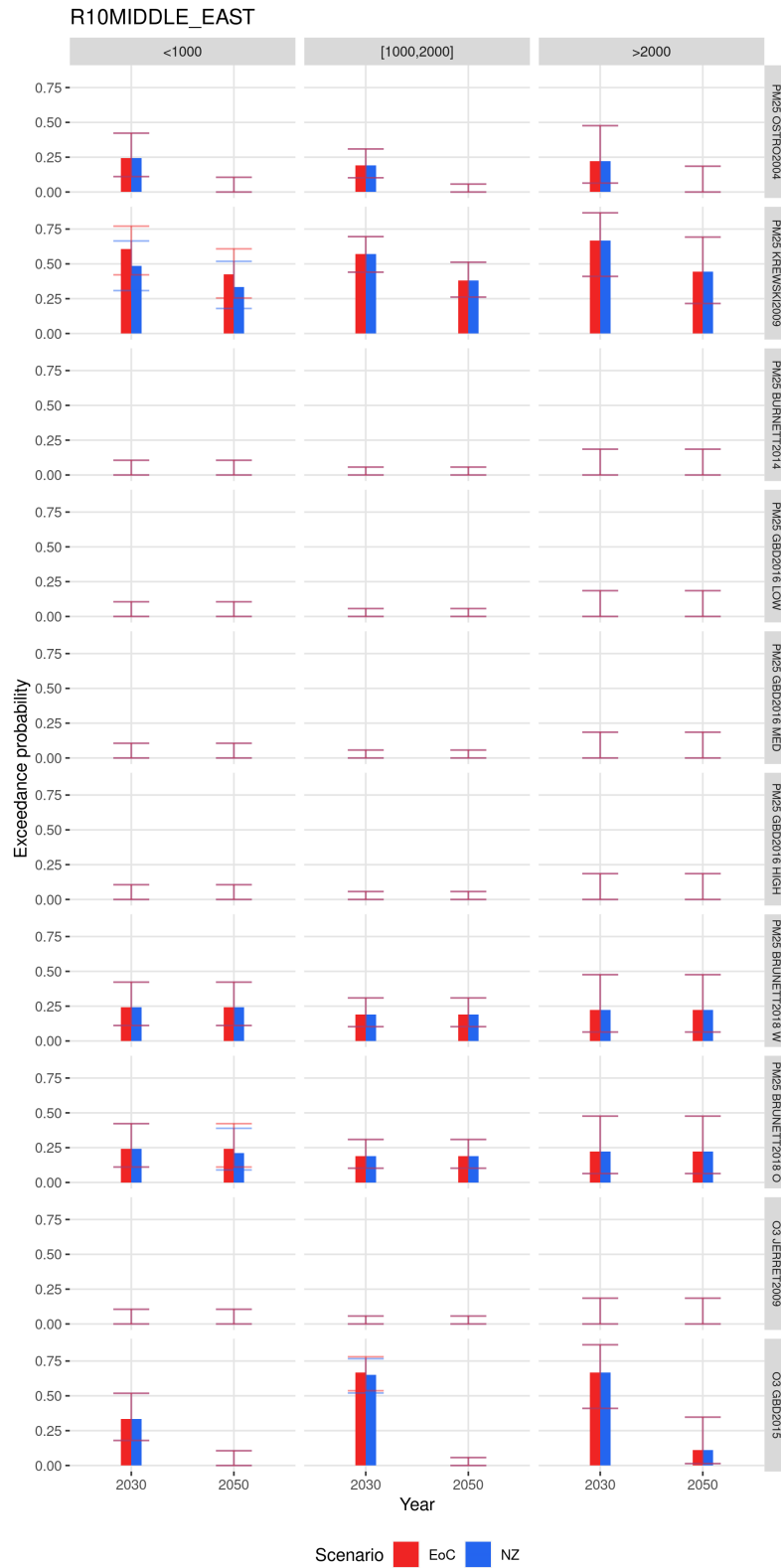
Figure 76: Exceedance probability for NZ and EoC climate policy for R10MIDDLE-EAST with 95% CI. Impact functions are ranked according to their publication date.
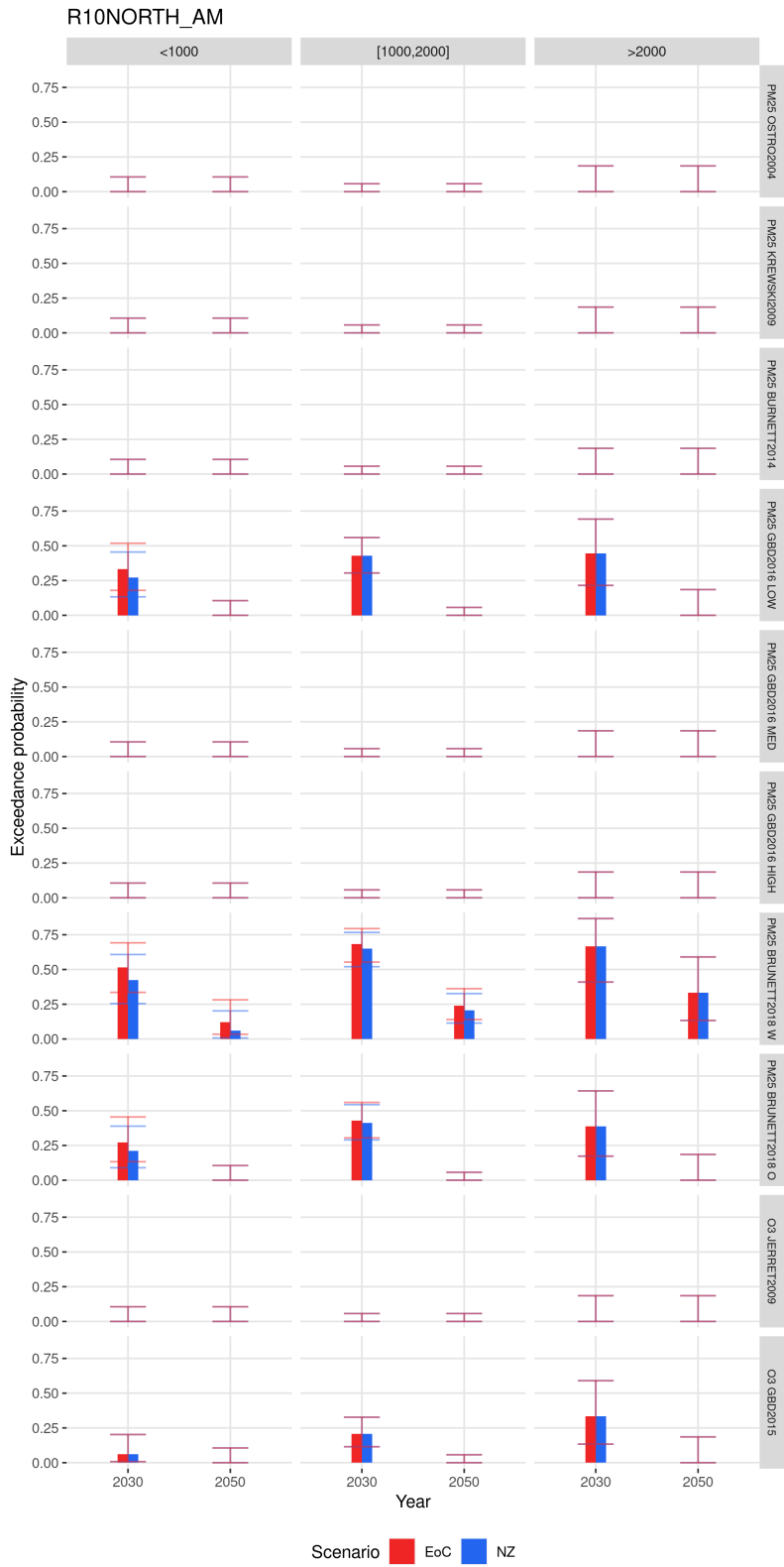
Figure 77: Exceedance probability for NZ and EoC climate policy for R10NORTH-AM with 95% CI. Impact functions are ranked according to their publication date.
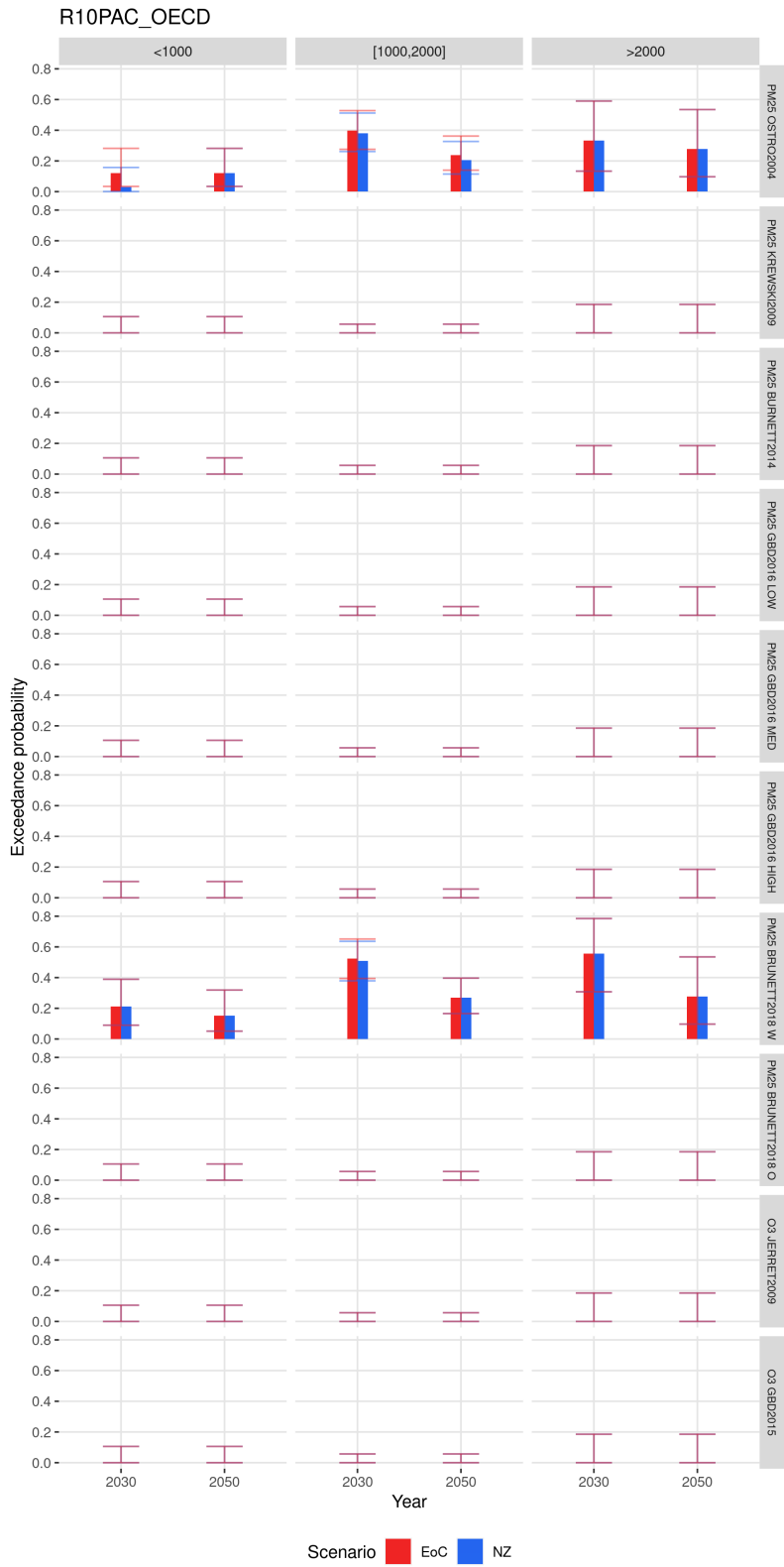
Figure 78: Exceedance probability for NZ and EoC climate policy for R10PAC-OECD with 95% CI. Impact functions are ranked according to their publication date.
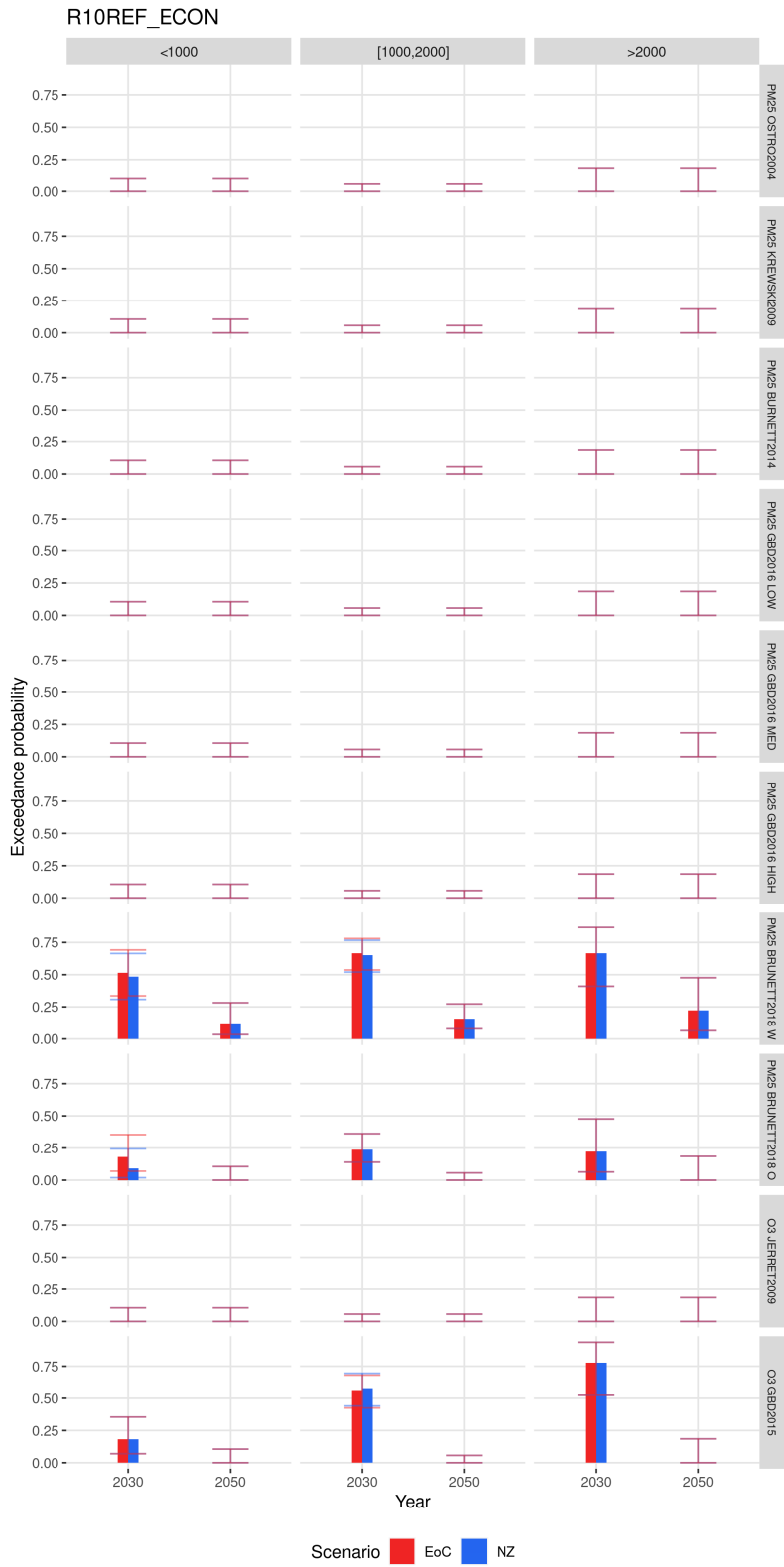
Figure 79: Exceedance probability for NZ and EoC climate policy for R10REF-ECON with 95% CI. Impact functions are ranked according to their publication date.
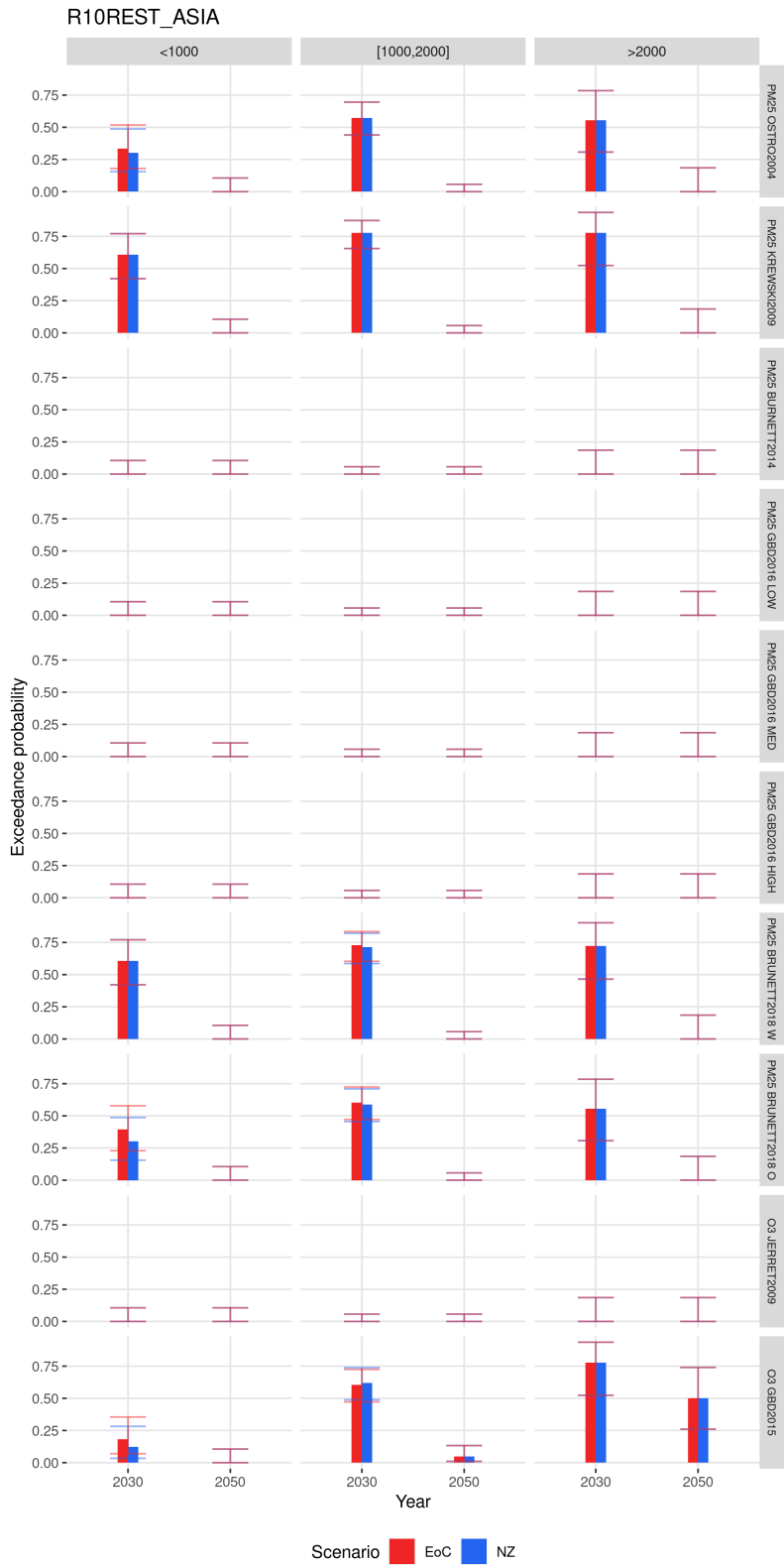
Figure 80: Exceedance probability for NZ and EoC climate policy for R10REST-ASIA with 95% CI. with 95% CI. Impact functions are ranked according to their publication date.

E.3 Premature deaths and avoided deaths
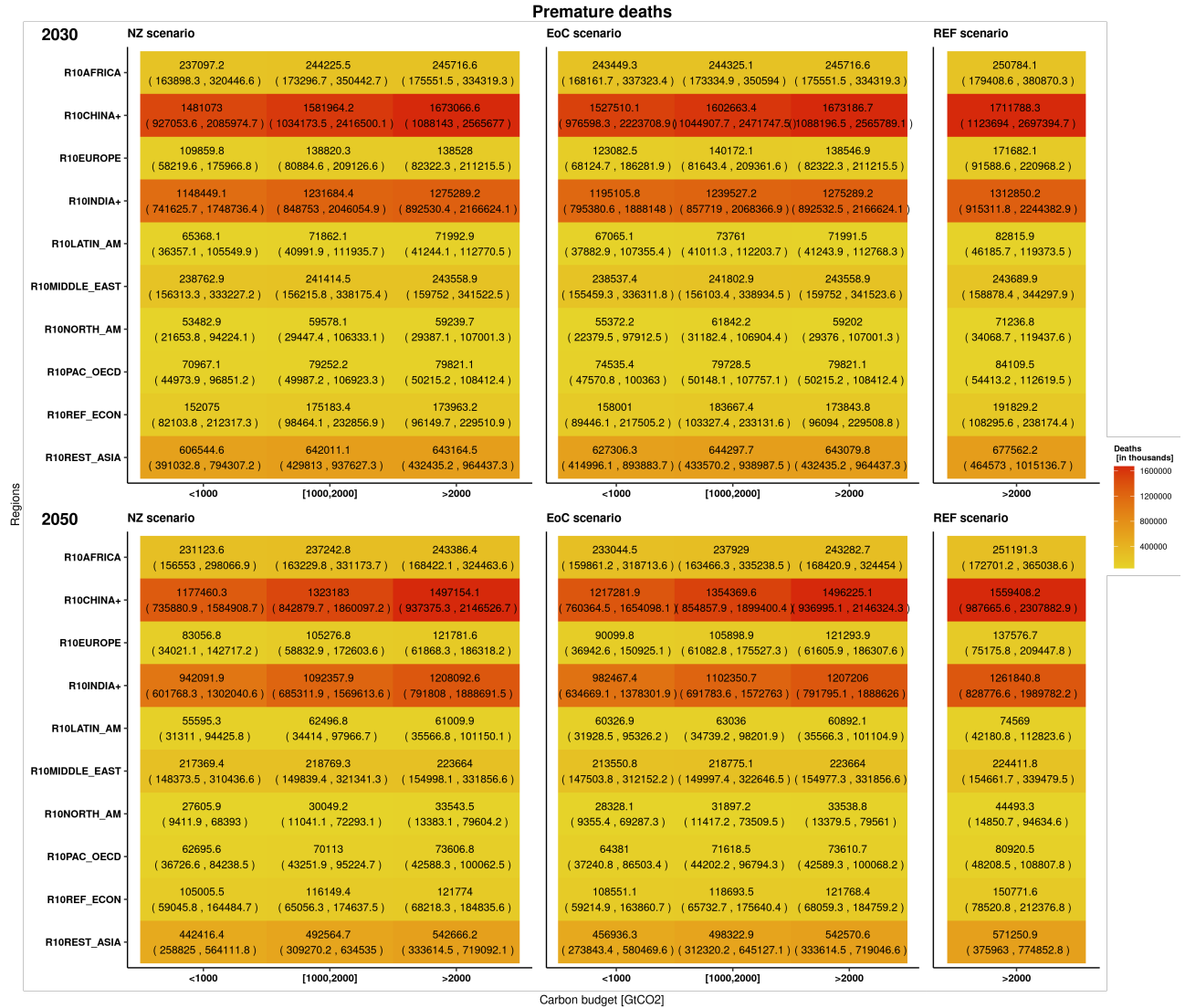
Figure 81: Overall ($PM_{2.5}$+ O_3) premature deaths by region and carbon budget in 2030 and 2050 using the premature deaths mean among the projections done by all impact functions. The colors correspond to the median value, and there is also displayed the 95% CI.
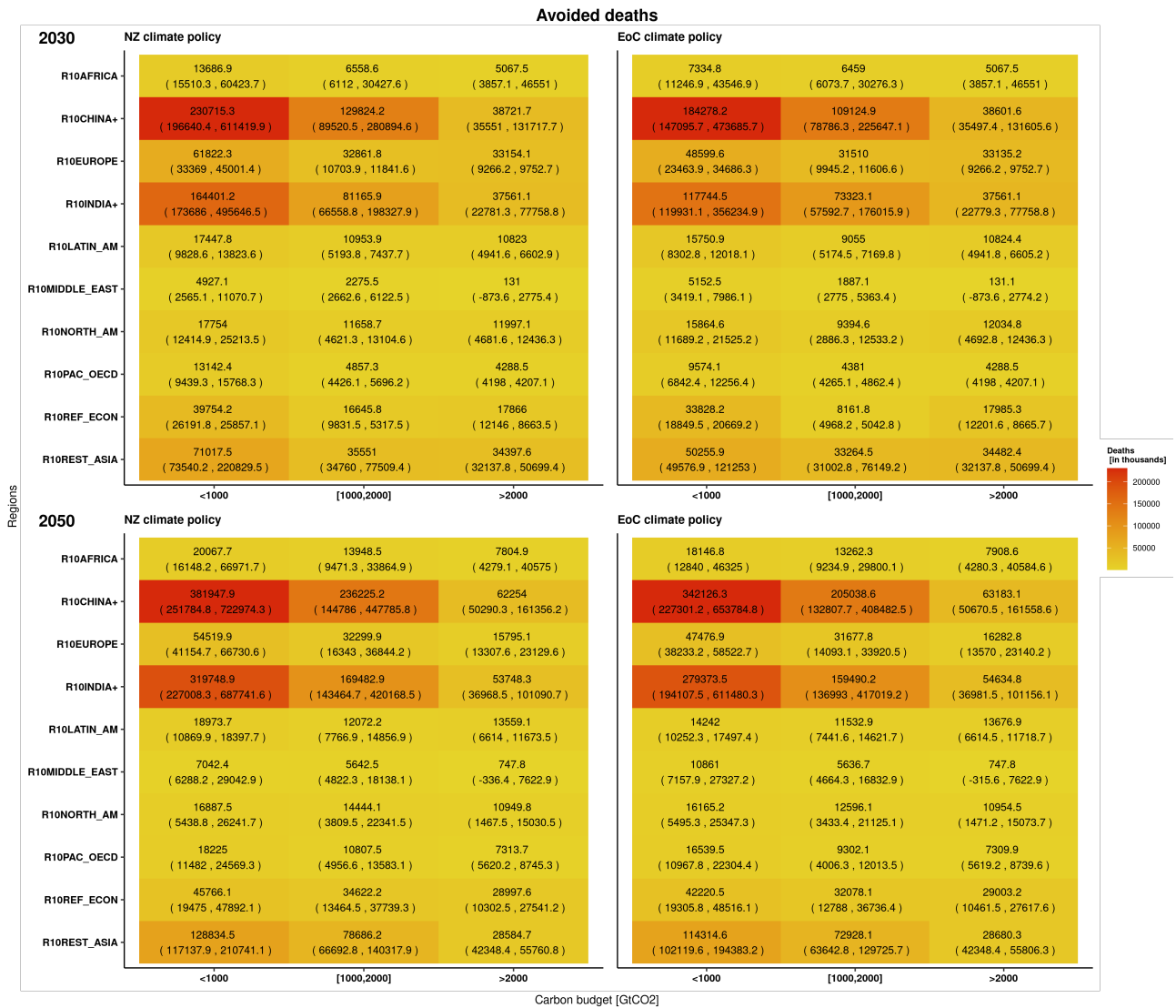
Figure 82: Overall (PM$_{2.5}$+ O$_3$) avoided deaths by region, carbon budget, and climate policy in 2030 and 2050 using the premature deaths median among the projections done by all impact functions. The colors correspond to the median value, and there is also displayed the 95% CI. To compute the avoided deaths, the premature deaths estimated by the each climate policy are subtracted to the ones estimated by the REF.
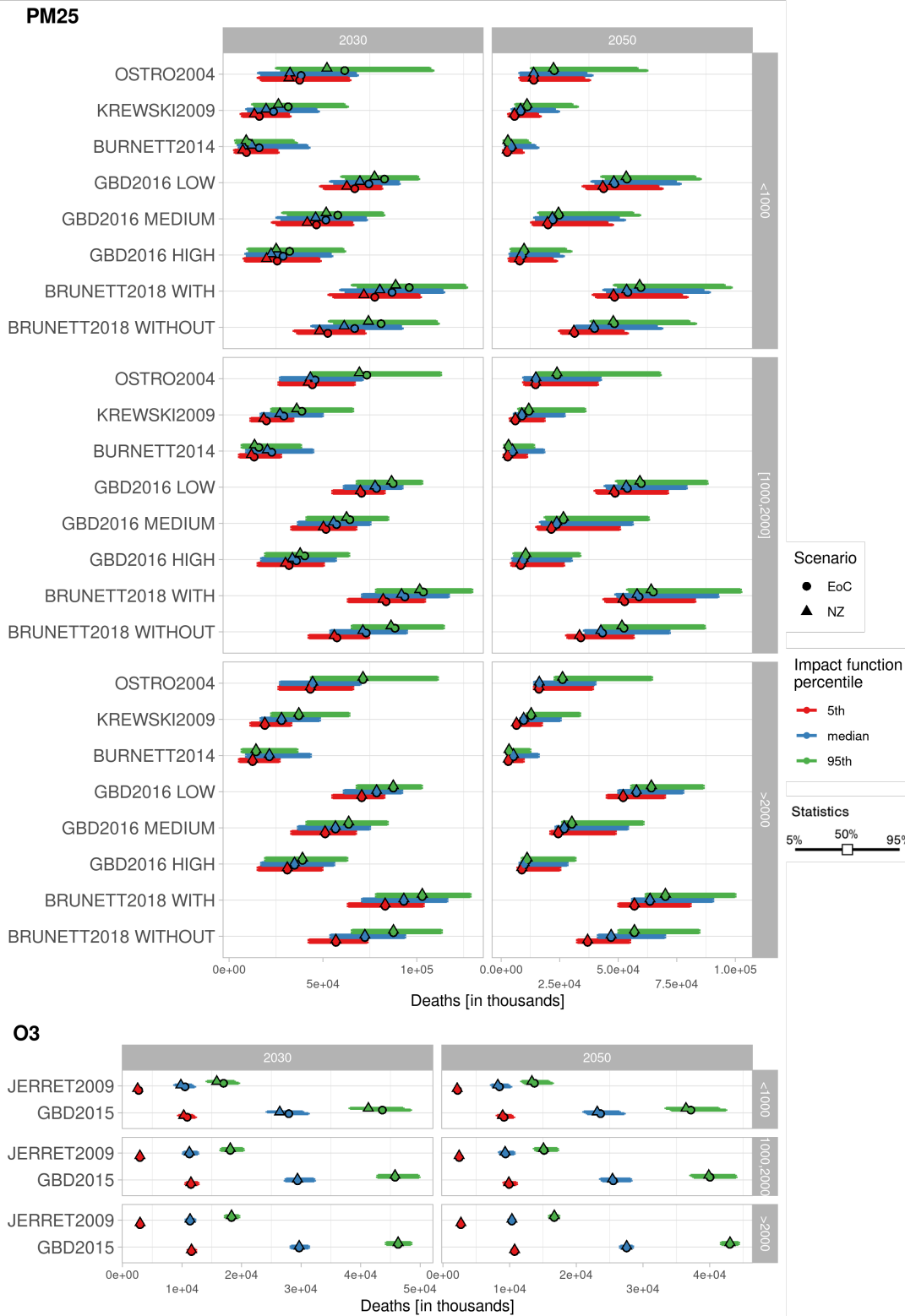
E.4 Impact function's parameters values sensitivity graphs
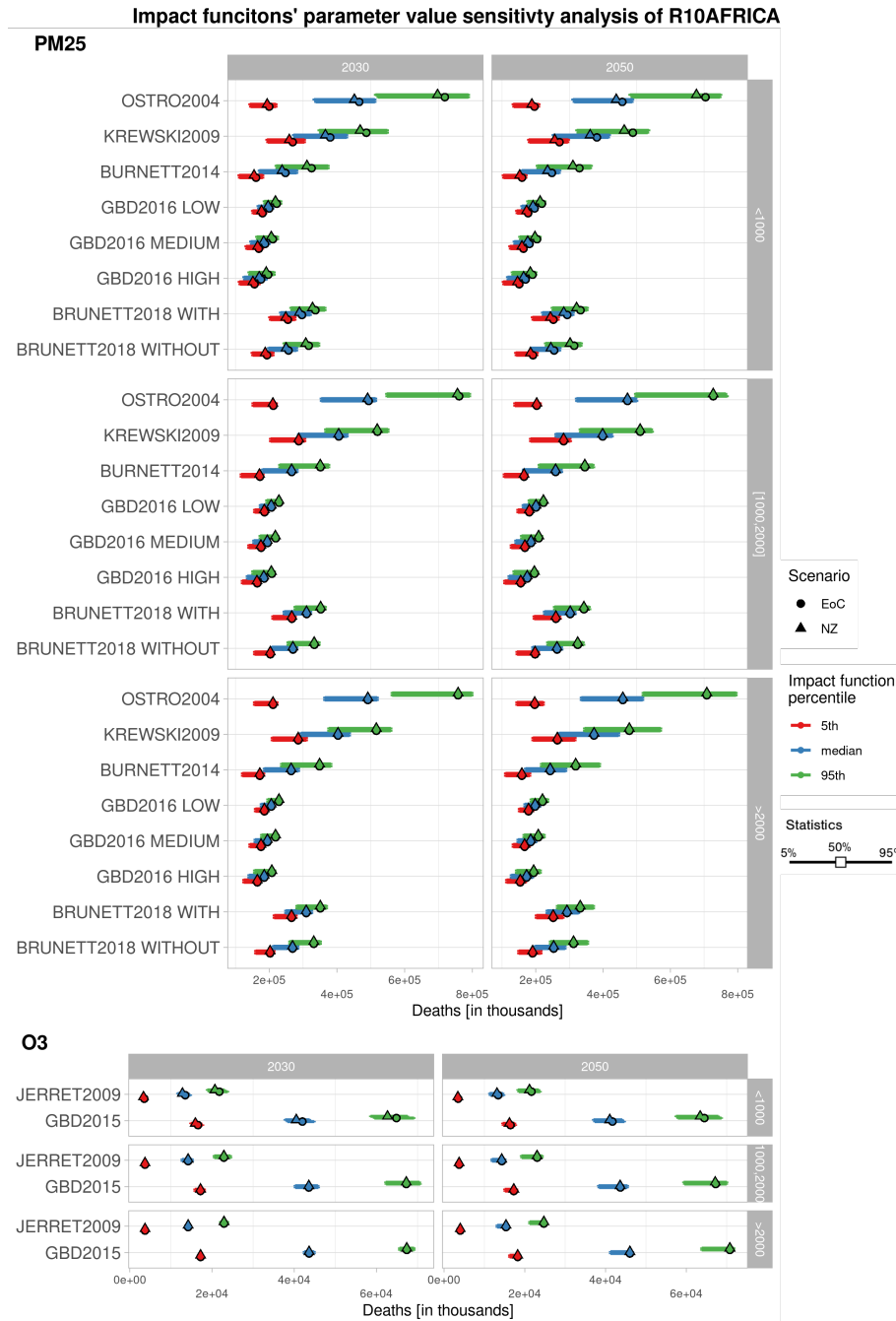
Figure 83: Influence of the impact function percentile on the estimation of premature deaths, regarding impact function, regarding impact function, carbon budget, year, and scenario for R10AFRICA. Each error bars report the uncertainty range (5-95%) across parameters' sets. The middle points represent the median of the impact function RR median. Colours represent the impact functions' parameter percentile. Impact functions are ranked according to their publication date. Parameters of the impact functions are reported in Table 3.
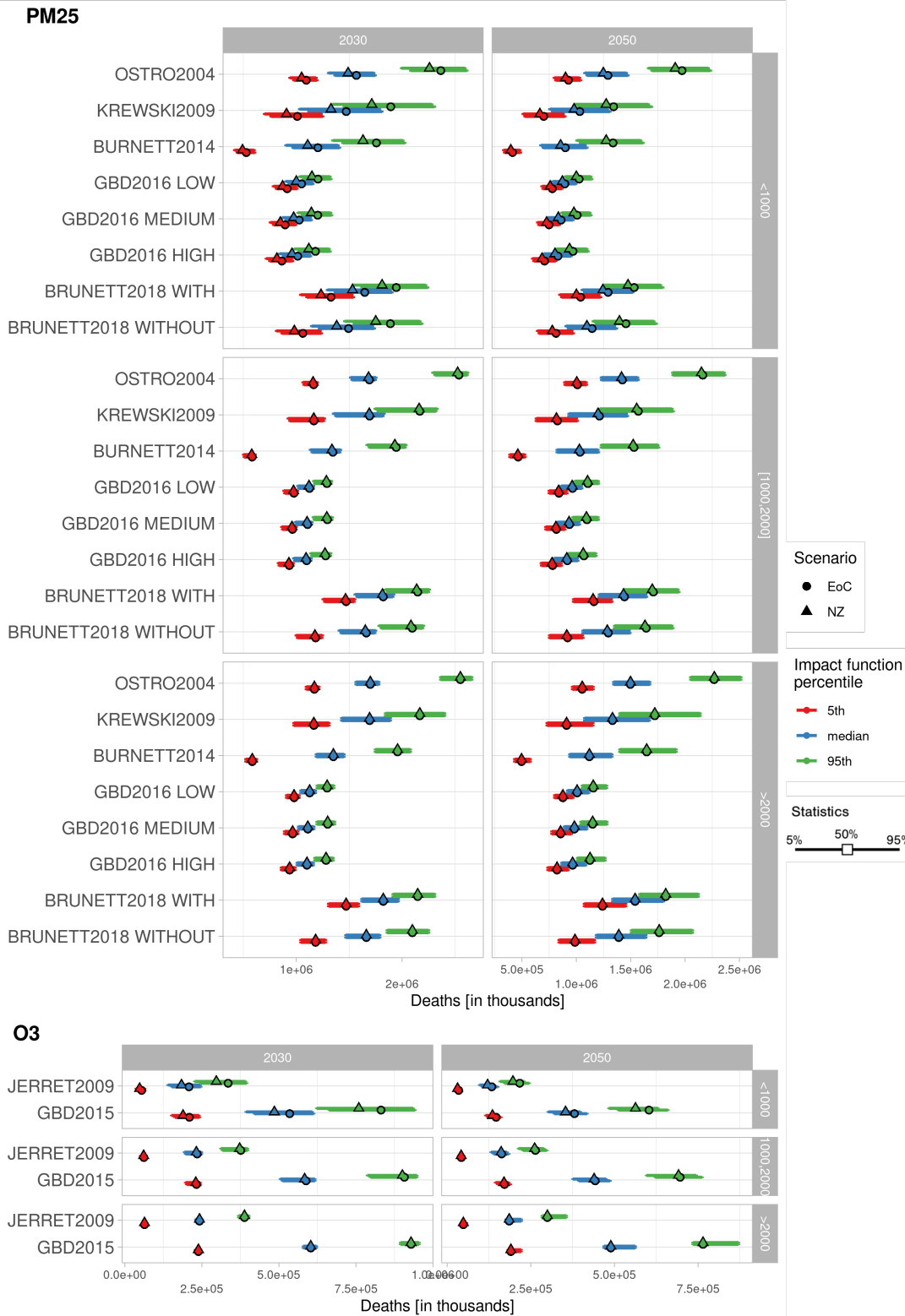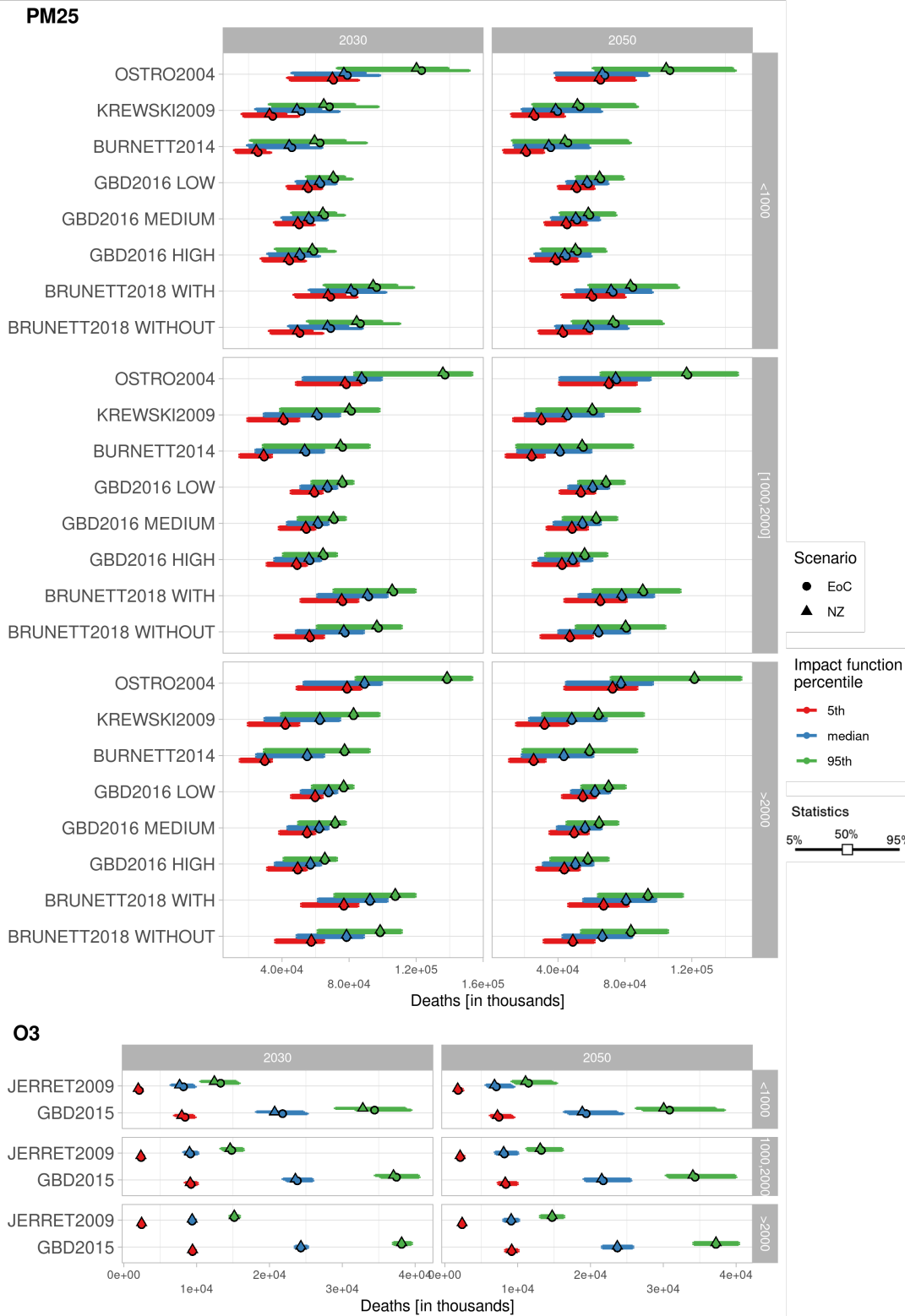
Figure 84: Influence of the impact function percentile on the estimation of premature deaths, regarding impact function, carbon budget, year, and scenario for R10CHINA+. Each error bars report the uncertainty range (5-95%) across parameters' sets. The middle points represent the median of the impact function RR median. Colours represent the impact functions' parameter percentile. Impact functions are ranked according to their publication date. Parameters of the impact functions are reported in Table 3.
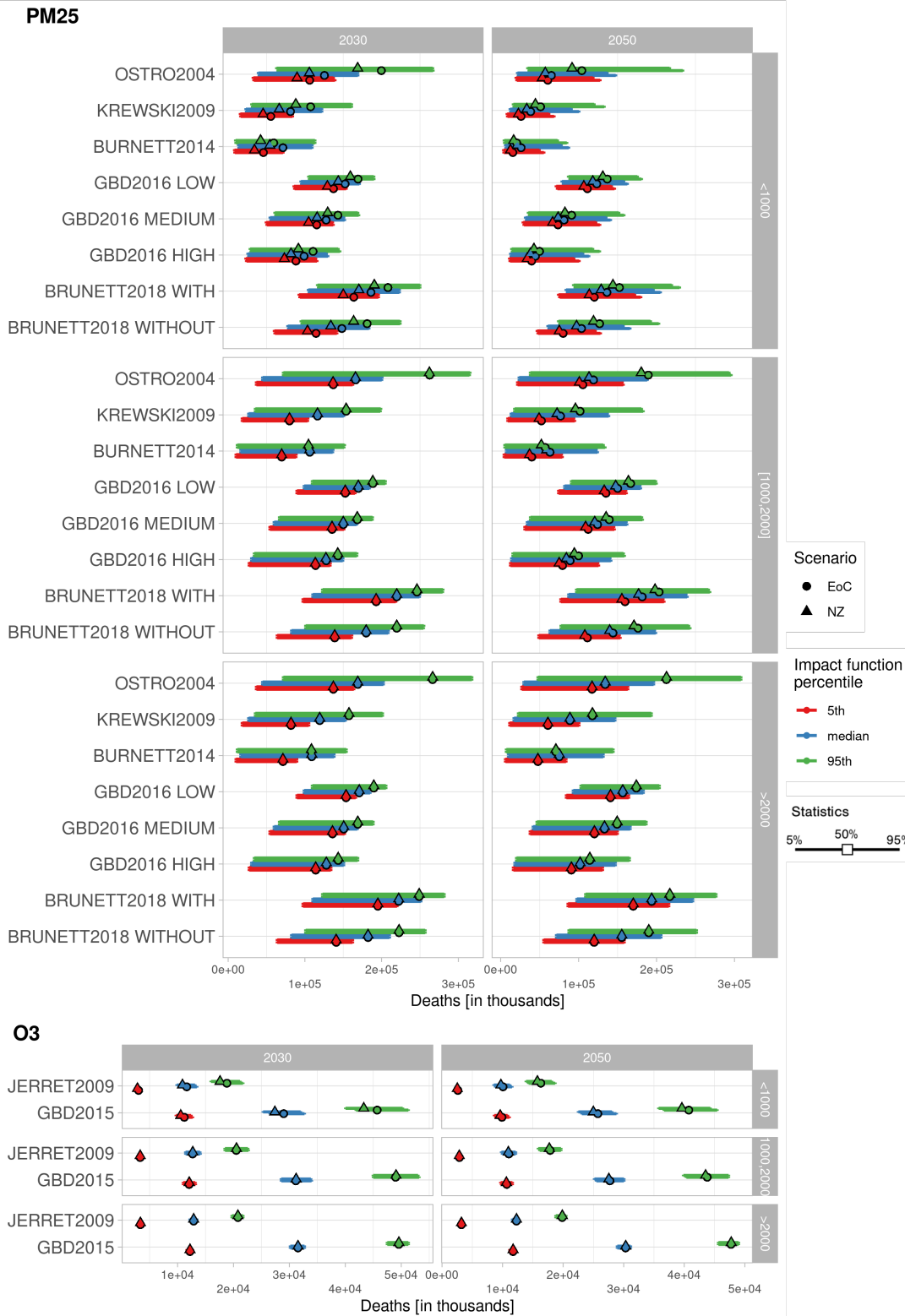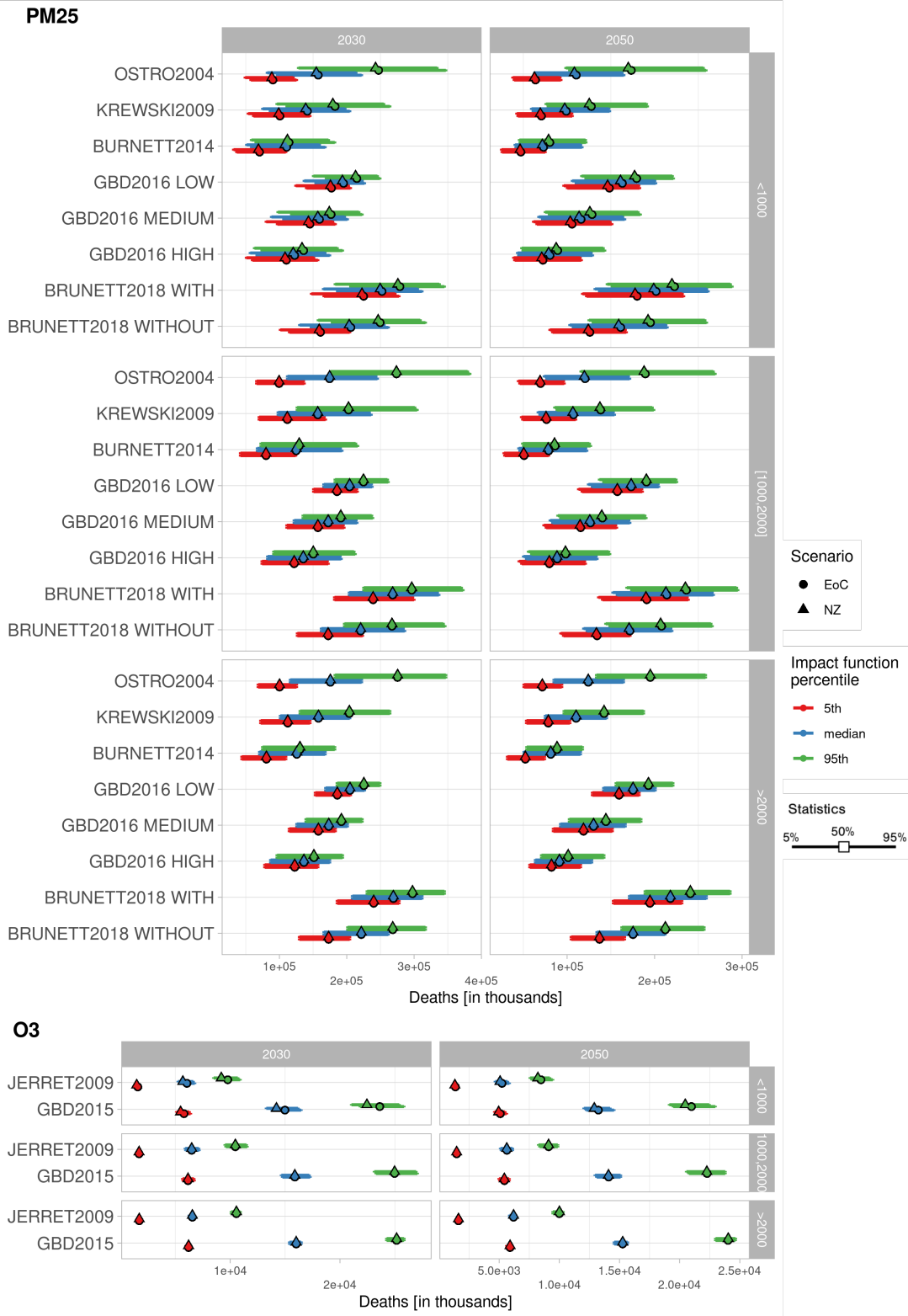
Figure 85: Influence of the impact function percentile on the estimation of premature deaths, regarding impact function, carbon budget, year, and scenario for R10EUROPE. Each error bars report the uncertainty range (5-95%) across parameters' sets. The middle points represent the median of the impact function RR median. Colours represent the impact functions' parameter percentile. Impact functions are ranked according to their publication date. Parameters of the impact functions are reported in Table 3.
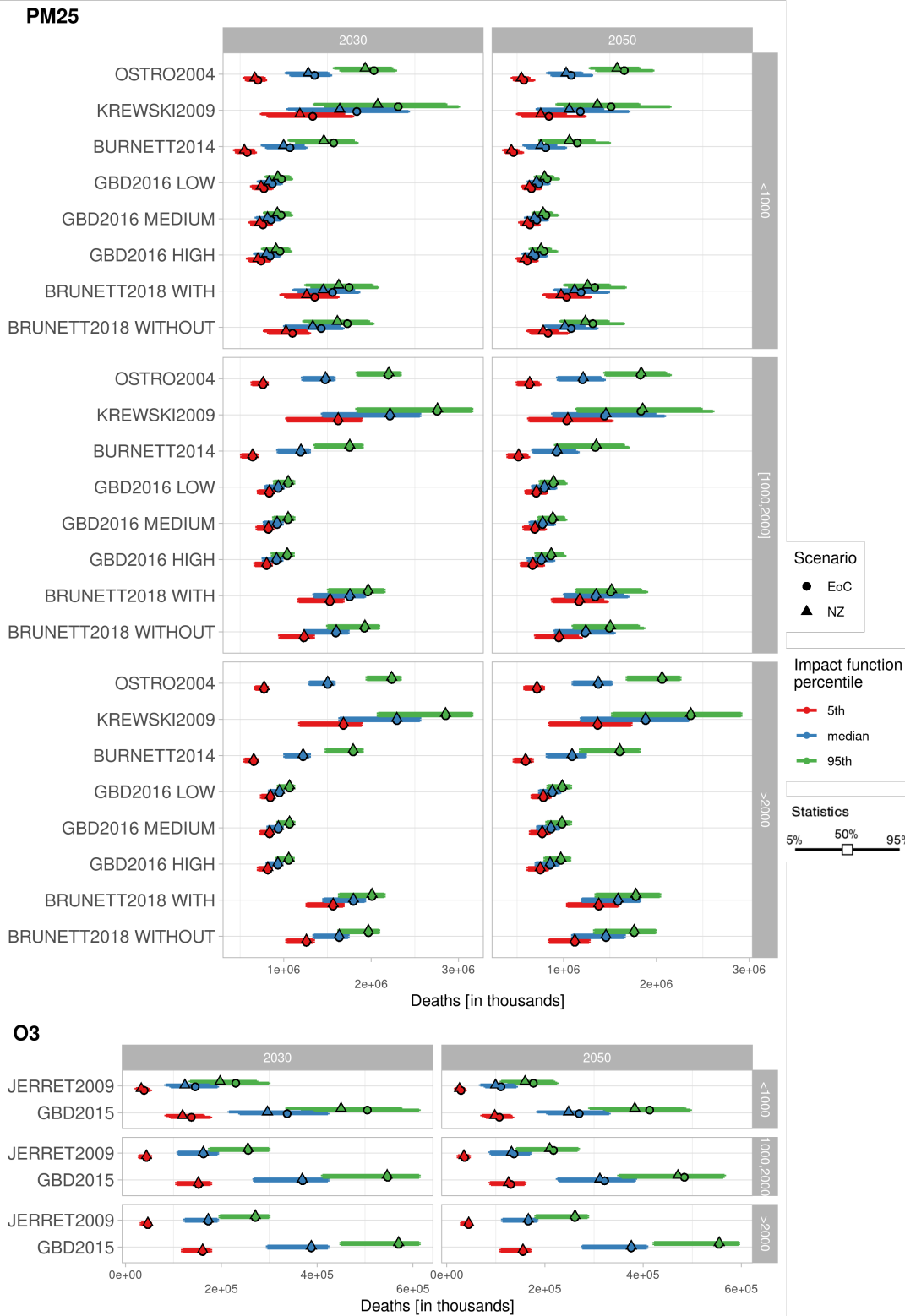
Figure 86: Influence of the impact function percentile on the estimation of premature deaths, regarding impact function, carbon budget, year, and scenario for R10INDIA+. Each error bars report the uncertainty range (5-95%) across parameters' sets. The middle points represent the median of the impact function RR median. Colours represent the impact functions' parameter percentile. Impact functions are ranked according to their publication date. Parameters of the impact functions are reported in Table 3.
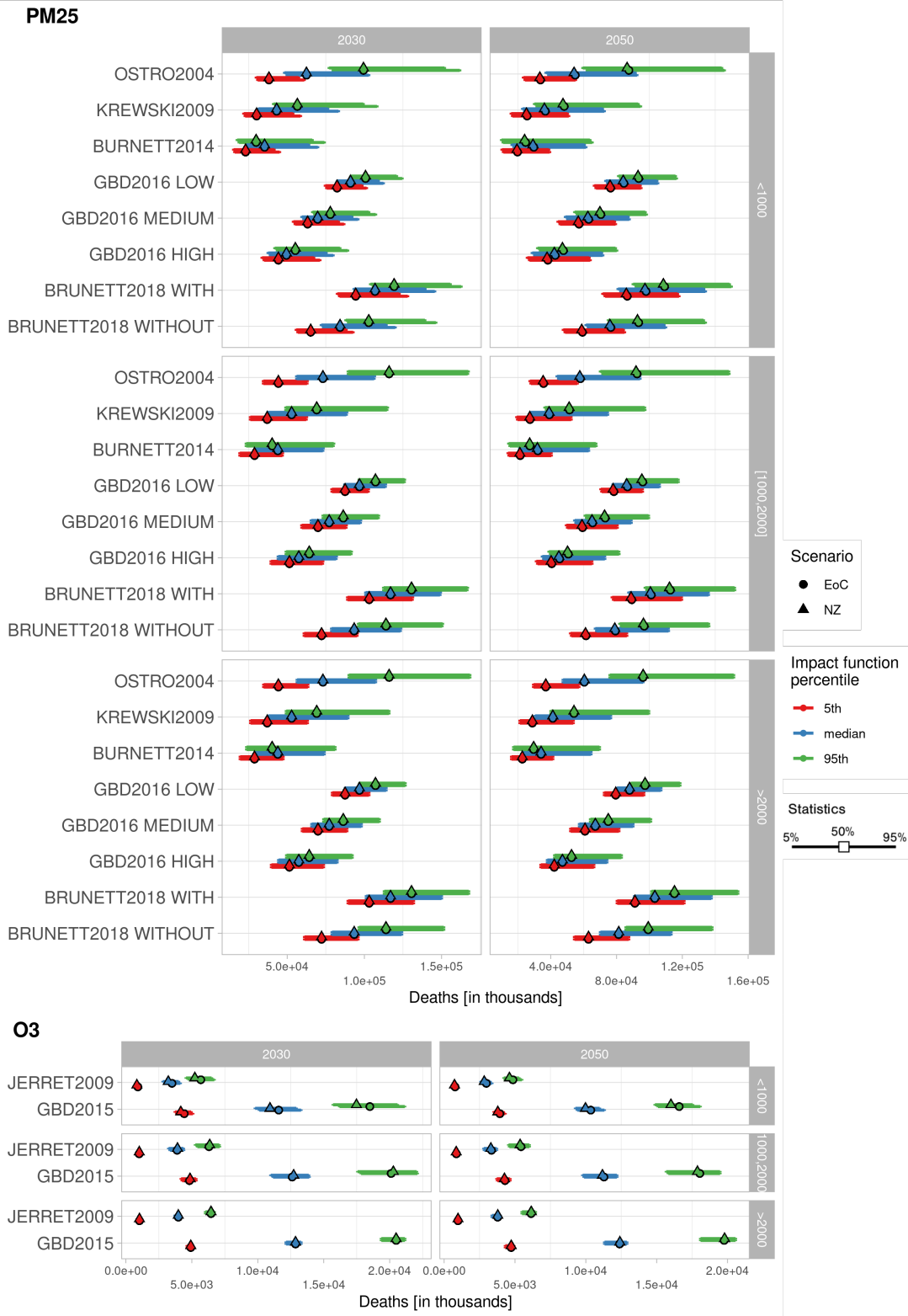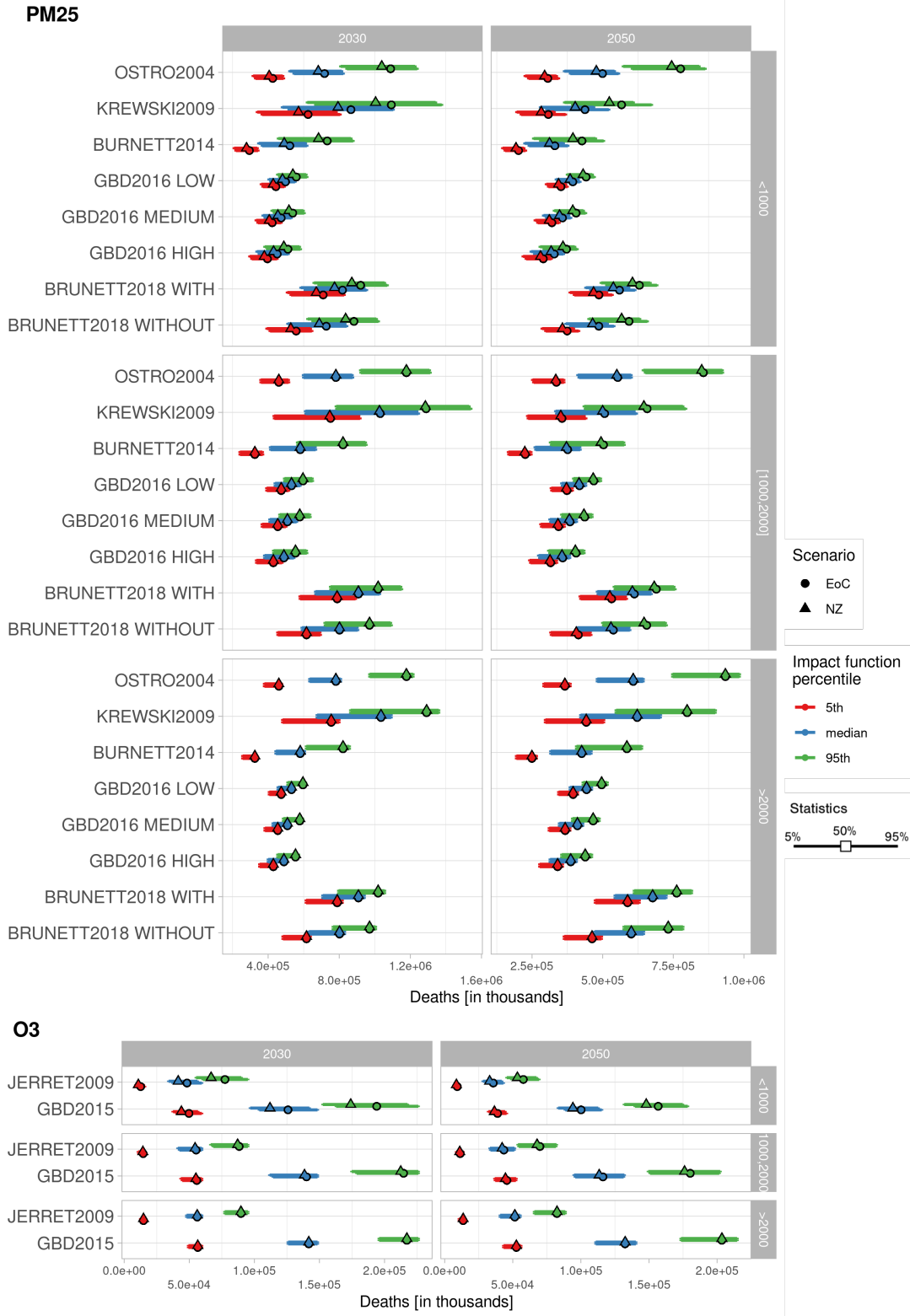
Figure 87: Influence of the impact function percentile on the estimation of premature deaths, regarding impact function, carbon budget, year, and scenario for R10LATIN-AM. Each error bars report the uncertainty range (5-95%) across parameters' sets. The middle points represent the median of the impact function RR median. Colours represent the impact functions' parameter percentile. Impact functions are ranked according to their publication date. Parameters of the impact functions are reported in Table 3.
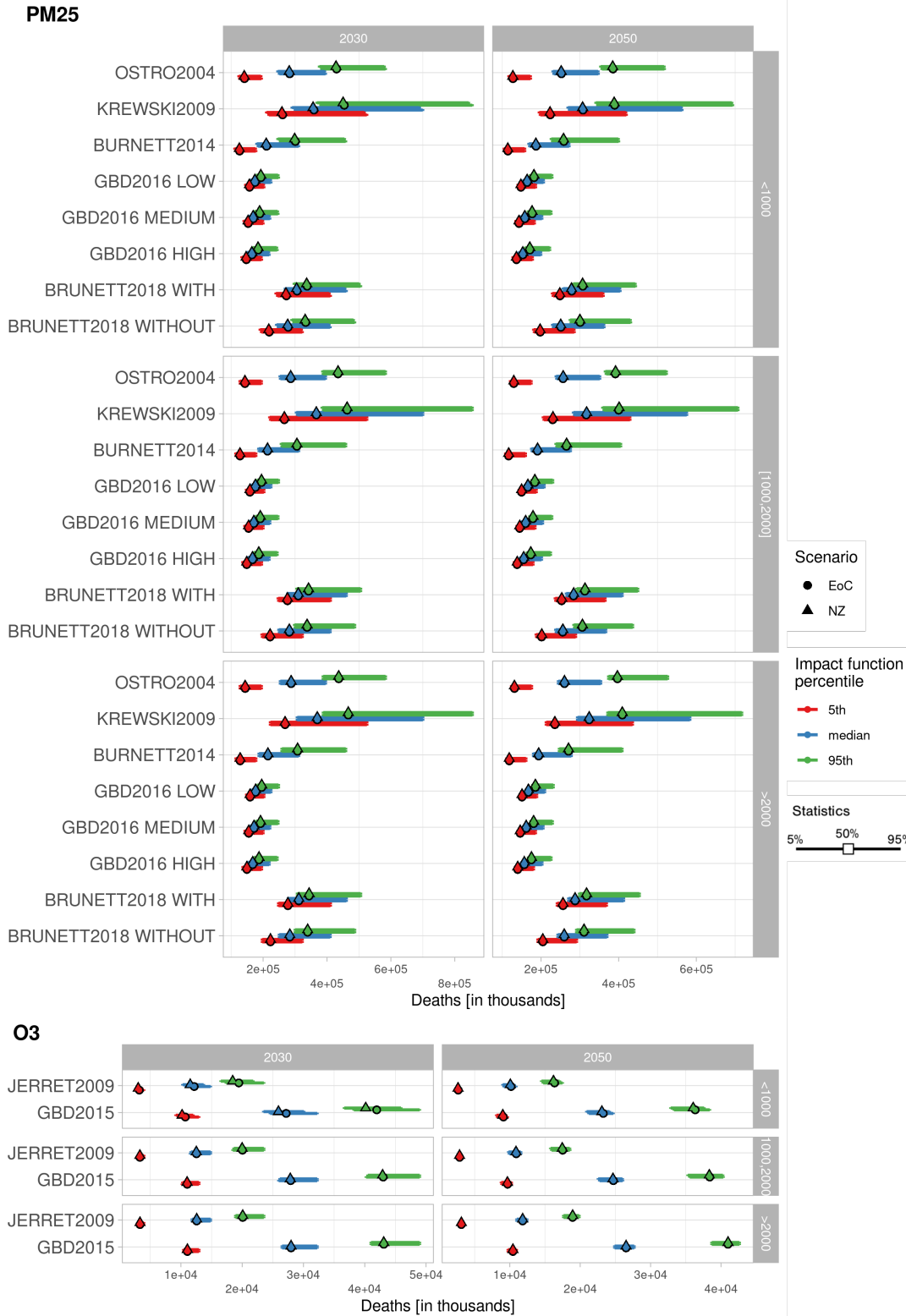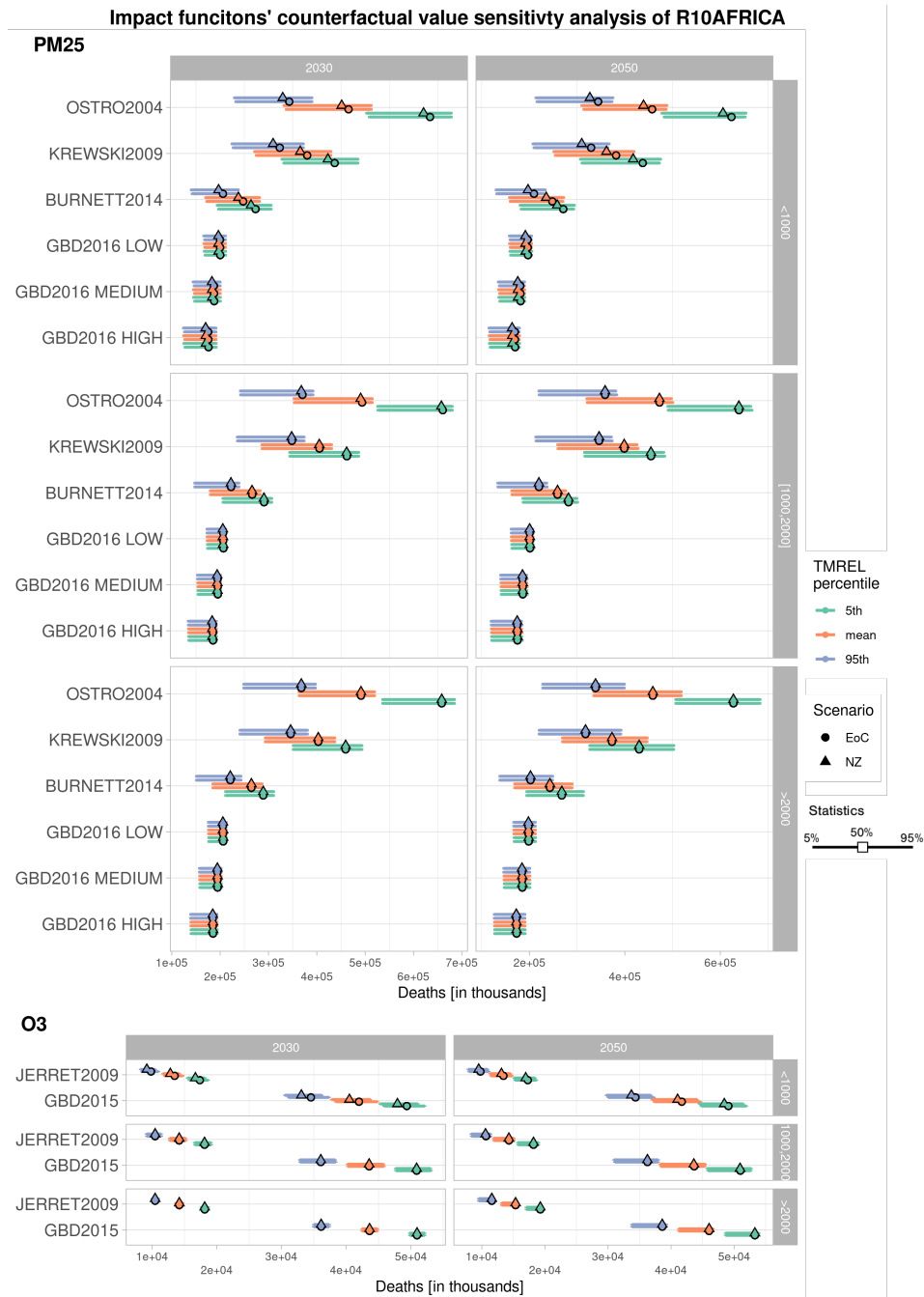
Figure 88: Influence of the impact function percentile on the estimation of premature deaths, regarding impact function, carbon budget, year, and scenario for R10MIDDLE-EAST. Each error bars report the uncertainty range (5-95%) across parameters' sets. The middle points represent the median of the impact function RR median. Colours represent the impact functions' parameter percentile. Impact functions are ranked according to their publication date. Parameters of the impact functions are reported in Table 3.
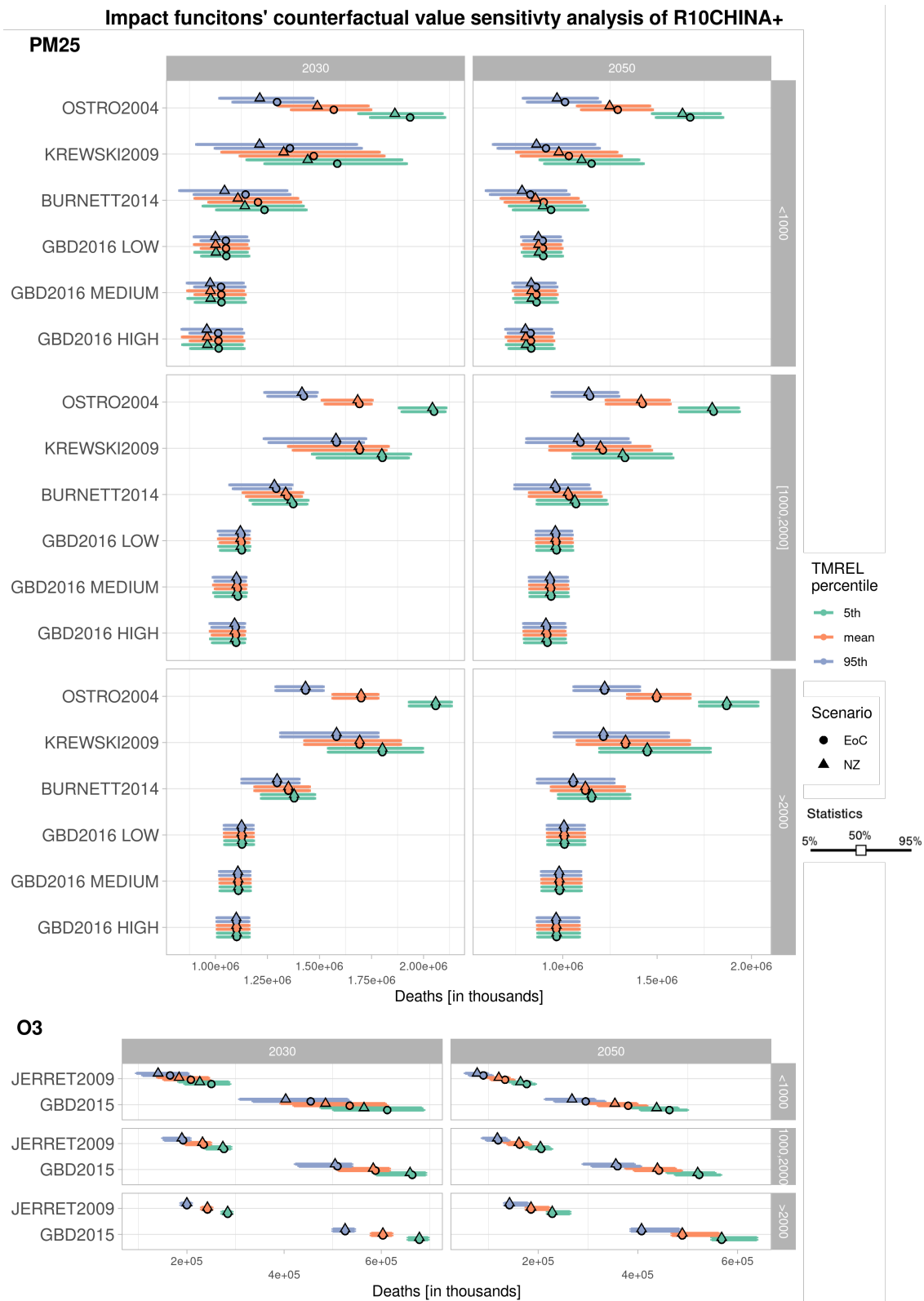
Figure 89: Influence of the impact function percentile on the estimation of premature deaths, regarding impact function, carbon budget, year, and scenario for R10NORTH-AM. Each error bars report the uncertainty range (5-95%) across parameters' sets. The middle points represent the median of the impact function RR median. Colours represent the impact functions' parameter percentile. Impact functions are ranked according to their publication date. Parameters of the impact functions are reported in Table 3.
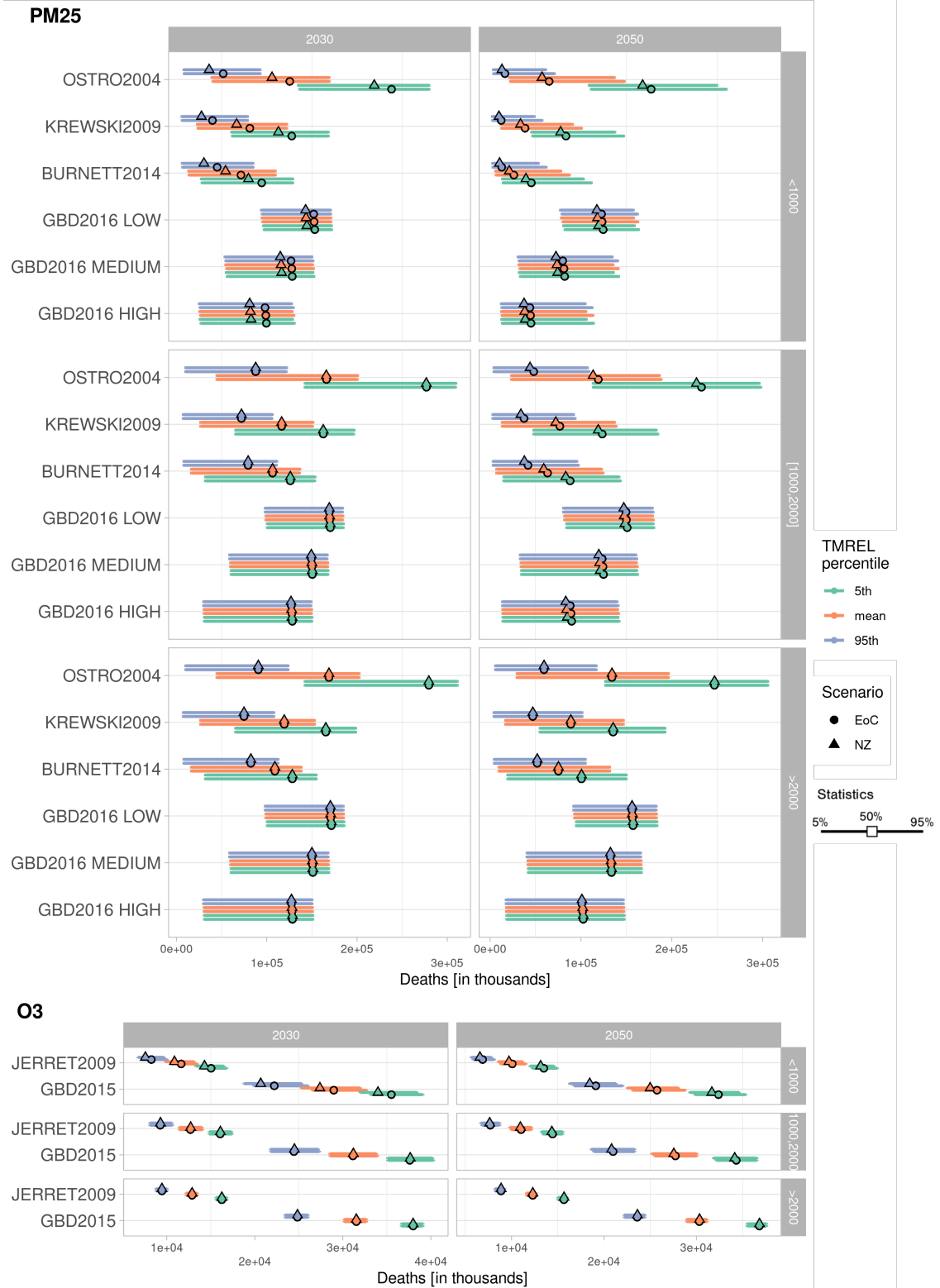
Figure 90: Influence of the impact function percentile on the estimation of premature deaths, regarding impact function, carbon budget, year, and scenario for R10PAC-OECD. Each error bars report the uncertainty range (5-95%) across parameters' sets. The middle points represent the median of the impact function RR median. Colours represent the impact functions' parameter percentile. Impact functions are ranked according to their publication date. Parameters of the impact functions are reported in Table 3.
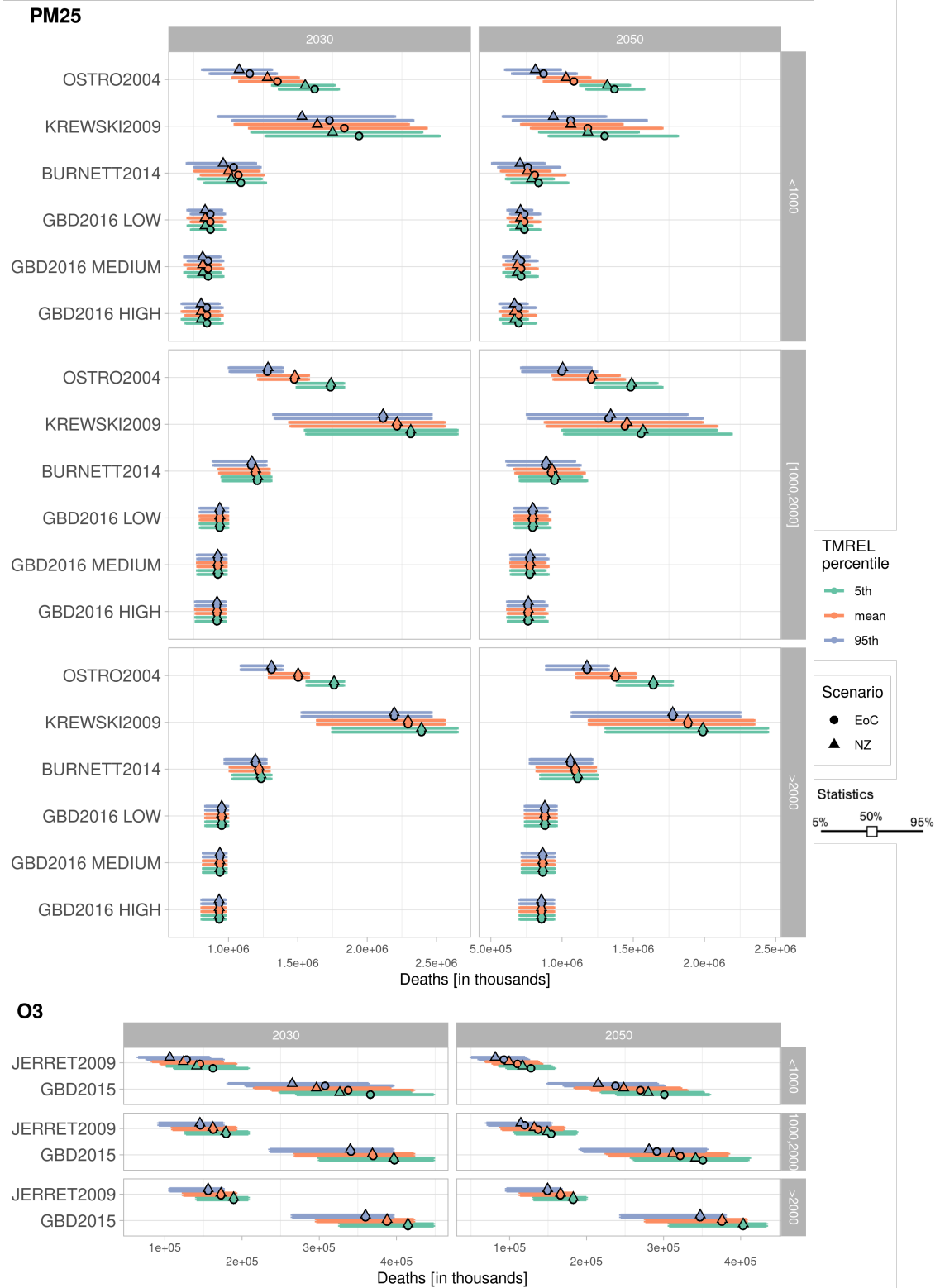
Figure 91: Influence of the impact function percentile on the estimation of premature deaths, regarding impact function, carbon budget, year, and scenario for R10REF-ECON. Each error bars report the uncertainty range (5-95%) across parameters' sets. The middle points represent the median of the impact function RR median. Colours represent the impact functions' parameter percentile. Impact functions are ranked according to their publication date. Parameters of the impact functions are reported in Table 3.

Figure 92: Influence of the impact function percentile on the estimation of premature deaths, regarding impact function, carbon budget, year, and scenario for R10REST-ASIA. Each error bars report the uncertainty range (5-95%) across parameters' sets. The middle points represent the median of the impact function RR median. Colours represent the impact functions' parameter percentile. Impact functions are ranked according to their publication date. Parameters of the impact functions are reported in Table 3.
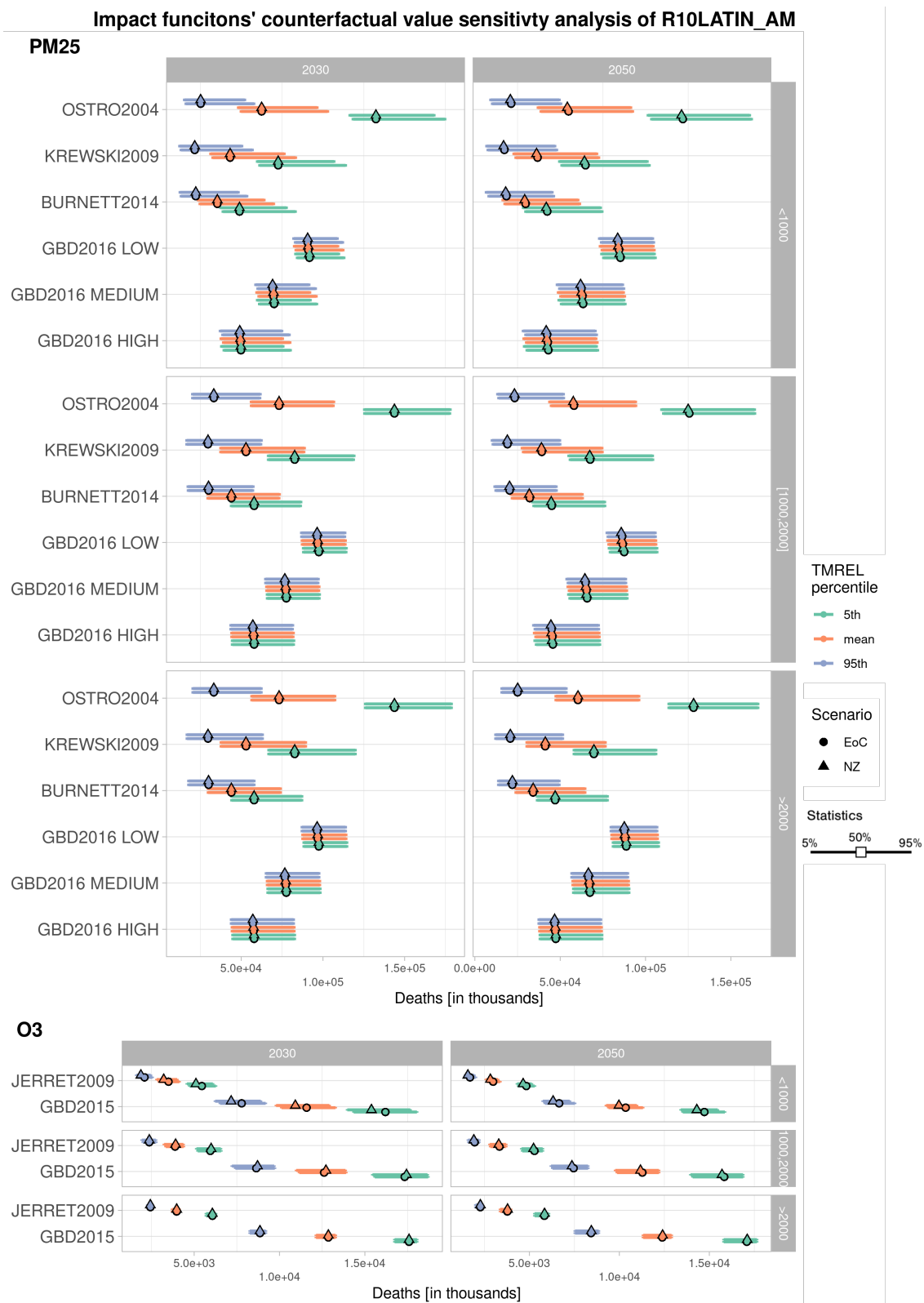
E.5 Impact function's counterfactual values sensitivity graphs

Figure 93: Influence of the impact function percentile on the estimation of premature deaths, regarding impact function, carbon budget, year, and scenario for R10AFRICA. Each error bars report the uncertainty range (5-95%) across parameters' sets. The middle points represent the median of the impact function RR median. Colours represent the impact functions' parameter percentile. Impact functions are ranked according to their publication date. Parameters of the impact functions are reported in Table 3.
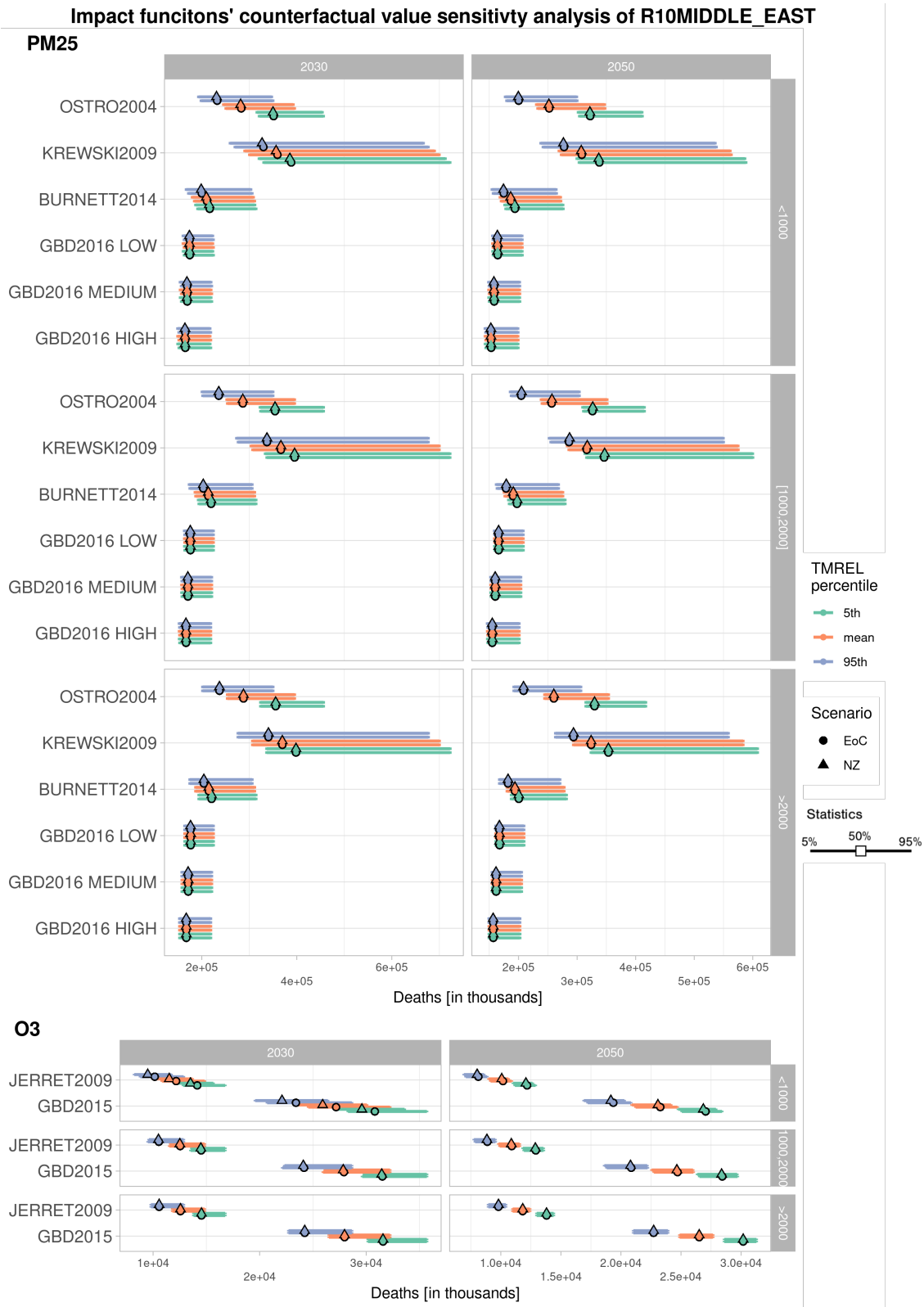
Figure 94: Influence of the impact function percentile on the estimation of premature deaths, regarding impact function, carbon budget, year, and scenario for R10CHINA+. Each error bars report the uncertainty range (5-95%) across parameters' sets. The middle points represent the median of the impact function RR median. Colours represent the impact functions' parameter percentile. Impact functions are ranked according to their publication date. Parameters of the impact functions are reported in Table 3.
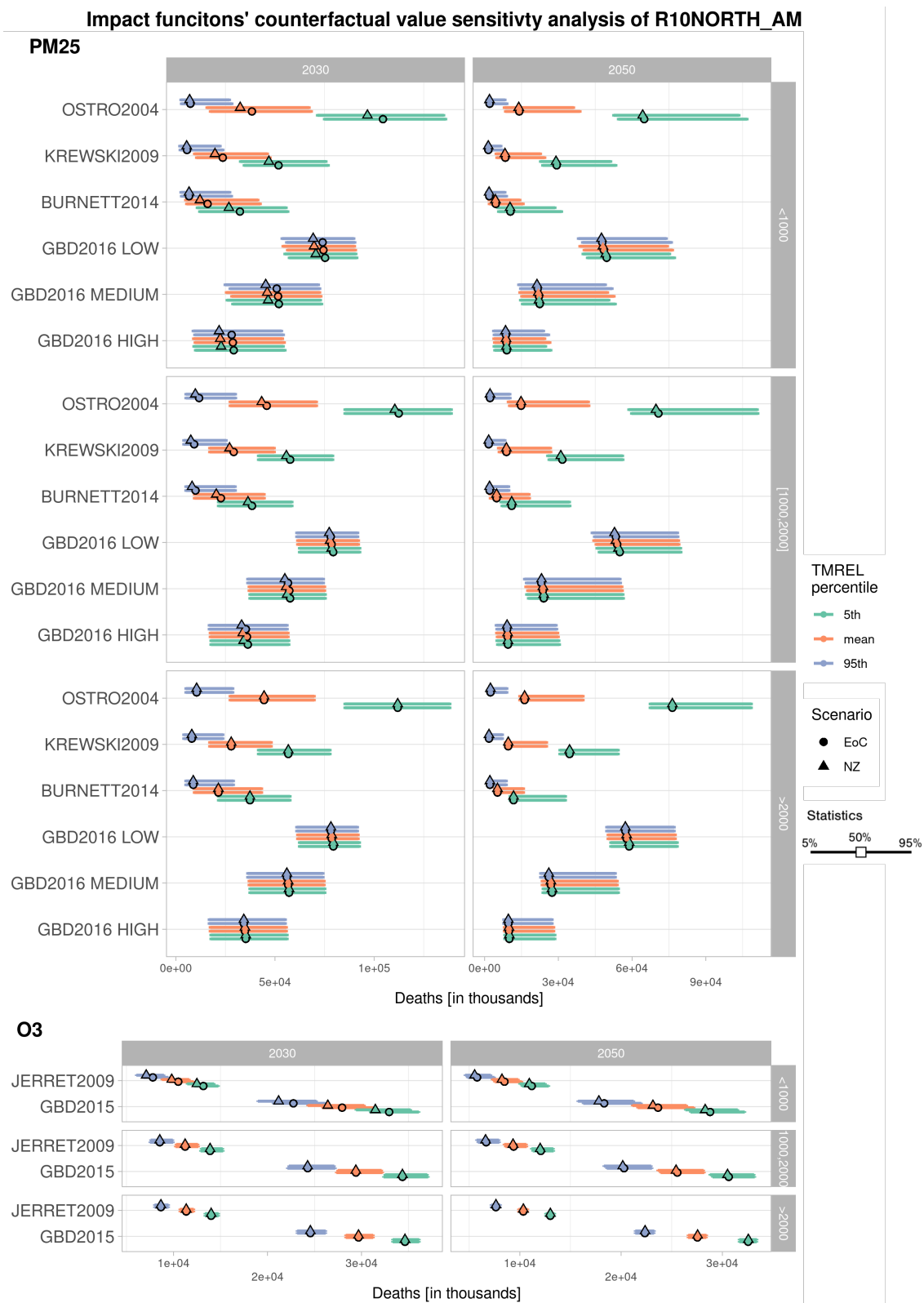
Figure 95: Influence of the impact function percentile on the estimation of premature deaths, regarding impact function, carbon budget, year, and scenario for R10EUROPE. Each error bars report the uncertainty range (5-95%) across parameters' sets. The middle points represent the median of the impact function RR median. Colours represent the impact functions' parameter percentile. Impact functions are ranked according to their publication date. Parameters of the impact functions are reported in Table 3.
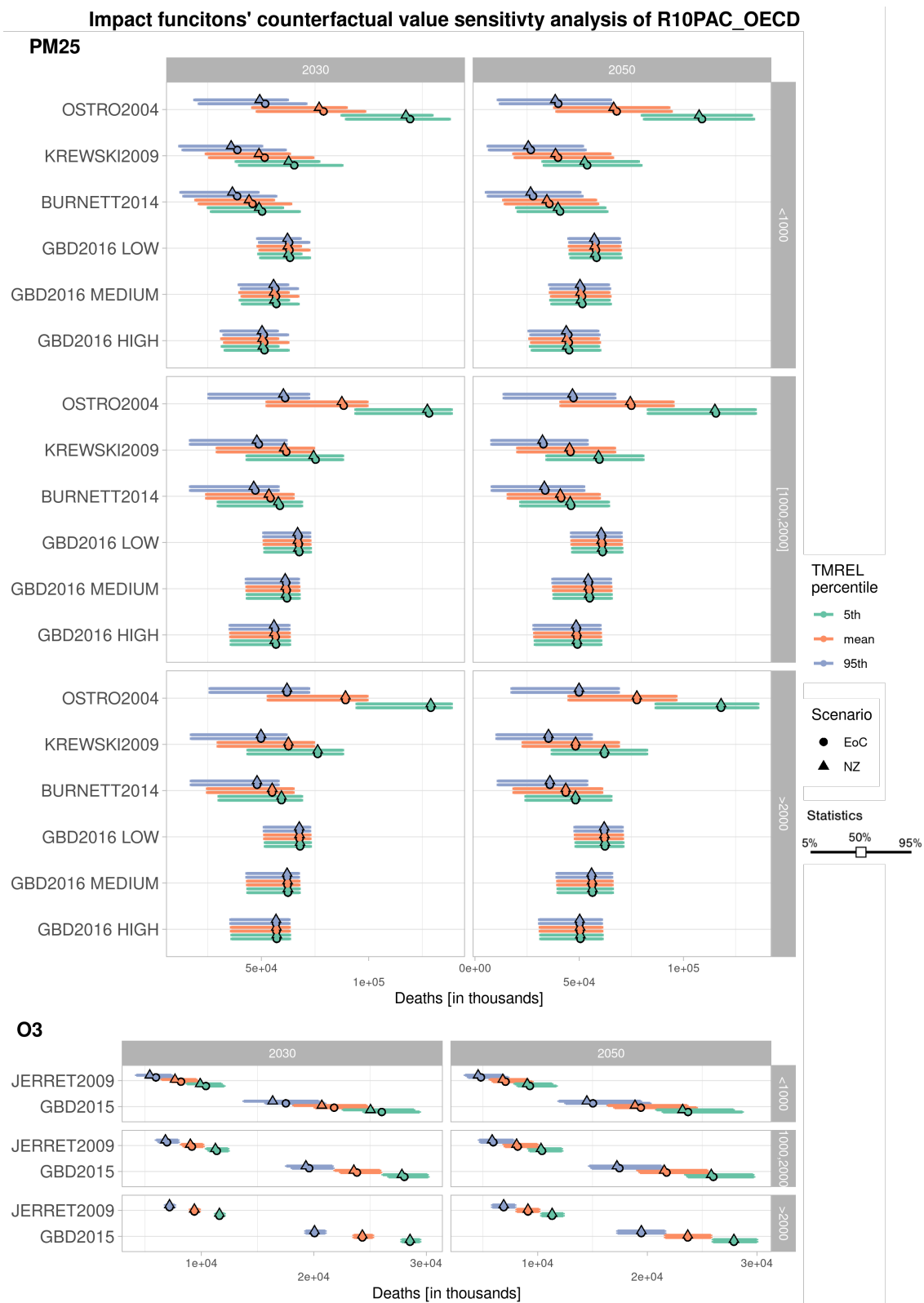
Figure 96: Influence of the impact function percentile on the estimation of premature deaths, regarding impact function, carbon budget, year, and scenario for R10INDIA+. Each error bars report the uncertainty range (5-95%) across parameters' sets. The middle points represent the median of the impact function RR median. Colours represent the impact functions' parameter percentile. Impact functions are ranked according to their publication date. Parameters of the impact functions are reported in Table 3.
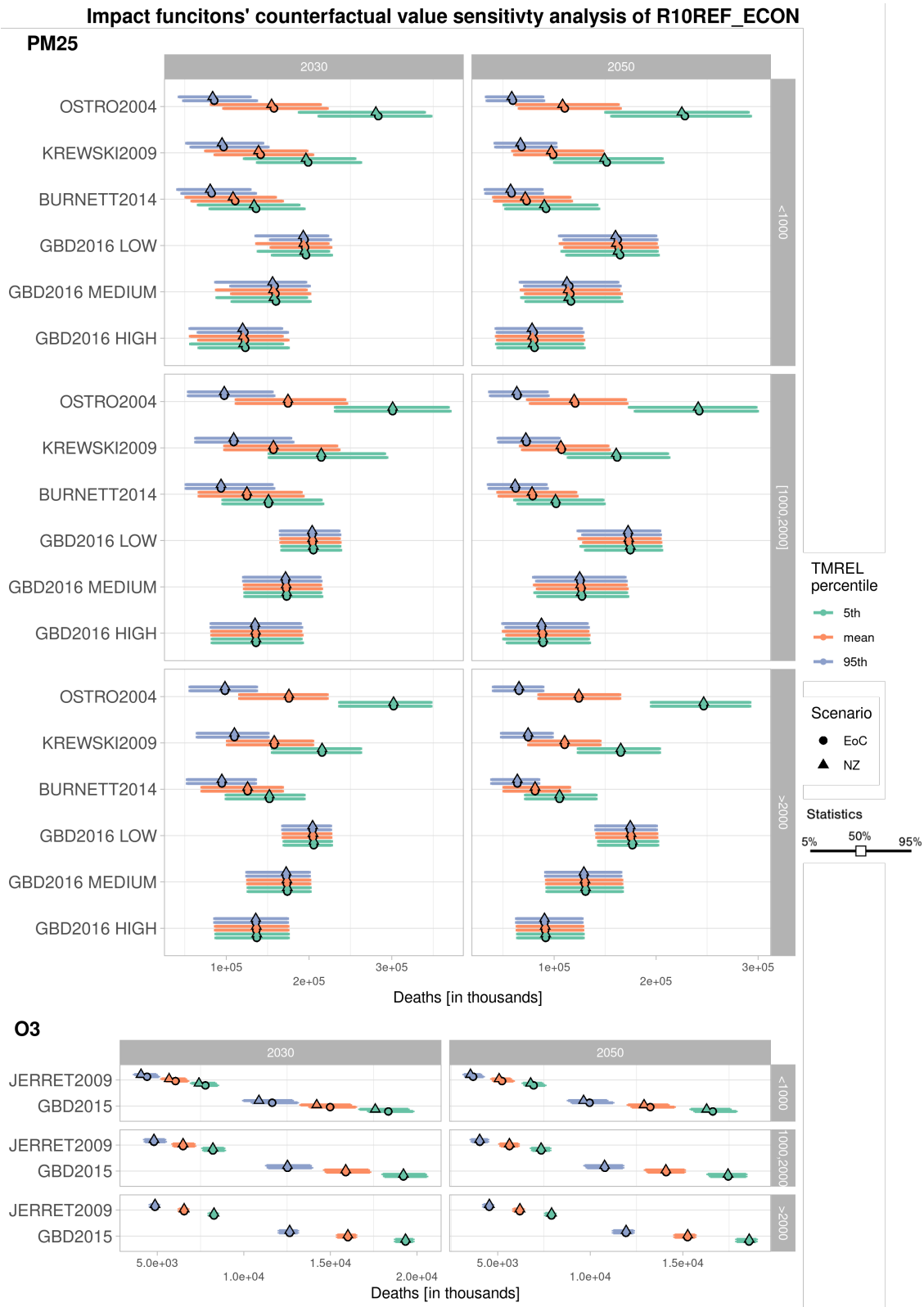
Figure 97: Influence of the impact function percentile on the estimation of premature deaths, regarding impact function, carbon budget, year, and scenario for R10LATIN-AM. Each error bars report the uncertainty range (5-95%) across parameters' sets. The middle points represent the median of the impact function RR median. Colours represent the impact functions' parameter percentile. Impact functions are ranked according to their publication date. Parameters of the impact functions are reported in Table 3.
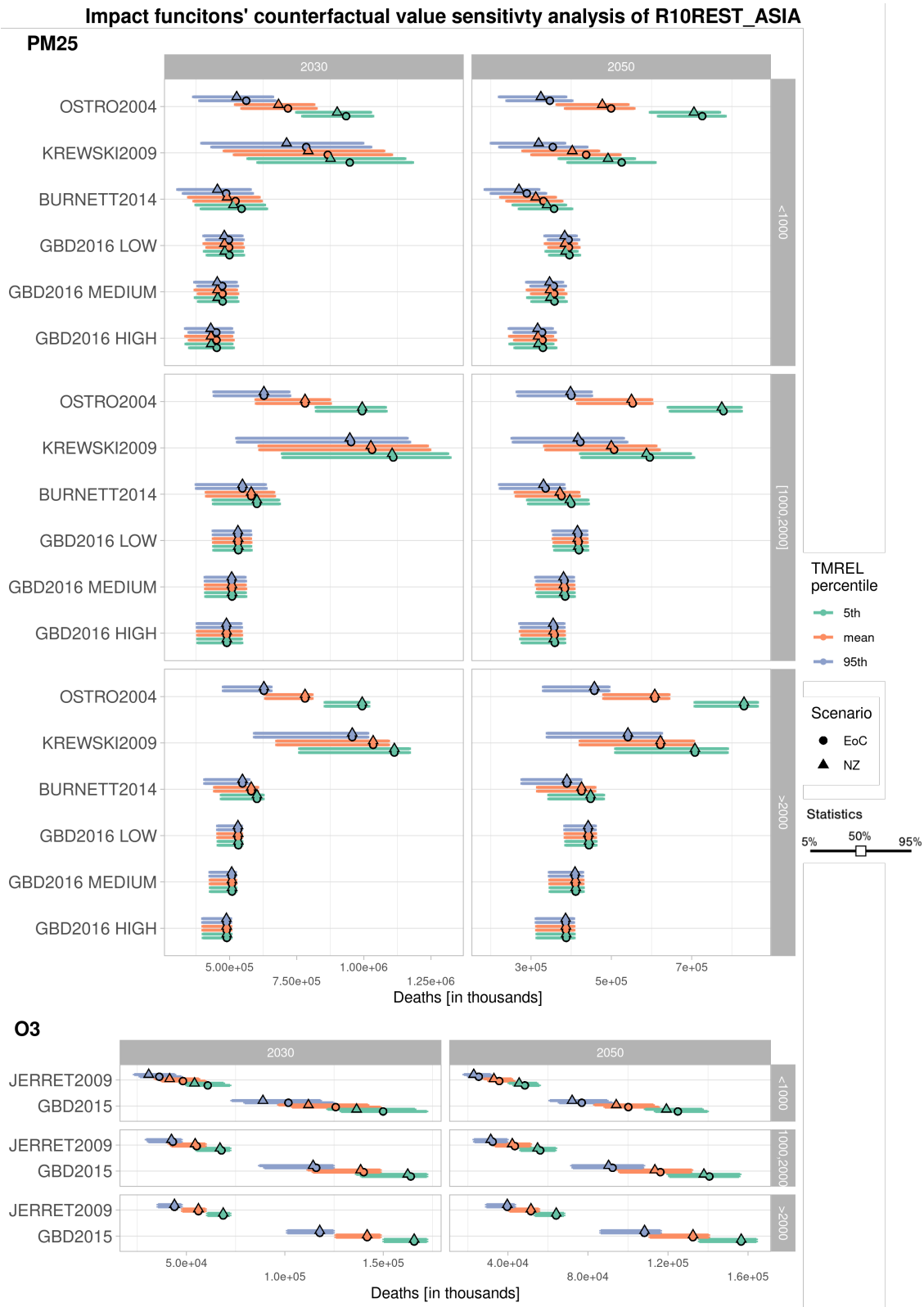
Figure 98: Influence of the impact function percentile on the estimation of premature deaths, regarding impact function, carbon budget, year, and scenario for R10MIDDLE-EAST. Each error bars report the uncertainty range (5-95%) across parameters' sets. The middle points represent the median of the impact function RR median. Colours represent the impact functions' parameter percentile. Impact functions are ranked according to their publication date. Parameters of the impact functions are reported in Table 3.

Figure 99: Influence of the impact function percentile on the estimation of premature deaths, regarding impact function, carbon budget, year, and scenario for R10NORTH-AM. Each error bars report the uncertainty range (5-95%) across parameters' sets. The middle points represent the median of the impact function RR median. Colours represent the impact functions' parameter percentile. Impact functions are ranked according to their publication date. Parameters of the impact functions are reported in Table 3.

Figure 100: Influence of the impact function percentile on the estimation of premature deaths, regarding impact function, carbon budget, year, and scenario for R10PAC-OECD. Each error bars report the uncertainty range (5-95%) across parameters' sets. The middle points represent the median of the impact function RR median. Colours represent the impact functions' parameter percentile. Impact functions are ranked according to their publication date. Parameters of the impact functions are reported in Table 3.
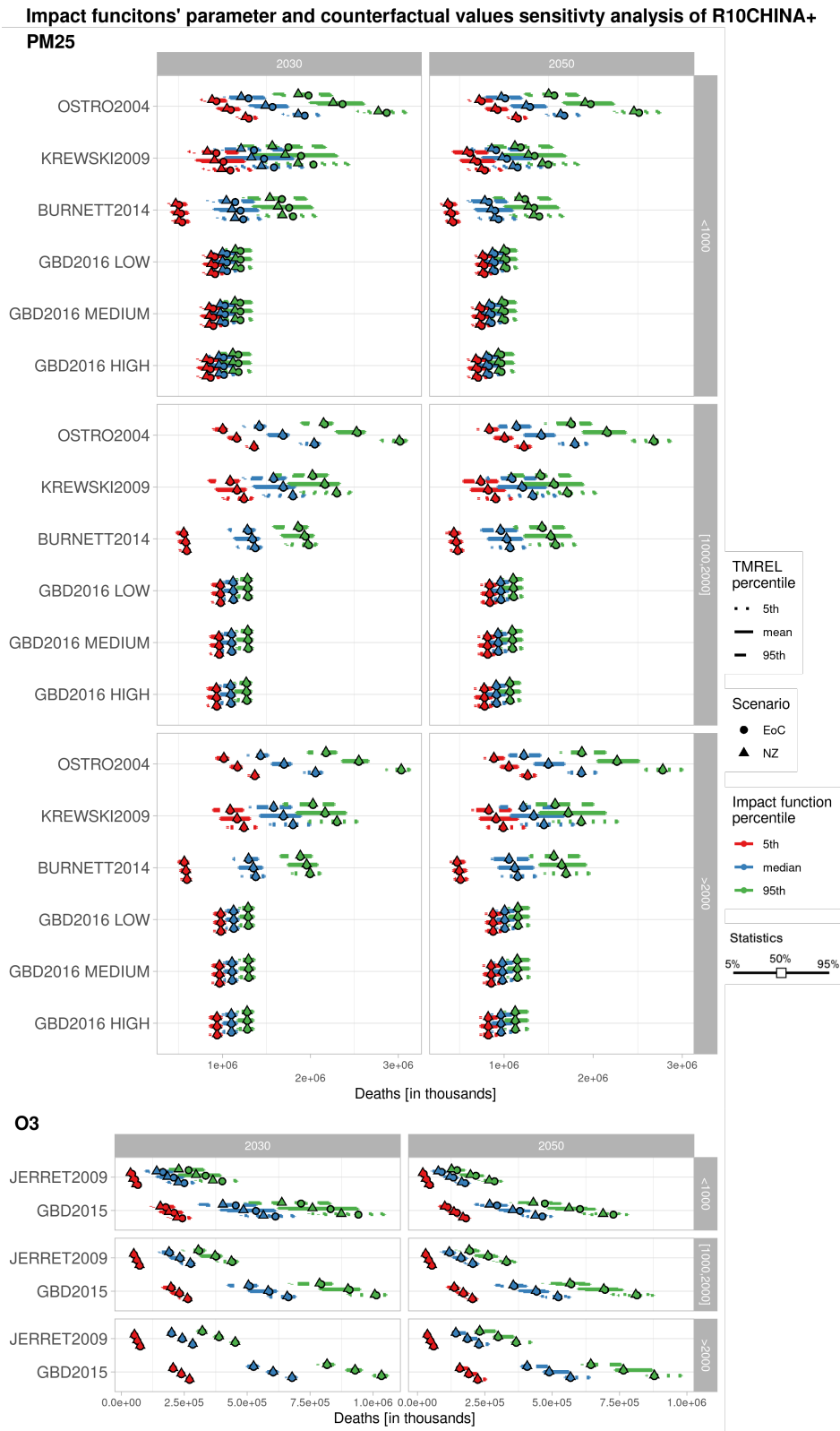
Figure 101: Influence of the impact function percentile on the estimation of premature deaths, regarding impact function, carbon budget, year, and scenario for R10REF-ECON. Each error bars report the uncertainty range (5-95%) across parameters' sets. The middle points represent the median of the impact function RR median. Colours represent the impact functions' parameter percentile. Impact functions are ranked according to their publication date. Parameters of the impact functions are reported in Table 3.

Figure 102: Influence of the impact function percentile on the estimation of premature deaths, regarding impact function, carbon budget, year, and scenario for R10REST-ASIA. Each error bars report the uncertainty range (5-95%) across parameters' sets. The middle points represent the median of the impact function RR median. Colours represent the impact functions' parameter percentile. Impact functions are ranked according to their publication date. Parameters of the impact functions are reported in Table 3.
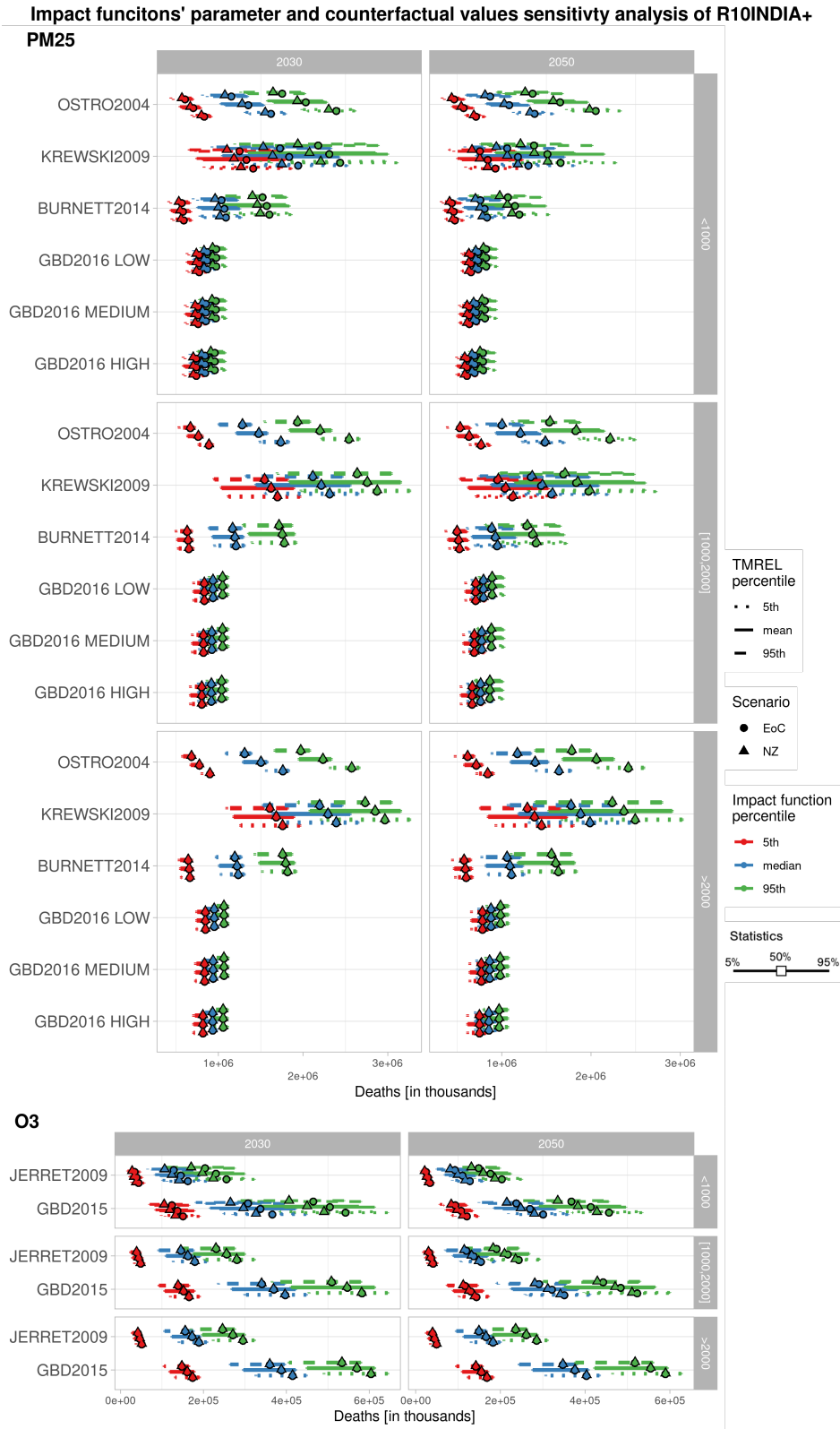
E.6 Impact function's parameters and counterfactual sensitivity graphs
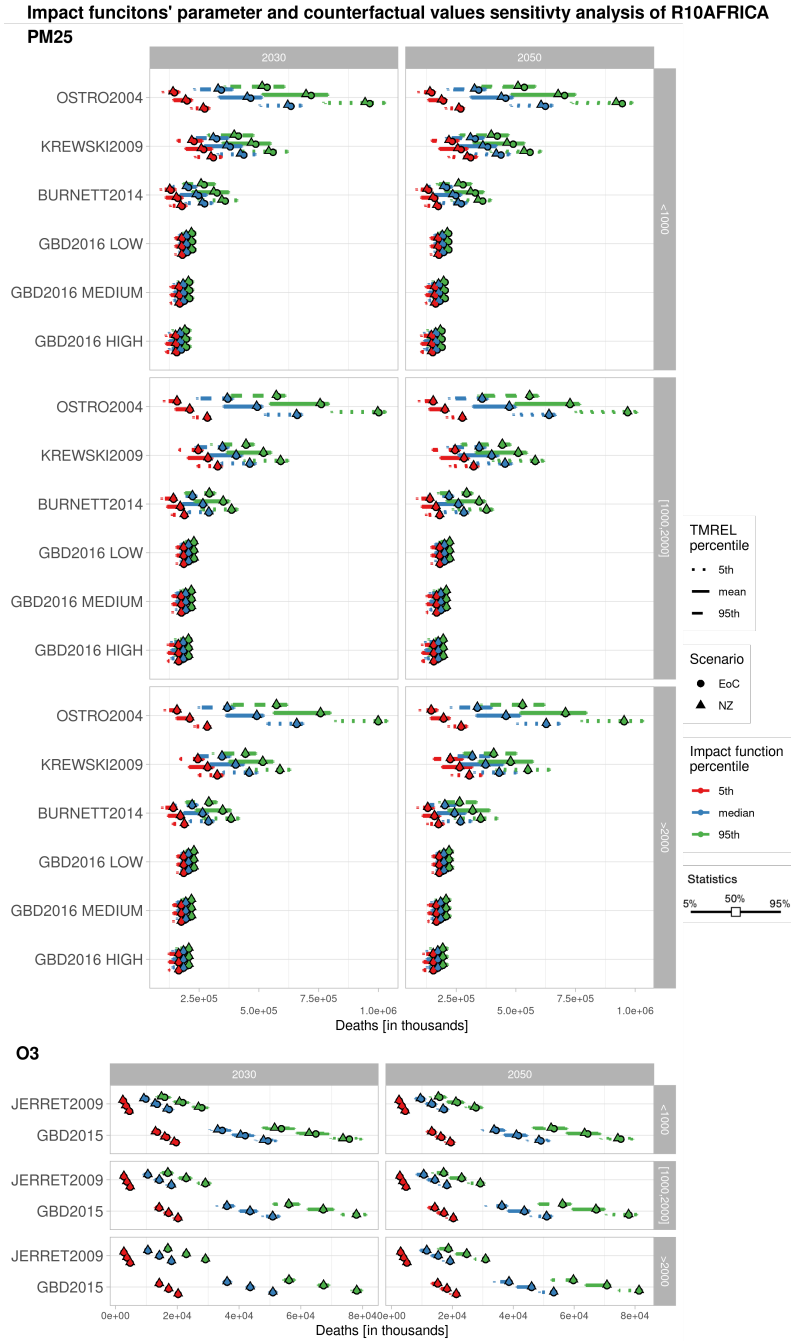
Figure 103: Influence of the relation between the impact function percentile and the counterfactual percentile on the estimation of premature deaths, regarding impact function, carbon budget, year, and scenario for R10AFRICA. Each error bars report the uncertainty range (5-95%) across parameters' sets. The middle points represent the median of the impact function RR median. Colours represent the impact functions' parameter percentile. Impact functions are ranked according to their publication date. Parameters of the impact functions are reported in Table 3.
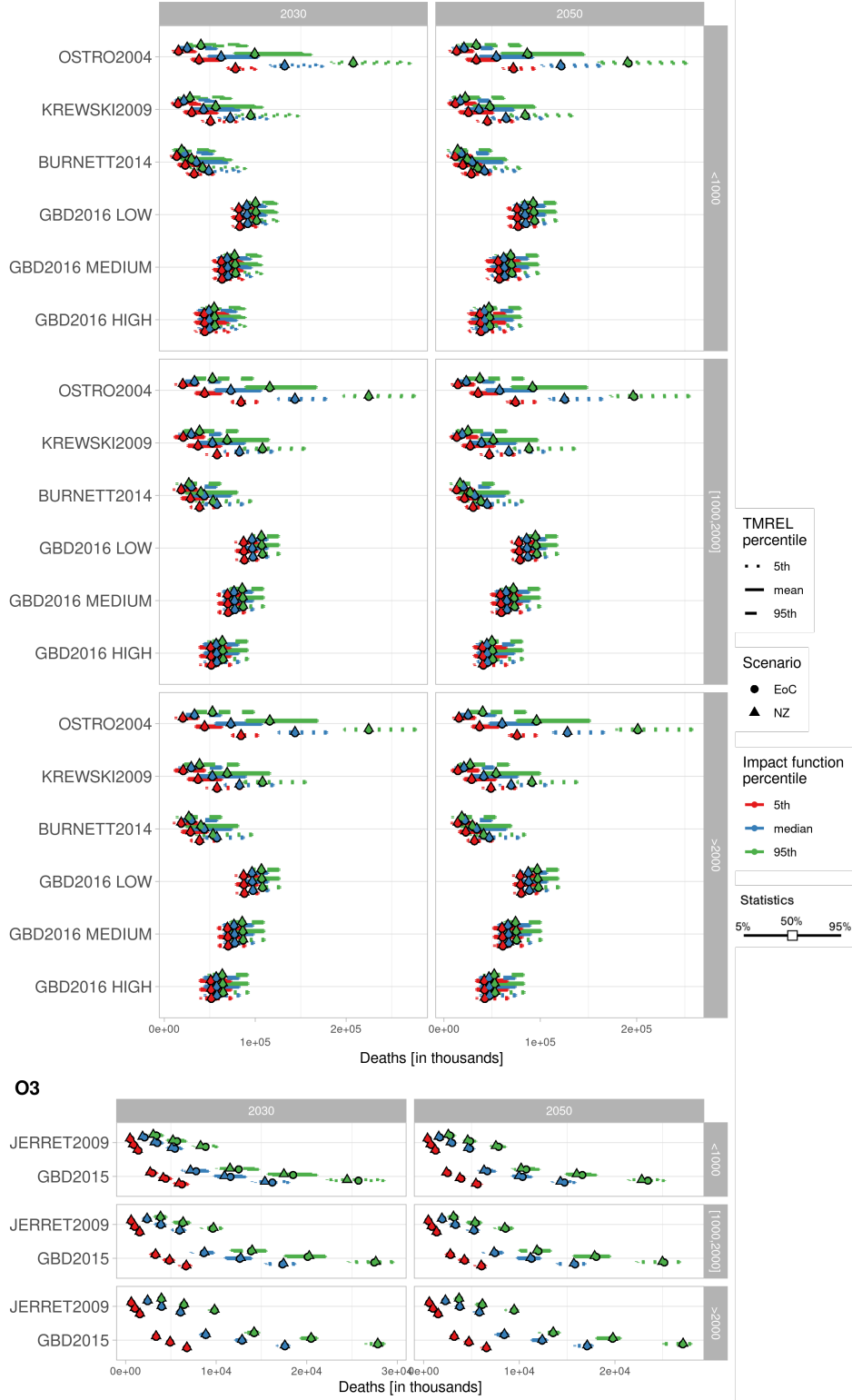
Figure 104: Influence of the relation between the impact function percentile and the counterfactual percentile on the estimation of premature deaths, regarding impact function, carbon budget, year, and scenario for R10CHINA+. Each error bars report the uncertainty range (5-95%) across parameters' sets. The middle points represent the median of the impact function RR median. Colours represent the impact functions' parameter percentile. Impact functions are ranked according to their publication date. Parameters of the impact functions are reported in Table 3.
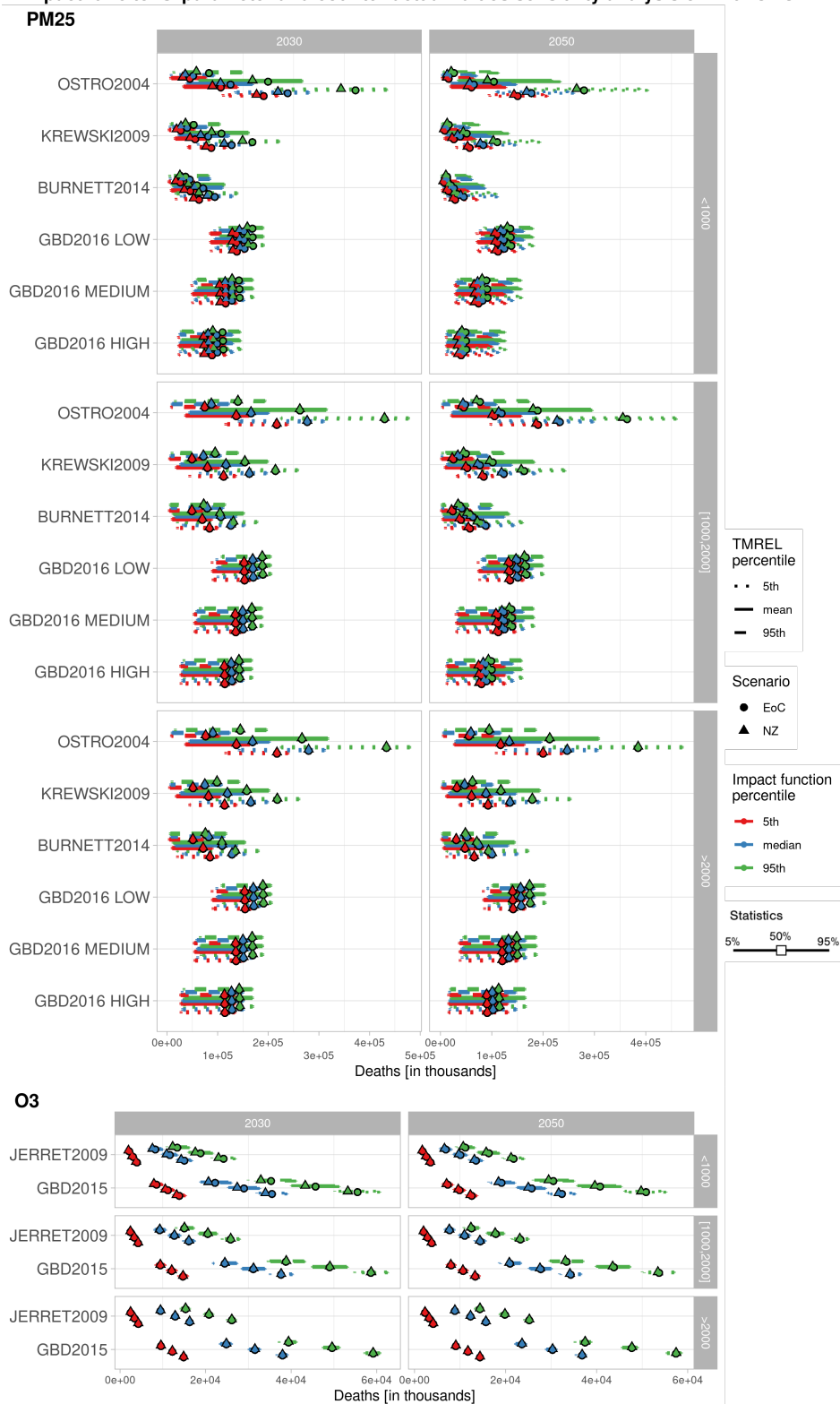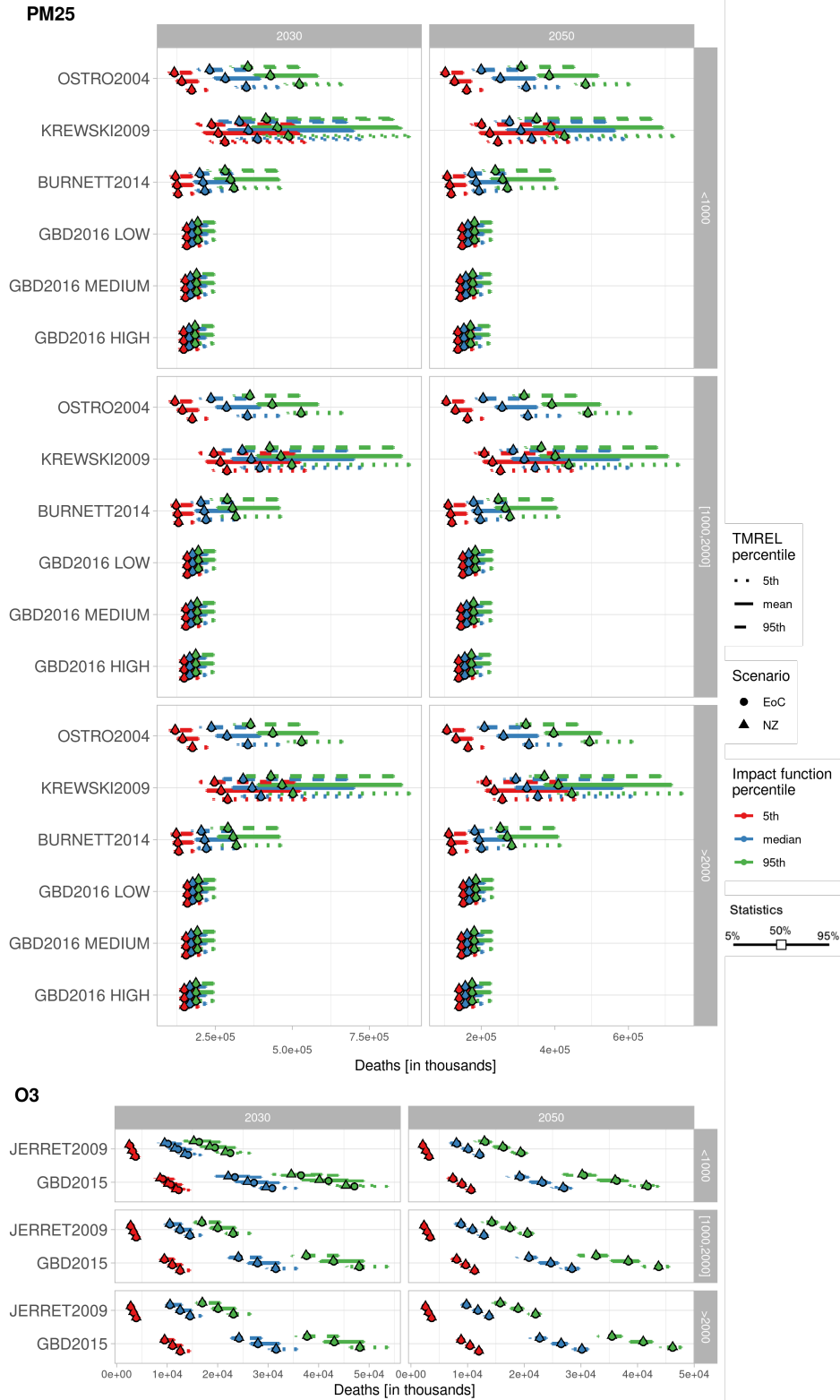
Figure 105: Influence of the relation between the impact function percentile and the counterfactual percentile on the estimation of premature deaths, regarding impact function, carbon budget, year, and scenario for R10EUROPE. Each error bars report the uncertainty range (5-95%) across parameters' sets. The middle points represent the median of the impact function RR median. Colours represent the impact functions' parameter percentile. Impact functions are ranked according to their publication date. Parameters of the impact functions are reported in Table 3.

Figure 106: Influence of the relation between the impact function percentile and the counterfactual percentile on the estimation of premature deaths, regarding impact function, carbon budget, year, and scenario for R10INDIA+. Each error bars report the uncertainty range (5-95%) across parameters' sets. The middle points represent the median of the impact function RR median. Colours represent the impact functions' parameter percentile. Impact functions are ranked according to their publication date. Parameters of the impact functions are reported in Table 3.
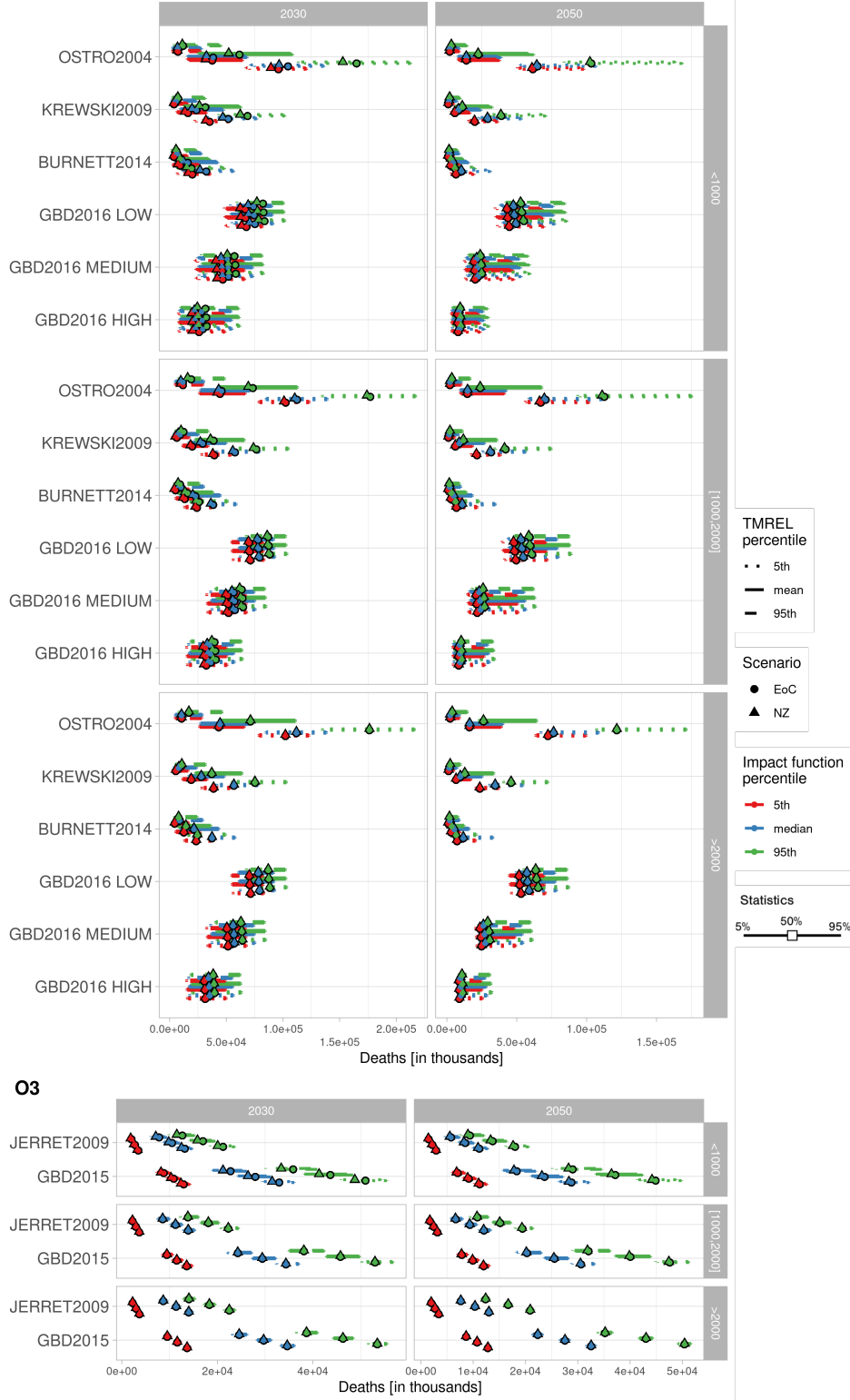
Figure 107: Influence of the relation between the impact function percentile and the counterfactual percentile on the estimation of premature deaths, regarding impact function, carbon budget, year, and scenario for R10LATIN-AM. Each error bars report the uncertainty range (5-95%) across parameters' sets. The middle points represent the median of the impact function RR median. Colours represent the impact functions' parameter percentile. Impact functions are ranked according to their publication date. Parameters of the impact functions are reported in Table 3.
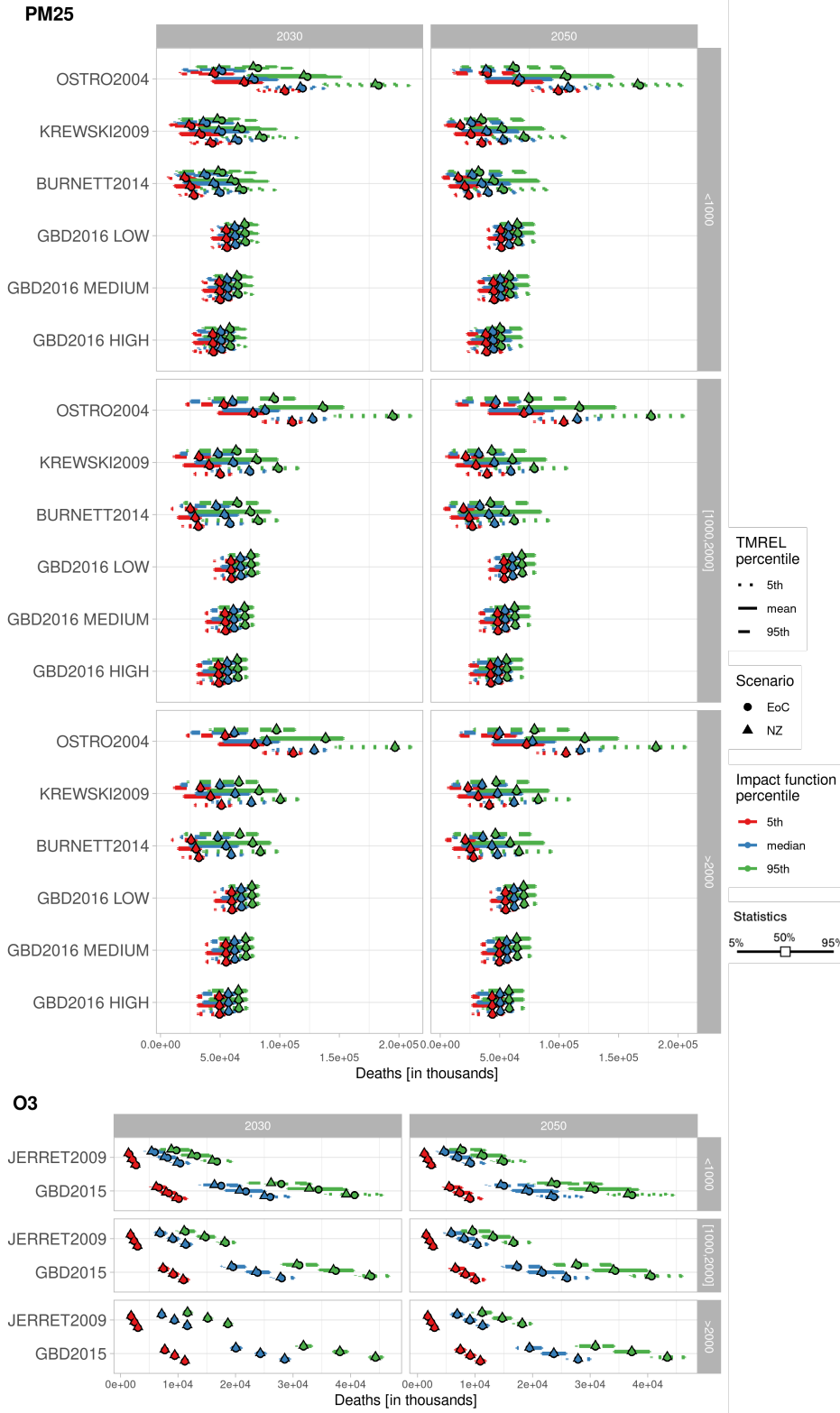
Figure 108: Influence of the relation between the impact function percentile and the counterfactual percentile on the estimation of premature deaths, regarding impact function, carbon budget, year, and scenario for R10MIDDLE-EAST. Each error bars report the uncertainty range (5-95%) across parameters' sets. The middle points represent the median of the impact function RR median. Colours represent the impact functions' parameter percentile. Impact functions are ranked according to their publication date. Parameters of the impact functions are reported in Table 3.
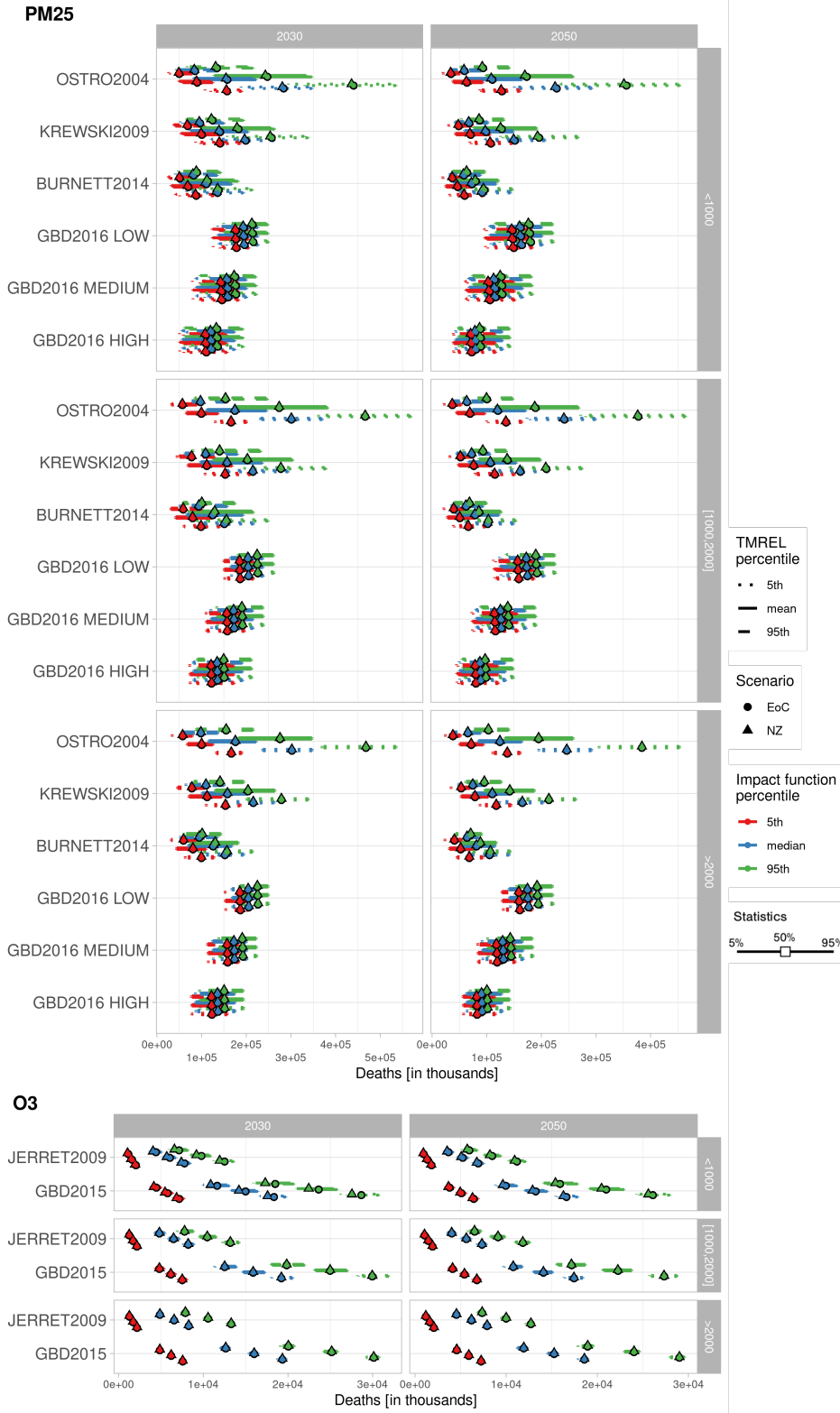
Figure 109: Influence of the relation between the impact function percentile and the counterfactual percentile on the estimation of premature deaths, regarding impact function, carbon budget, year, and scenario for R10NORTH-AM. Each error bars report the uncertainty range (5-95%) across parameters' sets. The middle points represent the median of the impact function RR median. Colours represent the impact functions' parameter percentile. Impact functions are ranked according to their publication date. Parameters of the impact functions are reported in Table 3.
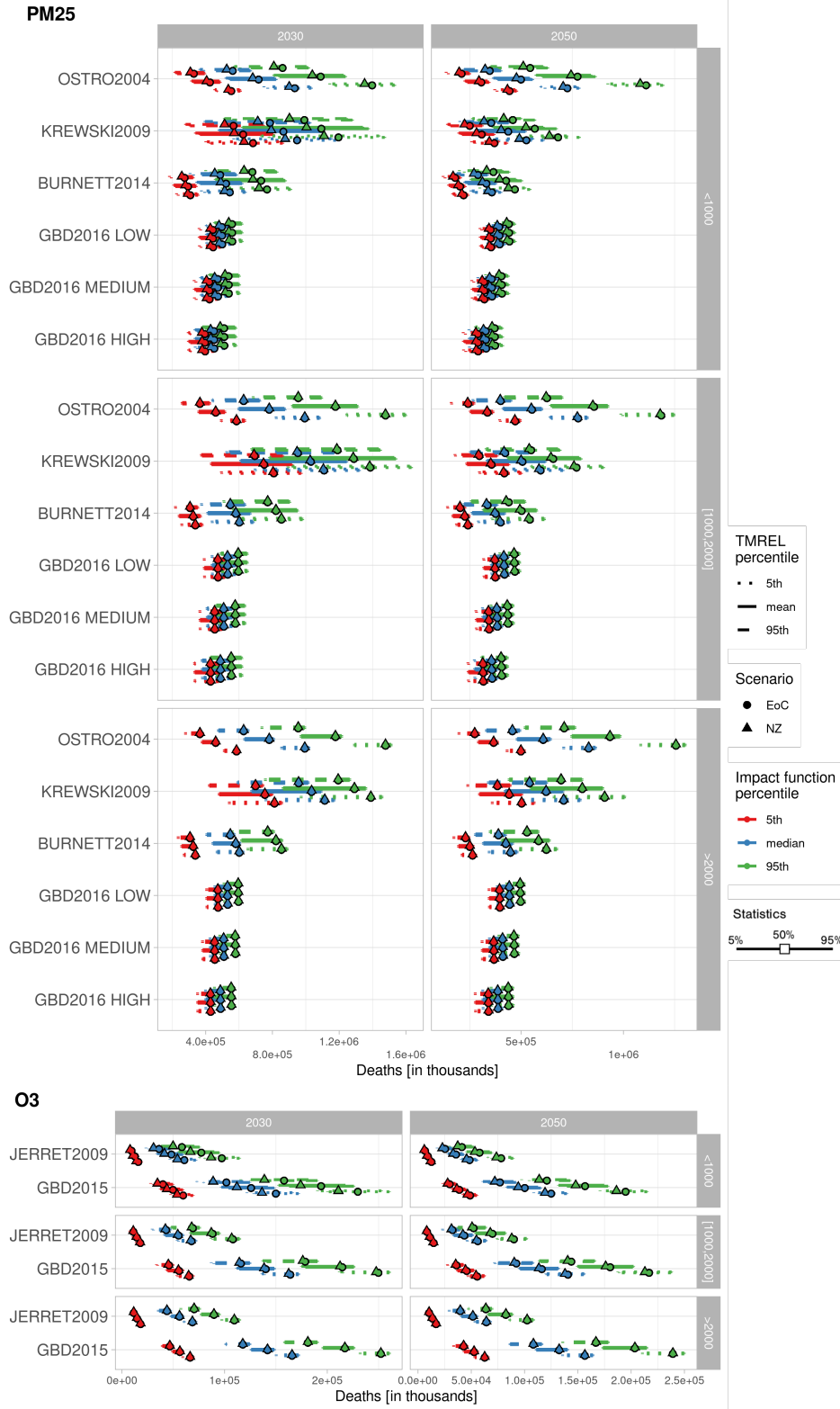
Figure 110: Influence of the relation between the impact function percentile and the counterfactual percentile on the estimation of premature deaths, regarding impact function, carbon budget, year, and scenario for R10PAC-OECD. Each error bars report the uncertainty range (5-95%) across parameters' sets. The middle points represent the median of the impact function RR median. Colours represent the impact functions' parameter percentile. Impact functions are ranked according to their publication date. Parameters of the impact functions are reported in Table 3.

Figure 111: Influence of the relation between the impact function percentile and the counterfactual percentile on the estimation of premature deaths, regarding impact function, carbon budget, year, and scenario for R10REF-ECON. Each error bars report the uncertainty range (5-95%) across parameters' sets. The middle points represent the median of the impact function RR median. Colours represent the impact functions' parameter percentile. Impact functions are ranked according to their publication date. Parameters of the impact functions are reported in Table 3.

Figure 112: Influence of the relation between the impact function percentile and the counterfactual percentile on the estimation of premature deaths, regarding impact function, carbon budget, year, and scenario for R10REST-ASIA. Each error bars report the uncertainty range (5-95%) across parameters' sets. The middle points represent the median of the impact function RR median. Colours represent the impact functions' parameter percentile. Impact functions are ranked according to their publication date. Parameters of the impact functions are reported in Table 3.

E.7 IAMs and impact functions uncertainty graphs
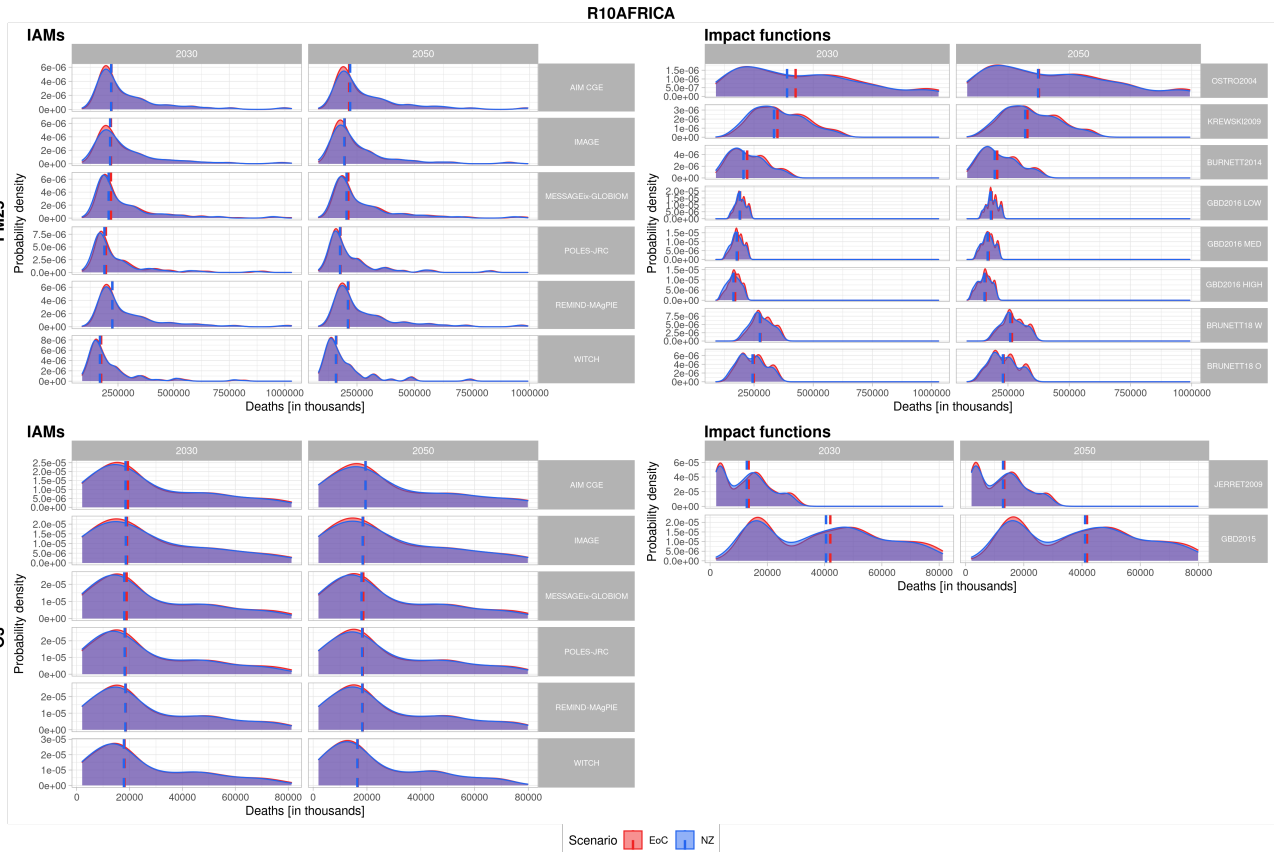
Figure 113(): Probability density distribution (left) and cumulative frequency (right) for R10AFRICA. Includes median line by climate policy. Impact functions are ranked according to their publication date.
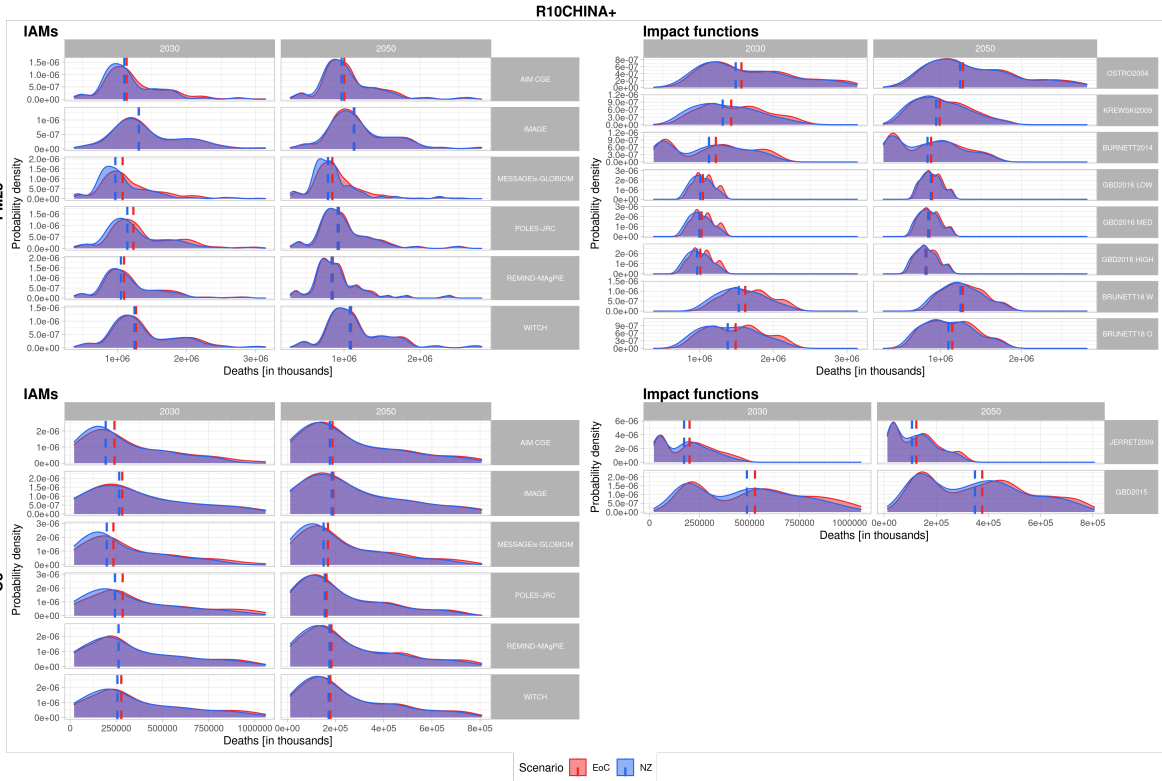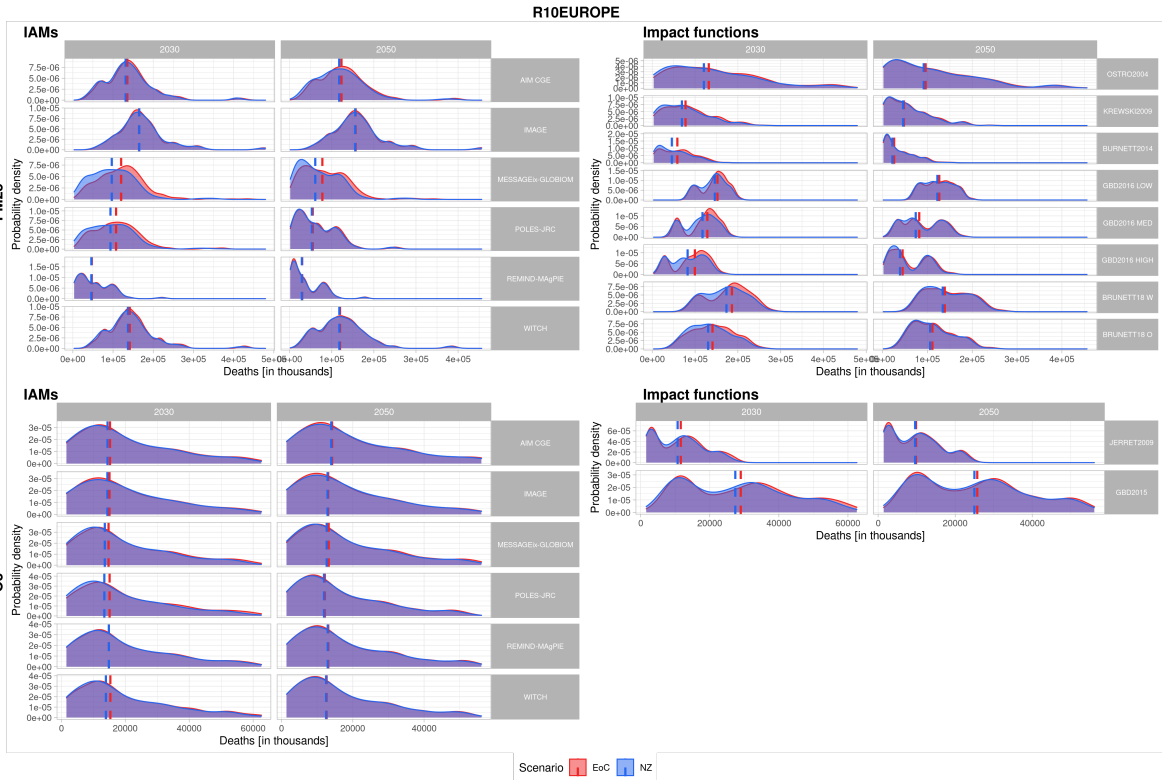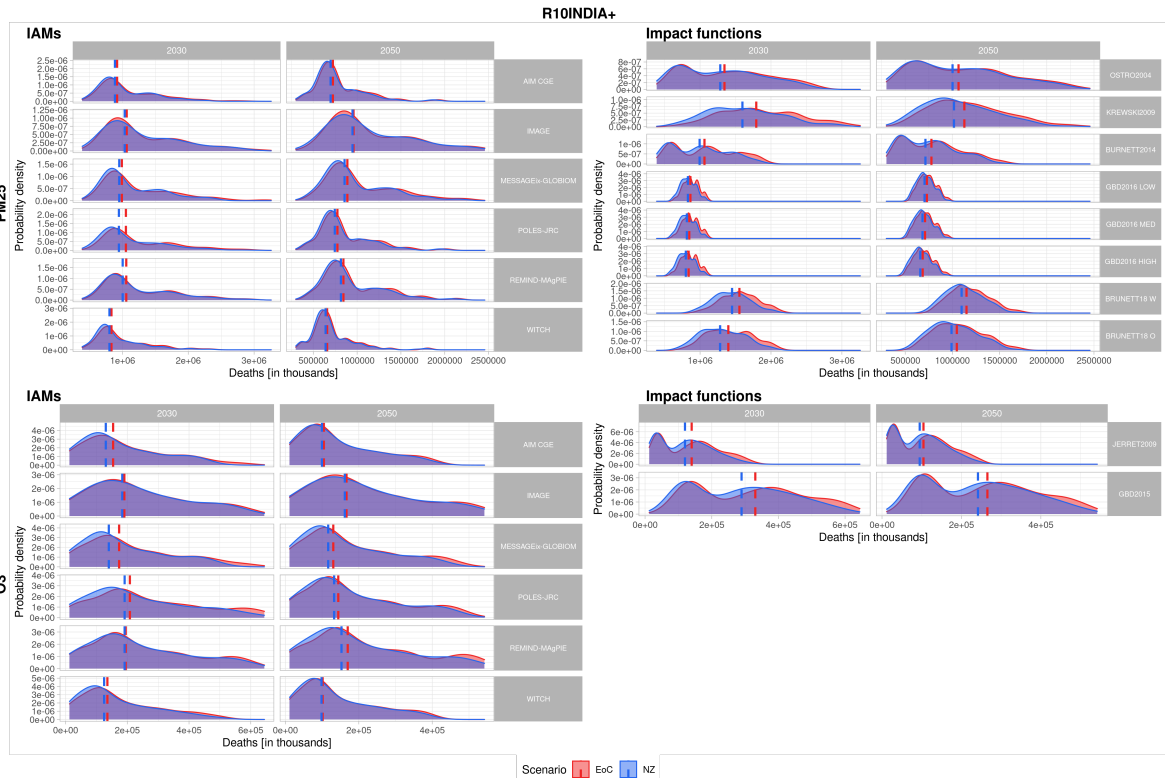
Figure 114(a): Probability density distribution (left) and cumulative frequency (right) for R10CHINA+. Includes median line by climate policy. Impact functions are ranked according to their publication date.

Figure 114(b): Probability density distribution (left) and cumulative frequency (right) for R10EUROPE. Includes median line by climate policy. Impact functions are ranked according to their publication date.

Figure 115(a): Probability density distribution (left) and cumulative frequency (right) for R10INDIA+. Includes median line by climate policy. Impact functions are ranked according to their publication date.
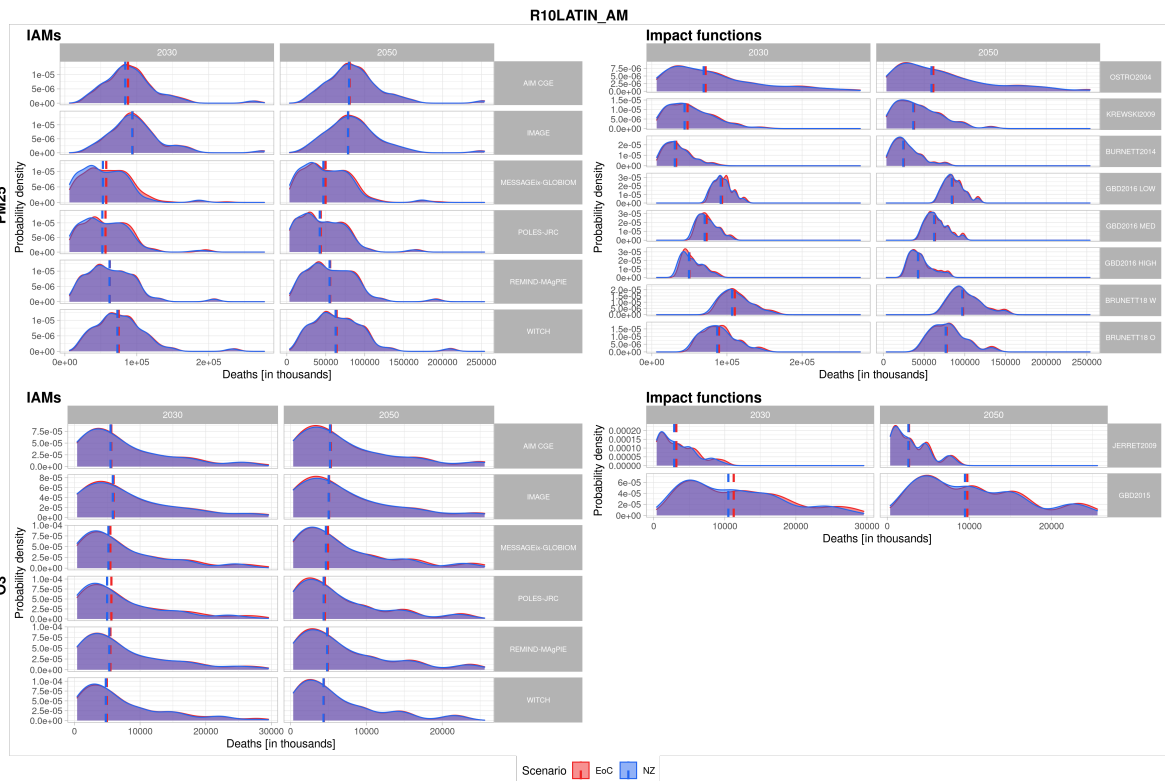

Figure 115(b): Probability density distribution (left) and cumulative frequency (right) for R10LATIN-AM. Includes median line by climate policy. Impact functions are ranked according to their publication date.
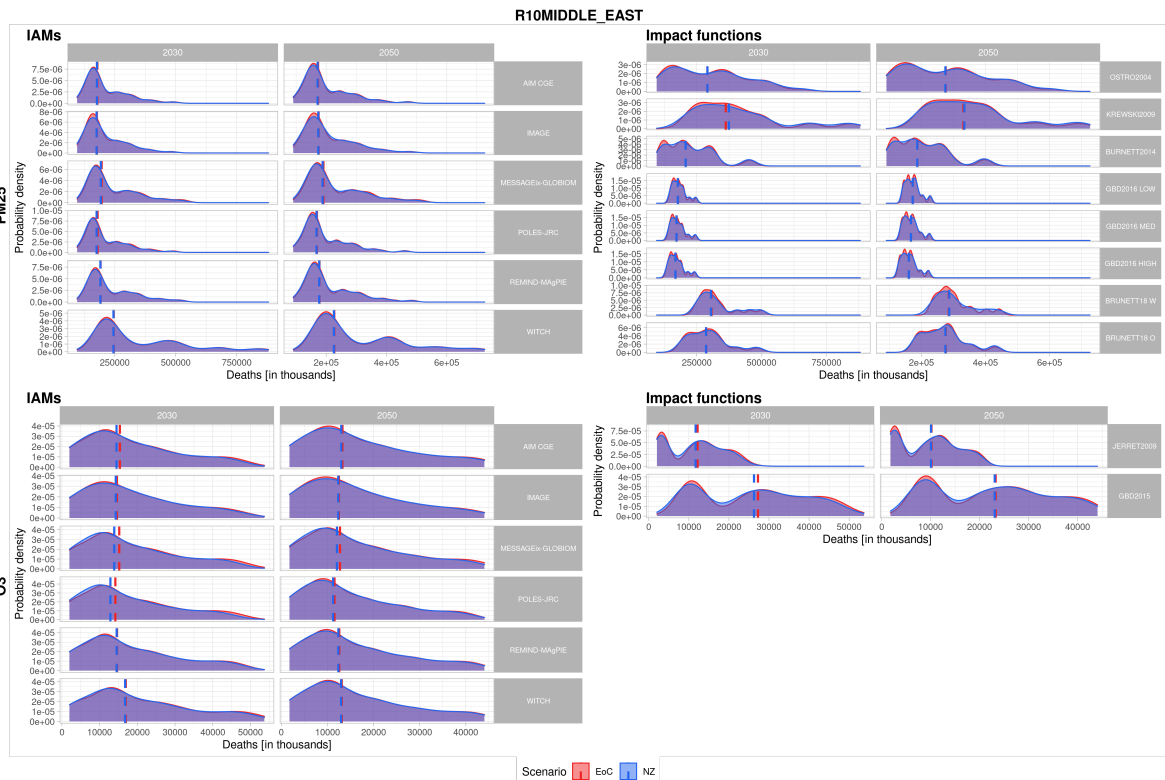
Figure 116(a): Probability density distribution (left) and cumulative frequency (right) for R10MIDDLE-EAST. Includes median line by climate policy. Impact functions are ranked according to their publication date.

Figure 116(b): Probability density distribution (left) and cumulative frequency (right) for R10NORTH-AM. Includes median line by climate policy. Impact functions are ranked according to their publication date.

Figure 117(a): Probability density distribution (left) and cumulative frequency (right) for R10PAC-OECD. Includes median line by climate policy. Impact functions are ranked according to their publication date.
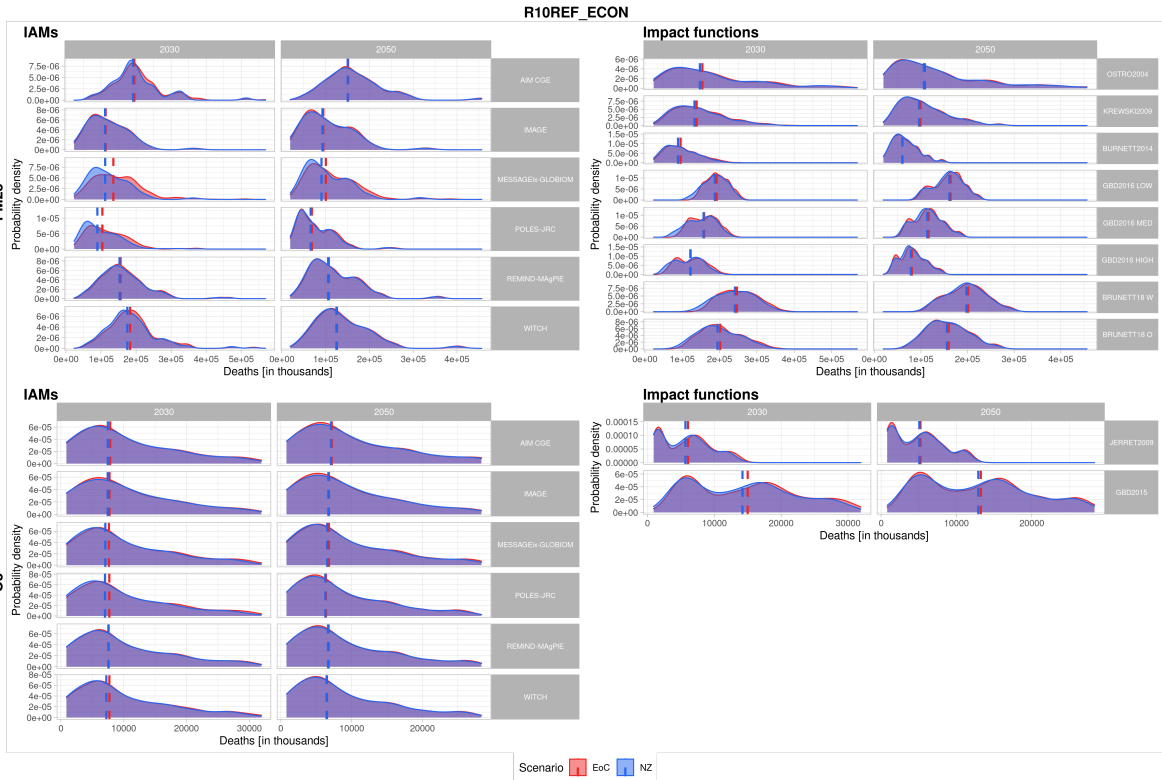

Figure 117(b): Probability density distribution (left) and cumulative frequency (right) for R10REF-ECON. Includes median line by climate policy. Impact functions are ranked according to their publication date.
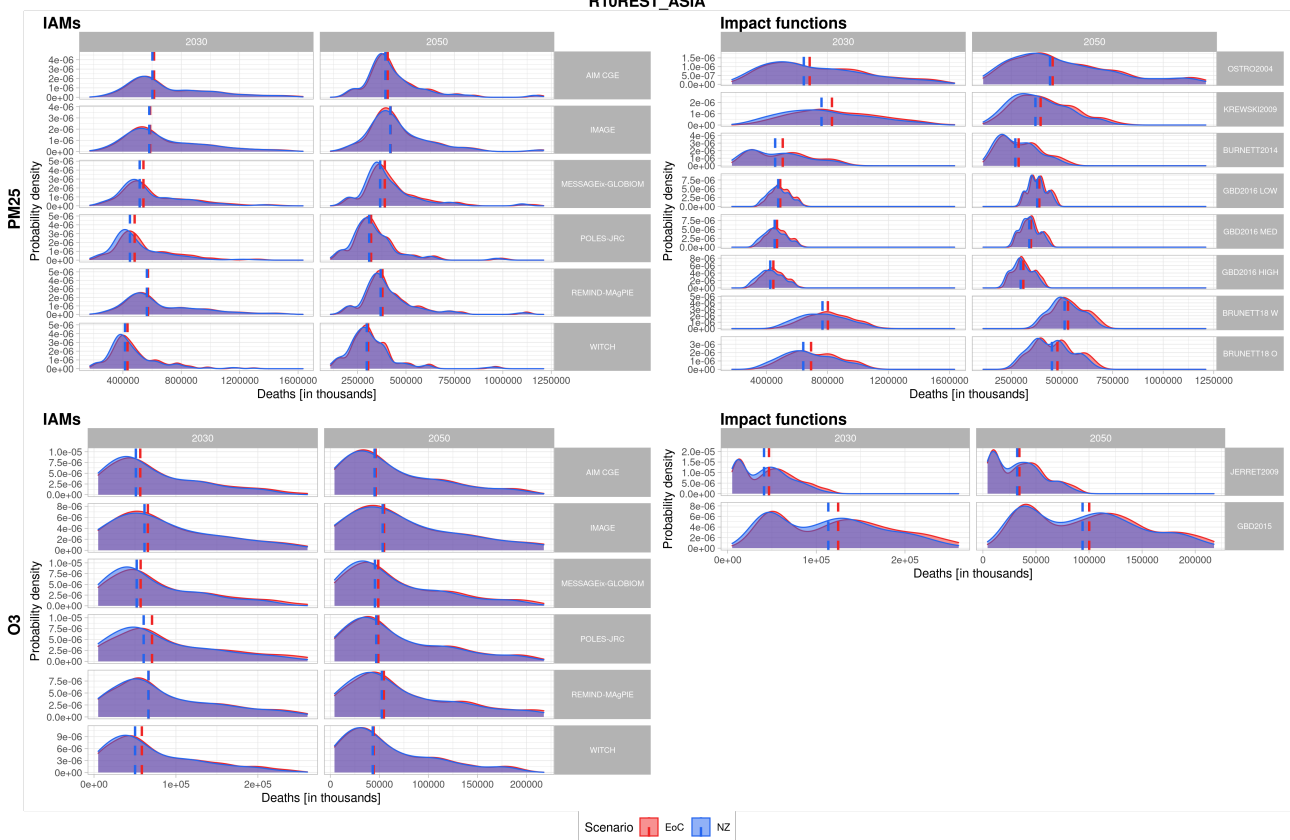
Figure 118(): Probability density distribution (left) and cumulative frequency (right) for R10REST-ASIA. Includes median line by climate policy. Impact functions are ranked according to their publication date.

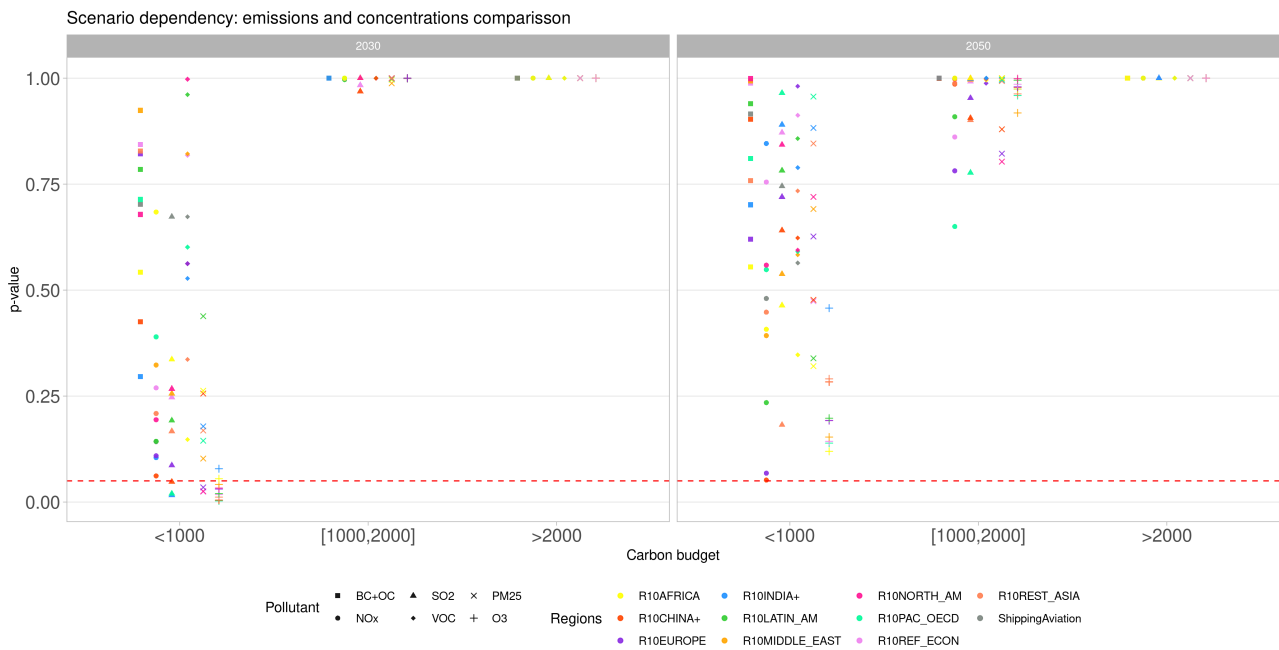# F. Emission and concentration sensitivity comparison

Figure 119: Climate policy dependence by region, year, and carbon budget. On the Y-axis there is the p-value of the K-S two-samples test done separately by pollutant, region, year, and carbon budget. The dashed red line indicates the significance level threshold.